THE OCCULTATION OF POLARISED LIGHT FROM STELLAR ENVELOPES

By

Geoffrey Kevin Fox

Thesis

submitted to the

University of Glasgow

for the degree of

Ph.D

Department of Physics and Astronomy

University of Glasgow

Glasgow

G12 8QQ

April 1990

ProQuest LLC.
789 East Eisenhower Parkway
P.O. Box 1346
Ann Arbor, MI 48106 – 1346

" I hope you don't think that I have been speaking too long about astronomical matters, for there is one other important thing connected with astronomy that I must speak of. You see, I have had almost nothing practically to do with astronomy, and hence I have a strong interest in the subject. It is very curious, but quite true, that men practically engaged in any pursuit are almost unable to see the romance of it. This is what the imaginative outsider sees. But the overworked astronomer has a different point of view. As soon as it becomes one's every-day work, the thing loses a great deal of its interest".

Spinning Tops and Gyroscopic Motion

By John Perry, 1957 (Dover).

Summary

Following the discovery of the spectral variability in a number of emission line B type stars (so called Be stars) at around the turn of this century, extensive theoretical and observational campaigns have since been an ongoing process in an attempt to understand the controlling physics of the star and its environment. Although it is now known that variability occurs on all time scales the mechanisms responsible for the variability are still not well understood. The consensus is that the stars are rapidly rotating (approximately up to 80% of the critical rotational velocity) which appears to have a major influence upon the characteristics of the star and its environment as is inferred by the observed spectral variability.

The observed high intrinsic polarisation of Be stars also implies that the rapidly rotating star rotationally distorts the surrounding circumstellar envelope. This suggests that by using current geometrical model envelopes together with polarisation theory, constraints upon the distribution of scattering material, the geometry and mass of the scattering envelope could be inferred from polarimetric observations.

In this thesis the theory of optically thin, Thomson (or Rayleigh) scattering polarisation from stellar envelopes for both single and binary star systems (Brown and McLean, 1977; Brown et al., 1978) are considered and extended to include finite light sources in order to provide more stringent constraints upon Be star envelopes and also to enable inferences to be made as to the density structure of regular polarimetric variations in single and binary star systems.

The spectral variability characterising the Be star phenonena is reviewed in chapter 1 with particular reference to γ Cas. Current spectroscopic geometric models are also discussed in some detail. Following this, the polarimetric theory and observations related to Be stars are discussed which also includes a brief section on binary diagnostics as Be stars are frequently observed in binary systems and a qualitative account of the observational consequences of scatterer occultation in binary systems is also included.

Continuing with polarimetric variability in binary systems, in chapter 2 the polarimetric variability of the Be/X-ray transient A0538-66 is investigated with a view to understanding the mass transfer from the primary (Be) star disc envelope to the secondary (neutron) star. This chapter is in a slightly different vein to the remainder of the thesis in that the scattering material is assumed not to be occulted (in fact due to the scanty data set this question cannot even be asked). It is included here partially because Be stars in binary systems seem to exhibit spectral behaviour similar to that of single stars and hence this may throw some light upon possible underlying mechanisms and also as an example of how the density structure within a binary system can be inferred from the polarimetric data which is one of the questions addressed in this thesis.

In chapters 3 - 5 the effects of incorporating a finite size (spherical) light source into the optically thin, single Thomson scattering polarimetric theory is developed for various geometrical models with particular reference to understanding what constraints are needed to be imposed upon Be star models in order to produce the necessary degree of observed intrinsic polarisation. Also addressed is the question to what extent the density structure can be inferred

from the polarimetric variability of a system when there is only one important light source. This may be considered as a density perturbation in a stellar envelope around a single star or a binary system in which the secondary is important as a light source (eg. a neutron star).

In chapter 6 the effects of occultation in obliquely rotating envelopes are discussed and the error in inferring the inclination and obliquity angle by Fourier analysing the polarimetric data of such systems is assessed when no account of occultation is made but is present within the data.

Finally in chapter 7 a brief summary of the conclusions of this thesis is made and suggestions are put forward for future work with particular reference to the application of polarisation theory, as an independent method, to understanding the underlying structure of UV discrete absorption line components is discussed.

Preface

This thesis is primarily concerned with the consequences of incorporating finite light sources into the Thomson (or Rayleigh) scattering polarisation in an optically thin media. The effects are two fold. First, account must be made of the fact that each scatterer sees a finite light source, the effect being a range of permissible scattering angles through which light from the source may be scattered towards the observer (Cassinelli et al., 1987; Carlow, 1988). Second, there exists the possibility of scatterer occultation i.e. there exists scatterers that are not visible to the observer (Milgrom, 1978). Both contributions are considered and their combined effects are investigated for various geometries, progressing from a planar distribution (chapters 3 and 4) to generalised axisymmetric envelopes in chapter 5.

The modified polarimetric theory is then used to answer two questions. First, what is the permissible parameter space for each of the geometrical models representing Be stars in order to account for the observed intrinsic polarisation ? Second, from the observed polarimetric variation from single and binary star systems, to what extent can the geometry of the envelope be inferred and can the inclination of the system be determined ?

In chapter 6 the occultation of obliquely rotating envelopes (ORE) is considered. The treatment is by no means rigorous, but is intended to examine with what certainty the inclination and obliquity angle of an ORE can be estimated using the point light source treatment of Brown et al. (1978) (cf. McGale, 1988).

The work of chapter 2 was carried out in cooperation with Dr. G.C. Clayton, Prof. J.C. Brown and Dr. I.B. Thompson at Wisconsin University (Madison) during October 1987 and is published in *Mon.*

Not. Roy. Astr. Soc. (**236**, 901). Whilst in Wisconsin chapter 3 was formulated by Prof. J.C. Brown and myself and is now published in *Ap. J.* (**347**, 468). Chapters 4 and 5 are intended to be submitted to *Ap. J.* as continuation papers of chapter 3.

The work of this thesis began in the Astronomy Department of Glasgow and continued through the merger of the Natural Philosophy and Astronomy Departments to form the Department of Physics and Astronomy.

I am grateful that I have been able to carry out this research under the supervision of Prof. John C. Brown who, amongst his many talents, has a world wide reputation for the development of polarimetric theory that began during the late seventies.

I would like to thank the astronomers at Wisconsin who made my stay there a warm and welcome one, particularly Prof. Joe Cassinelli, Dr. Geoff Clayton, Dr. Jason Cardelli and Dr. Regina Schulte-Ladbeck.

I would also like to thank the Amsterdam Astronomy institute for their kind hospitality during my visit in April 1989. Particularly I would like to thank Dr. Huib Henrichs and his wife Beb for her cooking, Lex Kaper and Dr. Rens Waters.

I would like to thank the following visiting astronomers to Glasgow; Dr. George Collins II, for his useful critisisms of chapter 1 and Bert van den Oord for some fruitful discussions.

I would like to acknowledge the SERC for three years postgraduate support and Glasgow Computing Services for the use of their computing facilities.

Finally my most sincere thank you's go to all the members of the Astronomy group, both past and present, who have been a great pleasure to have known. Particularly I must thank Mrs Margaret

Waterson and Mrs Margaret Morris for making such an excellent job of the diagrams within this thesis, Fraser Gordon who has (apparently) willingly put up with me for in excess of three years and Alec McKinnon who, apart from the numerous scientific discussions, together with Fraser Gordon, introduced me to the Aragon (public house) where the staff (Mary, Steve, Debbie, Jeanette and Jayne) have always made me feel most welcome.

I would like to dedicate this thesis, if I may, to my mother (Sandra Gibson), father (Kenneth Fox) and especially to my step-mother and dearest friend (Yvonne Fox).

Contents

Chapter 1.

Observations and Theory Relevant to Understanding the Underlying Structure of Be star Circumstellar Envelopes.

1.1 Introduction.

Be stars exhibit temporal spectroscopic variations on all time-scales. These variations are generally irregular and often extreme with the possibility of spectral lines alternating from emission to absorption lines over a period of years (Baldwin, 1941). Be stars have also been observed polarimetrically (Shakovskoi, 1963, 1965; Coyne and Gehrels, 1967). It has been found that these stars can exhibit high degrees of polarisation (up to 1.5% for EW Lac, Poeckert and Marlborough, 1976). The very fact that these stars are intrinsically polarised implies that the envelope, which gives rise to the polarisation, is asymmetric with respect to the observer, contrary to standard wind model calculations (Castor Abbot and Klein, 1975; henceforth CAK; see also Hearn, 1988 for a recent review) which assume spherical envelopes.

1.2 Be Star Phenomena.

Examples of anomalous emission lines from stars can be found throughout the HR diagram. Stars are only noted for their emission characteristics if, in the visible wavelengths, emission lines are observed when the classical theory of stellar atmospheres instead predicts absorption lines, implying the presence of some (hot) matter beyond the normal atmosphere.

Be stars are of particular interest because they are the most frequently observed emission stars, with observations spanning over a century from the first observations of the Be star γ Cas in 1866 by

Secchi (1867). Today over 3000 Be stars are known (Wackerling, 1970), making up about 20% of the total B star population. From such a large sample of stars and observations it should be possible to construct models representing the physical conditions within the envelope. The resulting models should also be applicable to rapidly rotating emission line stars of higher (Oe) and lower (Ae, Fe) temperatures.

1.2.1 The Definition of a Be Star.

According to Collins (1987) Be stars are defined as B stars of luminosity classes III-IV (non supergiants) whose spectra have, or have had at one time, one or more Balmer lines in emission superposed on the normal B spectra. (Luminosity classes I and II are excluded as Balmer emission lines are considered to be a normal characteristic of B supergiants). This definition is somewhat ambiguous in that it depends upon (i) the instrument being used (i.e. whether or not the instrument is sensitive enough to detect emission); (ii) how well the observer can identify possible weak emission and (iii) the epoch at which the observations are made, as most emission features are relatively short lived phenomena. On consideration of the ambiguity in the definition, the 20% value quoted for the Be/B star ratio must be considered as an underestimate.

Be stars are subdivided according to their (high resolution) spectra :

(i) Be spectrum; emission lines showing either no reversal or more or less central reversal (Underhill and Doazan, 1982, p. 280). These stars are often referred to as "Classical" Be stars. They are known to be fast rotators (Slettebak, 1976) and often exhibit Fe II in emission (Slettebak, 1982). In addition there is also a subgroup which also show

many forbidden lines in emission (eg. O I, Fe II, N II, S II and Fe III) and are designated Bep or B[e].

(ii) Be shell spectrum; Hydrogen Balmer lines exhibit sharp, very deep absorption cores (generally bordered by emission wings) and ionised metal lines (eg. Fe II, Ti II, Cr II) appear as sharp absorption lines with (or without) emission wings (see Fig. 1.1 for a comparision of line profiles).

This definition for the "shell" spectrum is relatively new. Historically the term shell was reserved for Be stars exhibiting the most pronounced absorption features (e.g. Plieone, 48 Lib) indicating that they are being observed equatorially (Slettebak, 1988).

1.2.2 Variability.

Spectroscopic observations of Be stars have shown that at any given time a star classed as Be may exhibit B or Be/shell spectra and indeed some stars (eg. γ Cas; Cowley et al., 1976: Pleione; Gulliver, 1977) have repeatedly exhibited each characteristic spectrum over a number of decades (non-periodic). It seems almost certain now that since such extreme spectral variability exists, that the spectral types (Be, Be/shell) are merely different aspects of a single phenomenon (Underhill and Doazan, 1982, p. 286) - so called phase changes - rather than representing intinsically different kinds of objects or different stages of evolution (i.e. phase change time scales are much shorter than evolutionary time-scales).

Associated with these spectral variations in any particular star are changes in magnitude, colour temperature, radial velocities of lines, the V/R (violet to red) and E/C (emission to continuum) ratios for example. How these changes are related to each other depends upon

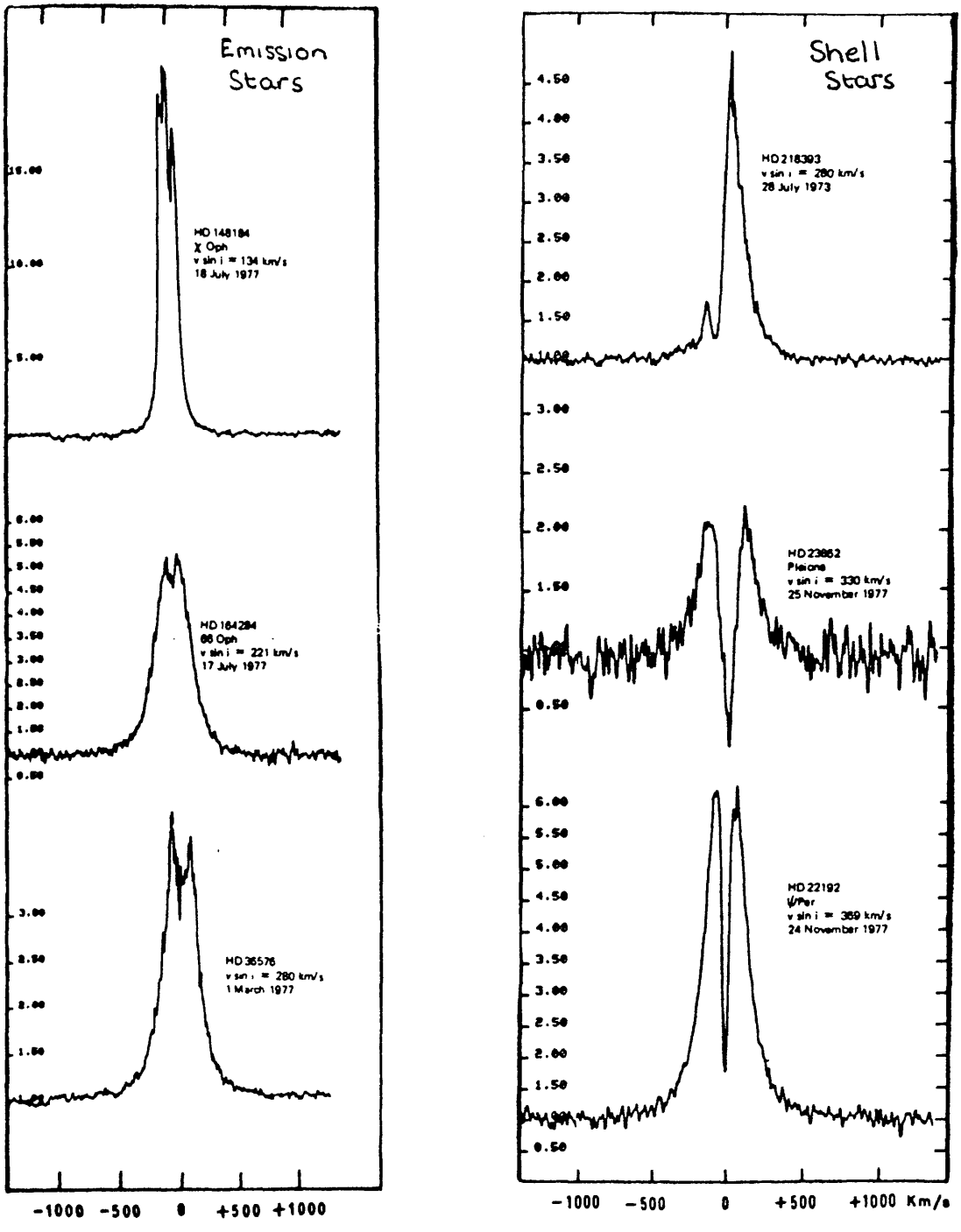

Figure 1.1

Emission and shell line profiles.

(Taken from Underhill and Doazan, p. 282)

the individual star.

The spectral phase changes (and associated changes) are particularly well illustrated in the case of γ Cas (Baldwin, 1940; Edwards, 1956; Cowley and Marlborough, 1968; Underhill and Doazan, 1982, p. 326 et seq).

From the first spectral observations of γ Cas in 1866 and until 1915, the star was seen to be in a quiescent Be phase exhibiting emission in the Balmer series up to H 8 and the He I(D_3) line. Thereafter small variations were noticed in the V/R of H_γ and only minute variations in the visual magnitude (mean 2.2) were recorded until 1932 when suddenly large variations in the V/R of the Balmer emission lines were observed, indicating that the rotating extended atmosphere was expanding (V/R $>$ 1 - expanding; V/R $<$ 1 - contracting). The emission lines became increasingly strong and the two emission peaks (observable only in high resolution spectrometry) became narrow and closer together until the appeared only as a single line. Emission reached a maximum in 1934, by which time there was emission in the Balmer series up to H 18 (with the emission widths greatest for the lowest members) and also strong emission in Fe II, He I, Mg II, Si II and Ca II. Whilst emission had increased, the photospheric absorption lines had weakened due to veiling (line infilling) from the continuum.

By 1935 a dramatic decrease in emission occurred, leaving only the lowest Balmer lines in emission and the whole process was reversed with the V/R ratio and the visual magnitude decreasing. The 'single line' appearance of the emission lines transformed into two emission peaks and the photospheric lines strengthened. Thereafter He I (388.9 nm) appeared as a sharp absorption core line which was followed by

developing deep absorption cores in the Balmer and the helium emission lines. By mid 1936 γ Cas had lost all traces of photospheric veiling and exhibited a fully developed shell spectrum. Three months later, however, this spectrum had completely disappeared and the spectral variations observed from 1933 - 1936 were then immediately repeated but with much greater intensity, such that the visual magnitude increased to a maximum of 1.7 whilst the colour temperature reddened to 8×10^3 K. (The reddening is due to an excess radiation in the Paschen continuum caused by free-free, free-bound emission from an ionised gas that is optically thin in the continuum.) At the time of maximum emission the Balmer lines were in emission up to H 32 and many ionised metals were also seen in emission.

Following this emission phase a further shell episode occurred reaching a maximum in 1940 whereby the visual magnitude had decreased to 3.3 and the colour temperature had become bluest (3×10^4K). By 1942 the shell spectrum had completely disappeared leaving a normal B spectrum star (with slight emission in H_α).

Perhaps the most important (and somewhat overlooked) feature during these spectral changes is the variation associated with the photospheric line profiles because these lines essentially affect the determination of spectral classification, the effective gravity and Vsini. Since it is assumed that the photospheric lines are not modified by the presence of the envelope, standard model atmospheres of normal B stars can be applied to Be stars.

To date, the value of Vsini (for any star) has not been calculated during all its various phases but its variation with time has been observered in some Be stars, particularly during maximum emission, (e.g. β^1 Mon; Cowley and Gugula, 1973). Such a variation, however, is

in contradiction to the method of construction of empirical models for Be stars, whereby the emission width is fixed by Vsini. Furthermore, neither the rotational speed (V) nor the inclination (i) can reasonably be expected to change rapidly as either implies the application of a huge torque to the star. The very fact that the photospheric line profiles do change would indicate that, in the absence of detailed atmospheric models, very little meaning can be attached to the Doppler half width of these lines which is interpreted as Vsini. The possible variation of Vsini (with time) would explain, to some extent, why there appears little correlation of (the mean) Vsini value with certain parameters when a strong correlation might be expected (e.g. Polarisation versus Vsini - Poeckert and Marlborough, 1977, McLean and Brown, 1978). However it must be borne in mind that accurate determination of Vsini is a difficult one (Slettebak, 1976) and during times of veiling it may not be possible to determine the value of Vsini with any certainty.

Spectral variability is also observed on shorter time scales of months to minutes, most of which is chaotic in nature and on the shorter time-scales may in fact be unreal (Clarke and Wyllie, 1977). In particular, small rapid profile variations on time scales of the order of minutes have been observed across H_β (Hutchings, 1976) and H_α (Slettebak and Snow, 1978) for several stars. The variations on these short time-scales are weak and in general irregular. They are impossible to observe without good spectral and time resolution and merely affect the structure of the line rather than the total line intensity.

The most frequently observed variations are of the order of a day. They can be non-periodic, such as those observed in the radial

velocities of some lines, which have been explained in terms of expansion and contraction in the envelope of the star - mass ejection followed by fallback - (Doazan, 1965; Doazan and Peton, 1970) and by the rotation of an object with triaxial deformations (Chandrasekhar, 1969; Bossi et al., 1982). However most variations are strictly periodic and have been attributed to various mechanisms. Baade (1982, 1984a) found regular spectroscopic variations in 28 CMa with a period of 1.37 day which he attributes to non-radial pulsations (NRP). Stagg (1987) has confirmed this period photometrically (during 1983-4). However Balona and Engelbrecht (1986, 1987) were unable to find such a periodicity photometrically during 1985-6. NRP have been suggested for the short regular variations in many Be stars eg. λ Eri (Bolton, 1982; Baade, 1984a), ε Cen and μ Cen (Baade, 1984b). It is as yet unknown what role NRP play in Be stars, they may be either an underlying cause or an effect of the Be phenomena (or they may in fact be superfluous to the Be phenomena; for a recent review of NRP see Baade, 1987).

Periodic spectral and/or photometric variations however can usually be explained in terms of spot features or rotational modulation (see discussion at the end of Baade, 1987; Balona and Englebrecht, 1986; Sareyan et al., 1987), binary motion or magnetic effects (see review article by Barker, 1987). In particular, for a small number of Be stars, which exhibit amomalously strong helium abundances, it is becoming evident that the magnetic field of the star can play an important role in determining the structure of the stellar wind. These helium strong stars have dipolar kiloGauss fields in which the observed longitudinal magnetic field varies strictly with the rotation of the star (e.g. Landstreet and Borra, 1978; Barker et al., 1982). For one

star (HD 37776) Thompson and Landstreet (1985) have found evidence for a quadrupole field. The prototype star, σ Ori E, has also been observed photo-polarimetrically by Kemp and Herman (1977) and interpreted by Clarke and McGale (1988 b) as an off-centre obliquely rotating magnetic dipole with a polar field strength of ~12 ± 1 kG.

1.3 The Modelling of Stellar Envelopes.

In order to explain the visual spectral observations of Be stars, Struve (1931) suggested that because large Vsini values (close to the theoretical critical velocity) are observed, then the escape velocity at the surface of the star would be least at the equator and greatest at the poles. This led him to the conclusion that preferential equatorial mass loss enhancement would occur.

Struve's geometrical model has since been elaborated upon by many authors (see Sec. 1.3.1 below) all of which assume equatorial enhanced mass loss.

These ad hoc geometrical models are able to explain the visual and IR spectrometry and the degree of polarisation observed from Be stars but generally fail to explain the V/R variations and high energy spectrum.

An alternative method to modelling stellar atmospheres is to consider the possible physical mechanisms that dominate the (global) structure of the wind (for a review of wind mechanisms see Holtzer, 1988).

In the particular case of hot stars CAK modelled radiatively driven winds in O stars by considering the basic hydrodynamic equations. They assume that the radiative force, resulting from a mixture of optically thick and thin absorbing lines, is proportional to the velocity

gradient raised to some power [$(dv/dr)^{\alpha}$, where α is a free parameter ($0 < \alpha < 1$)] that is fixed by observations. They also assume that the Sobolev approximation (Sobolev, 1960; i.e. probability of a photon being absorbed is proportional to the reciprocal of the velocity gradient of the wind) to be valid throughout the wind. Their theory predicts a simple velocity distribution for the wind, viz

$$v^2 = v_*^2 + (v_\infty - v_*)^2 \, (1 - R_*/r) \qquad (1.1)$$

where v, v_∞, v_* are the radial ouflow velocities at r , infinity and at the surface of the star respectively. Since $v_\infty >> v_*$ then

$$v = v_\infty \, (1 - R_*/r)^{1/2} \qquad (1.2)$$

where $v_\infty = (1/\alpha - 1)^{-1/2} \, v_{esc}$.

In the interpretations of observations, the velocity distribution (eq. 1.2) is usuallly parameterised by setting the power of the distance function equal to β. Therefore in the CAK theory $\beta = 0.5$ in agreement with observations. Using a large number of UV line data (250,000 lines) they predict that $\alpha \sim 0.7$ and thus $v_\infty/v_{esc} \sim 1.5$. Observations, however, (e.g. Abbot, 1982) indicate a value between 2 and 4.

Pauldrach et al. (1986) and Poe and Friend (1986) found that the inclusion of a finite size star correction into the basic CAK theory agrees well with observations . By incorporating magnetic fields and rotation (Friend and McGregor, 1984; McGregor and Friend, 1987) it has also been possible to account for the observed dispersion in the estimates of mass loss and v_∞ for O stars.

Further investigations of the effects of rotation and magnetic fields has shown that a two component wind may in fact exist (Poe et al., 1988; Maheswaren and Cassinelli, 1988) with an enhancement of mass loss (and lower terminal velocity) from the equatorial region compared to the polar regions.

There are, however, several problems that arise when applying these standard models to Be stars. A primary objection is that the models assume that mass loss is spherically symmetric whereas polarimetric and IR observations show unequivocally that Be winds are highly non-spherical (Dachs et al, 1986; Waters, 1986; McLean and Brown, 1978). A second objection arises in the validity of applying radiative driven winds to Be stars because such a mechanism is not self-initiating for Be stars which would indicate that there are other mechanisms at work (Hearn, 1988; Holtzer, 1988).

We shall now discuss in more detail Struve's rotational model (because of its historical importance and simplicity) and two current competing geometric models of Be envelopes, namely the Marlborough et al. (1978) rotationally enhanced mass loss model and the Doazan and Thomas (1982) spheroidal/ellipsoidal mass loss model.

1.3.1 The Rotational Model.

Struve, Shajn and Elvey had by 1930 (Shajn and Struve, 1929; Elvey, 1930; Struve, 1930) established that the broadening of spectral lines in many hot stars are due to Doppler broadening produced by rotation of the star and its envelope. By considering these observations and conclusions Struve suggested (Struve, 1931) that rapidly rotating stars will be oblate spheroids (or in his words "lens shaped bodies") which eject matter preferentially at the equator (his original idea being that this was a one-time ejection) forming an equatorial ring, or disc, that is responsible for the observed emission lines. Variation in the observed inclination of such systems would then give rise to the range of widths in the emission lines (Fig. 1.2) observed in these emission stars.

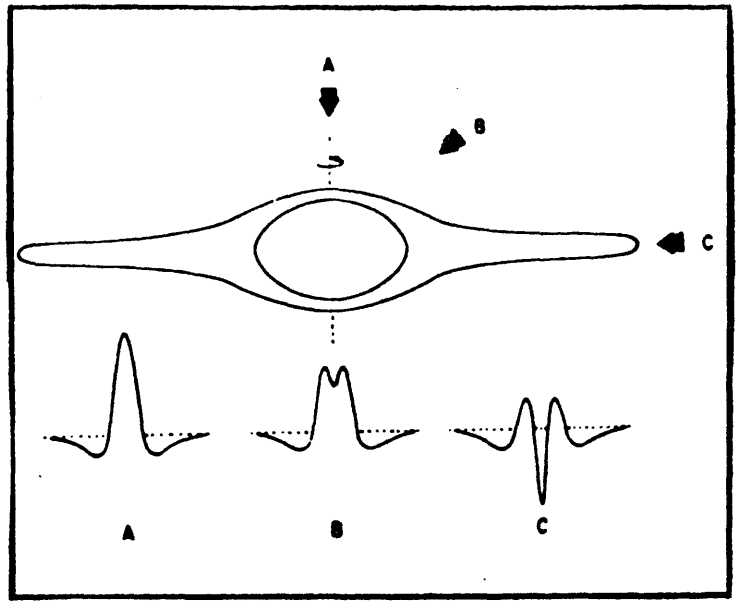

Figure 1.2

Sketch of Struve's Rotational model. The different types of profiles, A, B and C, are interpreted in terms of the line of sight on the rotation axis.

The shell absorption line spectra are explained within the framework of this model by the fact that these (shell) stars (eg. Pleione) show the largest line broadening (largest Vsini) and therefore presumably viewed equatorially. Such shell lines exhibit narrow absorption cores, indicating that the envelope disc is optically thick across that line. Struve's model has since been elaborated upon by Limber and Huang.

Limber (1964, 1967, 1969) considered mass loss through rotationally forced ejection of matter consequent to structural changes in the body of the star (eg. stellar contraction). From such modelling Limber was able to reproduce the radial velocity variations of the Balmer H 5, H 15 and H 25 shell lines in addition to the variation of the line intensities with time for Pleione's shell episode (1938 - 1954). Apparao et al. (1987) have suggested that such forced ejections are due to the transport of angular momentum from the core of the star to the surface layers which are confined by the magnetic field of the star. They suggest that the star differentially rotates, which twists the magnetic field and the resulting force enables the angular momentum to be transported to the surface. In doing so, the outer layers of the star expand due to the additional centrifugal force. Eventually the surface layers become unstable and results in episodic mass loss from the star. They estimate the frequency of such events to be of the order of decades in agreement with the observed Be phase change time-scale.

Huang (1972, 1973, 1977) considered variable (and continuous) mass ejections from the equatorial regions of the star which result in a rotating elliptical ring of material that is quasi-stable. This gave a natural explanation to the quasi-periodic phase changes of Be stars as

well as the periodic variations observed in the V/R ratio.

1.3.2 Rotational Model of Marlborough, Snow and Slettebak (1978)

Their model is the latest generation of Struve's original rotational model and is based on a previous geometric model by Poeckert and Marlborough (1978a) which was constructed in order to explain the variation of polarisation across the H_α and H_β lines for γ Cas. Marlborough et al. (1978; henceforth MSS) extended the model to explain the high energy spectra (UV lines and xrays) from γ Cas. Although their model is specifically intended to explain the observations related to γ Cas, their model should, at least in general terms, be able to reproduce the main features of the Be star phenomena (values quoted are those used by MSS for γ Cas).

MSS envisage a cool ($T \sim 10^4$ K) equatorially enhanced envelope, with a high density ($n_H \sim 10^8 - 10^{13}$ cm^{-3}) and low outflow velocity ($V_r < 20$ kms^{-1}) extending to a radius of 3 - 15 R_* in the equatorial plane (Fig. 1.3). The envelope increases in geometrical thickness with increasing radius to a height of $\sim \pm 5$ R_*. This region is responsible for the shell lines and Balmer emission, for the IR excess and (due to the asymmetry of the envelope) the intrinsic polarisation.

The inner part of this envelope rotates rapidly and differentially which causes turbulence that is supersonic along the disc edge (where the density falls rapidly) and shocks form. (It is assumed by MSS that Be star discs can be considered as analogous to accretion discs.) The shocks result in the nonthermal heating of the outer edge of the disc (called the transition zone).

Out of the disc a corona exists (Icke, 1976) with a high temperature ($T_C \sim 10^6$ K), high outflow velocities ($V_r \leqslant 1000$ kms^{-1}) and a low

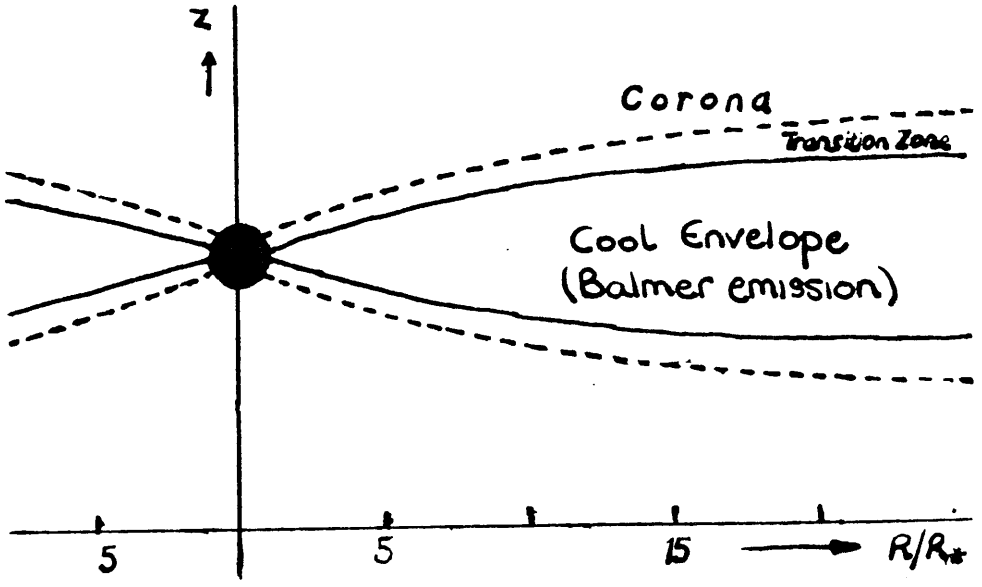

Figure 1.3

Sketch of MSS disc model. (See text.)

density ($n_H \sim 10\ cm^{-3}$). Within the corona highly ionised species (N^{5+}, O^{6+}) are produced by collisional ionisation giving rise to the observed UV line spectra (Marlborough, 1977a).

In their model, MSS speculate that the x-ray emission is produced via mass accretion on to a neutron star and it is through this mass flow that the variable V/R ratio is explained. In the context of a generalised model, however, we must account for the x-ray emission observed from Be stars (Peters, 1982) in another way. Marlborough (1977b) showed that the x-ray flux produced in an optically thin Maxwellian plasma surrounding the star (a corona) composed of completely ionised hydrogen would require a temperature of $T \sim 10^7$ K and a density $n_e < 10^{11} cm^{-3}$ (again the calculations are for γ Cas). To date, however, it is unknown where the x-ray emission is produced within the envelope (Vaiana and Sciortino, 1988). Current theories concerning x-ray emission include a coronal origin (Hearn, 1975; Waldron, 1984) and shock structures via density perturbations throughout the wind (Lucy, 1982).

The V/R ratio has been observed for some Be stars over a long period of time and has been found to be quasi-periodic. (The same phenomenon has also been observed in other emission stars, notably T Tau stars [e.g. DR Tau, Krautter and Bastien, 1980] and so there may possibly exist a single physical mechanism for the V/R variation.) The V/R ratio indicates that the envelope expands (V/R > 1) and contracts (V/R < 1) with time. In the present MSS model the stellar envelope is in dynamic equilibrium and so no time dependent phenomena occur .

Their ad hoc model is able to explain all the main observed features of Be stars (including the observing angle dependency, Poeckert and Marlborough, 1976, 1978b). Their model implicitly assumes, via the

geometry adopted for the envelope, that all Be stars are rapidly rotating, as inferred from observational data (Slettebak, 1976; Warren, 1976). Since the model is static it cannot explain any of the time dependent phenomena associated with Be star such as V/R changes or the so-called phase changes i.e Be - Be/shell - B (and not necessarily in that order). On a more basic level, as the authors admit, their model is primarily geometrical in construction and has not been tested for physical self-consistency.

Recent spectral observations (Dachs et al., 1986; Waters, 1986) support this cool H_α emitting disc envelope scenerio of MSS and interferometric observations of γ Cas (Granes et al., 1987) indicate that the H_α envelope extends to ~7 R_* consistent with the MSS model.

1.3.3 Spheroidal/Ellipsoidal Model of Doazan and Thomas (1982).

Doazan and Thomas (1982; henceforth DT) initally assume a spherically symmetric solar-like extended stellar atmosphere. By using the conservation laws of mass, momentum and energy together with spectral observations they construct an empirical model which they claim is thermodynamically and hydrodynamically self-consistent (for the mathematical details see Doazan and Thomas, 1982, Ch.13 and for a complete review of the model see Doazan, 1987). In actuality they write down the conservation laws in their most general form and then define regions in which certain physical mechanisms dominate (eg. radiative/thermal equilibrium). They then estimate (order of magnitude), using the detailed numerical results of Mihalas (1972), how the density varies (i.e. r^{-2}, by the conservation of mass) throughout the atmosphere and give typical values for the density, temperature and outflow velocity in each region. They do not solve the equations

governing the physics of the atmosphere.

In their analysis, they break down the atmosphere into several physically different regions (Fig. 1.4) of which the exact size and observed phenomena in any region at any epoch will depend not only upon each other region but also upon previous epochs.

The model atmosphere consists of a photosphere, which is in both radiative and thermal equilibrium (T_{ph} ~ 30,000 K , outflow velocity ~ $1ms^{-1}$ and n_H ~ $10^{14}cm^{-3}$). They suggest that within this photosphere the characteristic shell spectra is produced by enhanced mass outflow (Doazan et al., 1986). However, no radiative transfer modelling is carried out to prove this and furthermore spectral observations show that the shell spectra cannot be produced in this region by the line widths (Collins, 1989; Private communication).

The photosphere is followed by a chromosphere where thermal equilibrium holds but radiative equilibrium does not. Energy is conserved by the dissipation of mechanical energy (eg. acoustic noise) which heats up the chromosphere to a temperature of T_{chr} ~ 80,000 K. (In the sun the chromosphere is believed to be heated by acoustic noise that has its origin in the convective zone [Durrant, 1988]. In stellar evolution modelling it has become apparent that such a convective zone also exists in B stars [Hofmeister et al., 1964].) Throughout the chromosphere (which extends to ~1.01 R_*) the density (varying as r^{-2}) decreases (n_H ~ 10^{11} cm^{-3} and the radial outflow velocity increses to V_r ~ 10 kms^{-1}.

Beyond the chromosphere lies the lower corona (T_C ~ $5x10^6$ K, outflow velocity V_r > $100kms^{-1}$ and n_H ~ 10^8cm^{-1}) where non radiative and non-hydrodynamic equilibrium exists and the outflow is transsonic. Within this region superionised species exist and nonthermal x-ray

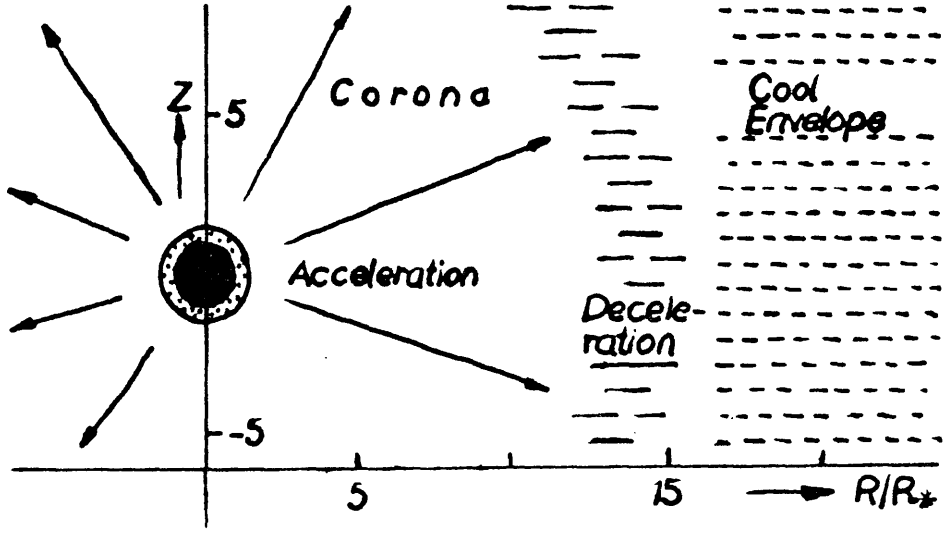

Figure 1.4

Sketch of DT spheroidal model. (See text.)

emission occurs. The lower corona ends where the ouflow velocity becomes supersonic (called the upper corona) and is terminated when non-radiative energy dissipation becomes insignificant.

From the photosphere to the upper corona, the flow is accelerated. Beyond the corona the flow cools (no radiative heating) but it can still be accelerated by the radiation field arising from the chromosphere-coronal region. Thereafter shocks form and the density increases to $n_H \sim 10^{10}cm^{-3}$ and the flow decelerates. Beyond this region lies a cool, low velocity envelope where H_α emission and the colour excess originate. The location of this envelope is such that the outflow velocity is close to the escape speed ($V_r \sim 100kms^{-1}$). The amount of momentum that is transferred from the shock forming region to the H_α emitting envelope will be variable (because mass loss from the star is variable) and thus at some epochs the transferred momentum will be sufficient to drive the material up to escape speed and thus mass loss will occur ($V_r > V_{esc}$). At other epochs, however, there will be insufficient momentum to drive the material up to escape speed (i.e insufficient momentum to overcome gravity) and so the envelope will act as a 'storage balloon' that will expand ($V/R > 1$) and contract ($V/R < 1$) with time (Doazan et al., 1985). DT invoke such a mechanism in order to explain the observational fact that the inferred mass loss rates in the UV and H_α are not the same. However, since the mass loss rates for the UV and H_α depend on a knowledge of the exact ionisation balance and composition of the wind, one cannot expect agreement (see Snow, 1982 for a discussion of the problems concerning the interpretations of mass loss).

DT suggest that the shell lines are formed in the photosphere of the star. However, observations show (cf. Sec. 1.2) that the shell

episodes are characterised by a developing narrow absorpion line (centrally) superposed upon the emission line and would therefore indicate that the shell lines are produced in a region close to the H_α emitting region, which in the DT model is likely to be the shock forming region because it is here that it is possible for a velocity plateau to exist (Mullan, 1984) and thus the velocity gradient across this region becomes small. For such a region the opacity of a line increases (Sobolev, 1960; the opacity of a line is inversely proportional to the velocity gradient) and therefore the neutral hydrogen in this region will appear as deep narrow absorption lines, giving rise to the observed shell spectra. If, once the shell spectra appear, increased mass loss occurs from the star, the shocks within the shock forming region will become stronger and result in the heating of the neutral hydrogen gas to higher excited states which will result in emission. Therefore, once emission begins, the Balmer lines will steadily change from a shell line to an emission line. Observations in the UV and visible spectral regions for 59 Cyg (Snow and Marlborough, 1980; Doazan et al., 1980a, b; Barker, 1979) indicate that during the shell phase of 59 Cyg (~ 1974) the expansion velocity of the shell lines were greatest (~ 50 kms^{-1}) when the UV absorption lines of highly ionised species were least (~ 180 kms^{-1} for N V) and weakest. The onset of Balmer emission was characterised by an increased displacement and strength of the UV absorption lines (Doazan et al., 1985) which infers an enhanced mass loss from the star. The increased mass flux then produces a stronger shock when it reaches the cool envelope boundary which heats the gas and results in Balmer emission. In addition, UV observations also indicate that the expansion velocity is variable and thus one can expect that the velocity plateau in the

shock forming region may not be established and so the opacity of the line decreases (i.e. a velocity gradient exits in the shock forming region).

The model of DT does not require a fast rotating star, but in order that some asymmetry is present the star must indeed rotate. The effect of rotation will be to cause an asymmetry in the photospheric mass outflow with the total velocity at the equator being greater than that at the poles and so shock interactions will also be stronger at the equator and this region, together with the cool envelope, will be ellipsoidal in shape which they claim will give rise to the observed net degree of polarisation.

On the basis of spectral observations alone it is not possible to distinguish between the MSS and the DT models because they use these observations as a basis for their models and thus observations other than spectral observations must be used. Polarimetry is particularly useful in this case as it enables (from polarimetric theory and observations) important inferences to be drawn regarding the geometry and mass of the scattering envelope. In particular, given a specific geometrical shaped envelope (eg. an equatorial disc or an ellipsoid) then by comparing the theoretical variation of polarisation with certain stellar parameters to observations (McLean and Brown, 1978) it is possible to infer the typical mass and oblateness of the envelope required which may then be tested against model predictions (see Section 5.4 for a comparision of the MSS model to DT model predictions).

1.4 Polarised Radiation.

In order to calculate the theoretical intrinsic polarisation from a circumstellar envelope one has to solve the equations of radiative transfer through the envelope (Chandrasekhar, 1950). The solutions are found numerically (Hummer et al, 1973; Poeckert and Marlborough, 1977; Kalkofen, 1987). This particular method of solution is model dependent and requires extensive computing time. The results, however, simplify in the case of optically thick and thin limits. In the optically thin limit (which we shall concern ourselves with), when the optical depth is so small that single scattering is an adequate approximation, the equations of radiative transfer are minimised as it is then not necessary to consider the scattering of polarised radiation (provided that the light source is unpolarised) and absorption may also be neglected.

Brown and McLean (1977) first generalised the theory of optically thin scattering (with a point light source). They found that for Thompson scattering in an axisymmetric envelope the net polarisation depends on the inclination of the system and the envelope geometry in a very simple way, viz

$$P = \tau(1 - 3\gamma)\sin^2 i \qquad (1.3)$$

where i is the inclination (defined as the angle between the observer and the rotation axis of the star), τ is a measure of the optical depth (averaged over the entire envelope) and γ is a shape factor that depends on the envelope geometry. Other authors (e.g Dolginov and Silant'ev, 1974; Shakovskoi, 1965, Poeckert and Marlborough, 1977) had previously obtained similar results for specific geometries but had then not generalised their results.

Brown et al. (1978; henceforth BME) generalised the theory to

general envelope distributions and multiple (point) light sources. They found that for a rotating system the normalised Stokes parameters could be written as a Fourier (time) series (up to the second harmonics) which has enabled important conclusions to be drawn from the polarimetric data (see Sec. 1.4.2).

The analysis of Brown amd McLean (1977) neglects absorption in the envelope and therefore, their results are only applic.able to broad band photometry. Haisch and Cassinelli (1976) investigated the theoretical wavelength dependence of the polarisation across the continuum for a distorted, extended electron scattering envelope that produces the observed polarisation. The polarisation is modified by an absorptive opacity due to bound-free and free-free absorption, which reduces the degree of polarisation by the absorption of polarised light and subsequent thermal emission of unpolarised light. They numerically calculated the radiative transfer of polarised flux through model atmospheres and found that for disc models a maximum polarisation of ~ 1.2% is predicted shortward of 500 nm which is significantly less than is sometimes observed. McLean (1979) considered the wavelength dependence of polarisation for both the continuum and across spectral lines using the analysis of Brown and McLean (1977). In this way he was able to determine the wavelength dependence for any axisymmetric envelope by including optically thin absorption and envelope emission. His results agreed with those of Haisch and Cassinelli (1976) and also with observations. By investigating the change in polarisation across emission lines he found that the polarisation decreases from the wings to the line centre where a possible increase may occur. Furthermore, he predicted that the change in position angle could be ~ 5°, agreeing with the observations of Poeckert and Marlborough (1977) for the H_α

emission line in γ Cas.

In general it is impossible to separate the inclination dependence from the polarimetric observations. Cassinelli et al. (1987), however, have suggested a novel way of analysing the polarimetric behaviour with wavelength, independent of the inclination and geometrical factors by analysing the 'Colour' polarisation, viz

$$C(\lambda_1, \lambda_2) = \{P(\lambda_1) - P(\lambda_2)\}/P(\lambda_1) \qquad (1.4)$$

which depends on the wavelenth and the electron density structure. This has the rather interesting result that in the continuum if scattering within the envelope is due entirely to Thomson scattering then $C(\lambda_1,\lambda_2) = 0$ whilst for Rayleigh scattering $C(\lambda_1,\lambda_2) = 1 - (\lambda_1/\lambda_2)^4$.

Simmons (1982, 1983) generalised the work of Brown and McLean (1977) and Brown et al. (1978) to arbitrary scattering mechanisms (provided that the density and scattering matrix are smoothly varying functions). He found that under certain conditions the Stokes parameters (to a first approximation) are equivalent to the results of Brown and McLean (1977) with Rayleigh scattering.

Complex numerical studies, involving multiple scattering and absorption (Daniel, 1980; Dolan, 1984; Poeckert and Marlborough, 1976; Haisch and Cassinelli, 1976) have verified that the single scattering ($\tau < 1$, no absorption) approximation correctly predicts the polarimetric dependence on certain parameters (eg. time, wavelength, envelope shape) only the predicted absolute polarisation is overestimated (in the optically thin approximation).

One inadequacy of the single scattering, optically thin treatment (Brown and Mclean, 1977; BME), however, is the assumption of a point light source. Cassinelli et al. (1987), using radiative transfer techniques, found that for a finite spherical isotropic light source the

polarisation from each electron is reduced compared to that for a point light source because with the inclusion of a finite light source there now exists a range of possible scattering angles through which a ray leaving the surface of the star may be directed towards the observer and thus net polarisation (summing over all possible rays) will be reduced. This depolarisation factor depends solely on the radial distance from the star, varying from 0 at the surface of the star (totally unpolarised light) to 1 at infinity where the scatterer sees a point light source.

BME obtained general expressions for the polarisation expected from an envelope illuminated by any number of point light sources. In principle, at least, it is therefore possible to calculate the polarisation from an envelope with an extended light source from their results by suming over all points on the light source. Carlaw (1988), however, reformulated their work to explicitly include any arbitrarily shaped light source. She was able, from these general results, to obtain explicitly not only the depolarisation factor for the second Stokes parameter but also an intensity modification factor for the direct scattered light (I_1), equivalent to the depolarisation factor, for a spherical and a disc light source assuming that the polarisation was due to Thomson or Rayleigh scattering (see Brown et al., 1989, for a discussion of depolarisation factors for non Rayleigh scattering mechanisms).

1.4.1 Statistical Studies.

McLean and Brown (1978) investigated the statistics of intrinsic circumstellar polarisation with apparent rotation speeds (Vsini) for 67 Be stars. Their analysis of the rotational speeds agree with previous

investigations (Chandrasekhar and Műnch, 1950; Slettlebak, 1976) - see below. By subdividing their polarimetric data into two spectral regions (O6 - B4 and B5 - A0) McLean and Brown (1978) found that the polarisation histograms are only slightly different from each other, but they note that in the spectral group B5 - A0 no star with a polarisation greater than 1.2% exists. The Vsini histograms for the two groups showed no significant differences, however, (Slettebak, 1976) and both histograms exibited a maximum Vsini at 300 kms^{-1}. Assuming that the rotation velocity in someway determines the geometry of the stellar envelope (MSS, DT), then since there appears to be no significant differences between the distribution of Vsini for the early (O6 - B4) and the later stars (B5 - A0), the lower observed polarisation for the later stars has been explained as a consequence of the fact that the later stellar envelopes are cooler and consequently will have a lower free elctron density and increased absorption (McLean and Brown, 1978).

McLean and Brown (1978) plot the intrinsic polarisation against Vsini for their program stars (their Fig. 2, see Fig. 1.5). With reference to this figure, one can see that stars with low Vsini values consistently exhibit a low degree of polarisation whereas for high Vsini the intrinsic polarisation is on the whole higher than compared to stars of low Vsini, but show a greater scatter. For any given Vsini there appears to be a maximum intrinsic polarisation given approximately by

$$P_{max} \sim 0.006 \text{ Vsini} \quad (\%) \qquad (1.5)$$

(with Vsini measured in kms^{-1}) which would indicate that the maximum observed polarisation would be $P_{max} \sim 2.5\%$ (for Vsini $\sim$ 400 kms^{-1}).

Another interesting feature of Fig. 1.5 is that there appears to be

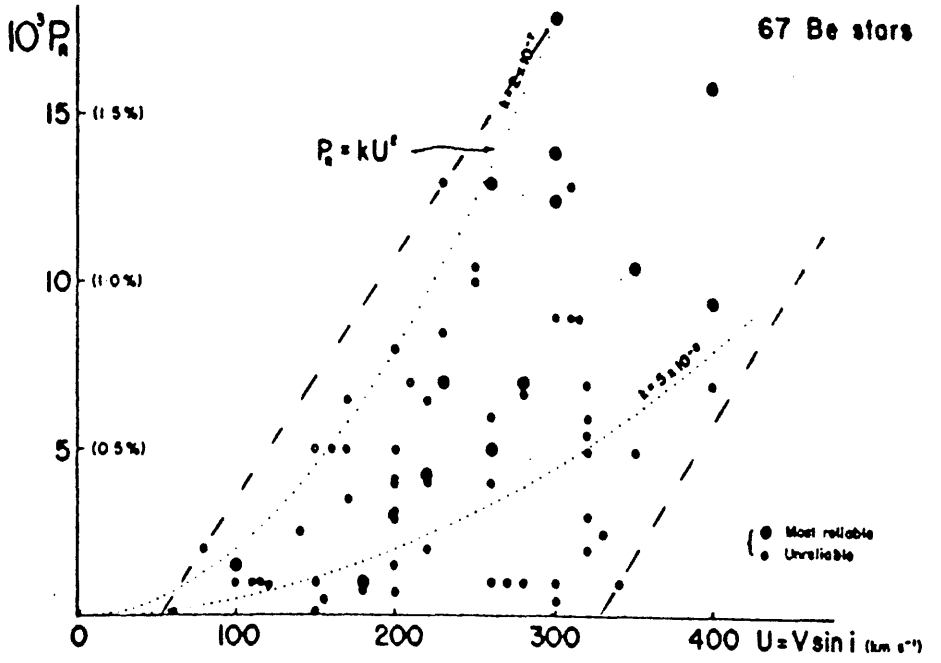

Plot of values of P_R versus $U = V \sin i$ for the stars of Table 1. Solid dots are for the "best" stars (with the largest filled circles indicating data of the highest quality) and open circles for the less reliable data as discussed in the text. The two superposed lines are from the theoretical Equation (10) with the displayed values of k corresponding to P_R as a decimal fraction (not %) and $U = V \sin i$ in $\mathrm{km\,s^{-1}}$

Figure 1.5

Plot of polarisation versus Vsini for 67 Be stars. (From McLean and Brown, 1979: Fig. 2.) The upper and lower cut-off lines are indicated by the broken (- - -) lines.

a lower limit cut-off for stars with Vsini > 320 kms^{-1}. The gradient of this line is the same as that for P_{max}, thus

$$P_{low} \sim 0.006 \text{ (Vsini - 320) (\%)} \quad \text{(Vsini > 320 } kms^{-1}\text{)} \qquad (1.6)$$

This lower exclusion zone may just be an artifact of the limited sample of data available. If real, however, it may in someway be related to the Be phenonena.

One test for any model stellar atmosphere is thus to explain Fig. 1.5 . We reconsider therefore the models of MSS and of DT in the light of these data.

The Doazan and Thomas model explains the statistical polarimetric data of McLean and Brown (1978) by considering a complete (but otherwise unspecified) distribution of rotational velocities for Be stars that will give rise to a certain degree of envelope asymmetry (depending on the rotational velocity and also the inclination). Stars with low values of V_{rot} will exhibit little polarisation even at high inclinations because the envelope will be approximately spherical. Stars with high V_{rot}, on the other hand, will have highly distorted envelopes and will exhibit a large variation in the degree of polarisation depending on the inclination and the density. The result would qualitatively be a Polarisation against Vsini plot as observed (fig. 1.5).

The disc model of Marlborough et al. explains the statistical polarimetric data somewhat differently. It assumes that all Be stars rotate close to the critical rotational velocity ($V_{rot} \sim 400$ kms^{-1}). Now such a high degree of asymmetry means that at high inclination these stars will exhibit a high degree of polarisation and there will exist a scatter in the polarisation due to differences in the envelope densities. At low inclination (low Vsini) the degree of polarisation will also be low

($P \propto \sin^2 i$). The variation in the degree of polarisation for a given Vsini can be explained in the degree of flattening and density of the envelope. One would therefore expect that for high Vsini (ie. viewed equatorially) there shall be no stars exhibiting low degrees of polarisation - as observed. Essentially the only difference between the two explanations is that in the DT model the geometry of the envelope is allowed to vary (from spherical to planar) whereas in MSS the geometry is fixed as near planar.

Coté and Waters (1987) presented a plot of intrinsic polarisation (%, λ = 425 nm) against 12μ colour excess (their Fig. 4, see Fig. 1.6) for 46 of the Be stars considered by McLean and Brown (1978). They find that for any given 12μ excess there is a large scatter in the intrinsic polarisation and a well defined upper limit exists for the intrinsic polarisation given by

$$P_{max} \sim 0.83\ CE(V, [12])\ (\%) \qquad (1.7)$$

Both the intrinsic polarisation and colour excess depend on the inclination of the system, the geometry and density of the envelope. The P_{max} cut-off line represents the optically thin scattering limit ($\tau \sim 1$). For optically thick envelopes ($\tau > 1$) multiple scattering and absorption become important and the net polarisation is reduced.

The colour excess is defined as

$$CE(V, [12]) = CE(V, [12])_{obs} - CE(V, [12])_* \qquad (1.8)$$

$$= (m_{\lambda=0.425\mu} - m_{12\mu})_{obs} - (m_{\lambda=0.425\mu} - m_{12\mu})_*$$

where $CE(V, [12])_{obs}$ is the observed colour excess and $CE(V, [12])_*$ is the photospheric colour excess estimated from the observations of "normal" OBA stars. Waters et al. (1987) found that

$$CE(V, [12]) = (4.22 \pm 0.1)(B-V)_o + (0.22 \pm 0.04), \quad (B - V)_o < -0.09$$

$$CE(V, [12]) = (2.35 \pm 0.09)(B-V)_o + (0.07 \pm 0.01), \quad (B - V)_o > -0.09.$$

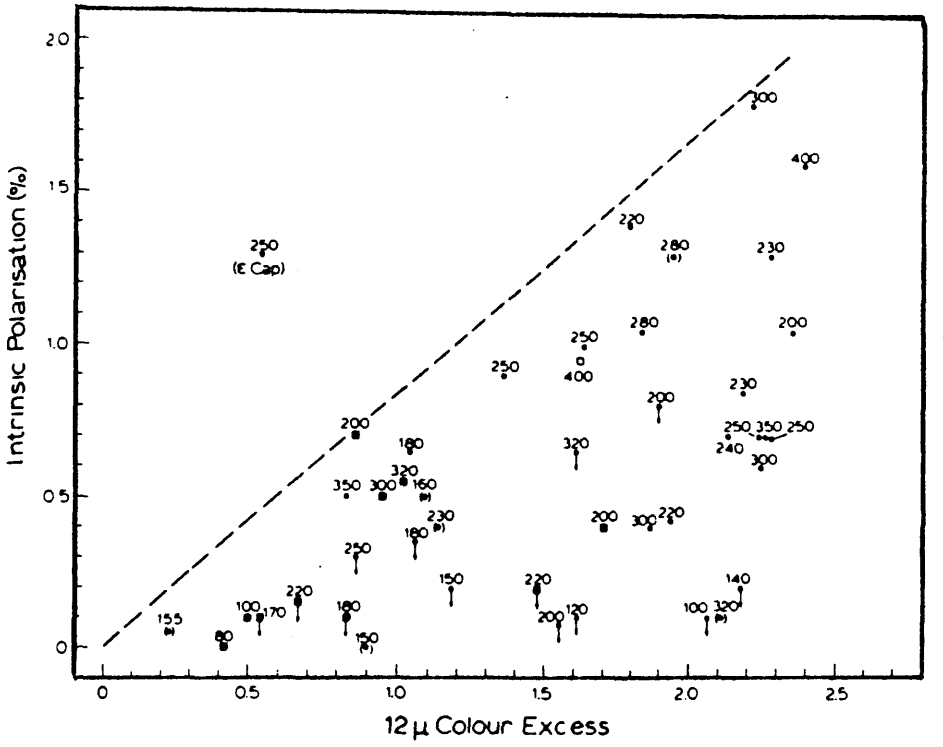

(V-[12]) colour excess CE(V,[12]) versus intrinsic linear polarisation at λ = 4250 Å (taken from Mclean and Brown, 1978). Dots indicate B0 to B4 stars, squares B5 to B9.5 stars. A point between brackets indicates an uncertain polarisation measurement. The numbers give the values of vsini for each star. Notice the triangle-like shape of the distribution, with a well-defined upper limit to the intrinsic polarisation. The upper limit is approximated by the dashed line (Eq. (10)).

Figure 1.6

Plot of polarisation versus colour excess CE(V,[12]). (From Coté and Waters, 1987: Fig. 6).

In obtaining these results they exclude all supergiants, peculiar and emission line stars and all stars with [12] - [25] > 0.25 mag. Their definition of a "normal" star is, therefore, one that radiates (at least approximately) a single temperature blackbody spectrum. In the visual wavelength region, Be star spectra are affected by the presence of ionised circumstellar material emitting free - bound radiation (Schild, 1978; Slettebak, 1985). They estimate that for early type stars (B0 - B3) the IR excess may be underestimated by up to 0.45 mag . For late type stars however it is negligible (Schild, 1978). Also at 12μ there is a hydrogen transition line in the Humphrey series (n = 6 $\leftrightarrow$ 7) that, if present, will affect the magnitude estimate at 12μ.

Collins (1987) has challenged the whole meaning of such plots (both McLean and Brown as well as Coté and Waters) because for rapidly rotating emission line stars (i.e Be stars) the definition of Vsini and $(B - V)_o$ are somewhat ambiguous. In particular Vsini is strictly the Doppler half width of a broadened sharp line and is measured as a velocity only because Struve's rotational model predicts that the half width is proportional to Vsini. For rapidly rotating emission stars (rotation speeds greater than 80% critical velocity) the surface distribution of temperature, luminosity, gravity etc. vary with the colatitude of the star due to rotation (either differential or rigid body) which will affect the Dopper widths of lines (Collins, 1987) and hence the Doppler width will no longer be proportional to Vsini. In the case of Be stars, which are believed to be rotating in excess of 50% critical velocity, there will be some Be stars in which the Doppler widths will be affected by the rotation of the star. The statisical analysis of McLean and Brown (1978) will, therefore, need to be re-examined in the light of a possible different dependence of the half

width with inclination (i.e not $\propto$ sini).

Collins (1987) has also demonstrated that the observed $(B-V)_o$ depends on the inclination of the star for rapidly rotating stars and so there exists no intrinsic value of $(B-V)_o$ for the star. Since $(B-V)_o$ may not be physically interpreted in the same way as for slowly rotating stars, then the corrections (equation 1.7) that Coté and Waters make to the colour excesses are dubious.

1.4.2 Binary Systems.

Out to a distance of 20pc approximately 50% of all stars are known to be components of binary or multiple systems (Voigt, 1974). It is therefore of great importance to be able to determine the orbital parameters of such systems in order to understand the physical nature of the system.

The most simple (easiest) method by which the orbital elements of binary systems are established is to observe the motion of the stars visually. Unfortunately only about 700 such visual systems are known (Finsen and Worley, 1970) because the components must be widely separated and hence must be long period binaries and/or close to the observer. Long term observations of such visual systems allow accurate and unique determination of all the orbital elements (except for the sign of the inclination of the orbit, i.e. cannot distinguish between retrograde and prograde motion).

In general, however, the components are too close to be resolved visually and so the orbital elements are determined spectroscopically by measuring the radial velocity of the stars which, with sufficient observations, allows the orbit of one or both components about the centre of mass to be determined. By analysing the variation of radial

velocity with time it is only possible to determine four of the orbital elements namely, the period, the eccentricity (e), the time of periastron passage and the periastron longitude (ω). The inclination of the orbit together with the semi-major axes of the orbits (and hence the masses of the stars) are left unknown (Heintz, 1978; p. 85 et seq.).

In order to establish reliable orbital element values, the radial velocity variation must be greater than the error in the measurements and so typically the orbital period of a spectroscopic binary is between 1 and 100 days (note that detection also relies on the binary being viewed at relatively high inclinations).

Many spectroscopic variable stars are single-lined (Heintz, 1978; p. 78 et seq.) which may indicate that the magnitude difference between the components is greater than ~1 mag. such that the secondary lines are swamped by the primary and consequently double-lined spectroscopic binaries have components of approximately the same mass. Historically, the single-line variability of radial pulsators (eg. δ Cep, RR Lyr) were interpreted as binary systems, giving certain characteristic ω and e values (so-called Barr effect; Barr, 1908). It is now know that such an interpretation is wrong because $R_{orbital} < R_{*}$.

For a minority of systems the light curve varies with time, indicating the eclipsing of one (or both) of the components and hence $i \sim 90^{\circ}$. For double-lined spectroscopic binaries this enables both the masses and radii of the binary components to be reliably estimated. (The study of photometric binary analysis is a lengthy and complex one and cannot be discussed here. The interested reader is referred to the treatise by Kopal, 1959.)

Shakhovskoi (1965) carried out polarimetric observations of the known eclipsing binary systems β Lyr and RY Per and found that the

normalised Stokes parameters exhibited phase-locked variations. Similar variations were later observed in AO Cas and u Her by Rudy and Kemp (1976, 1977). By considering the theoretical polarimetric variations arising from a general binary system in which extra-stellar clouds display mirror symmetry throughout the orbital period (i.e corotating envelope) BME were able to show, assuming point light sources and optically thin circumstellar material, that the polarimetric variations from such a binary system are strictly periodic and may be expressed as a terminating (second order) Fourier (time) series. By taking the ratios of the first and/or second order harmonic coefficients they (BME) were able to show that it is possible to directly obtain the inclination of the system. Rudy and Kemp (1978) came to the same conclusion even when the assumptions of BME were relaxed by including finite size light sources with limb darkening laws.

The analysis of BME (and Rudy and Kemp, 1978) has since been elaborated upon to include eccentric orbits (Brown et al., 1982) which allows the determination of the orbital elements. These canonical models have been successfully applied to data in order to determine the inclination of many binary systems (e.g. St.-Louis et al., 1988; Dolan and Tapia, 1984; Huovelin et al., 1987).

Despite the successful use of the canonical models, it has been found that for some binary systems the canonical polarimetric variations disagree with observations. In particular the synchronous polarimetric variations of Cyg X-1 with its 5.6^{d} rotational period (Kemp et al., 1978) have been analysed by many authors using the canonical models (BME, Kemp et al., 1978, 1979; Dolan and Tapia, 1989) and they all reach the same conclusion that the polarimetric variations are not consistent with the canonical models. The inconsistency between theory

and observation has been attributed to the occultation of part of the circumstellar envelope by the stars as they rotate (Milgrom, 1978) which is not accounted for by the canonical models. Such occultation effects can lead to temporal enhancemets/reductions in the polarisation compared to the predicted values, the exact change depending upon the distribution of material. The overall effect of including occultation (which the canonical models neglect) is that the canonical results no longer hold and so the orbital parameters are not correctly inferred from the data.

By considering a binary system with a primary and secondary of luminosity L_1, L_2 and a radius of R_1, R_2 respectively, in circular orbits, the effects of occultation can be analysed qualitatively by assuming that the observer lies in the plane of the orbit (i = 90) and that the circumstellar envelope corotates with the stars. It is apparent (Fig. 1.7) that there are two sets of regions that are of interest (by virtue that the stars are of finite size) which are neglected by the canonical models. The first consequence of including finite size stars is that there will be regions A_1 and A_2 which receive a reduced flux compared to considering point light sources. That is, region A_1 receives a reduced flux from the primary due to eclipsing of the primary by the secondary and similarly A_2 receives a reduced flux from the secondary due to eclipsing of the secondary by the primary. Such phenomena are well known and most commonly observed during solar and lunar eclipses (see for example Green, 1985, Ch 12). In the point source treatment the Stokes parameters for a binary system are given by BME (their eq. 5 - 7) with

$$f_j = \frac{L_j}{L_1 + L_2} \qquad j = 1, 2 \qquad (1.9)$$

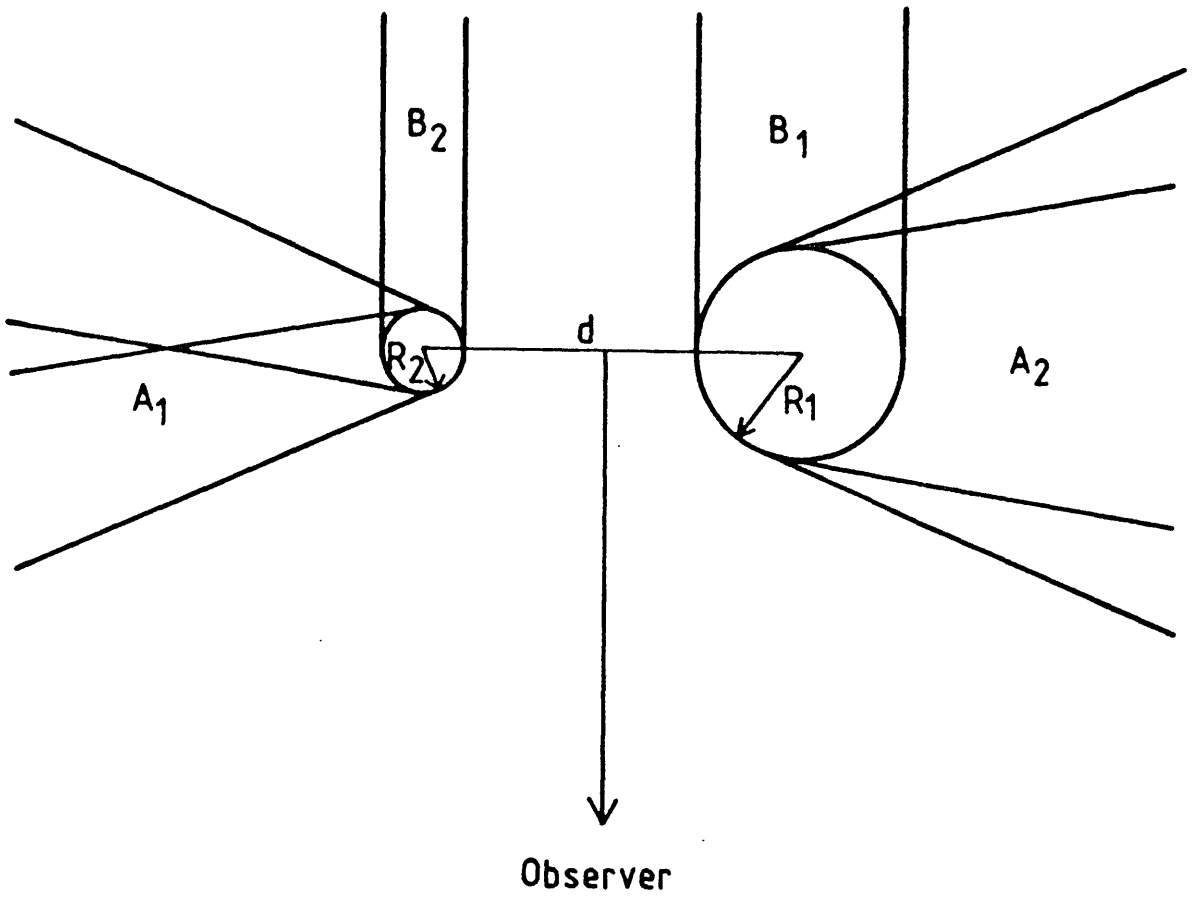

Figure 1.7

Schematic view of a binary system (looking down into the orbital plane) with a primary (radius R_1) and secondary (radius R_2) separated by a distance d from their centres, with an observer (E) in the equatorial plane.

The occulted regions (A_1, A_2, B_1, B_2) are indicated. A_1 is a region receiving a reduced flux from the primary. A_2 is a region receiving a reduced flux from the secondary. B_1 and B_2 are regions of the circumstellar envelope not visible to the observer due to the occultation of the envelope by the primary and secondary respectively.

To include the effcts of reduced flux in A_1 and A_2 (neglecting depolarisation, Cassinelli et al., 1987) we may introduce a general function $C_j(r_j,\theta_j,\phi_j)$ which represents the fraction by which the flux from the j^{th} star at a general point (r_j,θ_j,ϕ_j) is reduced by (compared to the point light source treatment). The function $C_j(r_j,\theta_j,\phi_j) = 1$ outside the region A_j and varies between 0 and 1 inside A_j. We may then replace eq. (1.9) by

$$f_j = \frac{L_j}{L_1 + L_2} C_j(r_j,\theta_j,\phi_j) \qquad (1.10)$$

Since eq. (1.10) is still independent of time (independent of λ) then only the magnitude of the polarisation will be changed and not the variation of polarisation with time. Therefore, the canonical results still hold and the number density in BME may be replaced by an equivalent effective number density without any loss of generality.

The other two regions of interest (B_1 and B_2) are the regions of the envelope not visible to the observer (and consequently observer dependent) due to the occultation of material by the two stars. The effects upon the net polarisation (at any given time) depends explicitly upon the distribution of material. For example, in the scenario of Fig 1.7 ($i = 90^\circ$) if all the material lies out of the orbital plane then no occultation effects will be observed. On the other hand, if the scattering material can be considered as a localised globule in the plane of the orbit then the polarisation variation will be as in the canonical prediction except at those phases when occultation occurs and the observed polarisation will be zero for the duration of the occultation (i.e. effectively a step function). In general, however, the material will be continuously distributed throughout space and thus

occultation will occur continuously such that higher than predicted orders of variation (i.e. greater than second order by the BME analysis) will be observed.

In the scenario depicted in Fig. 1.7, for a general scattering envelope, a rapid increase in the observed polarisation will occur during times of mutual stellar eclipsing. The change in polarisation during these times will be of the order of a factor ~ $(L_1 + L_2)/L_j$ larger than the pre- and post-eclipse values due to a rapid decline of the direct (unscattered) light (Pfeiffer and Koch, 1988) and the fact that the regions A_j, B_1 and B_2 will coincide so minimising any occultation effects. (In the foregoing chapters discussions concering the occultation effects in binary systems will be confined to those systems in which the secondary is dimensionally small and unimportant as a light source, compared to the primary, such that regions A_1, A_2 and B_2 can be neglected.)

1.5 Discussion.

Spectral and photometric observations of Be stars have shown that variablit y occurs on all time scales (seconds to decades). The short time scale variability is in general periodic and is attributed to surface features of the star, such as global oscillations (Baade, 1987), localised spots (Harmanec, 1989), or structural changes in the stellar wind (Prinja and Howarth, 1988; Bates and Halliwell, 1986). The longer time-scales on the other hand are non-periodic and indicate a long term variable mass loss from the star (Limber, 1967).

Polarimetric studies have so far investigated only the short term variability of Be stars (Clarke and Brooks, 1983; Clarke and McGale 1988a, b; Clarke, 1989). The indications are that the polarimetric

variability is consistent with corotating spot features.

Coordinated spectropolarimetric observations are potentially the best method for understanding the physical changes within stellar envelopes. (This is because spectrometry on the one hand observes photons passing through material along the line of sight whilst polarimetry, on the other hand, detects photons that are scattered into the line of sight.) There are two methods in which this may be done. One may either study the continuum polarisation with spectral changes (Sonneborn et al., 1988) which enables the global structure of the envelope to be studied (Brown and Henrichs, 1987) or the polarimetric changes across spectral lines may be investigated (Poeckert and Marlborough, 1977; McLean, 1979). This allows, to some extent, the local structure of the envelope to be studied since the variation of polarisation across a line will depend on the abundance and ionisation fraction of that species.

The mass loss mechanism for Be stars is still somewhat unknown. Observations of Be stars in binary sytems have been found to exhibit variability similar to single Be stars. This has been interpreted as meaning that all Be stars are members of binary systems (Křiž and Harmanec, 1975). This hypothesis has since been rejected (Harmanec, 1989).

In Be binary star systems mass transfer is believed to occur in some preferred plane (cf. Chapter 2). Since the Be phenomenon is similar for both single and binary Be stars this has led to the conclusion that such a preferred plane may also exist in single star stellar winds (eg. equatorial mass enhancements: MSS; Apparao et al., 1987; Maheswaren and Cassinelli, 1988).

Chapter 2

Polarimetric Analysis of Mass Transfer in the X-ray Transient A0538-66

2.1 Introduction

The X-ray transient A0538-66, more properly known as 0535-668 (Hutchings et al., 1985) in the Large Magellanic Cloud has been observed extensively since its discovery in 1977 (White and Carpenter, 1978; Johnston et al., 1979), largely due to its well established optical counterpart and the 16.65 day regularity of its outbursts when in the 'on' state. These outbursts, with an X-ray luminosity approaching 10^{39} erg/sec and a brightening of 2 mag or more in the V-band, are well fitted with the ephemeris of Skinner (1981),

$$N = (JD - 2443423.46)/16.6515 .$$

Physically these observations are interpreted in terms of a neutron star in a highly eccentric orbit about a B star primary, the outbursts occurring near periastron as the neutron star skims the outer layers of the B star (Charles et al., 1983; Skinner et al., 1982). However, the system sometimes turns into an 'off' state showing no outbursts for several years. This may be interpreted in terms of small readjustments in the primary radius corresponding (for small values of the atmospheric scale height as a fraction of radius) to large changes in the primary atmospheric density at the periastron point (Brown and Boyle, 1984). Analysis of the optical and near-UV data (Charles et al., 1983; Densham et al., 1983) suggest that the primary increases considerably in effective size during outburst and remains large well after periastron passage. Analysis of the X-ray light curve, and in

particular its asymmetry about periastron, has led Apparao (1985) to propose a model in which the neutron star orbits a B star with a characteristic equatorial disc but with the orbit highly inclined to the disc plane (cf. Johnston et al., 1979). However it is not clear that an inclined orbit is necessary to produce asymmetry in the X-ray light curve when account is taken of the differing radial velocities pre- and post-periastron and of the fact that accreted matter must have a finite residence time in the accretion disc so that $\dot{L}_X \propto \dot{M}_X$ is not proportional to $-\dot{M}_{primary}$ at each instant (Brown and Boyle, 1984), as assumed by Apparao (1985). Such conclusions about the system (Densham et al., 1983; Apparao, 1985) rest to some extent on ad hoc assumptions about the geometric interpretation of the spectrophotometric data. In principle, however, more direct information about the geometry of the system is obtainable by means of polarimetric observations (Brown et al., 1982; Boyle, 1984).

Clayton and Thompson (1982; hereafter CT) reported variable linear polarisation coincident with the optical outburst. They found that the broad-band optical polarisation rose from near zero to almost 2% near phase 0.0 of the outburst of March 10 1981 [outburst no. 75 according to the ephemeris of Skinner, (1981)]. The polarisation subsequently decayed but more gradually than the optical brightness, being still over 1% when the system had returned to near its pre-outburst brightness. CT also noted that the position angle of the polarisation varied during the outburst. They suggested an electron scattering model for their polarisation data in which most of the excess light occurs near periastron, when the compact companion in a highly inclined orbit intersects a gaseous disc surrounding the B star, accounting for the sudden onset of the polarisation increase. An

enhanced mass loss to the disc from the B star was proposed to account qualitatively for the sustained polarisation enhancement. Changing scattering geometry, due to orbital motion of the secondary and shifting of the main centre of the light emission from the primary to the secondary and back, were suggested as sources of variation in the polarisation direction.

Simmons and Boyle (1984; hereafter referred to as SB) gave an alternative interpretation of the CT data in which the variable degree of polarisation was shown to be interpretable entirely in terms of the variable scattering geometry of the system, as the companion swung rapidly through periastron, without any change in the physical amount or distribution of scattering matter. The SB analysis ignored changes in polarimetric position angle and required a periastron longitude λ_p satisfying $270^\circ \leqslant \lambda_p \leqslant 360^\circ$ or $90^\circ \leqslant \lambda_p \leqslant 180^\circ$, and the occurrence of an optical light maximum substantially before periastron (phase $\approx$ 0.86).

Since the CT data and SB analysis, we have obtained polarimetric data during a further outburst of A0538-66 and there have been two further attempts at determining the spectrophotometric orbital elements (Corbet et al., 1984; Hutchings et al., 1985). It is the purpose of this chapter to reconsider the CT and SB interpretations of the polarimetry of this system in the light of these new data and orbital elements.

2.2 New Observations.

Further polarimetric observations were obtained in April 1982 on the 2.5m Dupont telescope at Las Campanas Observatory. The Univerisity of Western Ontario's two-channel photoelectric Pockels cell polarimeter (Angel and Landstreet, 1970) was used to measure linear polarisation. The observations were unfiltered so the bandpass

(320-860 nm) was determined by the atmospheric transmission and response of the GaAs photomultipliers (RCA 31034A). The observations were corrected for instrumental efficiency and sky polarisation. Observations of the interstellar polarisation and null standards (Serkowski, 1973; Serkowski et al., 1975) were used to reduce the position angle to the standard equatorial system and to check for instrumental polarisation, respectively. The errors reported below are linear error estimates for photon counting statistics only. Uncertainties in the sky correction, interstellar polarisation, and rapid stochastic variations in the source itself (cf. Simmons and Stewart, 1985) will increase these errors substantially at times of low polarised flux prior to the outbursts. Galactic foreground polarisation was determined through observations of Dachs No. 20, a star lying only 2 arcmin from the A0538-66 line-of-sight. An average of four observations of this star gives $p = 0.24 \pm 0.04\%$, $\Phi = 7.1^{\circ} \pm 4.4^{\circ}$. This is very close to the foreground value used by CT.

The observations corrected for foreground are given in Table 2.1. Observations made while the moon was up, which are considered somewhat uncertain, are marked with a colon in Table 2.1. Figs 2.1 and 2.2 show, respectively, the values of p, Φ, Q and U (in the equatorial system) plotted against binary phase (using the Skinner ephemeris) in which the CT observations (filled squares) are from outburst 75, while the new data (open squares) are from outburst 99. In Fig. 2.3, we show the corresponding photometric variations during outbursts 75 and 99. The relative 'photometry' from CT has been re-plotted. These observations have now been scaled using some coincident B-band photometry (Tuohy, 1981, private communication). Differential photometry between A0538-66 and Dachs No. 20 was obtained coincident

Table 2.1 Observations

JD	Cycle	Phase	$p \pm \sigma_p$	$\phi \pm \sigma_\phi$	$p' \pm \sigma_{p'}$	$\phi' \pm \sigma_{\phi'}$	Q'	U'
4668.58	74	0.745	0.17 ± 0.21	116.0 ± 52.0	0.39 ± 0.21	104.9 ± 15.6	-0.34	-0.19
4670.57	74	0.864	0.25 0.22	41.9 24.7	0.28 0.22	68.4 22.4	-0.20	0.19
4671.62	74	0.927	0.08 0.16	36.5 52.0	0.21 0.17	88.0 23.0	-0.21	0.02
4672.62	74	0.987	0.51 0.08	62.9 4.4	0.64 0.09	73.1 3.9	-0.53	0.35
4673.52	75	0.041	1.66 0.10	74.2 1.7	1.84 0.10	76.9 1.6	-1.65	0.81
4673.76	75	0.056	1.24 0.11	73.9 2.5	1.41 0.12	77.4 2.3	-1.28	0.60
4674.52	75	0.101	1.44 0.11	90.9 2.2	1.68 0.12	91.8 2.0	-1.68	-0.10
4674.72	75	0.114	1.59 0.21	90.6 3.7	1.83 0.21	91.4 3.3	-1.83	-0.09
4675.69	75	0.172	1.22 0.14	96.1 3.4	1.46 0.15	96.2 2.9	-1.43	-0.32
4676.68	75	0.232	0.94 0.20	91.3 6.0	1.18 0.20	92.5 4.9	-1.17	-0.10
4677.59	75	0.286	0.90 0.19	92.0 5.9	1.14 0.19	93.1 4.8	-1.13	-0.12
5062.50:	98	0.402	0.50 0.08	167.7 4.6	0.34 0.09	154.9 7.3	0.22	-0.26
5063.49:	98	0.462	0.50 0.08	150.5 4.7	0.48 0.09	136.4 5.3	0.02	-0.49
5070.48	98	0.882	0.45 0.11	141.3 6.8	0.52 0.11	127.6 6.3	-0.13	-0.50
5071.50	98	0.943	0.59 0.09	158.5 4.5	0.50 0.10	146.8 5.7	0.20	-0.46
5072.48	99	0.001	0.70 0.06	170.8 2.7	0.51 0.07	163.5 4.2	0.43	-0.28
5072.50	99	0.002	0.52 0.06	178.6 3.1	0.30 0.07	172.0 6.3	0.29	-0.08
5073.50	99	0.062	0.30 0.05	62.1 4.7	0.44 0.06	77.3 4.0	-0.40	0.19
5073.52	99	0.063	0.32 0.06	77.7 5.4	0.53 0.07	85.9 3.9	-0.52	0.08
5074.50	99	0.122	1.14 0.08	76.9 2.1	1.33 0.09	80.2 2.0	-1.25	0.44
5074.52	99	0.124	1.10 0.08	74.8 2.2	1.28 0.09	78.5 2.0	-1.18	0.50

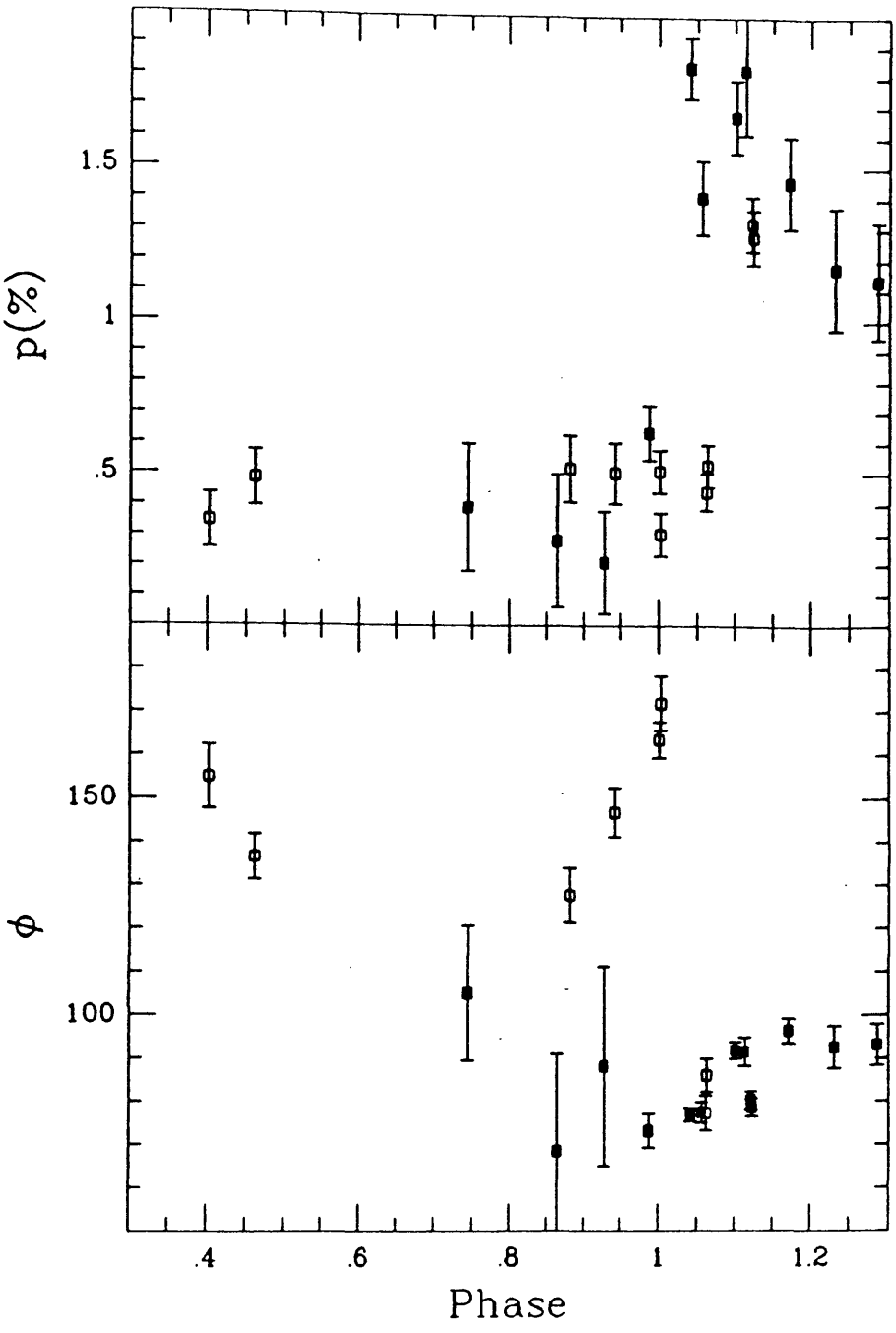

Figure 2.1

A plot of the magnitude and position angle of polarisation for both outbursts plotted against phase using the ephemeris of Skinner (1981). The filled squares represent observations from outburst 75 (CT) and the open squares represent the new data reported here from outburst 99. The error bars plotted here represent 1 σ. The plotted observations are corrected for foreground interstellar polarisation (see text).

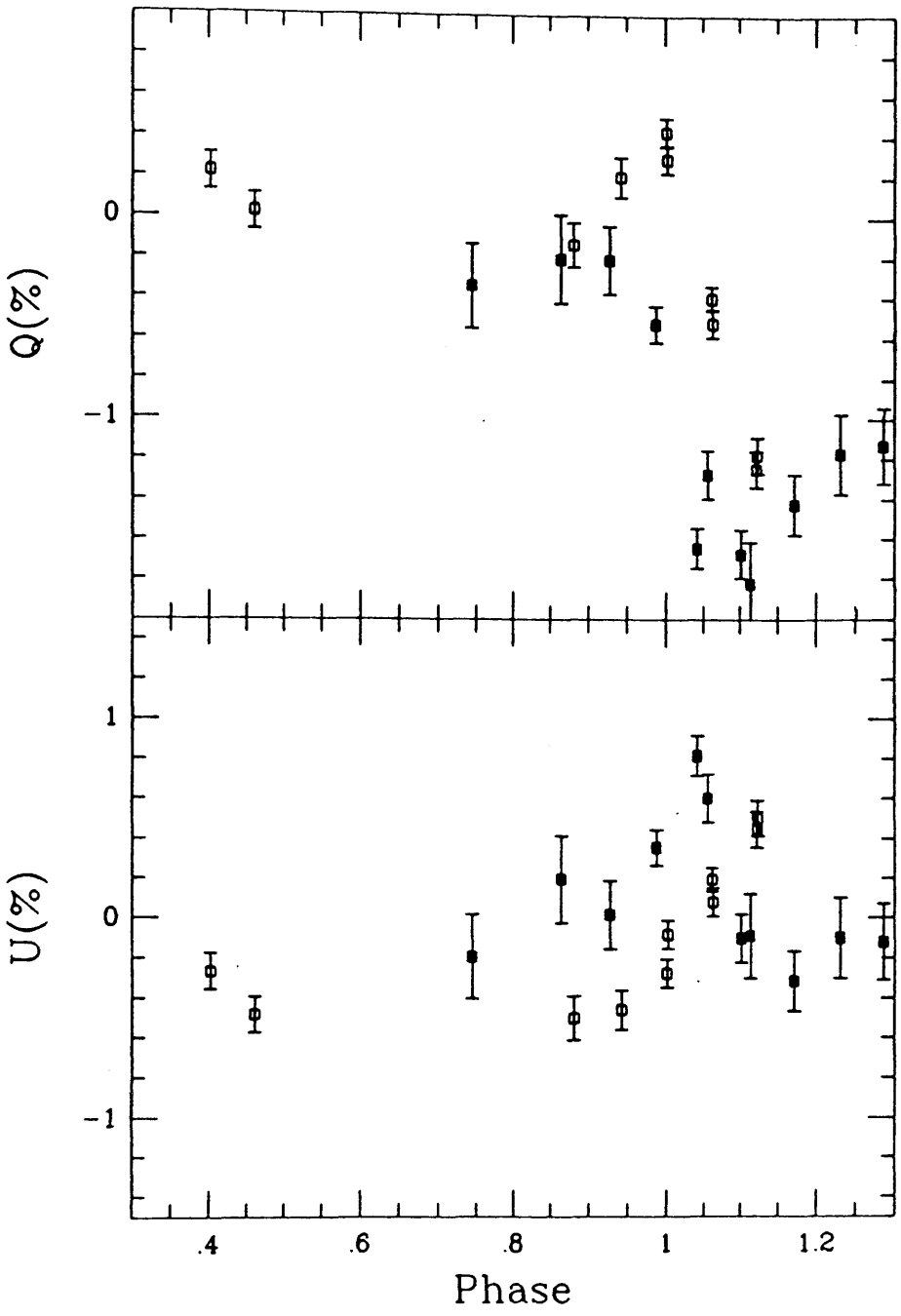

Figure 2.2

A plot of Q and U against phase for the same observations specified in Fig. 2.1. The symbols are the same as in Fig. 2.1

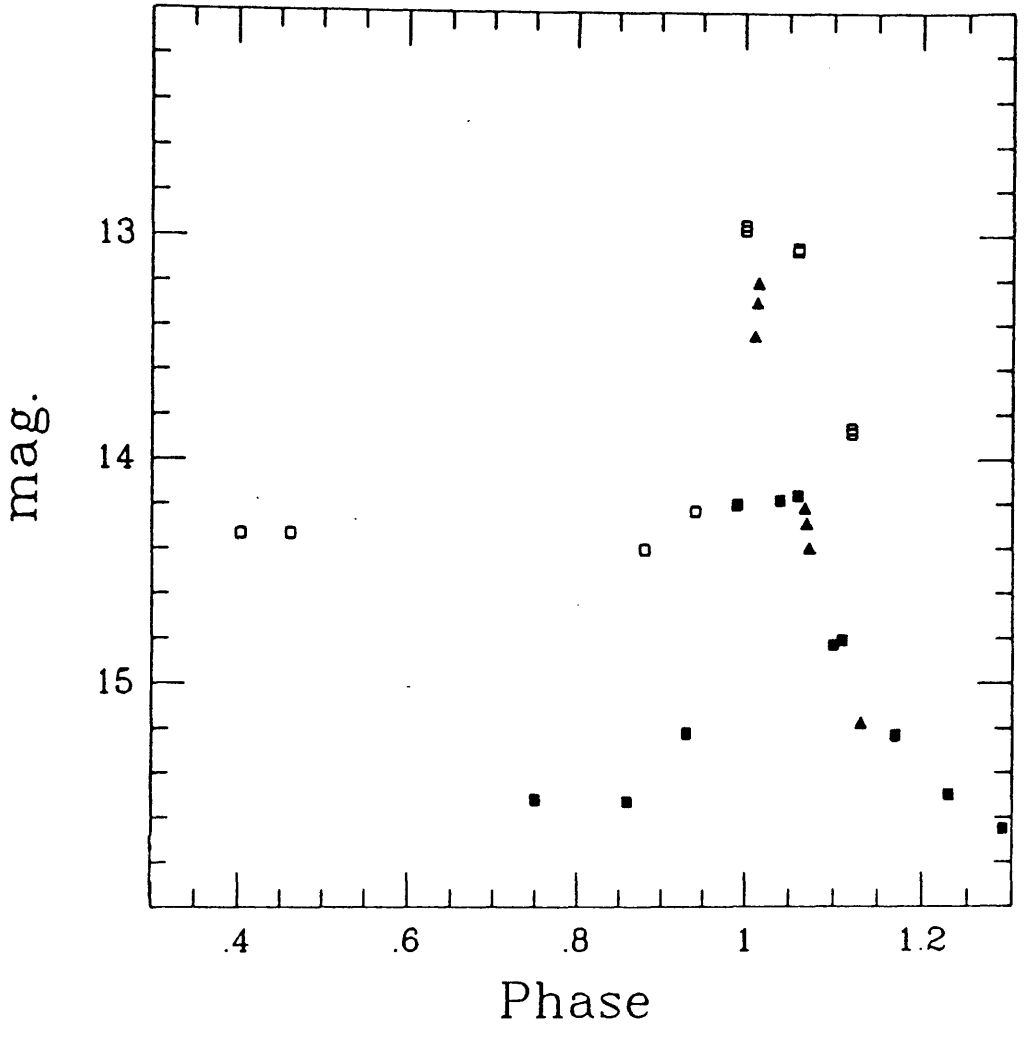

Figure 2.3

Photometry of A0538-66 taken during outbursts 75 and 99. The filled squares are magnitudes derived from polarimetric count rates from the observations of outburst 75 (see text). The triangles are B-band photometry taken during the same outburst (Tuohy, 1981 Private comm.). The open squares are differential photometry taken along with the polarimetry of ouburst 99.

with the new observations using a 10.4 arcsec aperture and the polarimeter count rates. The peak magnitude agrees well with the V = 13.1 ± 0.2 reported by van Paradijs et al. (1984). To assist in the interpretation, we show in Fig. 2.4 a plot of the data for the two outburst in terms of the locus desribed in the (Q,U) plane.

Reference to Fig. 2.1 shows that in both outbursts the main feature is a rapid rise in the degree of polarisation in the phase range 0.00 - 0.05 followed (after phase 0.1) by a comparatively slow decline on a time-scale considerably longer than that for the brightness of the system to decline (see Fig. 2.3). There is some indication that the polarisation rise in outburst 99 occurs at a later phase and has more prolonged light maximum than outburst 75, but the phase sampling of the data is too sparse to quantify these differences. Note that the quiescent brightness of the A0538-66 system differs by more than 1 mag between outbursts 75 and 99.

Fig. 2.1 suggests an apparently discrepant behaviour in the position angle between the two outbursts. However, the pre-outburst position angles in outburst 75 are rather poorly determined (noted by CT and SB) as can be seen from the (underestimated) formal errors in Fig. 2.1 at those phases. Therefore, we will henceforth discount these data for position angle interpretation. (If the pre-outburst Φ values were truly different the implications would be fascinating but problematic. They would imply a 90° rotation on the sky of the principal scattering plane in the non-outburst system, which would be normally taken as the plane of a Be star disc. Such a rotation might be attributed to major disruption of the disc in a preceding outburst by the action of a companion in an orbit highly inclined to the preceding disc plane. It is hard however, to see why repetition of

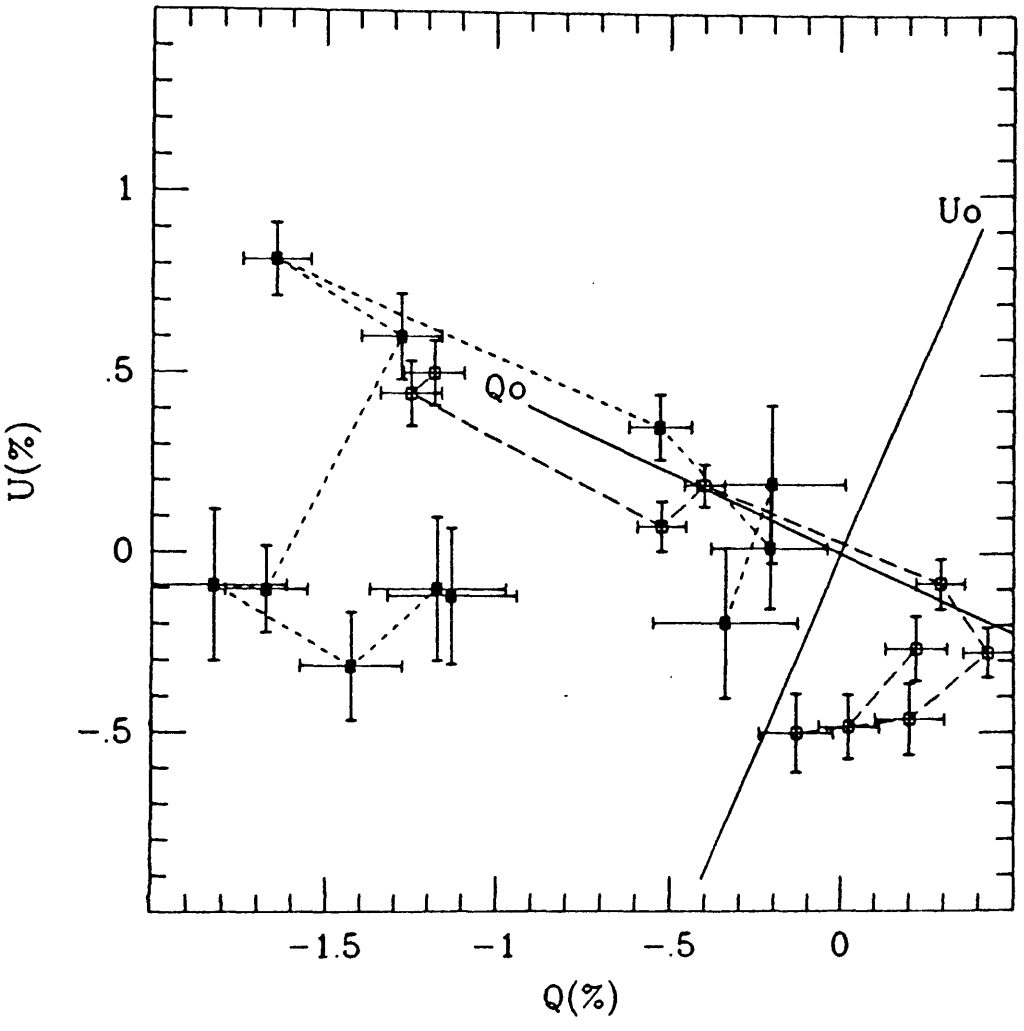

Figure 2.4

A (Q,U) diagram showing the same observations as plotted in Fig. 2.2. The symbols are the same. To follow the polarisation evolution with time of the two oubursts, the points are connected by short dashes (outburst 75) and long dashes (outburst 99). Also plotted, are the Q_o and U_o axes representing the natural axes of the A0538-66 system. They are rotatedby 12° on the sky and 24° in the (Q,U) plane.

such disturbances would not have quickly led to alignment of the disc and orbital axes). Then the main feature in the behaviour of Φ with phase is a possible slight increase just before phase 0.0, followed by a rapid rotation through about -90° at phase 0.00-0.05, and then by a slow recovery. In terms of the Q-U plane in Fig. 2.4, this can be seen in the form of a rapid near-linear transformation, mainly in the -Q direction, changing Q from positive to negative values (180° rotation in the (Q,U) plane ≡ 90° in Φ) followed by a trend at about right angles to this line (i.e. roughly in the -U direction), with Q moving back to less-negative values. Again the data are too undersampled to see detailed behaviour near phase zero or to see detailed differences between outbursts. In Fig. 2.4, we also show a set of axes (Q_0,U_0), used later, which are rotated by 12° from (Q_0,U) on the sky [24° in the (Q,U) plane] so that rapid changes in p lies along the Q_0 axis.

2.3 Qualitative Interpretation.

As is the case with spectrophotometry, the polarimetric light-curve modelling of an eccentric binary is a multi-parameter problem, demanding intensive observational coverage for an unambiguous solution. Thus, even with the improved spectrophotometric data and analysis of recent years (Hutchings et al., 1985, Corbet et al., 1984) there remains considerable doubt about the values of the orbital elements, some of the elements calculated by the two groups not agreeing at all, though a large eccentricity seems to be unanimously required. Because of the active nature of the A0538-66 system, the presence of small amounts of emission may affect the radial velocity measurements. In particular, Hutchings et al. (1985) comment that the mean spectrum of Corbet et al. (1984) contains blueshifted emission at

H_β, indicating that the star still had significant emission when their observations were made. Smale et al. (1984) reported similar problems with spectroscopic data they obtained around the same time. The Hutchings et al. data may be less affected, as the data were taken later when the system may have been more deeply in the 'off' state. The Hutchings et al. and Corbet et al. orbital elements are summarised in Table 2.2.

In the case of polarimetry, the problem will involve not only the geometrical effects related to the orbital elements (cf. Brown et al., 1982) but also the variable relative contributions of the two light sources (cf. CT, SB) and the variable amount and spatial distribution of the scattering material, which has not been considered quantitatively in any of the previous analyses. Given, therefore, the limited polarimetric coverage of A0538-66 even with our new data, a variety of possible interpretations is to be expected.

Our aim here, however, is to show that the available data are adequate to rule out certain interpretations, regardless of the orbital elements adopted, and to put some limits on the parameters of one possible interpretation. Specifically, we will restrict ourselves to an interpretation in which the system comprises a Be star primary surrounded by a disc accompanied by a neutron star, in a coplanar orbit, which disturbs and captures gas from the disc during close passage at periastron. While other interpretations would undoubtedly be possible, we will show that no more elaborate model is demanded by currently available data. Scattering of Be light from the disc is taken to be responsible for the polarisation outburst, the direction of this polarisation defining the projection of the system axis on the sky. Variations in the extent of the quiescent disc, which appear to be a

Table 2.2 Orbital elements.

	Corbet et al.	Hutchings et al.
Eccentricity (e)	$0.96^{+0.04}_{-0.23}$	0.82±0.04
Longitude of periastron	$330^{\circ}{}^{+30^{\circ}}_{-60^{\circ}}$	222°±21°
Mass function	4.7×10^{-7} $M_{\odot}$	0.027 $M_{\odot}$

Orbital elements of A0538-66 calculated with assumed period of 16.6515 days.

common Be phenomenon (Coyne, 1976; Hayes and Guinan, 1984), will cause variations in the quiescent polarisation (such are seen in Fig. 2.1). Disc variations will also cause considerable variation in the size and properties of different outbursts, since the mass transfer and loss at periastron passage is very sensitive to the size of the primary envelope (Brown and Boyle, 1984; Boyle and Walker, 1986). Indeed such variations may be responsible for the 'on-off' states in A0538-66 outburst behaviour (Brown and Boyle, 1984). Major enhancement of the disc by the disruptive effect of the periastron passage may contribute to the apparent enlargement of the optical primary at outburst (Charles et al., 1983; Densham et al., 1983) and to the amount of mass captured by the neutron star leading to the X-ray outburst.

One specific elaboration of the above model, proposed by CT and Apparao (1985) is that the orbit is highly inclined to the disc plane. CT proposed this as an explanation for the sudden onset of the polarisation as the neutron star enters the plane of the disc while Apparao claims the inclined orbit is necessary to explain the assymmetry of the X-ray and optical light curves near periastron. However, the steep radial density gradient in the disc and the rapidity of secondary approach alone will guarantee a steep rise in the light curves and polarisation, even for a coplanar orbit. Secondly, Apparao's argument rests on the assumption that the X-ray luminosity is a function only of secondary location, which is symmetric about periastron in the coplanar case. In reality, the mass accretion rate on to the neutron star (and hence the X-ray luminosity) is asymmetric about periastron because it is also affected by the sign of the radial velocity and by the storage time of the captured matter in the transient accretion disc (Brown and Boyle, 1984).

Quantitatively, the possible contributions to the polarisation are scattering of light from:

(i) the primary, X_1;

(ii) the secondary, X_2;

(iii) a disc, S_1, around X_1;

(iv) accreting gas, S_2, around X_2, and

(v) any additional gas, S_3, torn from X_1 and S_1 during periastron passage.

For reasons of symmetry, light from X_1 scattered around X_2, and light from X_2 scattered around X_1 show identical polarisation variations when the number of scatterers does not change with time. However, the net observed polarisation depends on the relative contributions, as a function of time, of the two sources of diluting unpolarised starlight (SB). Using only the earlier data (CT), SB argued that the observed variation in the degree of polarisation could be explained purely geometrically in terms of scattering in a fixed mass around X_1 of light L_1 and L_2, from both X_1 and X_2. Both L_2 and the position of X_2 vary rapidly through periastron, with L_1 fixed. This model is unrealistic in that it disregards the envelope redistribution which is bound to accompany the outburst. Furthermore, due to the high eccenticity, the light sources recede very rapidly from the scatterers around the other object so that the polarisation can only be sustained for very specific scattering-angle geometries soon after periastron, i.e. for very specific ω values for which SB also predict the position angle variation expected in their model. We show below that the more complete observational material now available do not agree with these SB predictions; see Fig. 2.6.

We have therefore considered a wide variety of light

source/scatterer geometries, including variation in the amount of scattering material to see what kind of coplanar situations can fit the observations. In doing so, we have assumed that the scattering polarisation can be adequately described by the single scattering treatment of Brown et al. (1978), corrected by the depolarisation factor required because of the large size of the primary (Cassinelli et al., 1987). Daniel (1980) and Dolan (1984) have shown that even multiple scattering situations are quite accurately described by this simpler treatment. (We have neglected, however, any effects of variable occultation or eclipsing by the large primary. If these were important they should also have shown up in the X-ray and optical light curves. Moreover, the polarimetric data are too scanty and noisy for occultation effects to be observed or studied.) In discussing the predictions of various models, we will refer the polarisation to the natural axis of the system i.e. the projection of the orbital/disc normal on to the sky. This is of course unknown *a priori* and in trying to fit the various models we have taken the system orientation on the sky to be a free parameter. We have done likewise with the system inclination i, but found model predictions to be insensitive over a wide range of i. Quantitative results are therefore given only for $i = 60^{\circ}$. In the following, all of the conclusions hold for any orbit with large eccentricity, regardless of the other orbital elements.

The simplest situation we considered was one in which all of the light variation was attributed to changes in the luminosity L_1 in the neighbourhood of X_1 and all of the polarimetric variations due to changes in the total number N_1 of scatterers in the disc S_1. Such a description could for suitable $N_1(t)$, reasonably describe the rise and fall of the degree of polarisation. However the position angle of the

polarisation should never change from that of the pre-outburst Be star/disc system, in contradiction to the observations (Fig. 2.1).

Secondly, we tried attributing the light enhancement entirely to the changing luminosity L_2 of X_2 and the polarimetric changes to scattering of L_2 on N_2 electrons in S_2 around X_2. This does give rise to changes in position angle (though more rapid than those observed). However the extra light L_2 must decline on the short decay time-scale of the optical light curve so that L_1 will again predominate and will dilute the polarisation of L_2 scattered on N_2 faster than the degree of polarisation is observed to decay (cf. Figs 2.1 and 2.3). Similarly, the position angle does not return to its pre-outburst value on this time scale (Fig. 2.1).

Therefore, we conclude that the polarisation cannot be described in terms of the predominance of L_1 on S_1 nor of L_2 on S_2. Next we consider the contribution of L_1 scattered on N_2 and of L_2 on N_1. One can at once conclude that the latter connot be predominant for the same reason as above i.e. the decline of L_2 demanded by the light curve would cause the polarisation to decline and the position angle to revert back to its pre-outburst value much faster than is observed. The scattering of L_1 on S_2 does not suffer from the same objection since the decline of the light curve does not change the polarisation as the polarised flux and the depolarising flux (both $\propto L_1$) decline together. The problem with this option is that the distance and angle X_1 and S_2 around X_2 change so quickly in a highly eccentric orbit. The consequences of this are best seen in the quantitative treatment below where we take L_1 to predominate throughout.

2.4 Quantitative interpretation with primary light source dominant.

In view of the problems posed by alternative interpretations, we consider here the possiblity of explaining the polarimetric data when the primary luminosity $L_1(t)$ is predominant throughout. In this model, the polarisation arises from scattering in the neighbouring disc material S_1 (which may be enlarged during outburst), and from some additional scattering material S_3. This material S_3 may, but need not, be identical with S_2 accreting on to X_2 so that the last scenario described in Section 2.3 is included in this analysis.

The analysis of Brown et al. (1978) in fact shows that the Stokes parameters of any electron distribution near the orbital plane may be described by those of an equivalent idealised scatterer at an appropiate site. Our procedure will be to consider the polarisation expected from an 'equivalent scattering volume' S containing N electrons and located at a distance R from X_1 at an angle (longitude) Λ in the orbital plane from the plane X_1EZ containing the Earth E and the orbital axis Z (see Fig. 2.5). the parameters N, R and Λ will be allowed to vary with time and, will identify the 'scattering centroid' properties when matched to the observations. These properties will therefore represent the sum of the contributions from S_1, S_2 and S_3.

A cloud of N electrons (R, Λ) in the orbital plane illuminated dominantly by X_1 with luminosity L_1, will result in the Stokes parameters Q_o, and U_o, with Q_o measured along the projection of X_1Z on the sky, given by,

$$Q_o = p\cos 2\Phi_o = \frac{\sigma_o N}{R^2}\left[1 - \frac{R_*^2}{R^2}\right]^{1/2}(\sin^2\Lambda - \cos^2 i\cos^2\Lambda) \qquad (2.1)$$

$$U_o = p\sin 2\Phi_o = \frac{\sigma_o N}{R^2}\left[1 - \frac{R_*^2}{R^2}\right]^{1/2}\cos i\sin 2\Lambda \qquad (2.2)$$

Figure 2.5

Two schematic views of the A0538-66 orbit. The positions of the primary, the secondary and periastron are given by X_1, X_2 and P respectively. The large double arrow shows the polarisation of the 'equivalent scattering volume' S containing N electrons and located in the orbital plane at a distance R from X_1 and at an angle (longitude) Λ from the plane X_1EZ containing the earth E and the orbital axis Z. The line X_1AX is the projection of X_1E in the orbital plane. The scattering angle is given by χ. The position of the secondary is r, υ in orbital polar coordinates. The longitude of periastron is ω and the true anomaly is λ.

Figure 2.5

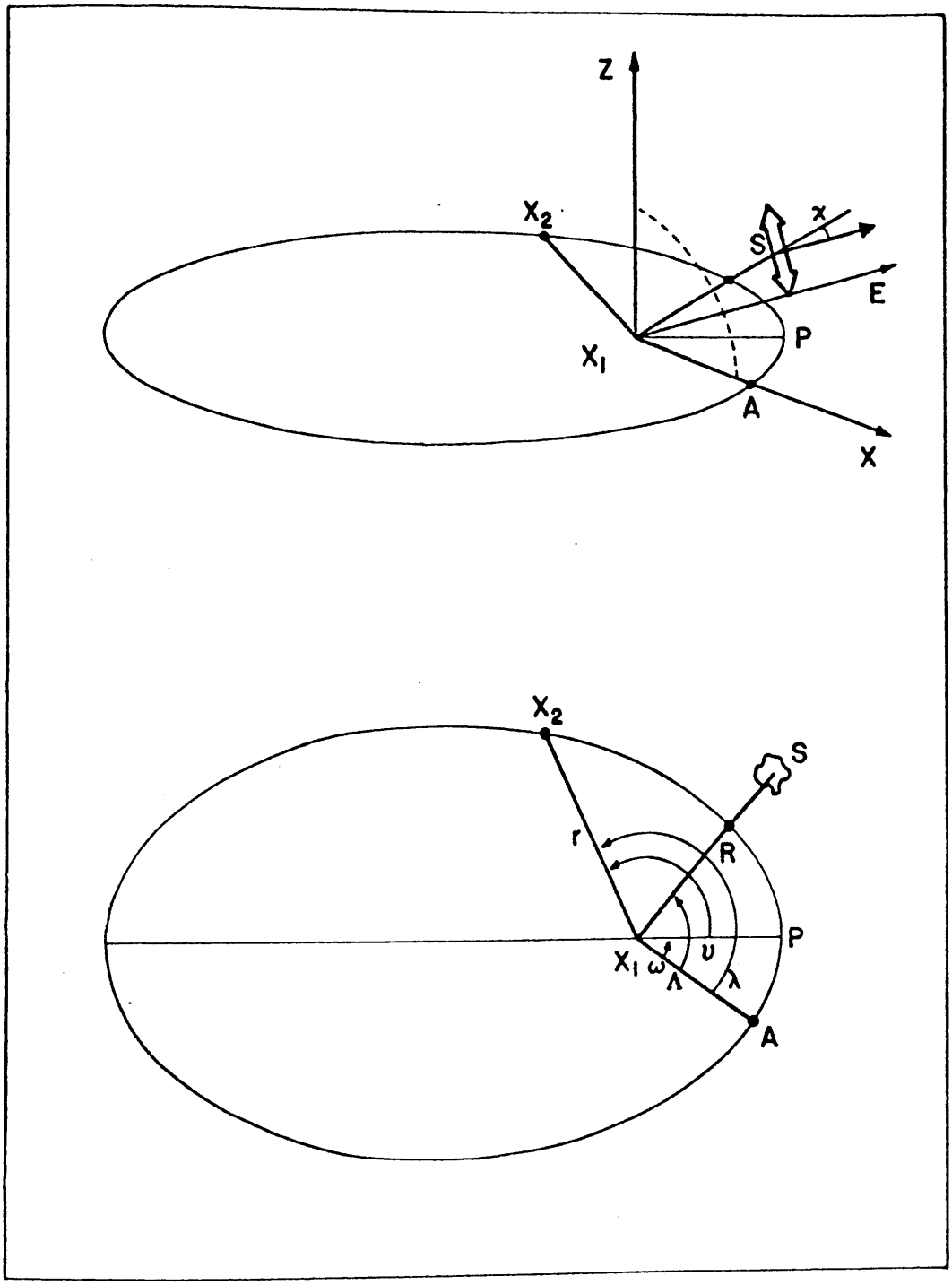

where Φ_0 is the position angle in this system, $\sigma_0 = (3/16\pi)\sigma_T$ with σ_T the Thomson cross-section, and R_* is the stelllar radius which arises in the depolarisation factor, $D = (1 - R_*^2/R^2)^{\frac{1}{2}}$ (Cassinelli et al., 1987).

Equations (2.1) and (2.2) can be used to predict the Q_0 and U_0 from a model where N, R and Λ are given (or from a sum of such contributions) for comparison with data, or to deduce the conbination of N, R and Λ needed from the data. We have used the equations both ways and we present here the results where the observed Q and U of Figs 2.2 and 2.4 have been rotated through $\Delta\Phi = 12^\circ$ on the assumption that the pre-outburst position angle indeed indicates the direction of the natural system Q_0 axis, i.e. that pre-outburst polarisation is the result of L_1 scattering from S_1 which can be considered a Be star disc in the orbital plane. In fact we have experimented with $\Delta\Phi$ as a free parameter and found that none of the conclusions stated below are modified, i.e. the $\Delta\Phi$ value adopted gives the most self-consistent interpretation.

First we used (2.1) and (2.2) to examine the physically plausible hypothesis that the variable polarisation arises from the scattering of L_1 on both S_1 and S_2, containing N_1 and N_2 electrons, respectively. Both the disc and the cloud scattering mass can be replaced by an equivalent uniform ring of N_1 electrons at radius R_1 and by averaging (1.2) and (2.2) over Λ_1. The scattering accretion cloud of N_2 electrons must have $R_2 \approx r$, $\Lambda_2 = \upsilon + \omega$ where r and υ are the orbital polar coordinates of the secondary at a time t (see Fig. 2.5). The total predicted polarisation is then given by,

$$Q_0(t) = \frac{\sigma_0 N_1}{2R_1^2}\left[1 - \frac{R_*^2}{R_1^2}\right]^{1/2} \sin^2 i$$

$$+\frac{\sigma_0 N_2}{r^2}\left[1 - \frac{R_*^2}{r^2}\right]^{1/2}[\sin^2(\upsilon + \omega) - \cos^2 i \cos^2(\upsilon + \omega)] \qquad (2.3)$$

$$U_0(t) = \frac{\sigma_0 N_2}{r^2}\left[1 - \frac{R_*^2}{r^2}\right]^{1/2} \cos i \sin[2(\upsilon + \omega)], \qquad (2.4)$$

where $r = a(1 - e^2)/(1 + e\cos\upsilon)$. If we express a, R_1, and R_2 in units of the primary star radius R_*, then for any given set of orbital elements the only unknown functions of time on the right sides of (2.3) and (2.4) are $\nu_1 = \sigma_0 N_1/R_*^2$ and $\nu_2 = \sigma_0 N_2/R_*^2$. With fixed ν_1 and ν_2 this is essentially the model discussed by SB. Thus for a given set of data, $Q_0(t)$, $U_0(t)$ and an assumed orbit, the equations (2.3) and (2.4) can be solved for $N_1(t)$ and $N_2(t)$ for a given orbit, and given values of R_*/a and R_1/R_*. In principle, this solution could yield valuable information on the redistribution of gas during the accretion outburst.

We have carried out this solution of the data in Table 2.1 for a variety of values of $\Delta\Phi$, i, R_*/a and R_1/R_* using both Corbet et al. (1984) and Hutchings et al. (1985) orbital elements. We use these for illustration of the procedure only. They are so different that neither can yet be taken seriously. On the other hand, the fact that conclusions below are the same in both cases shows them to be very insensitive to the orbital elements apart from high eccentricity. We found it impossible to obtain a physically acceptable solution, i.e. $N_1(t)$ and $N_2(t)$ both positive at all times. In those solutions with N_1, $N_2 \gtrsim 0$ for as many points as possible (namely with $\Delta\Phi \approx 12°$), we found that following periastron $N_2(t)$ became much larger (by 2 orders) than N_1

and continued to increase with phase. Such behaviour seems unphysical since N_2 presumably is drawn from N_1 and the transfer should decline rapidly as r/a increases. The negative N values in fact arise because of the incompatibility of predictions (2.3) and (2.4) with the observed position-angle changes. This is most clearly seen by considering the contributions of Q_2, and U_2 in (2.3) and (2.4) which would arise from N_2 alone if this were fixed in time, as follows. (These conclusions are unchanged for other ω values.) In Fig. 2.6 we show plotted against phase the observed polarisation, p, and the rotated position angle Φ_0. Superposed are the (arbitrarily scaled) p and Φ predicted for an accretion cloud of fixed N_2 around X_2 (SB), for the orbital elements of both Corbet et al. (1984) and Hutchings et al. (1985). In both of the predicted curves, we have used the largest value of $R_*/a(1 - e^2)$ (namely 0.5) compatible with the absence of eclipses for $i = 60^\circ$ (cf. Hutchings et al., 1985). This has the effect of maximising the reduction of the sharp peak in p(t) due to finite source depolarisation. Despite the error bars and undersampling of the data, it is clear that a fixed N_2 in orbit with X_2 cannot possibly explain the observations for either orbit, or indeed for any high-eccentricity orbit. The reason, as can be seen in (2.3) and (2.4), is simply that high eccentricity implies a more rapid variation in Φ_0 than observed because of the $(\upsilon + \omega)$ factors and a much more rapid decline in p than is observed of the $1/r^2$ factor. To offset the $1/r^2$ variation in p(t) would demand a correspondingly large rise in N_2 as found above.

We conclude therfore that N_1 and N_2 alone cannot explain our observations for any orbit. The only remaining way to interpret the sustained p(t) well beyond periastron and the near constancy of Φ_0 at

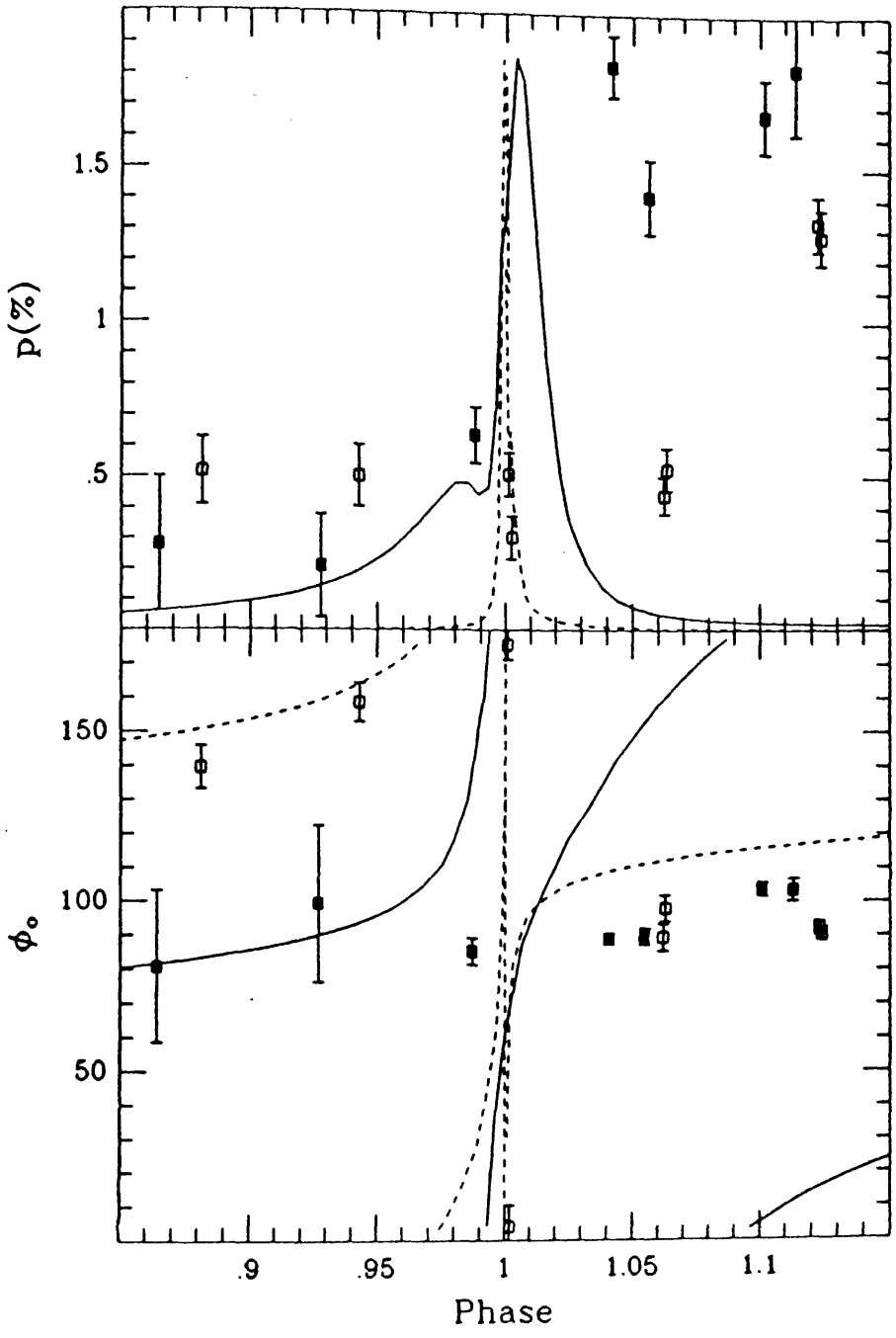

Figure 2.6

A plot similar to Fig. 2.1, rotated into the natural system of A0538-66 shown in Fig. 2.4. In this frame of reference, p is unchanged and the position angle, $\Phi_o = \Phi + 12^\circ$. Only the points from both outbursts occuring near phase 0.0 are plotted. The predictions of the Simmons and Boyle model for the orbital elements of Hutchings et al. (1985) (solid line) and Corbet et al. (1984) (dashed line) are also shown.

that time is to invoke a third scattering region S_3, the location of which changes only gradually. It should be noted that this conclusion does not conflict with the massive accretion cloud S_2 around X_2, as found in simulations (e.g. Boyle and Walker, 1986) and needed to explain the X-ray light curve. Rather it just means that this S_2 recedes from X_1 so quickly that it soon makes a negligible contribution to p compared to a persistent (possibly less massive) cloud that is located much nearer the light source.

To estimate the location and mass of S_3, we return to equations (2.1) and (2.2) and invert them to give,

$$\tan\Lambda = \cos i \left[\frac{\cos 2\phi_0 \pm 1}{\sin 2\phi_0} \right] \tag{2.5}$$

$$p_0 = \frac{\sigma_0 N}{R^2} \left[1 - \frac{R^2}{R_*^2} \right]^{\frac{1}{2}} \tag{2.6}$$

where p_0 is given by either (2.1) or (2.2) once Λ is obtained from (2.5).

We have used equations (2.5) and (2.6) to infer the longitude Λ and the quantity N of the 'effective scattering centroid' needed to fit the (rotated) data of Table 2.1 with well-defined ϕ_0. The results for $i = 60^\circ$ are shown in Table 2.3. The number of scatterers, N, has been shown in the scaled form,

$$fN = \frac{10^{24}}{\sigma_0} p_0 = 1.5 \times 10^{46} \, p_0 \text{ (per cent)(electrons)} \tag{2.7}$$

where the factor,

$$f = \left[\frac{10^{12}}{R_*} \right]^2 \left[1 - \frac{R_*^2}{R^2} \right]^{\frac{1}{2}} \left[\frac{R_*}{R} \right]^2 \tag{2.8}$$

Table 2.3 Effective Scattering Centroid.

JD	Cycle	Phase	p'	ϕ_o	fN(x10^{-46})	Λ	Λ+180°
4668.58	74	0.745	0.39	116.9	2.05	345.8	165.8
4670.57	74	0.865	0.28	80.4	1.67	4.6	184.6
4671.62	74	0.928	0.21	100.0	1.30	355.3	175.3
4672.62	74	0.988	0.64	85.1	3.79	2.4	182.4
4673.52	75	0.042	1.84	88.9	11.03	0.5	180.5
4673.76	75	0.056	1.41	89.4	8.54	0.2	180.2
4674.52	75	0.102	1.68	103.8	9.73	353.1	173.1
4674.72	75	0.114	1.83	103.4	10.61	353.2	173.2
4675.69	75	0.172	1.46	108.3	8.20	350.6	170.6
4676.68	75	0.232	1.18	104.5	6.83	352.7	172.7
4677.59	75	0.286	1.14	105.1	6.47	352.4	172.4
5062.5	98	0.402	0.35	166.9	0.60	295.0	115.0
5063.49	98	0.462	0.49	148.4	1.33	320.9	140.9
5070.48	98	0.881	0.52	139.6	1.76	329.6	149.6
5071.5	98	0.943	0.50	158.8	1.05	307.8	127.8
5072.48	99	0.001	0.51	175.5	0.78	278.9	98.9
5072.5	99	0.002	0.30	184.0	0.46	82.0	262.0
5073.5	99	0.062	0.44	89.3	2.66	0.3	180.3
5073.52	99	0.063	0.53	97.9	3.13	356.0	176.0
5074.5	99	0.123	1.33	92.2	7.96	358.9	178.9
5074.52	99	0.124	1.28	90.5	7.70	359.7	179.7

which reflects the fact that an N value at one R value, is polarimetrically equivalent to a different N at a different R. The maximum possible value of f is 0.38 $(10^{12}/R_*)^2$ attained when $R^2 = 1.5R_*^2$ so that N must take a value greater then those shown in Table 2.3 by a factor ~ $3(R_*/10^{12})^2$. The absolute values of N cannot be determined by the polarimetry since R is unknown (and may vary with time) but the numbers in Table 2.3 imply a value of N, near the polarisation peak, exceeding 3×10^{47} electrons. For ionised hydrogen this corresponds to a scattering mass of 5×10^{23} g. If a comparable mass is accreted by a neutron star (X_2) of $2M_\odot$ the resulting X-ray outburst should contain about 10^{44} erg or a peak luminosity of about 10^{39} erg s^{-1} over an X-ray burst peak of one day, closely comparable to that observed (Skinner 1980). Our data imply that comparable fractions of the material drawn from the Be star and its disc are accreted by X_2 and remain in the vicinity of X_1, though the relative proportions may vary greatly from one periastron passage to the next. Careful polarimetric monitoring with simultaneous X-ray coverage could thus reveal the variability of this episodic mass-loss fraction.

As far as the angular location of the scattering centroid is concerned, this is most readily seen from Fig. 2.7(a) and (b) which portray in polar coordinates the polar angle Λ of the scatterers, and a radial cordinate measuring the amount of scattering material (in terms of 10^{-46}fN) for those points in Table 2.3 where it is adequately determined. Of course every point can take the value Λ or $\Lambda + \pi$, but in plotting them we have adopted solutions in the same quadrant on the grounds of continuity. The loci of two sets of solution points are shown in Fig. 2.7(a) an (b) for the data in Table 2.3 in which Λ is adequately determined. For both outbursts, phase points are marked

Figure 2.7a

The curves in the upper part of the figure are the polar plots of the properties of the 'effective scattering centroid' inferred from the data. The radial coordinate here is $fN(x10^{-46})$, a measure of the number of scatterers, and the polar angle Λ, their longitude,for the Hutchings et al. orbit. While this cannot show where the scatterers are located, increased distance from the origin in this plot indicates an increase in the optical depth of the scattering centroid while Λ indicates its angular location. The filled circles derive from the observations of outbursts 75 and 99 at the following phase points corresponding to the adjacent labels. (the first three observations which have the largest errors have not been included).

Phase Points Outburst 75

a = 0.987, b = 0.056, c = 0.101, d = 0.114, e = 0.172, f = 0.232,

g = 0.286

Phase Points Outburst 99

1 = 0.40, 2 = 0.46, 3 = 0.88, 4 = 0.94, 5 = 0.001, 6 = 0.002

7 = 0.062, 8 = 0.063, 9 = 0.122, 10 = 0.124

The ellipse in the lower half of the figure is a polar (r,λ) plot of the A0538-66 orbit using the Hutchings et al. parameters with the location of the secondary marked for each data point. Peiastron lies near the marked number 6. Comparison of the upper and lower panels point by point enables comparison of the evolution of thescatterer location and effective mass with the orbital motion of the neutron star.

Figure 2.7a

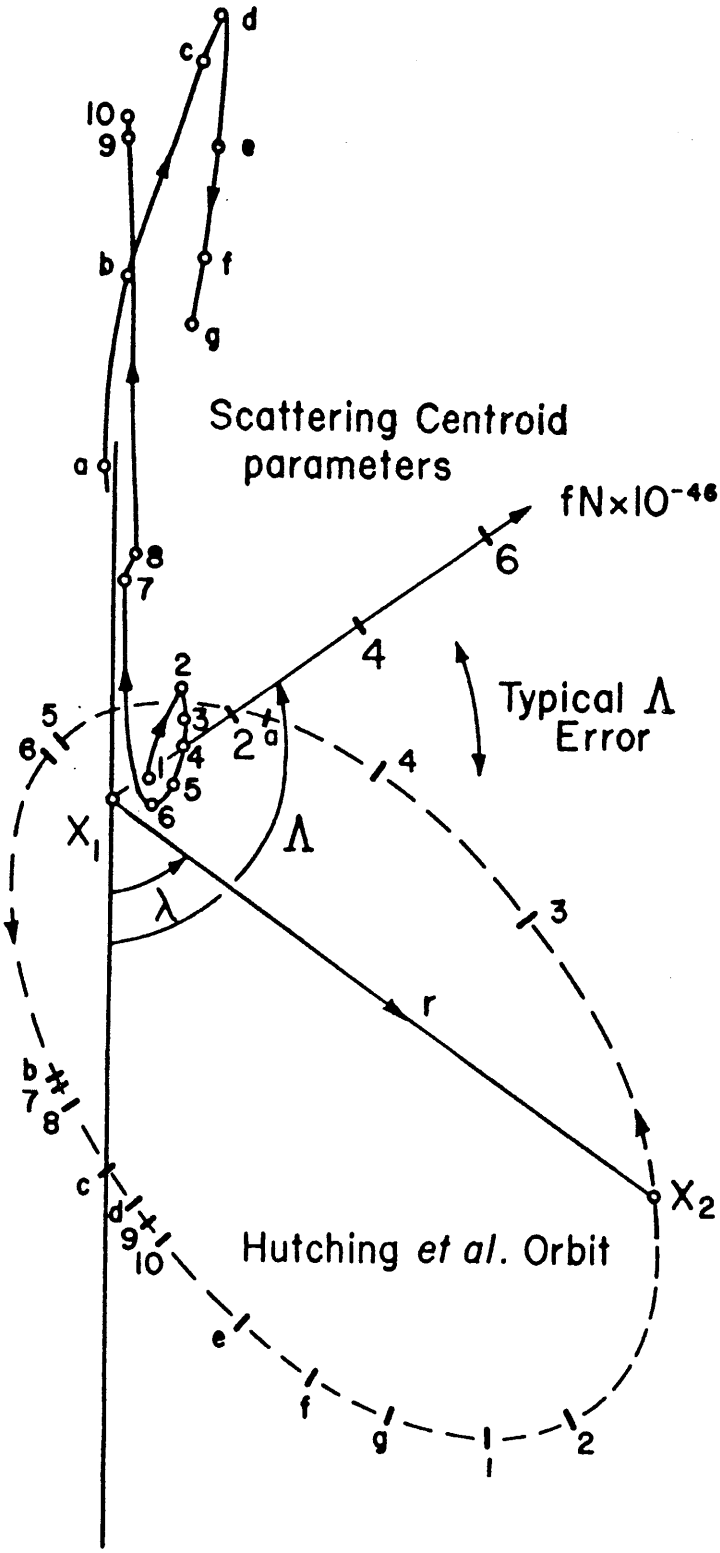
Scattering Centroid
parameters
fN×10⁻⁴⁶
Typical Λ
Error
Hutching *et al.* Orbit
X1
X2
Λ
λ
r

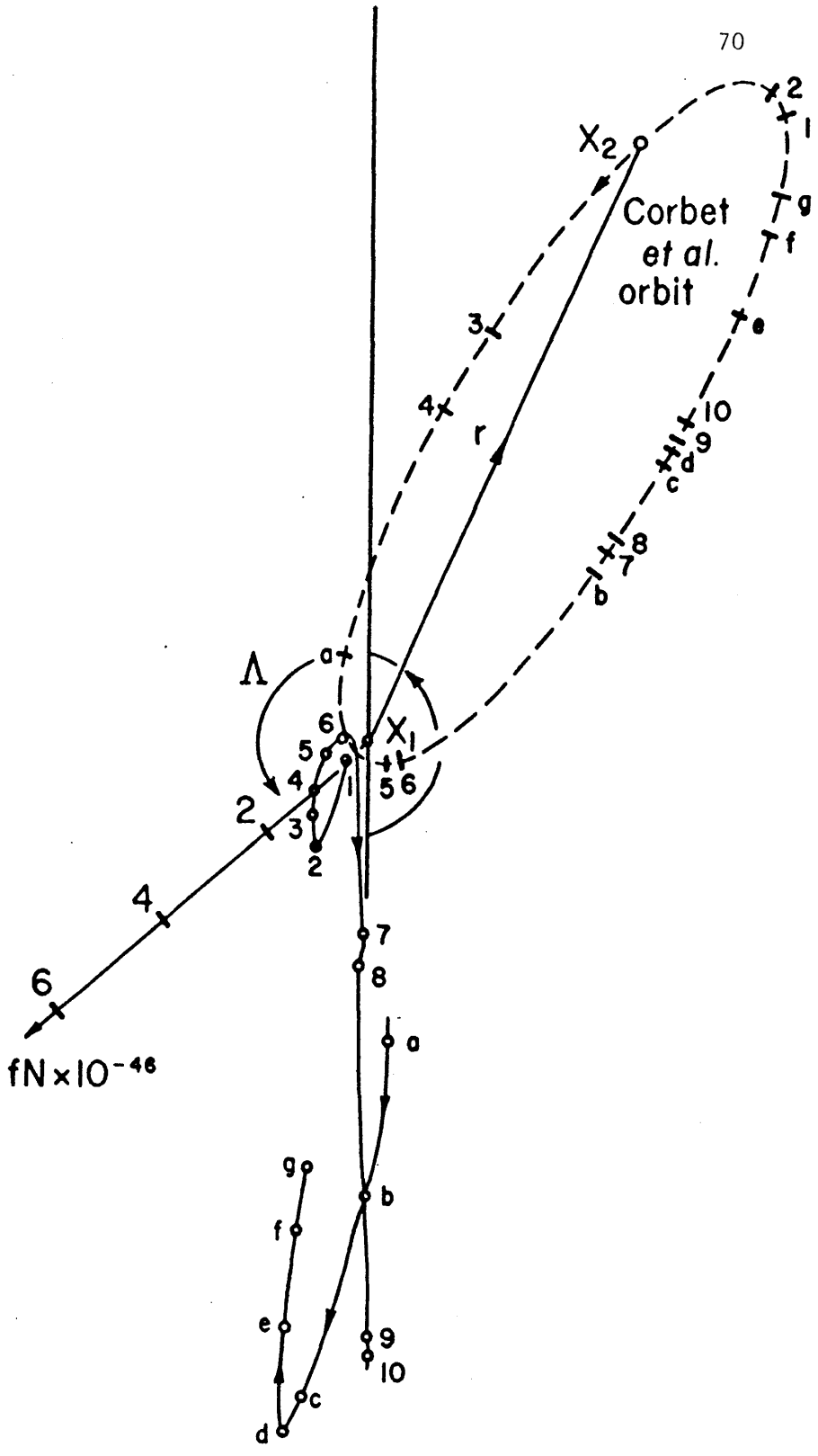

Figure 2.7b

The same as Fig.2.7a but for the elements of Corbet et al. (periastron lies between the points marked a and 5 in the lower panel). In this case the orbital ellipse is in the upper part of the diagram and the alternative scatterer longitudes Λ (shifted by 180°) have been adopted so that the scattering centroid locus lies in the lower part of the figure.

on the loci. Also shown are the phased positions of X_2 around its orbit for both Corbet et al. and Hutchings et al. parameters.

Assuming on physical grounds that the scattering material emerges near the periastron rather than the apastron longitude, we interpret the results as meaning that the scattering mass is either ejected around $\Lambda \approx 180^\circ$ close to the encounter ω value of Hutchings et al. (Fig. 2.7a) or around $\Lambda \approx 0^\circ$ close to the ω value of Corbet et al. (Fig. 2.7b). Prior to outburst 99, the Λ value is in the neighbourhood of 90° (or 270°) which is that of a point-scattering equivalent to a disc. This is not confirmatory of the model proposed, but only automatically consistent with it by our original choice of the Φ_o axis. Thereafter the small pre-outburst (disc) polarisation is rapidly swamped by the large polarisation associated with the large enhancement of scatterers N_3 near the periastron point. It is also worth noting that the pre-outburst value of $fN \approx 10^{46}$ implies there are $\sim 10^{47}$ electrons in the quiescent disc (again taking $f \leqslant 0.3$ and allowing for the factor of $^1/_3$ depolarisation due to the averaging of scattering angles around a flat disc (cf. Brown and McLean, 1977). If these disc electrons are spread throughout a volume of order R_*^3 the implied disc electron density is $n_e(cm^{-3}) \approx 10^{11}(10^{12}/R_*)^3$, typical of Be star disc density estimates (Poeckert and Marlborough, 1978a). At the phase points well after periastron in outburst 75, Fig. 2.7 shows a decline in N back toward the origin, presumably indicating that the circumstellar material is settling back toward its quiescent state. In the pre-periastron points of outburst 99, there may also be an indication that the circumstellar material is still reverting to its pre-outburst state after outburst 98 of the previous orbit, by redistribution in both longitude and radius.

The major features of physical interest in these results is the remarkable persistence of the mass and the direction Λ of the scattering centroid material. Thus, although X_2 presumably carries off and accretes a large mass which rapidly becomes polarimetrically negligible as already discussed, a comparable mass enhancement has to persist near the Be star, close to the periastron position for a long time (compared to the decay time of the photometric light curve). This time is longer than the orbital time for material close to the Be star and therefore longer than the inner Be star disc Keplerian rotation time-scale, and more comparable to the time-scale of the hydrodynamic travel across the disc $\approx R_*/v_s \approx 10$ days for a temperature of 10^4 K. Finally, it would be entirely consistent with the data if the scattering cloud were not a single material entity but rather a localised disc-density enhancement sustained by non-radial oscillations in and mass loss from, the stellar envelope set up by its distortion at periastron. The resulting outflow speed would have to be well above the escape speed so that rotation would not deflect the ejecta greatly. Secondly, the impulse delivered to the material in the disc and the star near the periastron point, during the rapid flyby of the neutron star, will be essentially radial and along the periastron line. thus the velocity field set up in the Be star matter will, at least initially, be in the direction of the enhancement required polarimetrically.

2.5 Discussion and Conclusions.

Whilst the data presented here are clearly undersampled compared to the rapidity with which the system geometry changes near periastron, our analysis shows the value of even limited polarimetric data as a diagnostic of recurrent transient mass distribution. The

analysis used here can be re-applied when more definitive orbital elements and better polarimetric data are obtained for this system. Clearly, frequent monitoring through the critical periastron encounter could be much more informative still, possibly containing the signature of the rapidly moving material accreted by the neutron star. Whatever this may reveal, we have established the necessity for there to be an additional major gas outflow from the Be star region near the periastron point and persisting there long after the neutron star has moved away. This result is strongly suggestive that mass loss and transfer in a highly eccentric binary must be treated in terms of tidal stripping rather than as a quasi-steady Roche lobe overflow or wind accretion phenomenon as suggested by some authors (Brown and Boyle, 1984; Apparao, 1985). An important theoretical question is whether the tidally stripped cloud producing the polarisation could also be hot enough to contribute significantly to the X-ray emission? Clearly the value of polarimetric coverage would also be greatly enhanced if good simultaneous optical and X-ray photometry were achieved.

It is unfortunate that our pre-outburst data are so scanty and, in the case of outburst 75, of low precision. Better coverage of this phase would test our interpretation that the pre-outburst polarisation is that of the normal Be star disc, and elucidate how fixed the plane of the disc is, and how variable it is in extent. The well known variability of single Be star discs inferred from polarimetric monitoring could well play a key role in determining the 'on-off' behaviour of outbursts in A0538-66 by presenting very different gas configurations to the neutron star at its periastron passages. Indeed a period of rising polarisation in the quiescent state could well presage a return of the system to its 'on' state.

Chapter 3

Stellar Occultation of Polarised Light from Circumstellar Electrons: I. Flat Envelopes Viewed Edge On.

3.1 Introduction.

Over the past decade there has been extensive use of light scattering off of circumstellar electrons as a diagnostic of geometric and physical conditions at the source. Applications (Poeckert and Marlborough, 1977; Brown et al., 1978; Dolan and Tapia, 1984, 1989; Drissen et al., 1986a, b; Huovelin et al., 1987; Brown and Henrichs, 1987) have been largely based on the point source/single scattering analytic treatment formulated by Brown and Mc.Lean (1977), Brown et al. (1978) and by Rudy and Kemp (1978). It has been shown by detailed numerical simulations that the results of this simplified treatment remain reasonably accurate even where multiple scattering and finite size light source effects are included (Daniel, 1980; Dolan, 1984) and even, in some cases, for non-Rayleigh scattering functions (Simmons, 1982, 1983). Most recently Cassinelli et al. (1987) have shown how a simple analytic depolarisation correction can be made to the point source results for a finite light source (cf. more general discussion by Brown, 1989).

Thus far almost no attention has been paid to the second effect of a finite stellar light source, namely its occultation of some of the scattering region, though Milgrom (1978) drew attention to its potential importance in complicating the interpretation of polarimetric variations by considering one special geometry and applying it to Cygnus X-1.

In this chapter we present the results of the first stage of a

general study of scatterer-occultation effects, examining the special case of oscillators confined close to the plane containing the observer. We will assume throughout that the light source is unpolarised (Collins, 1989) and that the envelope is purely a scattering one.

From previous analyses of polarimetric observations (Brown et al., 1978; Simmons et al., 1980; Drissen et al., 1986a, b) it appears that scatterers are distributed quite symmetrically about the orbital plane in a number of binaries. Indeed, physically we expect scatterers to be concentrated close to the orbital plane, in such cases as accretion discs, accretion streams, accretion wakes and focussed stellar winds. In the case of single stars (particularly Be stars) joint spectral and polarimetric analysis (Poeckert and Marlborough, 1977, 1978a; Brown and Henrichs, 1987) also point to almost planar disc distributions of circumstellar gas. We therefore believe that a theoretical study of the polarimetric effect of occultation of scatterers confined to a plane is a sound starting point. Clearly the results of such a study will depend on the observers direction. Our adoption in this chapter of a 90° inclination (i) - i.e. observer in the plane of the scattering material - is based on a desire to see what are the maximal effects of occultation and to obtain analytical simplification to reveal the primary features of occultation effects before proceeding to a more general analysis for arbitary inclination (chapter 4) and general axisymmetric envelopes (chapter 5). In an actual case of $i = 90°$ in an arbitrary system, there will inevitably also be the possibly important effects of stellar eclipses and scatterer occultation by both stars (even if the companion is faint and unimportant as a light source - cf. Sec. 1.4.2). Our analysis therefore, is to be understood as applying directly to those binary orbital phases when stellar eclipsing and secondary scatterer

occultation are not important.

After a general formulation of the problem (section 3.2) we will investigate (section 3.3) how Be star polarisation is affected when we include stellar occultation of a uniform disc scattering region, and how binary polarimetric variations could be used to infer properties of the radial and azimuthal scatterer distributions in the case of a one dimensional (plume like) scattering region (section 3.4) and a two dimensional (general planar) scattering region (section 3.5).

3.2 Polarisation of an Occulted Plane Electron Distribution.

Consider a near plane distribution of electron (or Rayleigh) scatterers of surface density $\Omega(x,\theta)$ (cm^{-2}) at polar coordinates (r,θ) ($r = xR_*$) centred on a uniform spherical star of radius R_* and luminosity L_*. By symmetry, all polarisation vectors are normal to the plane of Ω when the system is observed in this plane. An elementary area $dA = rdrd\theta$ at (r,θ) in the single Thomson scattering limit, contributes a polarised flux at the earth, distance d, of

$$dF_p = \frac{L_*\sigma_o}{4\pi d^2}\ \Omega(x,\theta)\ \frac{D(x)}{x}\ \cos^2\theta\ dxd\theta \qquad (3.1)$$

$$D(x) = \frac{(x^2-1)^{1/2}}{x} \quad , \quad \sigma_o = \frac{3\sigma_T}{16\pi} \qquad (3.2)$$

where D(x) is the depolarisation factor to allow for a finite range of incident light directions from the star (Cassinelli et al., 1987), and σ_T is the Thomson cross section.

The direct flux of unpolarised starlight is $F_* = L_*/4\pi d^2$, which will much exceed the total scattered flux in the single scattering limit, so that the net polarisation observed will be

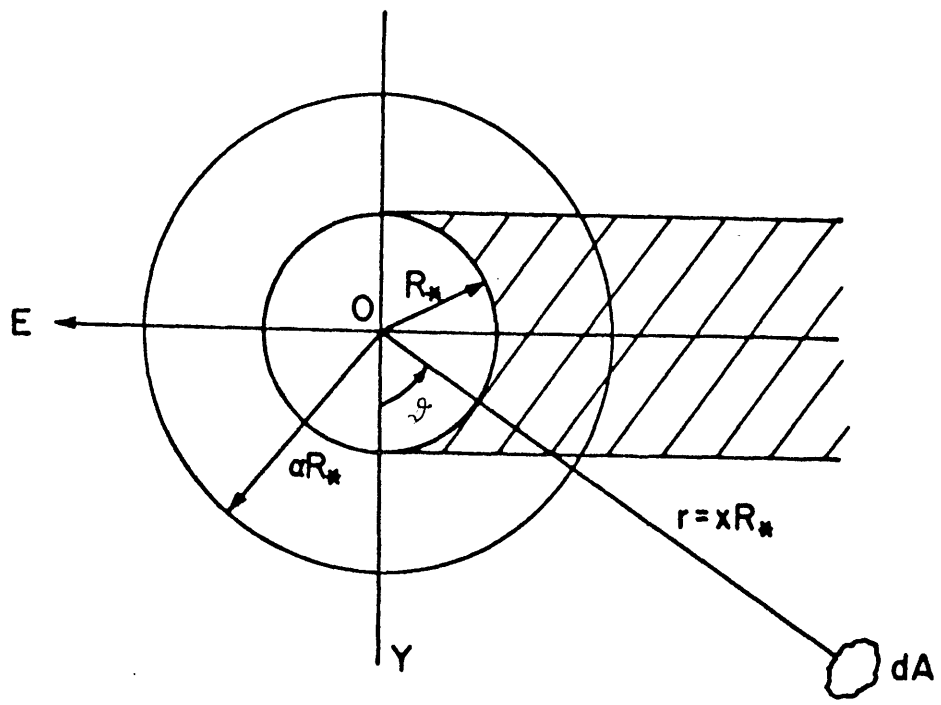

Figure 3.1

The coordinates (x,θ) are centered on the star, at O, of radius R_*. The observer is at E (along the x-axis) in the plane of the disc. The disc extends from the stellar surface to a finite radius, which is taken as αR_*. θ is measured anticlockwise from the y-axis. The occulted region is the hatched area.

$$P = \frac{F_p}{F_*} \tag{3.3}$$

$$\text{i.e.} \quad P = \sigma_o \iint_A \frac{D(x)}{x} \Omega(x,\theta)\cos^2\theta \, d\theta dx \tag{3.4}$$

where A = total area of Ω seen by observer.

Inspection of Fig. 3.1 shows that this can be written as

$$P = \frac{1}{2}\sigma_T \Omega_o \Big[\int_1^\infty \int_0^{2\pi} \frac{D(x)}{x} f(x,\theta)(1 + \cos 2\theta) \, d\theta dx - \int_1^\infty \int_{\sec^{-1}x}^{\pi - \sec^{-1}x} \frac{D(x)}{x} f(x,\theta)(1 + \cos 2\theta) \, d\theta dx \Big] \tag{3.5}$$

where $f(x,\theta) = \Omega(x,\theta)/\Omega_o$, measures Ω in units of a convenient (e.g. mean) surface density Ω_o. The outer upper integral limit has been set at ∞. In practice this is to be understood to mean either the finite disc radius or the maximum distance to which single scattering still applies - photons multiply scattered along large optical depths will contribute little to the polarisation.

3.3 Polarisation from a Single Be Star Disc with $\Omega = \Omega(x)$.

Be star envelopes have been modelled in terms of equatorial discs of matter (Poeckert and Marlborough, 1976; Rudy and Kemp, 1978; Kemp, 1980; Poeckert, 1982; Waters, 1986 and Dachs et al., 1986), which were initially proposed by Struve (1931), and sometimes in terms of approximately spherically symmetric shells (c.f. Doazan and Thomas, 1982; Doazan, 1987). In the latter case it is claimed that little deviation from spherical is needed to explain the observed polarisations of ~ 2%

for Be stars. This was similarly claimed by McLean and Brown (1978), who concluded from the statistics of the observed polarisations that extremely oblate envelopes presumably do not exist. We wish to emphasise that this is not correct for all stars. For a disc with a point source illumination from its centre, the highest (theoretical) polarisation achievable is ~14% before multiple scattering begins to reduce the polarisation (see Sec. 3.3.3). Since most of the scattering occurs near the star, however, the effects of finite source depolarisation and of scatterer occultation will both be substantial, and this 14% figure is a gross over estimate.

Here we will examine these two effects quantitatively and show that indeed flat discs are essential to obtain the observed degree of polarisation (c.f. Cassinelli, 1987).

We take the envelope to be axisymmetric with $f(x,\theta) = F(x)$ and to have an outer boundary at $x = \alpha$. Then the integration of the occulted region (see Fig. 3.1) can be written explicitly as

$$\iint_{A_{occ}} = \int_{1}^{\alpha} \int_{\sec^{-1}x}^{\pi-\sec^{-1}x} \qquad (3.6)$$

Then,

$$P = \pi\sigma_o\Omega_o \int_{1}^{\alpha} \frac{F(x)D(x)}{x}\left[\frac{1}{2} + \frac{1}{\pi}\left\{\sec^{-1}x + \frac{(x^2-1)^{1/2}}{x^2}\right\}\right] dx \qquad (3.7)$$

For comparison purposes we note that when no account is taken of depolarisation or occultation, the polarisation is,

$$P_o = \pi\sigma_o\Omega_o \int_1^{\alpha} \frac{F(x)}{x}\, dx \qquad (3.8)$$

When account is taken of depolarisation, but not occultation it is,

$$P_1 = \pi\sigma_o\Omega_o \int_1^{\alpha} \frac{F(x)D(x)}{x}\, dx \qquad (3.9)$$

and when account is taken of occultation but not depolarisation it is,

$$P_2 = \pi\sigma_o\Omega_o \int_1^{\alpha} \frac{F(x)}{x}\left[\frac{1}{2} + \frac{1}{\pi}\left\{\sec^{-1}x + \frac{(x^2-1)^{\frac{1}{2}}}{x^2}\right\}\right] dx \qquad (3.10)$$

Inspection of (3.7)-(3.10) shows that P_1, P_2 and P are always smaller than P_o whatever F(x) is. We now calculate how large the reduction is for two special cases of interest.

3.3.1 Uniform Finite Disc.

We set $F(x) = 1$ for $1 < x < \alpha$ and zero otherwise.

Then for equations (3.7)-(3.10) we obtain the following,

(i) point source with no occultation,

$$P_o = \pi\sigma_o\Omega_o \ln\alpha \qquad (3.11)$$

(ii) Extended source with no occultation,

$$P_1 = \pi\sigma_o\Omega_o\left[\ln(\alpha + \{\alpha^2 - 1\}^{\frac{1}{2}}) - \frac{(\alpha^2 - 1)^{\frac{1}{2}}}{\alpha}\right] \qquad (3.12)$$

(iii) Point source with occultation,

$$P_2 = \pi\sigma_o\Omega_o\left[\frac{1}{2}\ln\alpha + \frac{1}{2\pi}\sec^{-1}\alpha - \frac{(\alpha^2 - 1)^{\frac{1}{2}}}{2\pi\alpha^2} + \frac{1}{\pi}\int_1^{\alpha} \frac{\sec^{-1}x}{x}\, dx\right] \qquad (3.13)$$

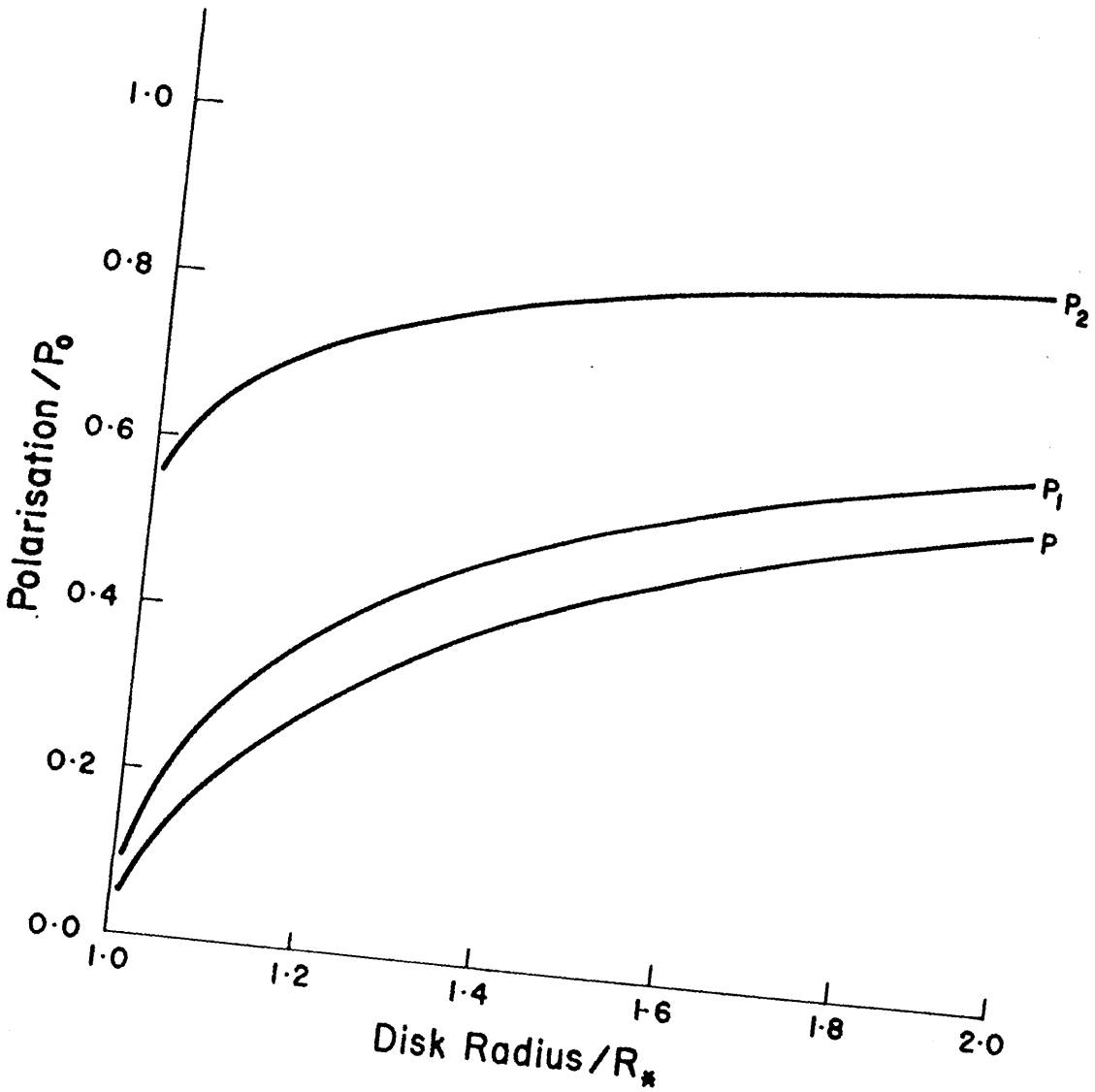

Figure 3.2

A plot of the polarisation values P, P_1, P_2 compared to P_o as a function of disc radius (α) for a finite axisymmetric disc.

(iv) Extended source with occultation.

$$P = \pi\sigma_o\Omega_o$$

$$P = \pi\sigma_o\Omega_o\left[\frac{1}{2}\left\{\ln(\alpha + (\alpha^2 - 1)^{\frac{1}{2}}) - \frac{(\alpha^2 - 1)^{\frac{1}{2}}}{\alpha}\right\}\right.$$

$$\left. + \frac{1}{\pi}\left[\frac{2}{3} + \frac{1}{3\alpha^3} - \frac{1}{\alpha}\right] + \frac{1}{\pi}\int_1^{\alpha} \frac{(x^2 - 1)^{\frac{1}{2}}}{x^2} \sec^{-1}x \, dx \right] \qquad (3.14)$$

In Fig. 3.2, we show the values of P, P_1, P_2 compared to P_o as a function of α. It is clear that even when a disc has uniform density over a considerable range ($x \sim 2$) the real polarisation is a factor of ~2 less than obtained by a point light source approximation. As α approaches 1, the polarisation $P_2 \sim P_o/2$ when only occultation is considered (because precisely half of the scatterers are hidden) and tends to zero (i.e. P_1, $P \rightarrow 0$) when depolarisation is included, as expected for material very close to the stellar surface.

3.3.2 Infinite Disc with $F(x) \sim x^{-n}$.

In a real stellar mass loss situation the scattering density will fall off with distance from the star (faster than r^{-2} for an accelerated wind in three dimensions - Waters, 1986).

Here we will examine the effects of depolarisation and occultation on such a structure in two dimensions, parameterising the density profiles as $\sim r^{-n}$, that is we adopt

$$F(x) = x^{-n} \qquad (3.15)$$

where Ω_o is now the surface density at the stellar boundary. We then obtain for,

(i) point source with no occultation,

$$P_o = \pi\sigma_o\Omega_o/n \qquad (3.16)$$

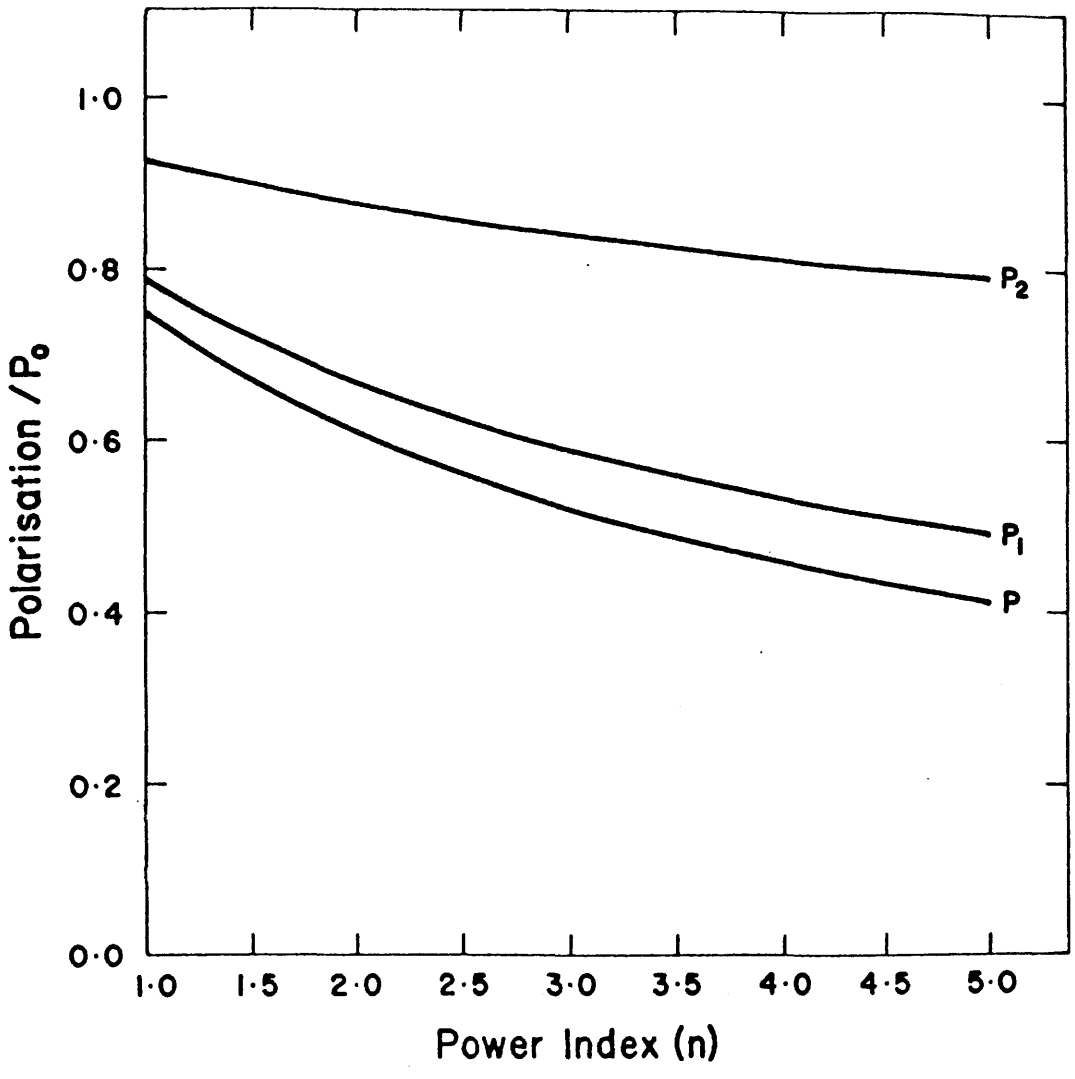

Figure 3.3

A plot of the polarisation values P, P_1, P_2 compared to P_0 as a function of power index n, for an infinite axisymmetric disc.

(ii) Extended source with no occultation, (setting $x = \sec\xi$)

$$P_1 = \pi\sigma_o\Omega_o\frac{1}{2}B(n/2, 3/2) \tag{3.17}$$

(iii) Point source with occultation,

$$P_2 = \pi\sigma_o\Omega_o\left[\frac{1}{2n} + \frac{1}{2n\pi}B((n+1)/2, 1/2) + \frac{1}{2\pi}B((n+1)/2, 3/2)\right] \tag{3.18}$$

(iv) Extended source with occultation,

$$P = \pi\sigma_o\Omega_o\left[\frac{1}{4}B(n/2, 3/2) + \frac{1}{2n\pi}B((n+1)/2, 1) + \frac{2}{\pi(n+1)(n+3)} + \frac{1}{n\pi}\int_0^{\pi/2} \xi\cos^{n+1}\xi\, d\xi\right] \tag{3.19}$$

where B is the beta function.

In Fig. 3.3 we show the values of P, P_1, P_2 compared to P_o as functions of n. As anticipated on the basis of Sec. 3.3.1 the effect of depolarisation is to greatly reduce the polarisation relative to the point source case, increasingly so as n increases.

3.3.3 Implications for the Shape of Single Star Envelopes.

The results of Cassinelli et al. (1987) and of the above sections, show that the combined effect of finite light source size and of envelope occultation is to reduce the scattering polarisation, in fact by a factor of about 2 for any realistic radial distribution of density. This means that the degree of envelope flattening needed to produce observed polarisations (for a given optical depth) is increased compared to estimates based on point star models. Since the necessary degree of flattening of circumstellar envelopes is controversial (cf. Doazan and Thomas, 1982; Cassinelli, 1987; Slettebak, 1988). We examine here the implications of these new results for the issue, assuming that

a similar factor of 2 reduction applies to envelopes which deviate from the plane (see chapter 5).

According to Brown and McLean (1977) the degree of polarisation in the optically thin scattering regime and for a point light source is

$$P_o < \frac{3\sigma_T}{16}\int_{-1}^{1}\int_{0}^{\infty} n(r,\mu)(1 - 3\mu^2)\, dr\, d\mu \qquad (3.20)$$

(equality applying for inclination i = 90°) where $n(r,\mu)$ is the density at radial distance r and colatitude $\cos^{-1}\mu$. The polarisation cannot be increased arbitrarily by increasing n because the onset of substantial optical depth reduces the polarisation by multiple scattering (Daniel, 1980). To model this approximately we assume that n(r) is uniform in latitude over an equatorial wedge of half angle $\sin^{-1}\mu_o$ for which equation (3.20) becomes

$$P_o < \frac{3}{8}\tau_*\mu_o(1 - \mu_o^2) \qquad (3.21)$$

where $\tau_* = \sigma_T\int_0^\infty n\, dr$ is the scattering optical depth.

Requiring roughly that $\tau_* < 1$ to avoid multiple scattering along any light path and maximising the right hand side of equation (3.21) over μ_o, we find that the maximum P_o is,

$$P_o < \frac{1}{4\sqrt{3}} \simeq 14\% \qquad (3.22)$$

occurring for a wedge of half angle $\sin^{-1}(1/\sqrt{3}) \simeq 35°$ (for an optically thick disc, a maximum theoretical value of 11.7% was obtained by Bochkarev and Karitskaya, 1983). When account is taken of the

reduction in polarisation for a finite stellar light source this gives

$$P \lesssim 7\% \qquad (3.23)$$

The intrinsic polarisations of B stars with P Cygni winds has been reported to be as high as 5% (Swings, 1981) and so these would appear, on the basis of equation (3.23), to require concentration of the wind into an equatorial sector as described above. On the other hand, most Be stars have polarisations $\lesssim$ 2% and so, on the strength of the argument above it might be believed that these could be consistent polarimetrically with envelopes either non-planar or more spherical than needed in the extreme P Cygni case. To probe this point further, it is necessary to consider a self consistent treatment in which the influence of geometry on the depolarising effect of multiple scattering is explicitly included. Such a treatment has not been carried out. However, we can obtain a fair first estimate by utilising the results of Daniel (1980) who has obtained contours of constant polarisation in the plane of equatorial optical depth and envelope oblateness, using a thick oblate ellipsoid as the envelope model. Here we will suppose Daniels' results apply when finite star effects are included by recalibrating the values of his isopolarisation contours downward by a factor of 2. Then from Daniel (1980, figure 5) we find that P Cygni polarisations of 5% (10% on his curves) can only be achieved, with optimised optical depth τ, for flattening factors E (polar/equatorial radius) $\lesssim 1/7$ while for more normal Be star polarisations of 2% (4% on Daniels' curves) flattening factors of $\lesssim 1/3$ are needed.

Given that envelope geometries and densities are hardly likely to conspire to provide the most optimal combination of E and τ and that most stars will not be seen at i = 90°, it is therefore clear that the polarisations of Be stars do demand highly equatorially flattened

envelopes. This conclusion will be further strengthened when absorption effects are included.

3.4 Variable Occultation as a Diagnostic of Scatterer Distribution in a Corotating System.

3.41 General Principle.

As is clear from section 3.3 (and from Brown and McLean, 1977) polarimetry of a single axisymmetric source yields essentially only one number describing the scattering envelope (the polarimetric position angle determining the orientation of the symmetry axis on the sky). Further, this number permits a multiplicity of interpretations depending on three distinct factors - envelope shape, density and inclination (Brown and McLean, 1977).

In systems where the envelope is non-axisymmetric and revolves about the light source, due to binary orbital motion or accretion disc precession for example, the situation is better because the variable scattering geometry in the observer's frame essentially enables an angular scan to be made over the envelope geometry and some of its parameters to be derived (Brown et al., 1978; Rudy and Kemp, 1978; Karitskya and Bochkarev, 1983; Carlaw and Brown, 1989). However only a rather small number of integral moments (or series expansion coefficients) can be derived from observations in this case. This is essentially because the Thomson scattering function which acts as the kernel of an integral equation relating the envelope angular distribution to the Stokes parameter variation (cf. Simmons, 1982, 1983) is slowly varying and of separable form (cf. Craig and Brown, 1986) such that all high spatial frequency components of the envelope

distribution are absent from the polarisation (cf. Brown, 1989).

However when we include scatterer occultation effects, we may anticipate that the situation may be further improved because the sharp boundary of the occulting star will scan across the scattering distribution as it rotates, so providing a one dimensional "narrow band" spatial filter with which to study the structure. It is also clear that the case of a flat distribution seen edge on is the easiest to treat theoretically in this problem and we illustrate the potential of the technique, starting with a one dimensional scatterer distribution which permits a unique inversion of the problem (section 3.4.2), and then proceeding to restricted and general two dimensional distributions (Appendix A).

3.4.2 Structure of One Dimensional (Plume Like) Envelope.

In the case of a mass-transferring binary, the circumstellar matter may, in some cases, approximate quite closely to an axisymmetric distribution of mass lost from the primary light source with a superposed one dimensional plume like structure. Such would be the case for example for accretion via a focussed stellar wind (Friend and Cassinelli, 1986) or a Roche lobe overflow accretion stream (Haisch and Cassinelli, 1976), or for stellar jets (e.g. Carlaw and Brown, 1989).

In the $i = 90^{\circ}$ case we are considering, the axisymmetric disc component will provide a constant polarisation (cf. section 3.3) which we will denote by P_D, provided occultation effects by the secondary are small (if not then a generalisation of the analysis in appendix A to the case of two occulters would be necessary).

The one dimensional plume we will represent in terms of a linear density $\Lambda(x)$ (cm^{-1}) of electrons per unit radial length (i.e. $\Lambda(x)R_{*}dx =$

number of electrons in dx) giving rise to a time dependent polarisation $P_L(t)$. If time t is chosen such that the plume is at $\theta = 0$ at time $t = 0$ (cf. later discussion) and rotates uniformly in period T (cf. fig. 3.1), then in (3.4) we must let

$$\Omega(x,\theta)R_*^2 x\,dx\,d\theta \rightarrow \Lambda(x)\delta(\theta-\omega t)R_* dx\,d\theta \ ,$$

where $\omega = 2\pi/T$ and δ is the delta fuction.

In this instance (3.4) becomes at phase angle $\theta = \omega t$

$$P_L(\theta) = \frac{\Lambda_o\sigma_o(1 + \cos 2\theta)}{2} \begin{cases} \int_1^\infty G(x)\,dx & \pi < \theta < 2\pi \quad (3.24) \\ \int_{|\sec\theta|}^\infty G(x)\,dx & 0 < \theta < \pi \quad (3.25) \end{cases}$$

$$\text{where } G(x) = \frac{\Lambda(x)(x^2-1)^{1/2}}{R_*\Lambda_o x^3} \quad \text{and } \Lambda_o = \Lambda(1) \qquad (3.26)$$

Observations of such a system should therefore exhibit pure second-harmonic ($\cos 2\theta$) phase variations, typical of an unocculted binary (Brown et al., 1978) on top of a constant contribution,

$$P_D + \frac{1}{2}\Lambda_o\sigma_o\int_1^\infty G(x)\,dx \qquad (3.27)$$

during half the rotation period ($\pi < \theta < 2\pi$), and more complex variations [depending on G(x)] during the other half as the value of $\sec\theta$ in the integral limit of (3.25) changes. Given any model of $\Lambda(x)$, P(t) can be computed throughout period T by means of (3.24) - (3.26).

It is also possible however, to invert this problem explicitly, thereby allowing inference of $\Lambda(x)$ from the data on P(t) as follows.

The time at which P(t) starts to exhibit variations other than on period T/2 identifies the time of zero phase. Once this is known we

can construct from the data, P(t), the function $2P(t)/(1 + \cos 2\theta)$ and on differentiation of (3.25) we get,

$$\frac{\Lambda(x)\sigma_o}{R_*} = \frac{x^2}{(x^2 - 1)}\left[\frac{-d}{d\theta}\left\{\frac{2P(\theta)}{1 + \cos 2\theta}\right\}\right]_{\theta=\cos^{-1}(1/x)} \qquad 0 < \theta < \pi \qquad (3.28)$$

Once the function $\Lambda(x)/R_*$ is found it can be integrated to give

$\frac{\Lambda_o\sigma_o}{2}\int_1^\infty G(x)\,dx$, and hence the disc polarisation contribution P_D.

In order to illustrate the potential of this inversion method, we shall construct a simple model calculation by considering an infinitely thin plume with effectively infinite radial extent ($r > 60R_*$ in our numerical simulation).

We let the plume density vary as x^{-2} and let the disc polarisation $P_D = 1.0\%$. Then the total polarisation may be written as

$$P(t) = 0.01 + \frac{\Lambda_o(1)\sigma_o}{R_*}\frac{(1 + \cos 2\theta)}{2}\begin{cases} \frac{\pi}{16} & \pi < \theta < 2\pi \\ \frac{1}{16}\left[\pi - 2\theta + \frac{\sin 4\theta}{2}\right] & 0 < \theta < \pi \end{cases} \qquad (3.29)$$

We set $\Lambda_o(1)\sigma_o/R_* = 0.001$ and so the polarimetric variation due to the plume is $\sim \pm 2\times10^{-4}$ (or 0.02%). We then evaluated P(t) for every $^1/_{36}{}^{th}$ of the phase (Fig. 3.4a).

Utilising (3.28) and making the approximation

$$\frac{df(\theta)}{d\theta} \approx \frac{f(\theta + h) - f(\theta - h)}{2h} \quad , \text{ with } h = {}^{\pi}/_{18} \qquad (3.30)$$

we obtain $\Lambda(x)\sigma_o/R_*$ as a function of x (Fig. 3.4b). In this particular case we need only apply (3.28) for $0 < \theta < {}^{\pi}/_2$ - due to symmetry.

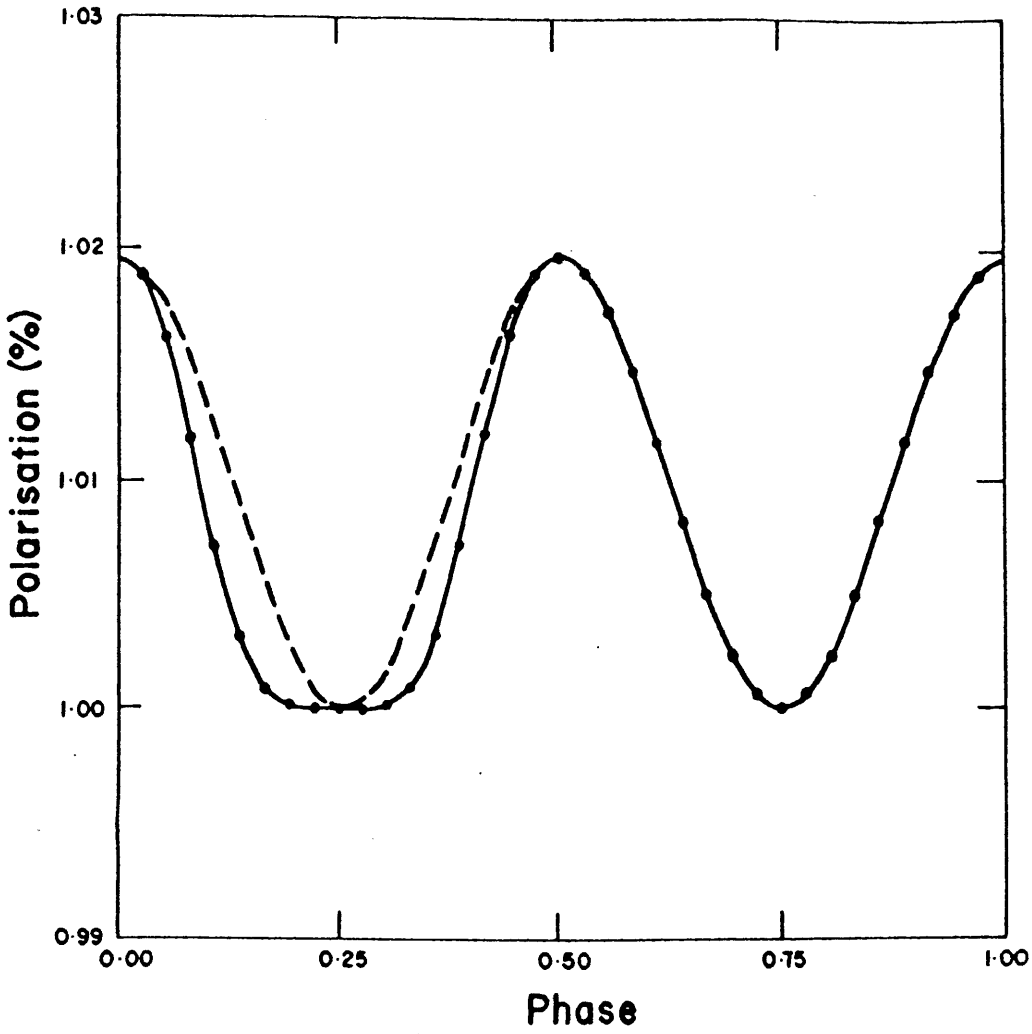

Figure 3.4a

A plot of the variation of polarisation (%) with phase for a corotating plume with occultation included (solid line) and with occultation neglected (dashed line).

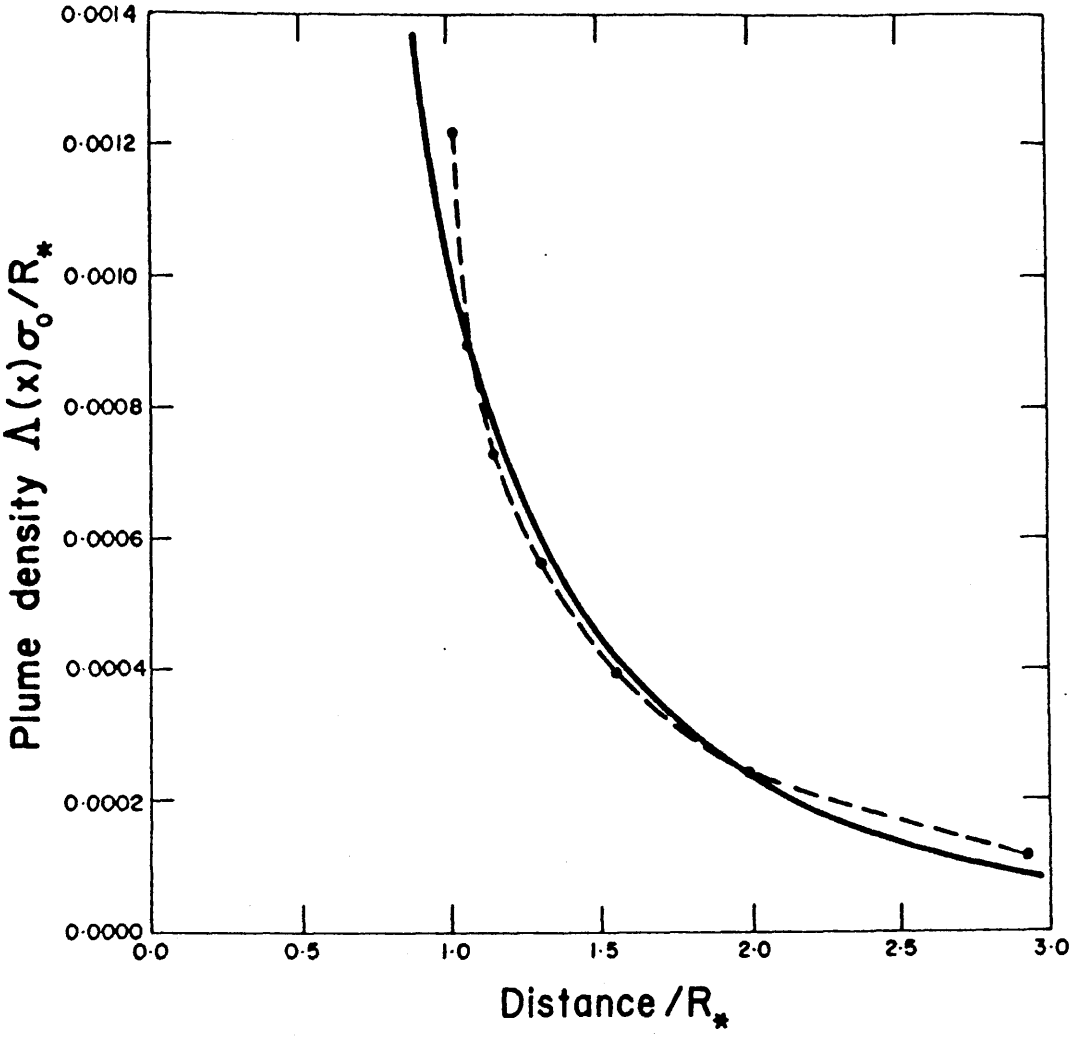

Figure 3.4b

Discretized (dashed line) and best fit (solid line) solutions for the variation of density with distance obtained from the inversion procedure.

From Fig. 3.4b we see that the method recovers a discrete form of $\Lambda(x)$ (dashed curve) close to the true x^{-2} distribution and with $\Lambda(1)\sigma_o/R_* = 9.75\text{x}10^{-4}$, very close to the correct value. Finally we find the disc polarisation to be $P_D = 0.10$ (1.00%).

In this particular example we have neglected noise and thus our inversion results are in excellent agreement with the input model. In practice problems may arise due to data noise, particularly if an attempt is made to push the discrete recovered solution toward the continuous limit ($h \rightarrow 0$), since then the approximation (3.30) to df/de may become swamped by changes in Δf due to noise rather than real changes. (On the other hand, too large a sampling interval, h, gives a poor recovery because of coarse discretisation errors). In such cases it will be necessary to apply a smoothness constraint on the solution to stabilize the inversion (differentiation) procedure against the effects of noise, as discussed by Craig and Brown (1986).

3.5 Conclusions.

We have shown in our analysis that the neglect of the finite size of the light source leads to a gross overestimate of the polarisation for a given disc geometry. By including occultation and depolarisation we found that B star envelopes are necessarily highly flattened disc type structures.

For a disc viewed edge on we find that the effect of occultation reduces the polarisation more than the inclusion of the depolarisation factor alone. This however is due to the fact that we have maximised the occulted region and one can expect that for a general inclination angle, the depolarisation factor will have the same reducing effect upon the observed polarisation, whereas occultation will become

decreasingly important as i decreases.

The analysis of a one dimensional plume led to a powerful technique that allows one to explicitly obtain the electron density distribution from the polarimetric data. Although we only inverted the problem for an infinite plume, it is a trivial matter to carry out a similar analysis for a finite plume (use of our formulation would just give $\Lambda(x) = 0$ for $x > \alpha$ in such a case).

The application of our present analysis is restricted to high inclination sources only. For Be stars therefore, such analysis will be limited to those stars with the largest apparent rotational velocities ($V\sin i \sim 400$ kms^{-1}).

Chapter 4

II. Flat Envelopes Viewed at Arbitrary Inclination.

4.1 Introduction.

In Chapter 3, we considered only the effect of scatterer occultation on circumstellar scattering polarisation for the case of an equatorial envelope seen at an inclination of 90°. In this chapter we generalise this problem to arbitrary inclination while retaining the other assumptions adopted and discussed in Chapter 3, namely

(i) Optically thin, single electron scattering envelope with no absorption.

(ii) A finite size, spherical light source that is unpolarised with constant intensity over its surface.

(iii) In a binary situation we assume the secondary is unimportant as a light source and we consider only those phases of the orbit when the secondary neither occults part of the scattering region, nor eclipses the primary.

The limitations of these assumptions will be discussed in Sec. 4.6.

After a general formulation of the problem we shall obtain expressions for the polarisation expected from the specific types of electron distributions considered in Chapter 3.

4.2 General Theory.

Consider (Fig. 4.1) a near plane distribution of electrons of surface density $\Omega(x,\Phi)$ (cm^{-2}) at polar coordinates (r,Φ) (where $r = xR_*$) centred on a uniform spherical star of radius R_* and luminosity L_*. Let the observer (E) have an inclination i between the line of sight

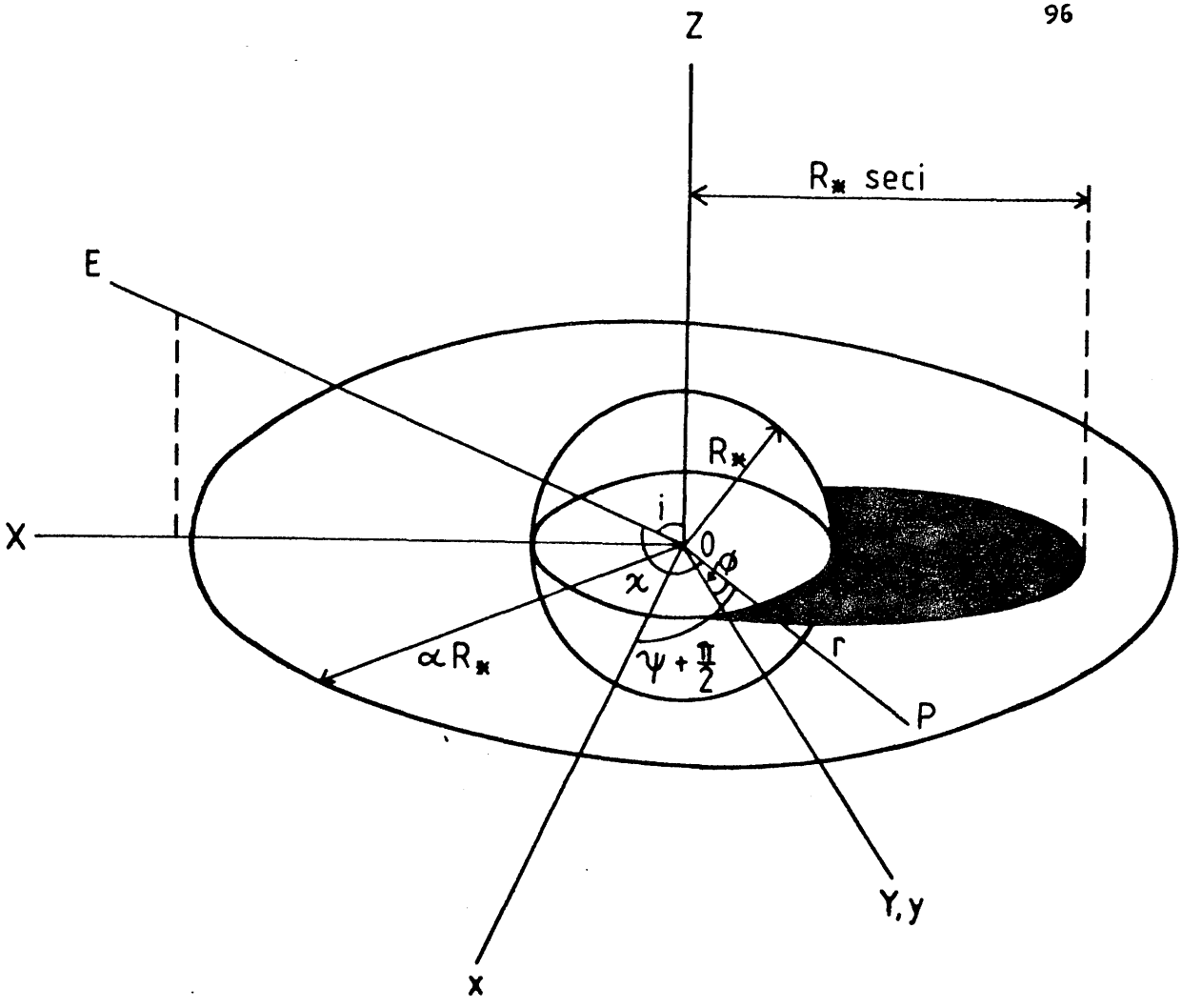

Figure 4.1

A star, centered at O, with a radius R_* rotates uniformly about the Z axis. A near plane distribution of electrons lie in the stars' equatorial (XY) plane. The electron distribution extends to a radius αR_*.

An observer (E) is inclined at an angle i to the rotation (Z) axis of the star. The observer-sky (x,y,E) axes (also centred on O) are oriented such that the y-axis coincides with the Y-axis of the stellar reference frame.

According to the observer, material directly behind the star is occulted. This occulted region (shaded area) is a half ellipse with a semimajor axis = R_*seci and a semiminor axis = R_*.

An electron at position P is described in spherical polar coordinates in the stellar frame by $(r,\pi/2,\phi)$ and in the observer frame by (r,χ,ψ).

and the normal to the plane containing Ω (Z axis).

In the frame of the observer, with associated spherical polar coordinates (r,χ,ψ), we can write the contribution to the Stokes fluxes at the earth associated with a scattering area dA, at a distance d

$$\left.\begin{matrix} dF_Q \\ dF_U \end{matrix}\right\} = \frac{L_*\sigma_o}{4\pi d^2 r^2}\,\Omega(x,\phi)\,dA \begin{cases} \sin^2\chi\,\cos 2\psi \\ \sin^2\chi\,\sin 2\psi \end{cases} \tag{4.1}$$

We transform from the (χ,ψ) observer oriented coordinates, to the (θ,ϕ) star centred coordinates which allows derivation of the polarisation from a general planar distribution of electrons.

The appropiate transformations are (Fig. 4.2)

$$\begin{aligned} \cos\chi &= -\sin i\,\sin\phi \\ \sin\chi\,\cos\psi &= \cos\phi \\ \sin\chi\,\sin\psi &= \cos i\,\sin\phi \end{aligned} \tag{4.2}$$

The direct flux of unpolarised starlight is $F_* = L_*/4\pi d^2$ at the Earth so that the observed normalised Stokes parameters are $Q = F_Q/F_*$ and $U = F_U/F_*$

which may conveniently be written as,

$$Q = \tau_o \sin^2 i + \tau_1(1 + \cos^2 i) \tag{4.3}$$

$$U = 2\tau_2 \cos i \tag{4.4}$$

where,

$$\tau_o = \frac{\sigma_o}{2}\iint_{A_o} \Omega(x,\phi)\,\frac{D(x)}{x}\,d\phi dx \tag{4.5}$$

$$\tau_1 = \frac{\sigma_o}{2}\iint_{A_o} \Omega(x,\phi)\frac{D(x)}{x}\,\cos 2\phi\,d\phi dx \tag{4.6}$$

$$\tau_2 = \frac{\sigma_o}{2}\iint_{A_o} \Omega(x,\phi)\frac{D(x)}{x}\,\sin 2\phi\,d\phi dx \tag{4.7}$$

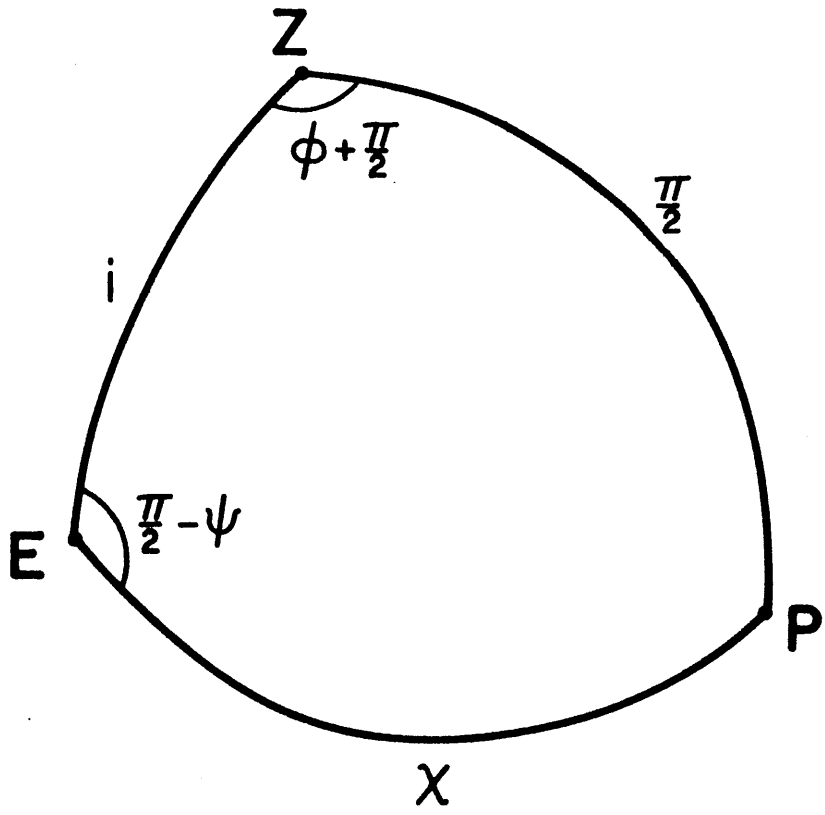

Figure 4.2

Spherical triangle from Fig. 4.1 for the transformation from (r,χ,ψ) to $(r,{}^{\pi}/_{2},\phi)$ coordinates.

with $D(x) = (1 - x^{-2})^{\frac{1}{2}}$ and $\sigma_o = \frac{3\sigma_T}{16\pi}$.

σ_T is the Thomson electron cross-section, D(x) is the depolarisation factor (Cassinelli et al., 1987) and A_o is the observed (unocculted) area of the electron distribution.

The integrals τ_o, τ_1, τ_2 are analogous to the integral moments τ_o, $\tau_o y_3$, $\tau_o y_4$ of Brown et al. (1978). In this case τ_o measures the effective scattering depth. τ_1 and τ_2 are measures of the rotational symmetry and antisymmetry (respectively) of the scattering material in the stars' reference frame, thus if the material is rotationally symmetric $\tau_2 = 0$.

The area A_o is the total area of the disc minus the occulted region. From Fig. 4.1 and Fig. 4.2 this may be written as

$$\iint_{A_o} = \int_1^{\alpha} \int_0^{2\pi} - \int_1^{\beta} \int_{\phi(x)}^{\pi-\phi(x)} \qquad (4.8)$$

where,

$\beta = \text{seci}$ for $\alpha \geqslant \text{seci}$

$\beta = \alpha$ for $\alpha < \text{seci}$

with the radius of the disc being α (in units of stellar radii)

and $\phi(x) = \sin^{-1}\left\{\frac{(1 - x^{-2})^{\frac{1}{2}}}{\text{sini}}\right\}$.

4.3 Axisymmetric Disc.

Recent observations (Dachs et al., 1986 and Waters, 1986) suggest that B type stars have extended, highly flattened circumstellar envelopes. In general such envelopes will be non-axisymmetric and thus give rise to polarimetric variations during the rotation of the system (see section 4.4).

In this section, however, we are concerned only with average polarisation expected from such a disc rather than its variation with phase and so we may write $\Omega(x,\phi) = \Omega(x)$. In this restricted case we have $U \equiv 0$ and so we may directly write $P = Q$. Using equations (4.3) - (4.8) we can obtain the expression for the polarisation of an axisymmetric disc, viz

$$P = \tau_0 \sin^2 i + \tau_1 (1 + \cos^2 i) \tag{4.9}$$

with $\tau_2 = 0$ and

$$\tau_0 = \frac{\sigma_0}{2}\left[\int_1^{\alpha} \int_0^{2\pi} \Omega(x)\frac{D(x)}{x}\, d\phi dx - \int_1^{\beta} \int_{\phi(x)}^{\pi-\phi(x)} \Omega(x)\frac{D(x)}{x}\, d\phi dx \right] \tag{4.10}$$

$$\tau_1 = \frac{\sigma_0}{2}\left[\int_1^{\alpha} \int_0^{2\pi} \Omega(x)\frac{D(x)}{x}\cos 2\phi\, d\phi dx - \int_1^{\beta} \int_{\phi(x)}^{\pi-\phi(x)} \Omega(x)\frac{D(x)}{x}\cos 2\phi\, d\phi dx \right] \tag{4.11}$$

Note that in equation (4.9) the τ_1 term vanishes if occultation is ignored, recovering the $P \propto \sin^2 i$ result of Brown and McLean (1977).

4.31 Uniform Finite Disc.

We set $\Omega(x) = \Omega_o$ for $1 \leqslant x \leqslant \alpha$

$= 0$ otherwise,

and substitute into equations (4.9) - (4.11) to obtain the following expressions for the polarisation,

(i) Point source with no occultation,

$$P_o = \pi\sigma_o\Omega_o \sin^2 i \ln\alpha \tag{4.12}$$

(ii) Extended source with no occultation,

$$P_1 = \pi\sigma_o\Omega_o \sin^2 i \left\{ \ln\{\alpha + (\alpha^2 - 1)^{\frac{1}{2}}\} - \frac{(\alpha^2 - 1)^{\frac{1}{2}}}{\alpha} \right\} \tag{4.13}$$

(iii) Point source with occultation,

$$P_2 = \pi\sigma_o\Omega_o \left\{ \sin^2 i \left[\ln\alpha - \frac{1}{2}\ln\beta + \frac{1}{\pi}\int_1^\beta \sin^{-1}\left[\frac{(x^2 - 1)^{\frac{1}{2}}}{x \sin i}\right] \frac{dx}{x} \right] \right.$$

$$\left. + (1 + \cos^2 i)\left[\frac{\cos i}{\sin^2 i}\right]\frac{1}{\pi}\int_1^\beta (x^2 - 1)^{\frac{1}{2}} \frac{(\sec^2 i - x^2)^{\frac{1}{2}}}{x^3} dx \right\} \tag{4.14}$$

(iv) Extended source with occultation,

$$P = \pi\sigma_o\Omega_o \left\{ \sin^2 i \left[\ln\{\alpha + (\alpha^2 - 1)^{\frac{1}{2}}\} - \frac{(\alpha^2 - 1)^{\frac{1}{2}}}{\alpha} - \frac{1}{2}\ln\{\beta + (\beta^2 - 1)^{\frac{1}{2}}\} \right.\right.$$

$$\left. + \frac{(\beta^2 - 1)^{\frac{1}{2}}}{2\beta} + \frac{1}{\pi}\int_1^\beta \frac{(x^2 - 1)^{\frac{1}{2}}}{x^2} \sin^{-1}\left[\frac{(x^2 - 1)^{\frac{1}{2}}}{x \sin i}\right] dx \right] \tag{4.15}$$

$$\left. + (1 + \cos^2 i)\left[\frac{\cos i}{\sin^2 i}\right]\frac{1}{\pi}\int_1^\beta (\sec^2 i - x^2)^{\frac{1}{2}} \frac{(x^2 - 1)}{x^4} dx \right\}$$

In Fig. 4.3 P_o, P_1, P_2, P are plotted as functions of inclination for various disc radii (α).

In general, it is found that for low inclination, occultation enhances the observed polarisation ($P_2 > P_o$, $P > P_1$) and for high inclination

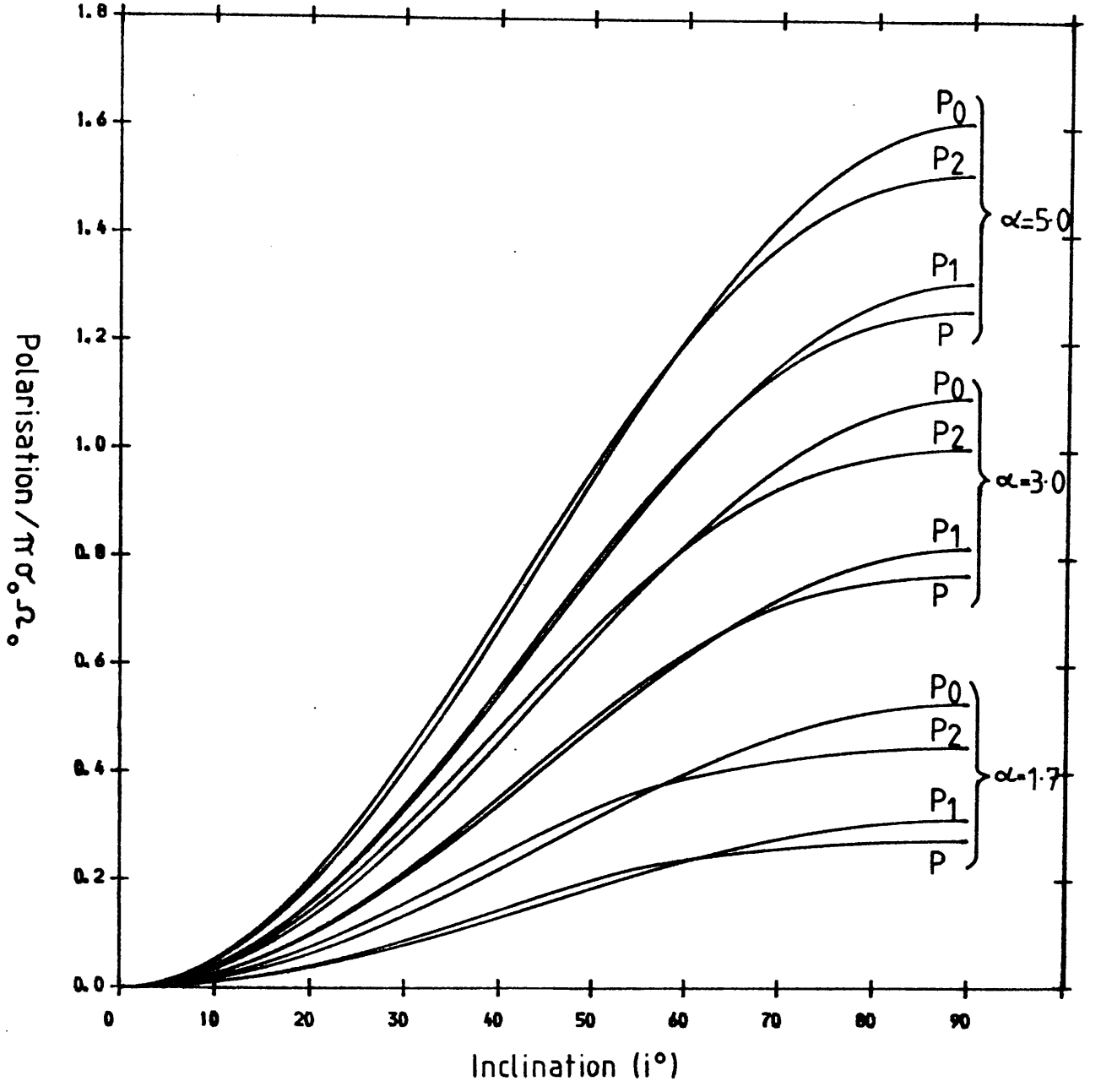

Figure 4.3

The variation of polarisation with inclination for a disc with uniform density Ω_0 (cm^{-2}) and of finite radial extent (αR_*). The definitions of P_0, P_1, P_2 and P are given in the text.

the polarisation is reduced ($P_2 < P_0$, $P < P_1$). For $\alpha > 2$ it is found that the "cross-over points" (i.e. when $P_0 = P_2$, $P_1 = P$) occur at a constant inclination independent of disc size, namely i ~ 58° for point light source calculations and i ~ 63° for extended light source calculations (we shall refer to the inclination at which this cross over occurs as the 'null' inclination).The explanation of this phenomenon results from the vector nature of polarisation and can understood geometrically.

Consider an equatorial disc of material viewed by a distant observer at an inclination i. At low inclinations the integrated polarisation of the whole disc will be near to zero, with the polarisation vector lying in a plane parallel to the system axis projected on the sky (see Brown, 1989; Poeckert and Marlborough, 1978a, their Fig. 13) whilst the occulted part of the disc will be polarised perpendicular to the projection axis. So when this is substracted from the net polarisation of the whole disc, the observable polarisation is enhanced and lies along the projected axis.

At high inclinations the plane of polarisation of the occulted region will be in the same plane as that of the disc as a whole (parallel to the projection axis) and so the net observed polarisation will be reduced.

There will be an inclination, therefore, when the plane of polarisation for the occulted region will switch orientation and at this inclination (the null inclination) the net polarisation of the occulted region will be zero, thus $P = P_1$, $P_0 = P_2$. It is clear that for a sufficiently large disc radius the null inclination will be independent of the disc size because the occulted region (a half ellipse with a semi-major axis of $R_* \sec i$) will be filled with scattering material (if the

radius of the disc is greater than $R_*\sec i$). In the point light source treatment this null inclination is 58° (from Fig. 4.3). Thus for a disc radius $r > 1.9R_*$ the null inclination will be always 58°. In the case of an extended light source treatment the emitted flux will be depolarised and thus in order for the polarisation of the occulted region to be zero this region will need to be larger than in the point light source approximation and therefore the null inclination will also be larger ($i \sim 63°$ and so the semi-major axis of the occulted region will be $2.2R_*$).

4.32 Infinite Disc with $\Omega(x) \sim x^{-n}$.

In a real stellar mass loss situation the scattering density will fall off with distance from the star.

We set $\Omega(x) = \Omega_o x^{-n}$,

where Ω_o is the surface density at the stellar boundary and in this instance $\alpha = \infty$ and $\beta = \sec i$. Substituting into equations (4.9) - (4.11) we then obtain,

(i) Point source with no occultation,

$$P_o = \pi\sigma_o\Omega_o \sin^2 i/n \tag{4.16}$$

(ii) Extended source with no occultation,

$$P_1 = \pi\sigma_o\Omega_o \sin^2 i \quad B(n/2, 3/2)/2 \tag{4.17}$$

(iii) Point source with occultation,

$$P_2 = \pi\sigma_o\Omega_o\Big\{ \sin^2 i\Big[\frac{1}{2n} + \frac{\cos^n i}{2n} + \frac{1}{\pi}\int_1^{\sec i} \sin^{-1}\Big[\frac{(x^2-1)^{1/2}}{x \sin i}\Big]\frac{1}{x^{n+1}}dx\Big] + (1+\cos^2 i)\Big[\frac{\cos i}{\sin^2 i}\Big]\frac{1}{\pi}\int_1^{\sec i} (\sec^2 i - x^2)^{1/2}\,\frac{(x^2-1)^{1/2}}{x^{n+3}}\,dx\Big\} \tag{4.18}$$

(iv) Extended source with occultation,

$$P = \pi\sigma_o\Omega_o\Big\{ \sin^2 i\Big[\tfrac{1}{2}B(n/2, 3/2) - \tfrac{1}{2}\int_1^{\sec i} \frac{(x^2-1)^{1/2}}{x^{n+2}}\, dx$$

$$+ \frac{1}{\pi}\int_1^{\sec i} \sin^{-1}\Big[\frac{(x^2-1)^{1/2}}{x \sin i}\Big]\frac{(x^2-1)^{1/2}}{x^{n+2}}\, dx \Big] \qquad (4.19)$$

$$+ (1 + \cos^2 i)\Big[\frac{\cos i}{\sin^2 i}\Big]\frac{1}{\pi}\int_1^{\sec i} (\sec^2 i - x^2)^{1/2}\, \frac{x^2-1}{x^{n+4}}\, dx \Big\}$$

where B is the beta function.

In Fig. 4.4 the polarisation values P_o, P_1, P_2, P are plotted as a function of inclination for power indices n = 1, 2 and 4 .

In general it is again found that at low inclination the net polarisation is enhanced by including occultation, whilst at high inclination the net polarisation is reduced when occultation is included.

For any given power index, the null inclination for a point light source (i.e. $P_o = P_2$) is always less than the corresponding null point for the extended source case (i.e $P = P_1$). This is again due to the depolarisation of the occulted region by the extended source which thus requires a greater inclination (i.e. a larger occulting region) than that of the point light source treatment in order for the net polarisation of the occulted region to be zero.

It should also be noted that as the power index increases the null inclination decreases. This can be physically explained by considering a star with most of the scattering material lying near the stellar boundary. Since most of the polarisation will arise near the star, it is reasonable to expect that the occulted region need only be small to

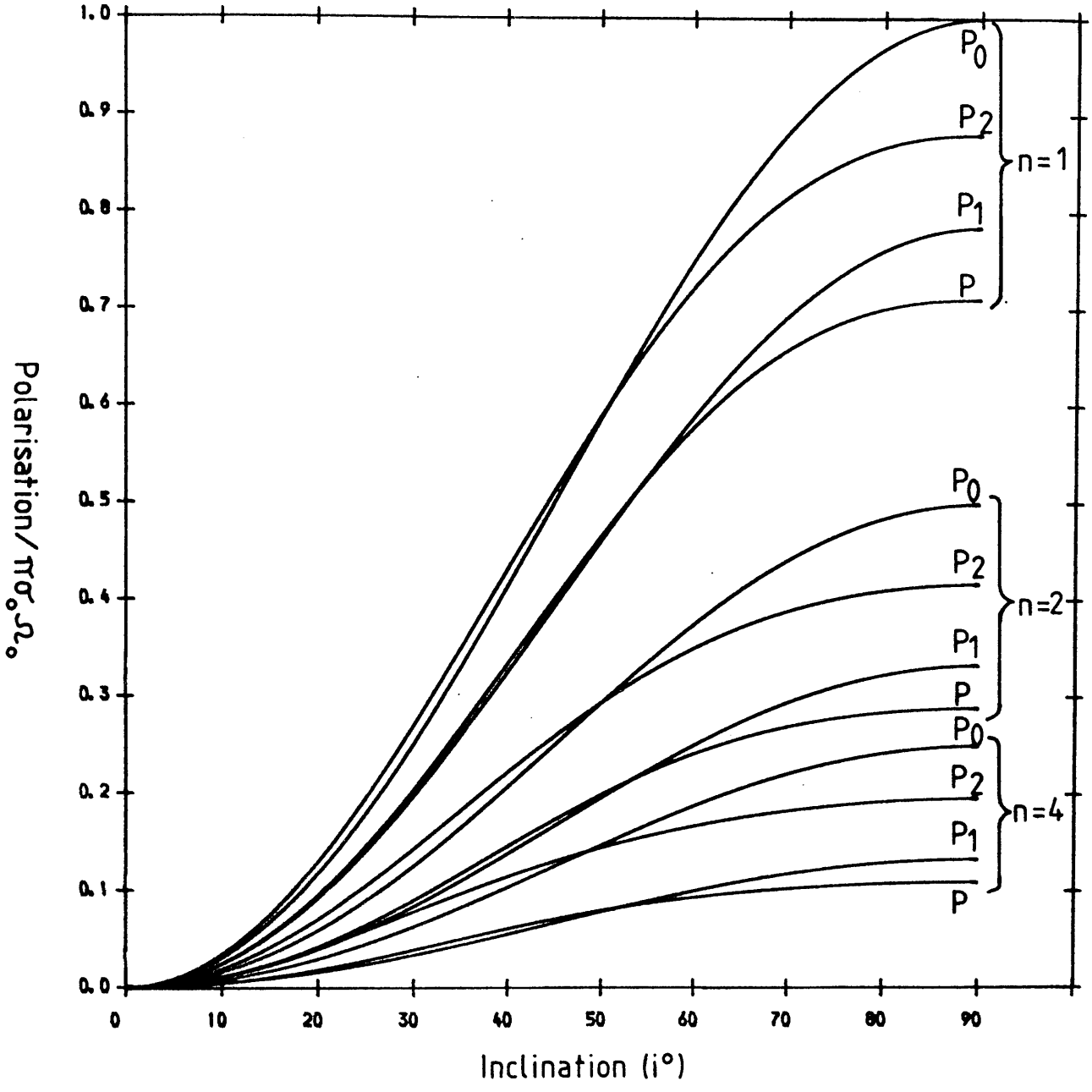

Figure 4.4

The variation of polarisation with inclination is shown for a disc with a number density of the form $\Omega(x) = \Omega_0 x^{-n}$. The definitions of P_0, P_1, P_2, and P are given in the text.

make a significant contribution to the polarisation. So the greater the concentration of the material about the star, the smaller the occulted region needed, and hence the smaller the null inclination for increasing power index.

4.4 One Dimensional (Plume Like) Density Structure.

We consider the phase variations of a rotating plume-like structure (e.g. accretion stream) superposed upon an axisymmetric disc.

Consider a plume in the equatorial plane of the star which rotates at a uniform angular frequency, ω. If the plume has linear density $\Lambda(x)$, then we must let

$$\Omega(x,\phi)R_*^2 x\,dx\,d\phi \longrightarrow \Lambda(x)\delta(\phi - \omega t)R_* dx\,d\phi.$$

At phase angle $\phi = \omega t$ an electron is just occulted at a distance ($r = xR_*$) where

$$x = \frac{1}{\sqrt{1 - \sin^2 i \sin^2\phi}} \tag{4.20}$$

Note that electrons at a distance $x > \sec i$ are never occulted, and for a plume of total length less than $\sec i$ total occultation will occur through some phase of the orbit.

In general at phase $\phi = \omega t = 2\pi t/T$ (where T is the orbital period) we have for the plume

$$Q = \tfrac{1}{2}\sigma_o\Lambda_o(\sin^2 i + (1 + \cos^2 i)\cos 2\phi) \begin{cases} \displaystyle\int_1^\infty G(x)\,dx \quad , \pi < \phi < 2\pi & (4.21) \\ \displaystyle\int_{x(\phi)}^\infty G(x)\,dx \quad , 0 < \phi < \pi & (4.22) \end{cases}$$

$$U = \sigma_o \Lambda_o (\cos i \sin 2\phi) \begin{cases} \int_1^\infty G(x)\,dx\,, & \pi < \phi < 2\pi \quad (4.23) \\ \int_{x(\phi)}^\infty G(x)\,dx\,, & 0 < \phi < \pi \quad (4.24) \end{cases}$$

where $x(\phi) = (1 - \sin^2 i \sin^2\phi)^{-\frac{1}{2}}$ and $G(x) = \frac{\Lambda(x)}{\Lambda_o} \frac{(x^2 - 1)^{\frac{1}{2}}}{R_* x^3}$ (4.25).

Equations (4.22) and (4.24) can be inverted to obtain $\Lambda(x)$ and i, viz

$$\frac{\sigma_o \Lambda_Q(x)}{R_*} = \frac{x^2}{(x^2 - 1)(1 - x^2\cos^2 i)^{\frac{1}{2}}} \left[\frac{-d}{d\phi}\left\{\frac{2Q_o}{\sin^2 i + (1 + \cos^2 i)\cos 2\phi}\right\}\right]_{\phi(x)} \quad (4.26)$$

$$0 < \phi < \pi$$

$$\frac{\sigma_o \Lambda_U(x)}{R_*} = \frac{x^2}{(x^2 - 1)(1 - x^2\cos^2 i)^{\frac{1}{2}}} \left[\frac{-d}{d\phi}\left\{\frac{U_o}{\cos i . \sin 2\phi}\right\}\right]_{\phi(x)} \quad (4.27)$$

where Q_o, U_o are the observed polarimetric data

and $\phi(x) = \sin^{-1}\left[\frac{(1 - x^{-2})^{\frac{1}{2}}}{\sin i}\right]$.

Equations (4.26) and (4.27) give two solutions for $\Lambda(x)$ for any chosen value of i. The general method of solution will be to seek simultaneous solutions of (4.26) and (4.27) in terms of $\Lambda(x)$ to noisy data, with i as an adjustable parameter with a range constrained by the condition that only solutions $\Lambda(x) \geqslant 0$ for all x are acceptable.

If there is sufficient coverage over the phase in which no occultation occurs, then it is possible to find the inclination of the system by use of equations (4.21) and (4.23) and therefore this will limit the parameter search required in (4.26) and (4.27). For low inclination systems it is apparent that the inversion procedure will not benefit us in any way as the density distribution will be determined over only a very short range. In fact in order to find the distribution to $1R_*$ beyond the stellar surface an inclination of 60° is required.

When noisy data is being inverted there is a limit (oversampling) to the number of data points that may be used to obtain meaningful results (Craig and Brown, 1986). In general the time lapse between any two measurements must be sufficiently large that they are significantly different (i.e. $Q(t + \delta t) - Q(t) \geqslant 2\delta Q$). This condition will depend upon both the inclination and the phase of the orbit. However it does mean that one cannot hope to obtain arbitrarily more information as to the density structure by increasing the data set. On the other hand, however, if the data are significantly undersampled or unevenly distributed throughout the period, then the density structure may be poorly inferred (undersampling) - that is, a wide range of density structures may have significant fits to the data.

We now illustrate the use of this inversion procedure by constructing noisy data for a plume viewed at an inclination $i = 70°$, with a density distribution of the form $\Lambda(x) = \Lambda_0(1)x^{-n}$ with $\Lambda(1)\sigma_0/R_* = 0.32/\pi$ and $n = 2.0$. We will assume, for simplicity, that the data is equally spaced (in time) in which case equations (4.21) and (4.23) can be manipulated so that the inclination of the system is obtained by calculating differences, thereby removing all constant polarimetric contributions, viz

$$\frac{Q(t + T/4) - Q(t)}{U(t + T/4) - U(t)} = \frac{1 + \cos^2 i}{\cos i} \operatorname{cotan}(2\Phi) \qquad \pi \geqslant \Phi \geqslant 3\pi/2 \qquad (4.28)$$

In equations (4.26) and (4.27) we make the approximation

$$\frac{df}{dx} \simeq \frac{f(x + h) - f(x - h)}{2h} \qquad (4.29)$$

Thus once the inclination has been found from equation (4.28), the density functions $\sigma_0\Lambda_Q(x)/R_*$ and $\sigma_0\Lambda_U(x)/R_*$ can be simultaneously obtained from equations (4.26) and (4.27).

In practice it has been found that the use of equation (4.29) makes equations (4.26) and (4.27) sensitive to the absolute value of the polarisation and so all constant contributions should be removed from the data before utilising this procedure (effectively the equations become dominated by the constant contributions). This is achieved by reconstructing the polarimetric data during out-of-occultation periods via (4.21) and (4.23) so that one is able to obtain the constant polarimetric contributions (Q_o, $U_o = 0$) due to the disc.

We wish then to find what is the single best fit density function of the form $(\sigma_o\Lambda_o(1)/R_*).x^{-n}$ for the data. We do this by varying $\sigma_o\Lambda_o(1)/R_*$ and n, in order to minimise χ^2 (Simmons et al., 1980) where

$$\chi^2 = \left[\frac{\sigma_o}{R_*}\right]^2 \sum_{j=1}^{J} \frac{(\Lambda_{o,j} - \Lambda_{T,j})^2}{\sigma_j^2} \qquad (4.30)$$

where $\Lambda_{T,j} = \Lambda(1)x_j^{-n}$ is the theoretical density distribution with free parameters $\Lambda(1)$ and n , $\Lambda_{o,j}$ is the binned average density of $\Lambda_q(x)$, $\Lambda_u(x)$ and σ_j is the standard deviation of the binned data. (In our particular case there are two sets of Λ_q and Λ_u in each bin because the data is symmetric about phase 0.25.)

In Fig. 4.5 we show the polarimetric variations, due to the plume (in the absence of noise), presented in the (Q,U) plane. The diagram bears much resemblance to those of Brown et al., (1978; their Figs 5 and 6). The general form will always be one ellipse totally enclosed within a second ellipse. The outer ellipse describes the polarimetric variation of the plume during phase 0.5 - 1.0 when no occultation occurs. The inner ellipse, however, is for phase period 0.0 - 0.5

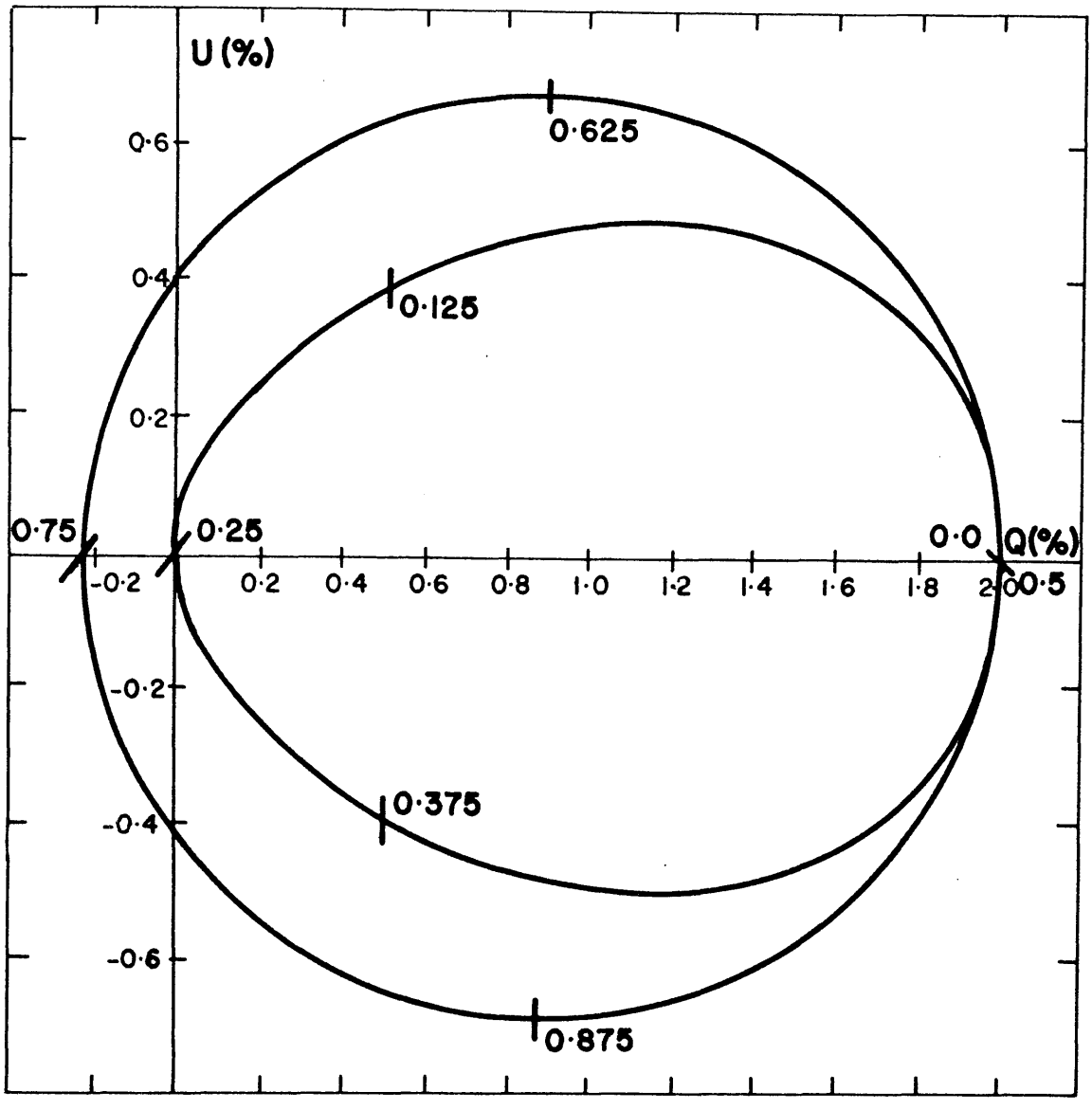

Figure 4.5

The variation of the Normalised Stokes parameters with phase for a plume of material viewed at i = 70° with a linear density distribution $\Lambda(x) = \Lambda_0(1)x^{-2}$ ($\Lambda_0(1) = 0.32/\pi$). Fiduciary marks are shown for every ¼ th of the phase.

during which occultation of the plume does occur. The polarimetric difference between the outer and inner ellipse is therefore the polarimetric contribution of the occulted part of the plume. The deviation between the two ellipses will depend upon the inclination and the density structure of the plume.

In Table 4.1 we present the results for i = 70° with a noise level of δQ = 0.001% and δQ = 0.01% ($\delta Q = \delta U$) with 180 data points

In both cases we have neglected data collected around phase 0.0 (1.0) because at this particular phase there is no measurable difference between Q(t + T/2) and Q(t) (and similarly for U) due to the error in the measurements and/or a negligible amount of material is being occulted. We have also neglected data collected at phase ~0.25 when the secondary may be occulted and at ~ 0.75 when the secondary may also play an important role in occulting some of the plume, or in eclipsing the primary.

We have purposely used oversampled data, i.e. 180 data points, to emphasise the fact that there is a limit to the number of data points that maybe meaningfully inverted. In the case of δQ = 0.001% we found it was possible to invert the data only if every other data point was neglected through the scanned phases. We can see (table 4.1 and Fig. 4.6a) that the density distribution is recovered very well with only significant deviation in the recovered data occurring near phase 0.25. By increasing the noise level to δQ ~ 0.01% we found that the step length had to be doubled and the sampling phase reduced near phase 0.25 as some of the $\Lambda_q(x)$ were negative. This is due to the fact that the Q data around phase 0.25 are approximately zero (therefore sensitive to any error present) and, coupled with the approximation of (29) can result in $\Lambda(x) \lesssim 0$. Fig. 4.6b shows the recovered density

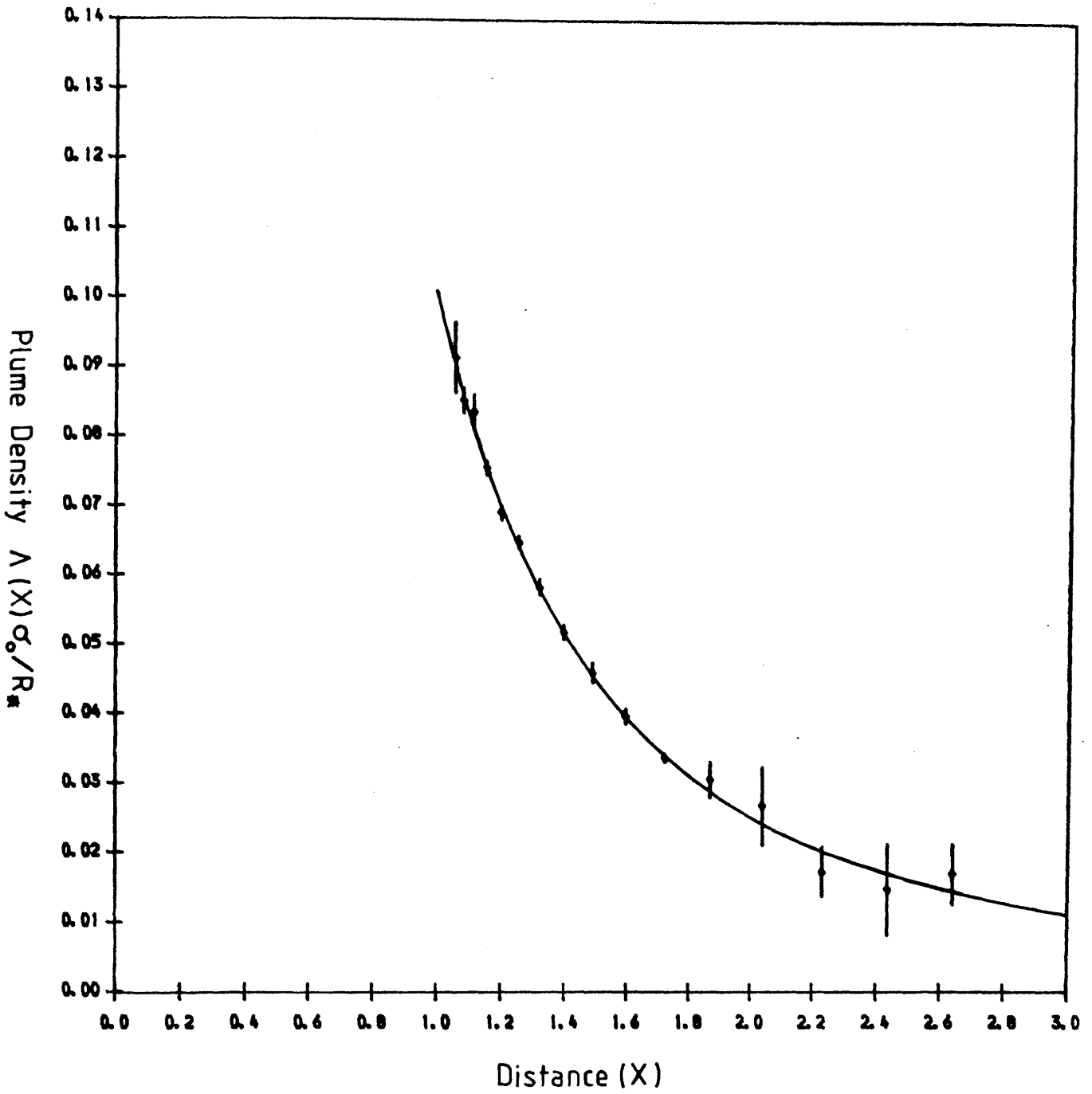

Figure 4.6a

The recovered density function is shown as a function of distance (x) with an error in the individual Stokes parameters of $\delta Q = \delta U =$ 0.001% . The inferred density parameters are given in Table 4.1

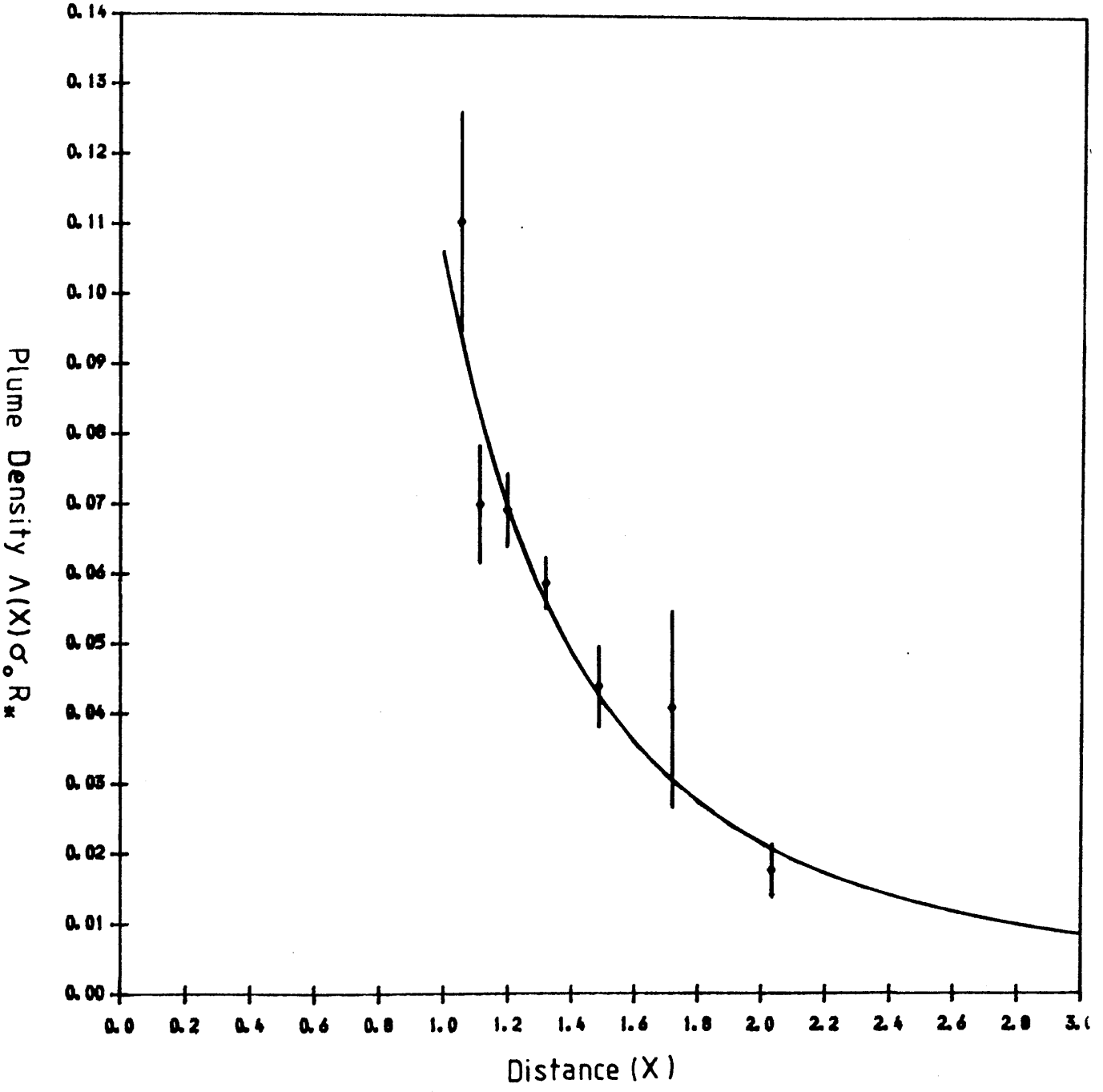

Figure 4.6b

As Fig. 4.6a except with δQ = 0.01%.

Table 4.1

Recovery of the input parameters with noisy data.

		Recovery	
	Input	δQ = 0.001%	δQ = 0.01%
Inclination	70.0	70.0±0.1	69.9±0.9
$\Lambda(1)\sigma_o/R_*$	$0.32/\pi$	0.10090	0.10045
n	2.00	2.00	2.20
χ^2 confidence	—	97.5%	50%
Sampling phase	—	$^{1}/_{18}$ - $^{4}/_{18}$ $^{6}/_{18}$ - $^{8}/_{18}$	$^{1}/_{18}$ - $^{35}/_{180}$ $^{55}/_{180}$ - $^{8}/_{18}$

distribution for the plume with a noise level of $\delta Q \sim 0.01\%$. In this case there is a marked increase in the scatter of the recovered density distribution compared to Fig. 4.6a.

4.5 The Structure of Two Dimensional Envelopes.

We now reconsider equations (4.3) - (4.8) and permit $\Omega(x,\Phi) = \Omega_o f_o(x,\Phi)$ to be distributed in Φ as well as x, and maintain the corotation condition $f_o(x,\Phi,t) = f_o(x,\Phi-\omega t)$, where $f_o(x,\Phi_o)$ is $\Omega(x,\Phi_o)/\Omega_o$ with Φ_o measured in a frame rotating with the envelope from a reference axis which coincides with that of Φ when $t = 0$.

We consider the extent to which properties of f_o can be obtained from the observations of Q(t), U(t) (c.f. Chapter 3).

4.51 $f_o(x,\Phi)$ Seperable With Known x - Dependence.

In this case we suppose

$$f_o(x,\Phi) = g_o(x)h_o(\Phi_o) \tag{4.32}$$

where $g_o(x)$ is known but $h_o(\Phi_o)$ is not.

We proceed in this case by the Fourier analysis of $h_o(\Phi_o)$ (c.f. Chapter 3), viz

$$h_o(\Phi_o) = x_o + \sum_{j=1}^{\infty} \{x_j \cos j\Phi_o + y_j \sin j\Phi_o\} \tag{4.33}$$

and obtain after some reduction, a Fourier series for Q and U as a function of ωt, viz

$$Q = p_o + \sum_{j=1}^{\infty} \{ p_j \cos j\omega t + q_j \sin j\omega t \} \tag{4.34}$$

$$U = u_o + \sum_{j=1}^{\infty} \{ u_j \cos j\omega t + v_j \sin j\omega t \} \tag{4.35}$$

with,

$$p_o = a_o[(\pi I - C)\sin^2 i + A_2(1 + \cos^2 i)] \tag{4.36}$$

$$\begin{Bmatrix} p_2 \\ q_2 \end{Bmatrix} = \begin{Bmatrix} a_2 \\ -b_2 \end{Bmatrix}[A_2\sin^2 i + \frac{1}{2}(\pi I - C + A_4)(1 + \cos^2 i)] \quad j = 2 \tag{4.37}$$

$$\begin{Bmatrix} p_j \\ q_j \end{Bmatrix} = \begin{Bmatrix} a_j \\ -b_j \end{Bmatrix}[A_j\sin^2 i + \frac{J_j}{2}(1 + \cos^2 i)] \text{ for even } j \ (j \neq 2) \tag{4.38}$$

$$\begin{Bmatrix} p_j \\ q_j \end{Bmatrix} = - \begin{Bmatrix} b_j \\ a_j \end{Bmatrix}[B_j\sin^2 i + \frac{K_j}{2}(1 + \cos^2 i)] \quad \text{for odd } j \tag{4.39}$$

$$u_o = 0 \tag{4.40}$$

$$\begin{Bmatrix} u_2 \\ v_2 \end{Bmatrix} = \begin{Bmatrix} b_2 \\ a_2 \end{Bmatrix}(\pi I - C - A_4)\cos i \qquad \text{for } j = 2 \tag{4.41}$$

$$\begin{Bmatrix} u_j \\ v_j \end{Bmatrix} = \begin{Bmatrix} b_j \\ a_j \end{Bmatrix} M_j \cos i \qquad \text{for even } j \ (j \neq 2) \tag{4.42}$$

$$\begin{Bmatrix} u_j \\ v_j \end{Bmatrix} = \begin{Bmatrix} a_j \\ -b_j \end{Bmatrix} N_j \cos i \qquad \text{for odd } j \tag{4.43}$$

where,

$$a_j = \sigma_o \Omega_o x_j \quad , \quad b_j = \sigma_o \Omega_o y_j \tag{4.44}$$

$$I = \int_1^{\infty} g_o(x) \frac{(x^2 - 1)^{1/2}}{x^2} \, dx \tag{4.45}$$

$$A_j = \int_1^{\sec i} g_o(x) \, \frac{(x^2 - 1)^{1/2}}{x^2} \, \frac{S_j^i(x)}{j} \, dx \tag{4.46}$$

$$B_j = \int_1^{\sec i} g_o(x) \, \frac{(x^2 - 1)^{1/2}}{x^2} \, \frac{T_j^i(x)}{j} \, dx \tag{4.47}$$

$$C = \int_1^{\sec i} g_o(x) \, \frac{(x^2 - 1)^{1/2}}{x^2} \left[\frac{\pi}{2} - \sin^{-1}\left[\frac{(x^2 - 1)^{1/2}}{x \sin i}\right]\right] dx \tag{4.48}$$

$$\left.\begin{aligned} J_j &= A_{j+2} + A_{j-2} \\ K_j &= B_{j+2} + B_{j-2} \\ M_j &= A_{j-2} - A_{j+2} \\ N_j &= B_{j-2} - B_{j+2} \end{aligned}\right\} \qquad (4.49)$$

and

$$S_j^i(x) = \sin\left\{j\sin^{-1}\left[\frac{(x^2-1)^{1/2}}{x\sin i}\right]\right\} \qquad (4.50)$$

$$T_j^i(x) = \cos\left\{j\sin^{-1}\left[\frac{(x^2-1)^{1/2}}{x\sin i}\right]\right\} \qquad (4.51)$$

where $S_j^i(x)$, $T_j^i(x)$ are the congruous related Chebyshev polynomials.

In order to find the coefficients a_j, b_j we need to know the inclination of the system. We can obtain the inclination by taking the ratios of the Fourier coefficients of the data (Brown et al., 1978; Simmons, 1983), viz

$$G_2 = \frac{p_2}{v_2} = -\frac{q_2}{u_2} = \left[\frac{2A_2\sin^2 i - (\pi I - C + A_4)(1+\cos^2 i)}{2(\pi I - C - A_4)\cos i}\right] \quad j = 2 \qquad (4.52)$$

$$G_j = \frac{p_j}{v_j} = -\frac{q_j}{u_j} = \left[\frac{2A_j\sin^2 i + J_j(1+\cos^2 i)}{2M_j\cos i}\right] \quad \begin{matrix}\text{for even } j \\ (j \neq 2)\end{matrix} \qquad (4.53)$$

$$H_j = \frac{p_j}{v_j} = -\frac{q_j}{u_j} = \left[\frac{2B_j\sin^2 i + K_j(1+\cos^2 i)}{2N_j\cos i}\right] \quad \text{for odd } j \qquad (4.54)$$

Since q_j/v_j , p_j/u_j and the form of $g_o(x)$ are known then the functions G_2, G_j and H_j will uniquely determine the inclination of the system. Once the inclination has been found the Fourier coefficients (a_j, b_j) of the Φ_o distribution are then obtained.

In Figs 4.7a-h we show as examples G_2, G_j, H_j for the first eight harmonics with $g_o(x) \sim x^{-n}$, for $n = 2.0 - 4.0$. We show up to the eighth harmonic only because according to the Riemann - Lebesque

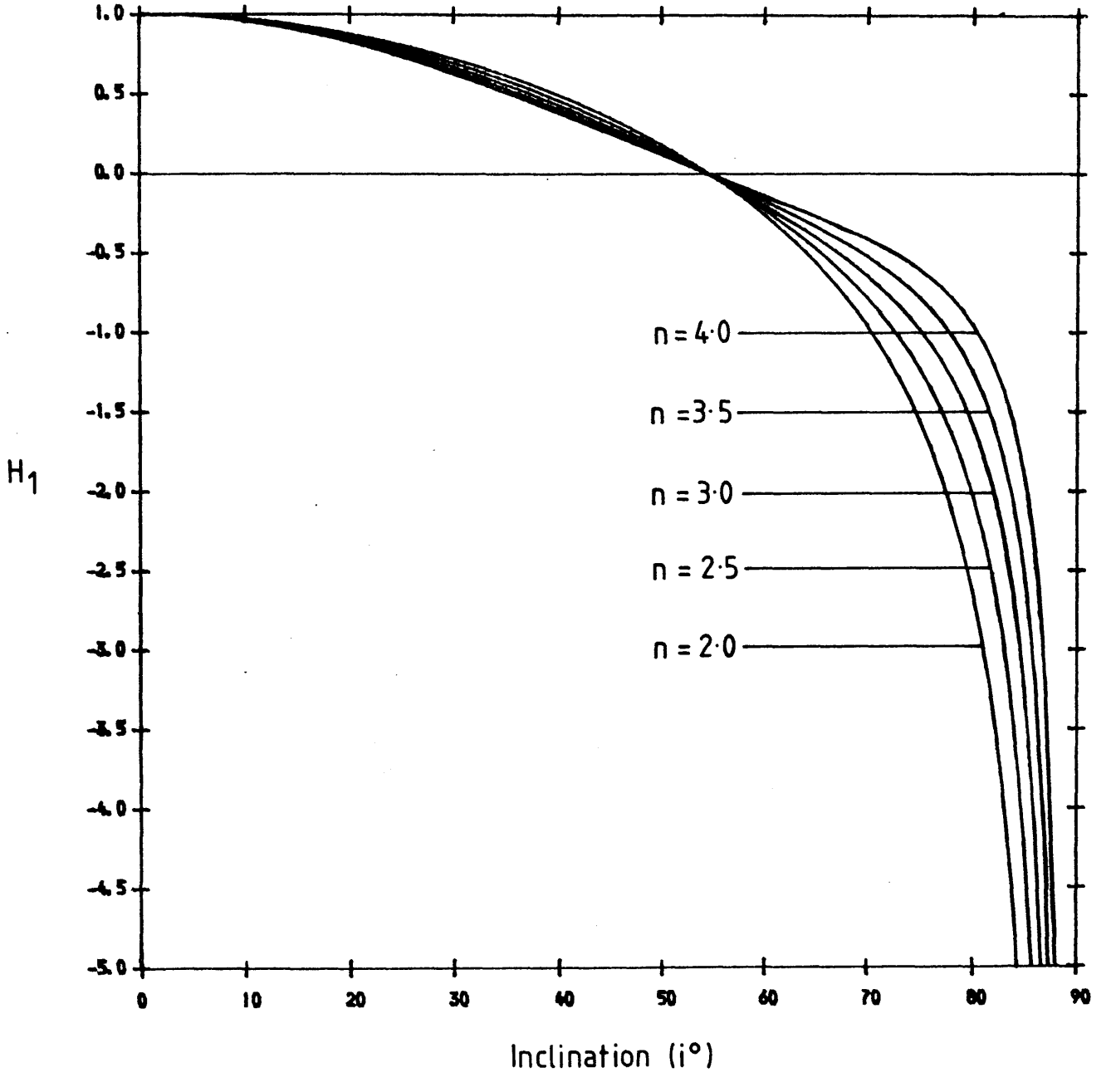

Figure 4.7a

The Fourier ratio H_1 is shown as a function of inclination (i) for power indices n = 2.0, 2.5, 3.0, 3.5 and 4.0.

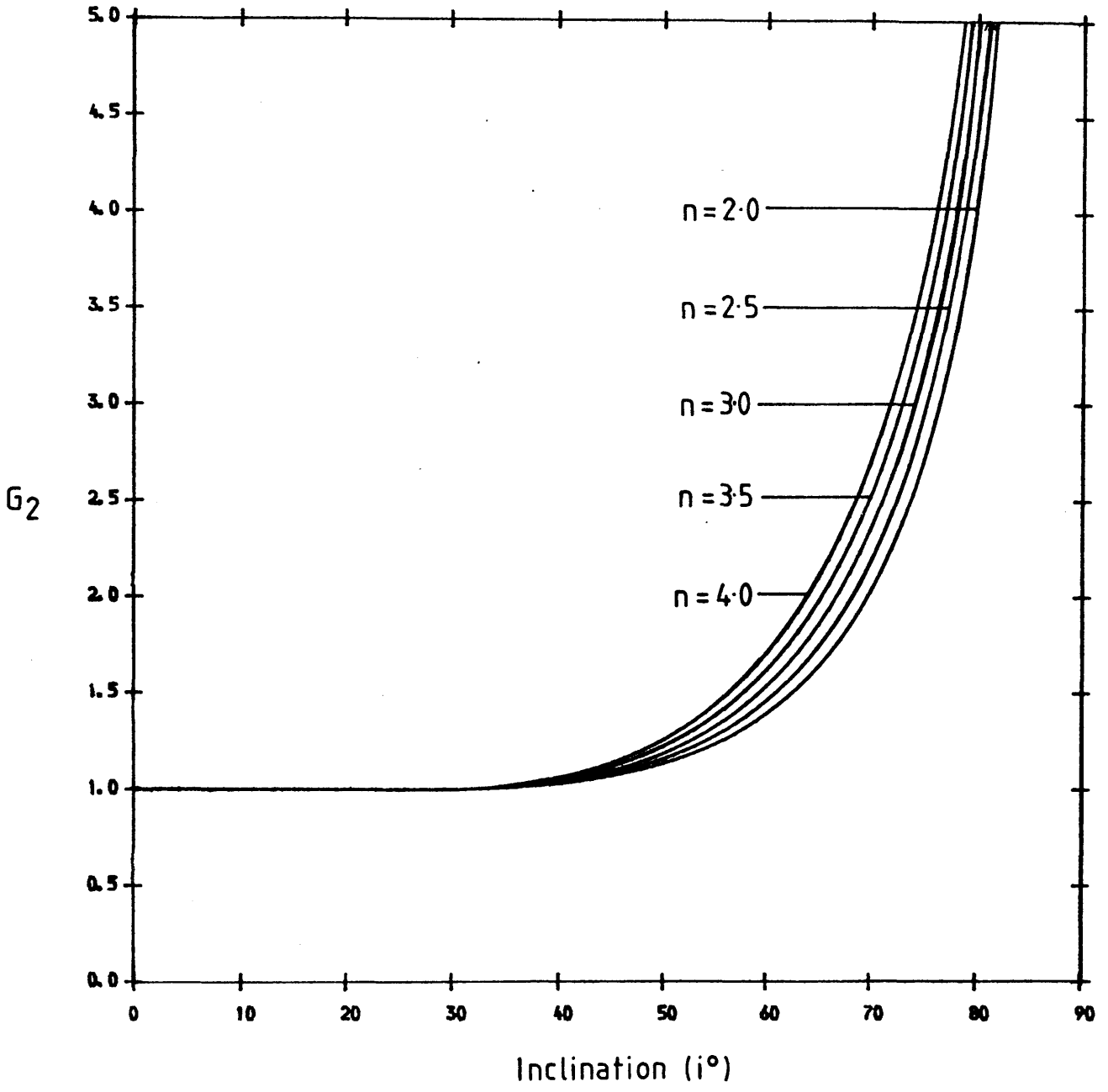

Figure 4.7b

As Fig 4.7a but for the Fourier ratio G_2

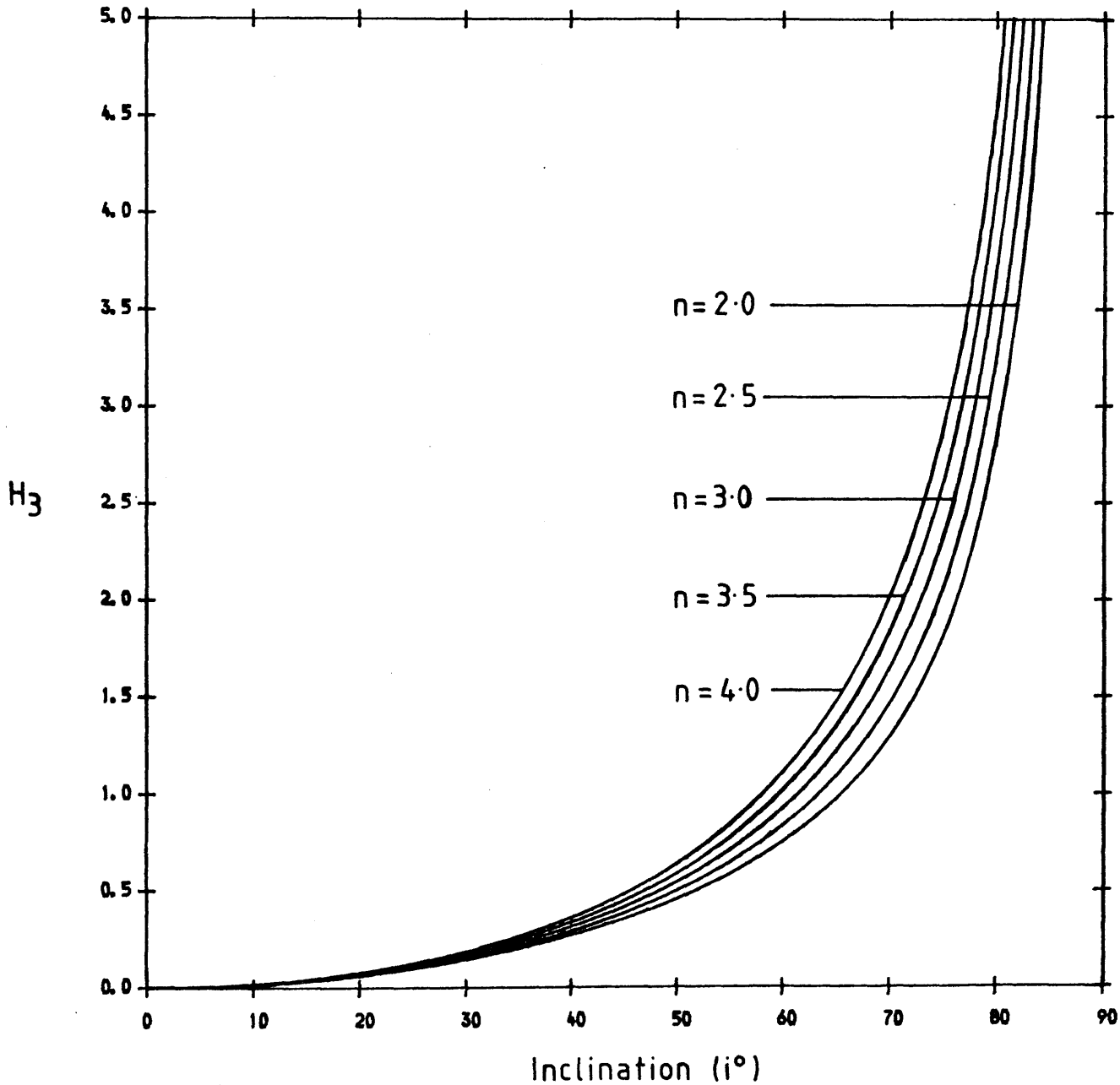

Figure 4.7c

As Fig 4.7a but for the Fourier ratio H_3.

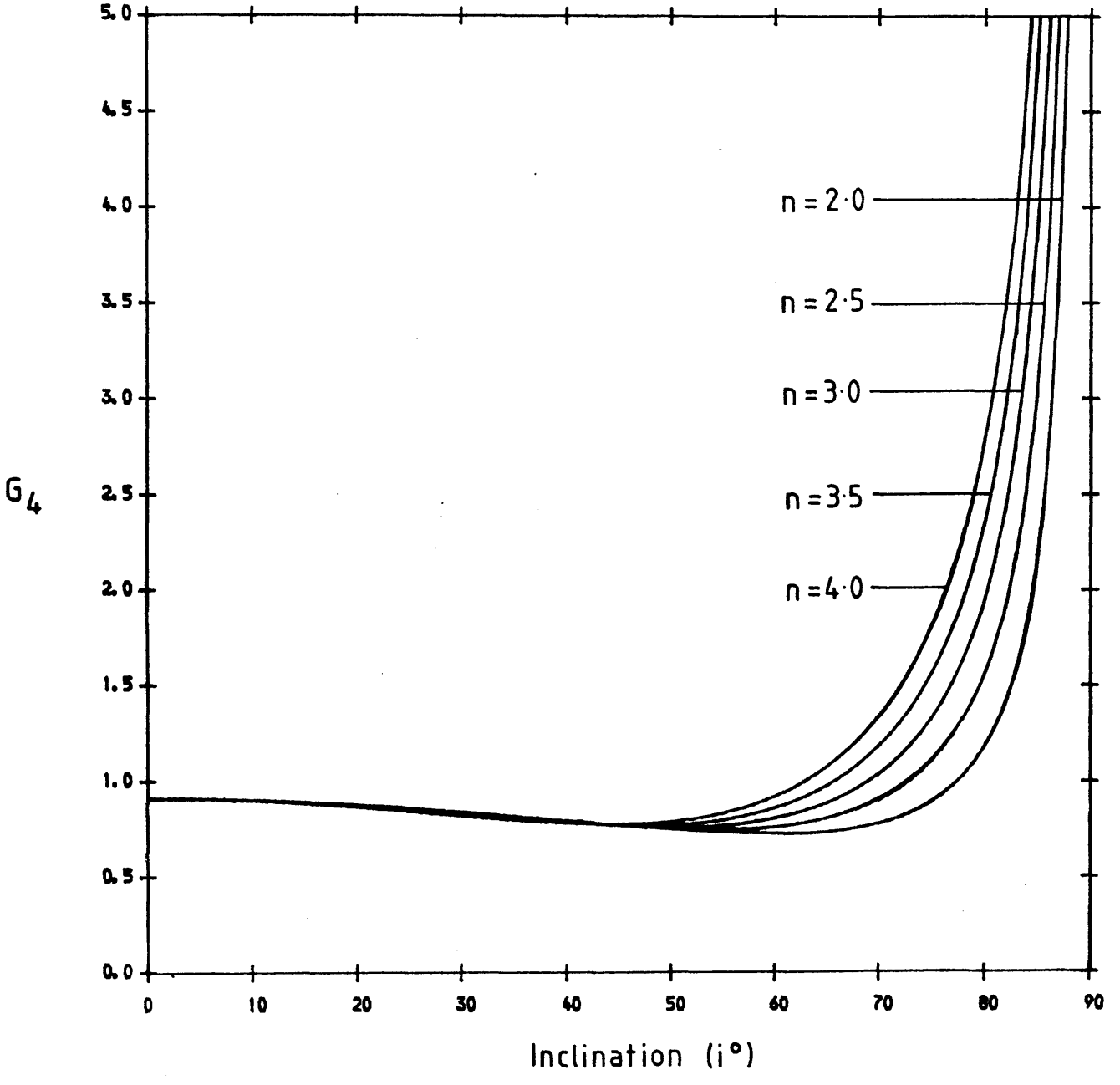

Figure 4.7d

As Fig 4.7a but for the Fourier ratio G_4.

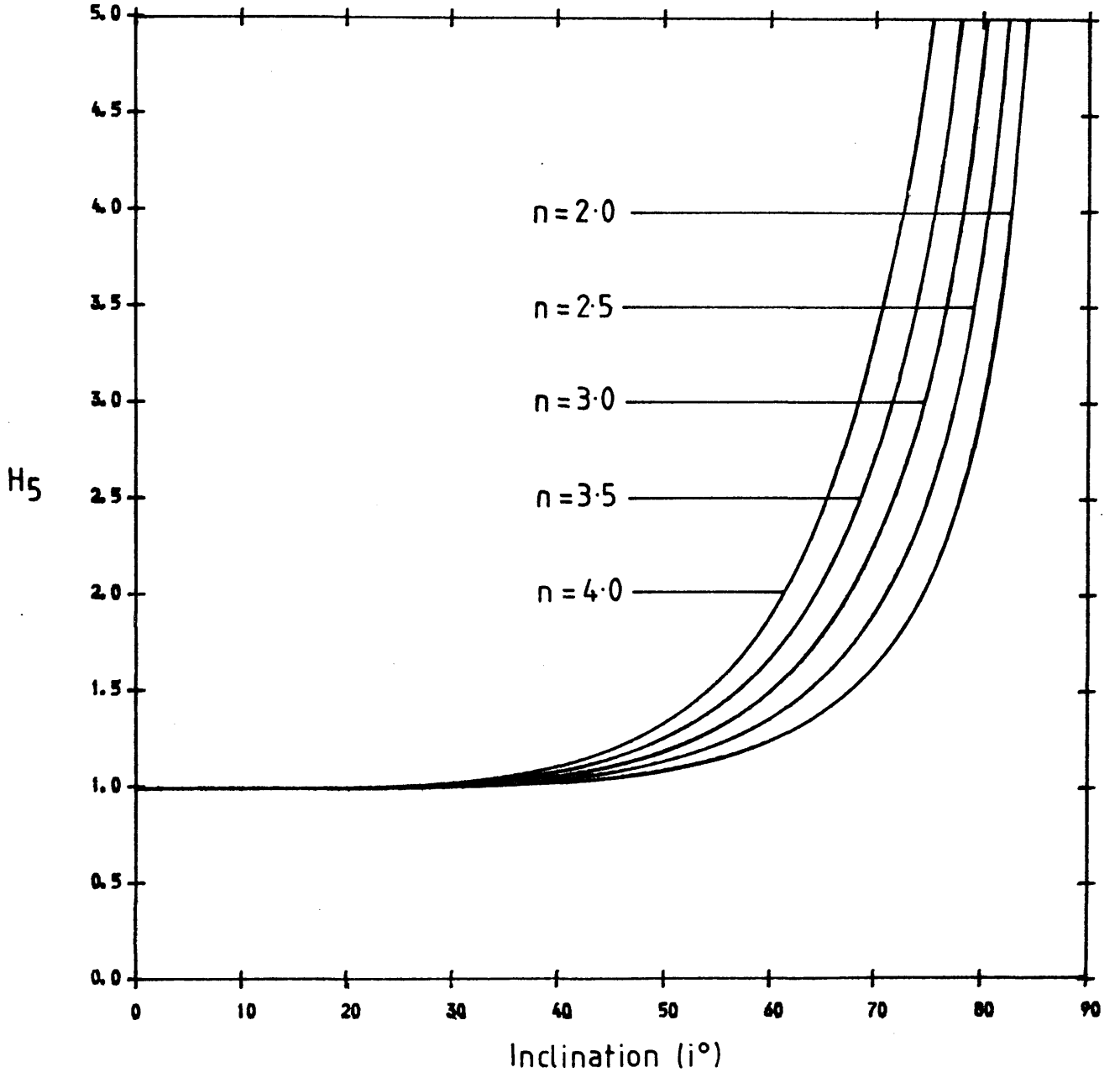

Figure 4.7e

As Fig 4.7a but for the Fourier ratio H_5.

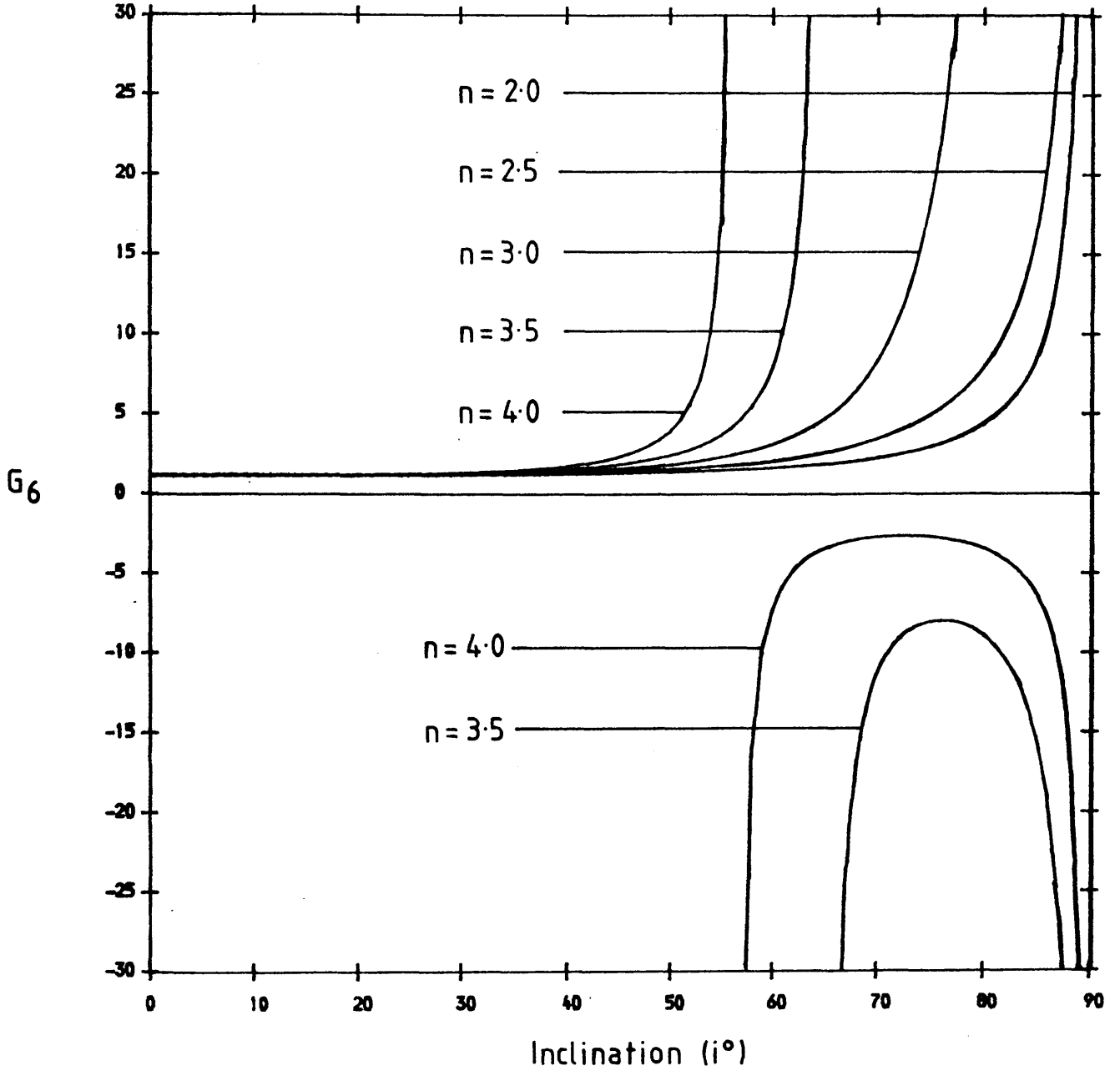

Figure 4.7f

As Fig 4.7a but for the Fourier ratio G_6.

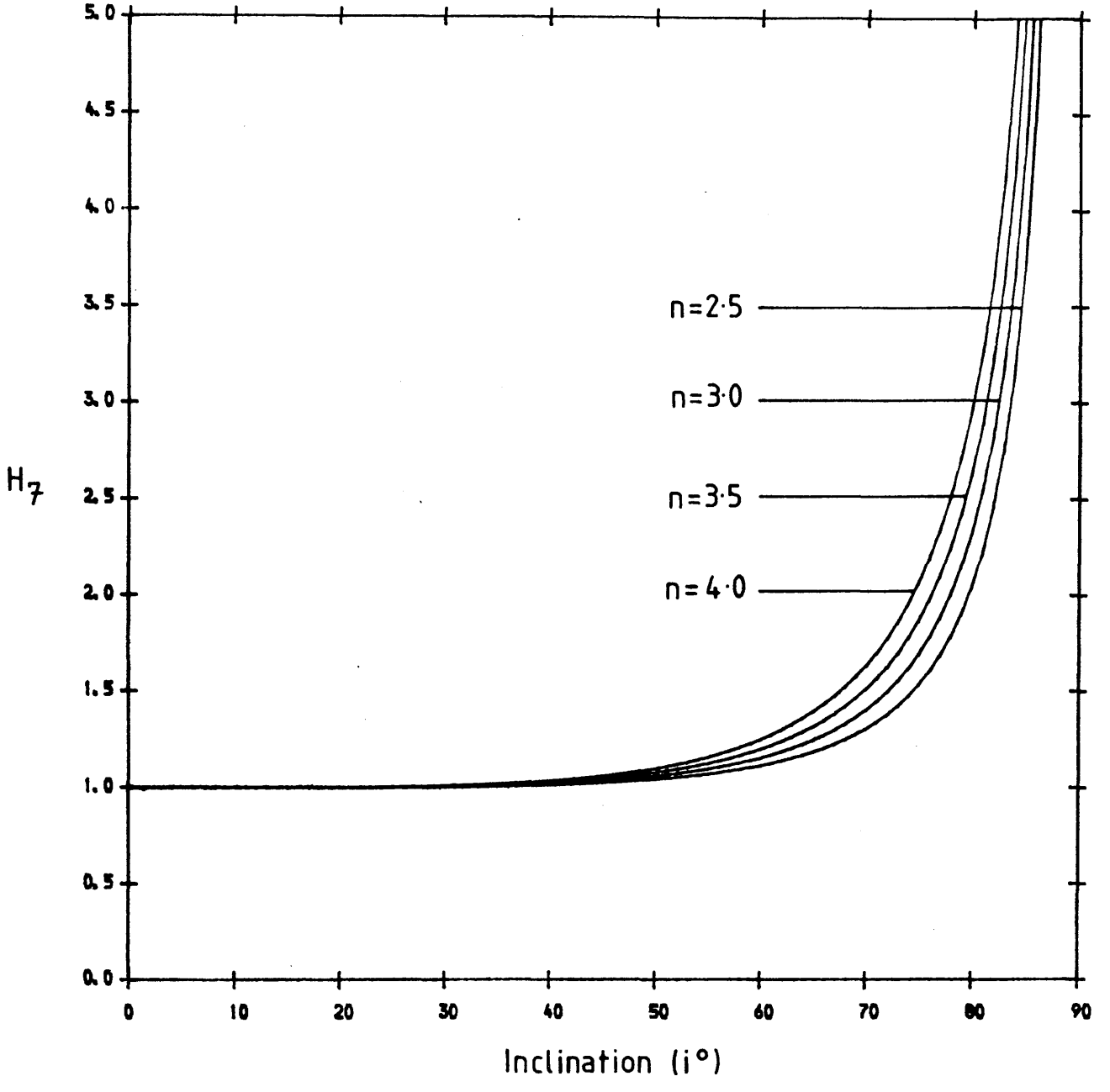

Figure 4.7g

As Fig 4.7a but for the Fourier ratio H_7. Note that the curve for n = 2 has been omitted since it is of indeterminate form (see text).

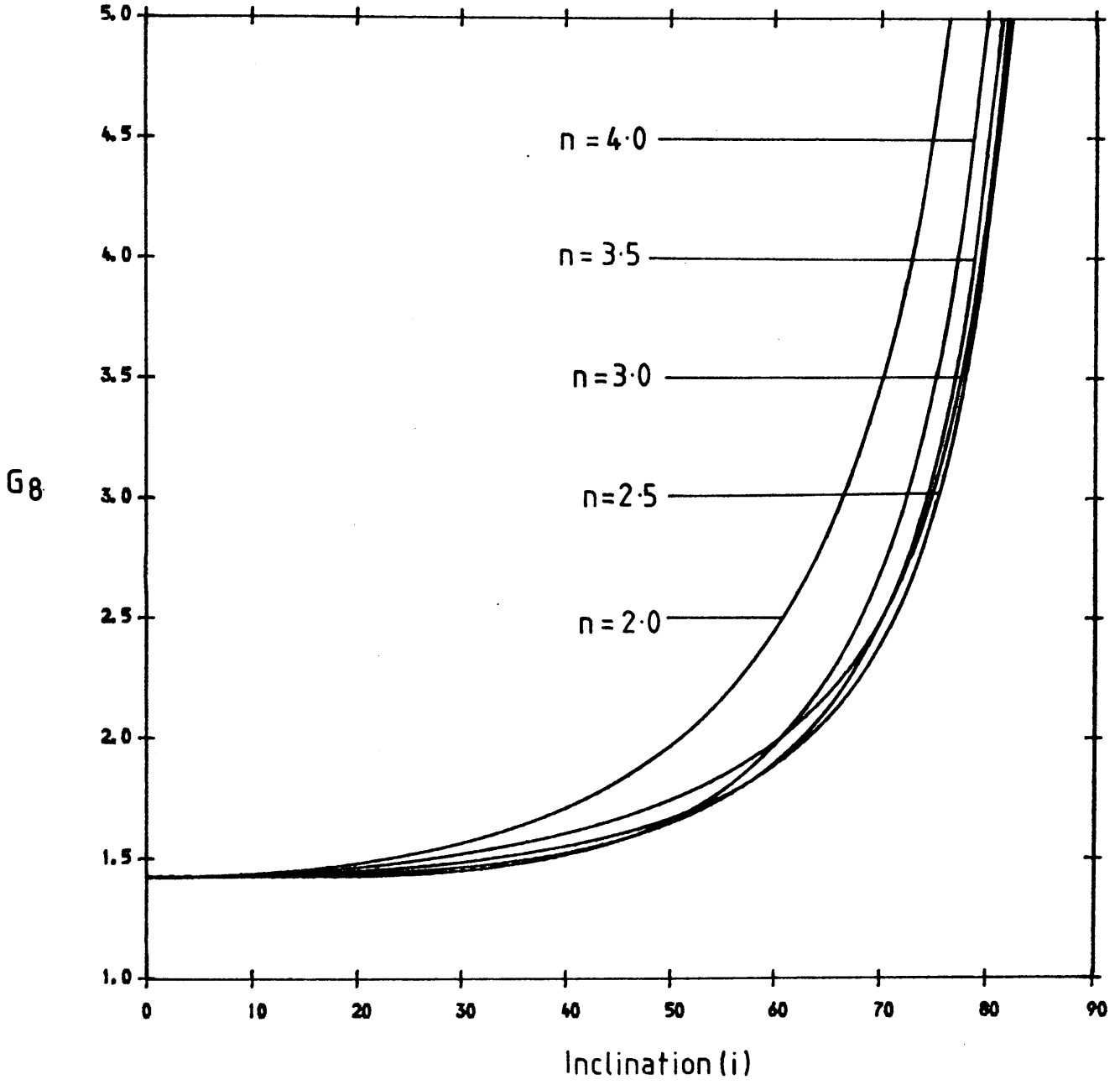

Figure 4.7h

As Fig 4.7a but for the Fourier ratio G_8.

Lemma the integrals A_j, $B_j \rightarrow 0$ as $j \rightarrow \infty$ (see Sneddon, 1972) and this, coupled with the fact that we have a finite data set means that the best we can hope to achieve will be typically the harmonics up to $j \sim 8$.

In Fig. 4.7f we see that G_6 (for $n = 3.5$ and 4.0) becomes infinite around $i \sim 60^\circ$. This is due to the fact that $M_6 \sim 0$ at this inclination and so [from equation (4.53)] G_6 becomes infinite (this may be verified analytically for $n = 4.0$, where $M_6 = 0$ at $\sin^2 i = {}^{13}/_{18}$).

In Fig. 4.7g the curve of H_7 ($n = 2$) has been excluded because this function is of indeterminate form (i.e 0/0) for all i and is due to the fact that $B_j = 0$ for $j \geqslant 5$ [see equation (4.54)]. In fact for $n = 2.0$, $H_j = 0/0$ for $j \geqslant 7$, whilst for $n = 4$, $H_j = 0/0$ for $j \geqslant 9$.

With the exception of these singular cases, the Fourier coefficient ratios (G_j, H_j) are insensitive to the power law index, except for the high order ratios at high inclinations.

We present now some model calculations with noisy data using 64 data points for a disc with a power index $n = 2.0$ and with cofficients $a_0 = 1$, $a_j = b_j = j^{-2}$ (for $j \geqslant 1$) viewed at an inclination $i = 70^\circ$.

In order to find the Fourier coefficients p_j, q_j, u_j, v_j we make use of the approximation (Champeney, 1985)

$$\begin{Bmatrix} p_o \\ u_o \end{Bmatrix} = \frac{1}{N} \sum_{n=1}^{N-1} \begin{Bmatrix} Q_n \\ U_n \end{Bmatrix} \tag{4.55}$$

$$\begin{Bmatrix} p_j \\ u_j \end{Bmatrix} = \frac{1}{N} \sum_{n=1}^{N-1} \begin{Bmatrix} Q_n \\ U_n \end{Bmatrix} \cos\left[\frac{2\pi nj}{N}\right] \tag{4.56}$$

$$\begin{Bmatrix} q_j \\ v_j \end{Bmatrix} = \frac{1}{N} \sum_{n=1}^{N-1} \begin{Bmatrix} Q_n \\ U_n \end{Bmatrix} \sin\left[\frac{2\pi nj}{N}\right] \tag{4.57}$$

(for more complicated transforms see for example Press et al., 1986 and references therein).

Using equations (4.55) - (4.57) with 64 data points it is possible to obtain (with any certainty) the Fourier coefficients up to j = 8. From these coefficients the Fourier ratios are then obtained. Table 4.2 shows the ratios for various amounts of noise. It can be seen (and is intuitively obvious) that as the noise increase the high order Fourier ratios become increasingly uncertain (i.e. $p_j/v_j \neq - q_j/u_j$)

When the Fourier ratios have been calculated it is then possible (by using Figs 4.7a - h) to find the inclination of the system, which we show in table 4.3 where we have calculated the average inclination for each available power index in order to illustrate how sensitive the choice of the power index is in determining the inclination. As can be seen from Table 4.3, the inferred inclination is consistant with the input value of i = 70° and is quite insensitive to the particular choice of the power index.

Once the inclination of the system has been established, it is then possible to obtain the Fourier coefficients of the envelope distribution (i.e a_j, b_j) via equations (4.36) - (4.43). The results are presented in Table 4.4 for n = 2.0 and n = 4.0 and are compared with the true values. We also show the error (super- and subscript values) introduced by taking the upper and lower limit of the inclination (as obtained in Table 4.1). One can see that, independent of the power index or the error in the data, the low j value coefficients are most sensitive to the value of the inclination. One can see that the errors associated with the coefficients for the power index n = 4.0 are greater than those for n = 2.0 which would indicate that we are trying to force a fit in the case of n = 4.0 . Since $H_7 = 0/0$, it is not possible

Table 4.2

Fourier ratio values obtained from data with varying amounts of noise.

	Error					
	$\delta Q = 0.001\%$		$\delta Q = 0.01\%$		$\delta Q = 0.1\%$	
Fourier Ratio	$\frac{p_j}{v_j}$	$-\frac{q_j}{u_j}$	$\frac{p_j}{v_j}$	$-\frac{q_j}{u_j}$	$\frac{p_j}{v_j}$	$-\frac{q_j}{u_j}$
G_2	1.90	1.90	1.90	1.90	1.90	1.90
G_4	1.22	1.22	1.21	1.22	1.21	1.26
G_6	2.03	2.03	2.48	1.71	-6.55	0.30
G_8	2.80	2.80	2.29	1.85	0.79	0.93
H_1	-0.61	-0.61	-0.61	-0.61	-0.61	-0.61
H_3	0.77	0.77	0.77	0.77	0.78	0.75
H_5	1.63	1.63	1.65	1.67	1.83	2.11
H_7	0/0	0/0	0/0	0/0	0/0	0/0

Table 4.3

Inferred inclination from Figs 4.7 using the Fourier ratios of Table 4.2.

	Error		
Index	SQ = 0.001%	SQ = 0.01%	SQ = 0.1%
2.0	68° ± 6°	67° ± 9°	70° ± 7°
2.5	67° ± 7°	66° ± 5°	68° ± 5°
3.0	65° ± 8°	64° ± 7°	70° ± 6°
3.5	63° ± 10°	62° ± 8°	65° ± 6°
4.0	61° ± 11°	60° ± 10°	64° ± 7°

Table 4.4

The resultant Fourier coefficients (a_j, b_j) of the envelope density distribution for power indices n = 2.0, n = 4.0 .

Coefficient	Input	δω = 0.0%		δω = 0.01%		δω = 0.1%	
		n = 2	n = 4	n = 2	n = 4	n = 2	n = 4
a_0	1.0	$1.02^{-0.05}_{+0.08}$	$3.9^{+0.7}_{-0.0}$	$1.03^{-0.07}_{+0.14}$	$3.87^{+0.57}_{+0.03}$	$1.00^{-0.04}_{+0.07}$	$4.01^{+0.05}_{-0.22}$
a_1	1.0	$1.20^{-0.31}_{-3.21}$	$26.6^{-25.3}_{-26.6}$	$1.10^{-0.49}_{-1.66}$	$-6.18^{+7.51}_{+6.22}$	$1.00^{-0.07}_{-0.50}$	$2.30^{-0.99}_{-3.17}$
b_1	1.0	$1.20^{-0.31}_{-3.21}$	$26.6^{-25.3}_{-26.6}$	$1.40^{-0.49}_{-1.66}$	$-6.18^{+7.51}_{+6.22}$	$1.00^{-0.07}_{-0.50}$	$2.29^{-0.90}_{-3.16}$
a_2	0.25	$0.24^{+0.05}_{-0.03}$	$0.77^{+0.63}_{-0.26}$	$0.23^{+0.00}_{-0.04}$	$0.74^{+0.49}_{-0.23}$	$0.25^{+0.07}_{-0.04}$	$0.89^{+0.42}_{-0.23}$
b_2	0.25	$0.24^{+0.05}_{-0.03}$	$0.77^{+0.63}_{-0.26}$	$0.23^{+0.00}_{-0.04}$	$0.74^{+0.49}_{-0.23}$	$0.25^{+0.07}_{-0.04}$	$0.89^{+0.42}_{-0.23}$
a_3	0.111	$0.11^{+0.02}_{-0.01}$	$0.14^{+0.00}_{+0.00}$	$0.105^{+0.020}_{-0.006}$	$0.146^{+0.024}_{+0.002}$	$0.11^{+0.03}_{-0.01}$	$0.152^{+0.022}_{-0.008}$
b_3	0.111	$0.11^{+0.02}_{-0.01}$	$0.14^{+0.00}_{+0.00}$	$0.105^{+0.020}_{-0.006}$	$0.146^{+0.024}_{+0.002}$	$0.11^{+0.03}_{-0.01}$	$0.151^{+0.022}_{-0.008}$
a_4	0.0625	$0.061^{+0.006}_{-0.001}$	$0.096^{+0.016}_{+0.005}$	$0.061^{+0.011}_{+0.001}$	$0.001^{+0.011}_{+0.005}$	$0.062^{+0.012}_{+0.003}$	$0.097^{+0.012}_{-0.003}$
b_4	0.0625	$0.061^{+0.006}_{-0.001}$	$0.096^{+0.016}_{+0.005}$	$0.061^{+0.011}_{+0.001}$	$0.001^{+0.011}_{+0.005}$	$0.062^{+0.011}_{+0.002}$	$0.097^{+0.011}_{-0.002}$
a_5	0.010	$0.0390^{+0.0032}_{+0.0002}$	$0.081^{+0.022}_{+0.000}$	$0.040^{+0.006}_{+0.002}$	$0.080^{+0.016}_{+0.001}$	$0.043^{+0.006}_{-0.000}$	$0.089^{+0.015}_{-0.005}$
b_5	0.040	$0.0390^{+0.0032}_{+0.0002}$	$0.081^{+0.022}_{+0.000}$	$0.040^{+0.006}_{+0.002}$	$0.080^{+0.016}_{+0.001}$	$0.038^{+0.005}_{-0.000}$	$0.078^{+0.012}_{-0.003}$
a_6	0.0278	$0.0270^{+0.002}_{+0.0005}$	$-0.14^{+0.16}_{+0.27}$	$0.026^{+0.003}_{+0.002}$	$-0.19^{+0.23}_{+0.32}$	$0.014^{-0.004}_{+0.003}$	$0.15^{-0.01}_{-0.27}$
b_6	0.0278	$0.0270^{+0.002}_{+0.0005}$	$-0.14^{+0.16}_{+0.27}$	$0.026^{+0.003}_{+0.002}$	$-0.29^{+0.29}_{0.42}$	$0.033^{+0.010}_{-0.003}$	$-0.19^{+0.09}_{+1.18}$
a_7	0.020	?	?	?	?	?	?
b_7	0.020	?	?	?	?	?	?
a_0	0.0156	$0.0155^{+0.0010}_{+0.0005}$	$0.0093^{-0.0008}_{+0.0039}$	$0.017^{+0.002}_{+0.001}$	$0.010^{-0.001}_{+0.003}$	$0.031^{+0.008}_{-0.002}$	$0.015^{-0.001}_{+0.002}$
b_0	0.0156	$0.0155^{+0.0010}_{+0.0005}$	$0.0093^{-0.0008}_{+0.0039}$	$0.023^{+0.004}_{+0.002}$	$0.014^{-0.001}_{+0.005}$	$0.098^{+0.025}_{-0.006}$	$0.050^{+0.001}_{+0.005}$

to calculate the values for a_7 and b_7. The fact that $H_7 = 0/0$ [see equation (4.54)], however, implies either $a_7 = b_7 = 0$ or that the power index is $n = 2.0$. As there is no reason to presume that $a_7 = b_7 = 0$ then $n = 2.0$. This inference is supported by the fact that the errors associated with the Fourier coefficients (Table 4.4) are least for $n = 2.0$.

4.6 Discussion and Conclusions.

In our analysis we have made certain simplifying assumptions about the the light source and the scattering material in order to analyse the effects of occultation alone.

We have considered the light source to be spherically symmetric despite the fact that Be stars are believed to be fast rotators and thus likely to be ellipsoidal in shape. This would primarily modify the geometrical factors of the problem, namely the depolarisation factor and the occulted region, making the calculations difficult but not changing the quantative results . A secondary effect however will be that the star itself will be intrinsically polarised (with the net polarisation vector lying in a direction parallel to the equatorial plane - Cassinelli, 1987). By confining our analysis to early type stars, however, photospheric polarisation can be neglected in the visible region (see Collins, 1989).

The effect of limb darkening is to decrease the effective stellar angular radius and thus increase the net polarisation, and although we have neglected limb darkening it can be incorporated into the theory (Brown, Carlaw and Cassinelli, 1989).

The circumstellar material is considered to be optically thin and thus absorption effects may be neglected. If absorption within the

envelope were to be included the problem would become wavelength dependent (e.g. McLean, 1978; Haisch and Cassinelli, 1976) and so our analysis is applicable to broad band photopolarimetry only.

Our results show that for an axisymmetric disc occultation enhances the net polarisation (compared to when occultation is neglected) at low inclination, whereas at high inclination occultation reduces the net polarisation.

In the case when a mass transferring binary can be approximated to an axisymmetric disc with a superposed one dimensional plume, it is then possible to obtain the inclination of the system, the polarisation of the disc and (for sufficiently high inclination) the density structure of the plume from the polarimetric data.

In general a circumstellar disc will be asymmetric and we have found that by Fourier analysing the data it is possible, when the radial structure of the disc is of of a presumed form, to obtain the inclination of the system and thereby obtain the Fourier expansion for the density distribution.

Chapter 5.

III. General Axisymmetric Envelopes.

5.1 Introduction.

So far, the effects of occultation upon the scattering of light from circumstellar envelopes has been restricted to envelopes that are confined to the equatorial plane of the star (i.e. planar distributions). It has been found that when occultation and the finite size of the star are incorporated into the single scattering treatment of Brown and McLean (1977; henceforth BM) the net theoretical polarisation is reduced by up to a factor of two compared to the point light source treatment.

It can be anticipated that for general scattering envelope distributions the net polarisation will again, in general, be reduced. The amount of reduction will depend upon the envelope shape, the density distribution and also the inclination of the system.

In the following Sections the normalised Stokes parameters are obtained for a general envelope distribution with the inclusion of depolarisation and occultation (Sec. 5.2). We then consider three specific (axisymmetric) distributions (Sec. 5.3) and investigate what the effects of occultation and depolarisation are upon the observed polarisation compared to the point light source treatment of BM.

5.2 The General Theory.

Consider a star (radius R_*, luminosity, L_*) centred at O (Fig. 5.1) surrounded by an extended envelope of scattering material with a number density $n(\underline{r})$. In the fixed stellar frame (X,Y,Z) the Z-axis

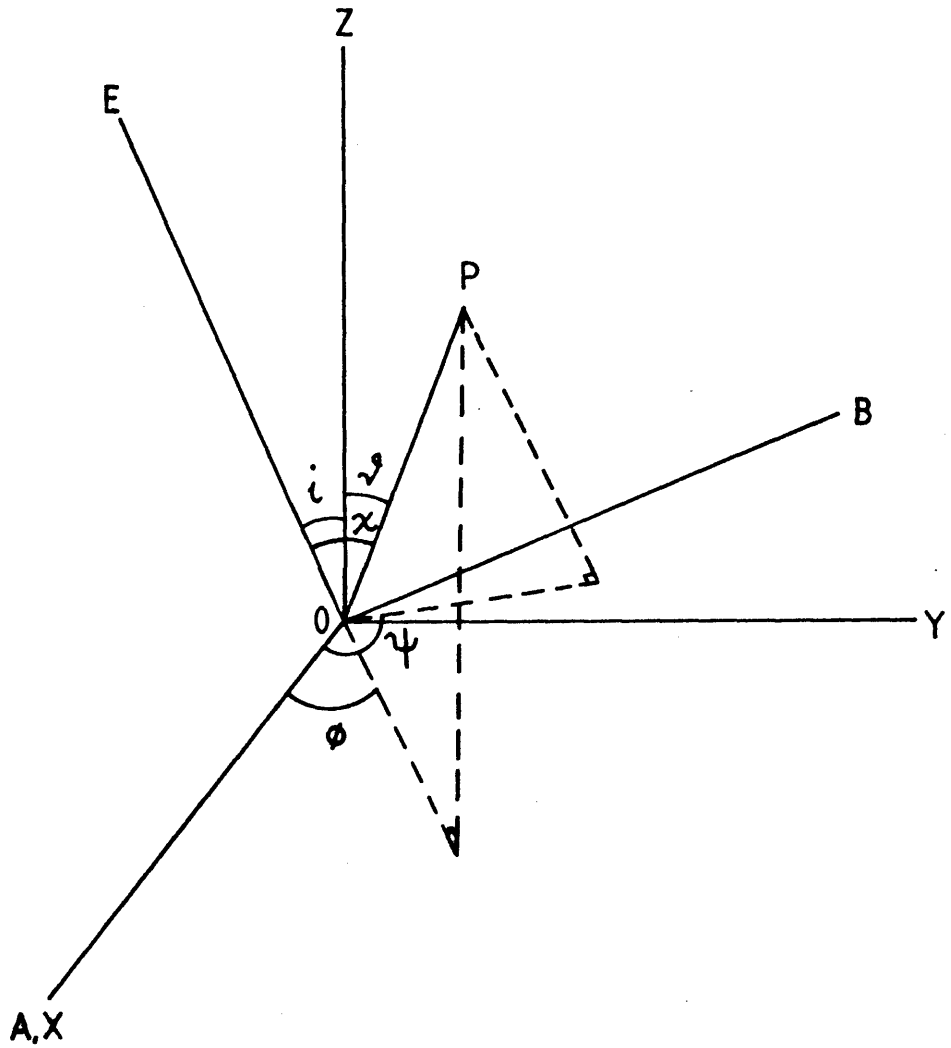

Figure 5.1

A star centred at O with a radius R_* (not shown) rotates uniformly about the Z-axis. An observer (E) is inclined at an angle i to the rotation (Z) axis of the star.

A general scattering point, P, at a distance r from the centre of the star, has position (r,χ,Ψ), in spherical polars, in the observer-sky (A,B,E) frame and has position (r,θ,ϕ) in the stellar frame. The observer-sky axes are orientated such that the A-axis coincides with the X-axis of the stellar frame.

defines the rotation axis of the star. An observer (E) is inclined to the rotation axis of the star by an angle i (the inclination) and the observer-sky frame (A,B,E) is oriented such that the Z-axis lies in the EB plane.

A general scattering point, P, at a distance r from O, in spherical polars has position (r,θ,ϕ) in the stellar frame and (r,χ,ψ) in the observer-sky frame.

In the frame of the observer, the normalised Stokes parameters can be written as

$$Q = \sigma_o \int_V D(r) n(r,\chi,\psi) \sin^2\chi \cos 2\psi \frac{dV}{r^2} \qquad (5.1)$$

$$U = \sigma_o \int_V D(r) n(r,\chi,\psi) \sin^2\chi \sin 2\psi \frac{dV}{r^2} \qquad (5.2)$$

where $D(r) = (1 - R_*^2/r^2)^{1/2}$ is the depolarisation factor for a finite spherical light source (Cassinelli et al., 1987) and $\sigma_o = 3\sigma_T/16\pi$, σ_T is the Thomson scattering cross-section.

Equations (5.1) and (5.2) are integrated over the observed scattering volume (Fig. 5.2), which is the total volume of the scattering region minus the occulted region that lies behind the star, according to an external observer. In the observer's frame the normalised Stokes parameters are

$$Q = \sigma_o \int_{\psi=0}^{2\pi} \int_{r=R_*}^{\infty} \int_{\chi=0}^{\pi - \sin^{-1}(R_*/r)} D(r)\, n(r,\chi,\psi) \sin^2\chi \cos 2\psi \frac{dV}{r^2} \qquad (5.3)$$

$$U = \sigma_o \int_{\psi=0}^{2\pi} \int_{r=R_*}^{\infty} \int_{\chi=0}^{\pi - \sin^{-1}(R_*/r)} D(r)\, n(r,\chi,\psi) \sin^2\chi \sin 2\psi \frac{dV}{r^2} \qquad (5.4)$$

In the polarimetric modelling of stellar winds the density is generally

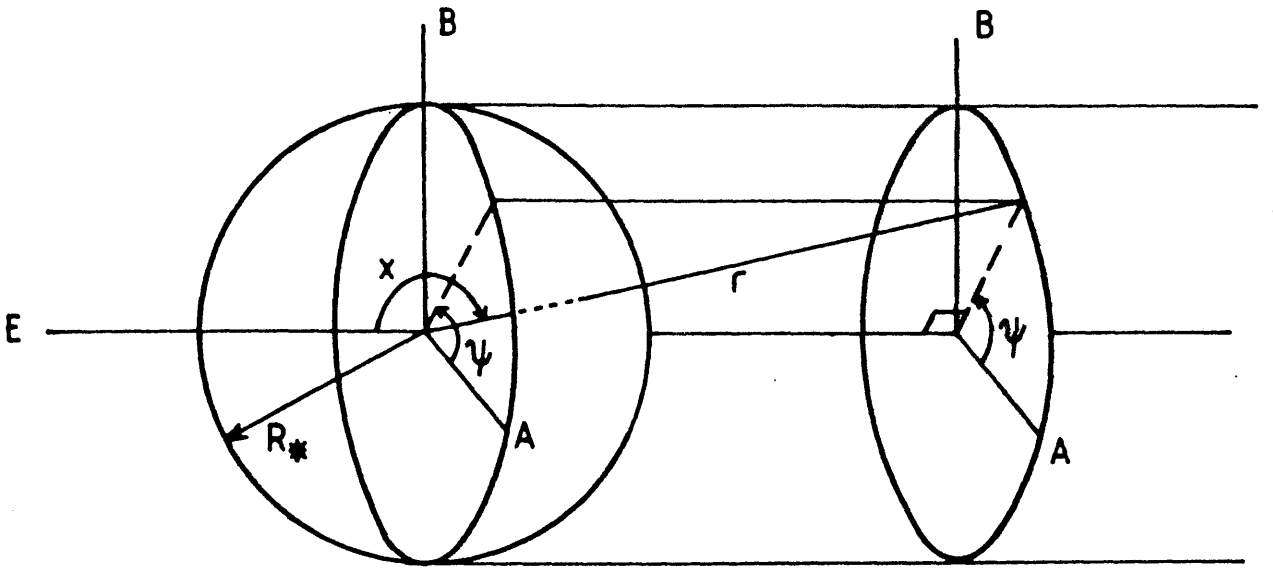

Figure 5.2

Occulting cylinder in the observer's frame.

of some presumed form in the stellar frame and it is, therefore, more convenient to transform from the observer's frame to the stellar (natural) frame via the following relations (Fig 5.3)

$$\left.\begin{aligned} \cos\chi &= \cos\theta\cos i - \sin\theta\sin i\sin\phi \\ \sin\chi\sin\psi &= \cos\theta\sin i + \sin\theta\cos i\sin\phi \\ \sin\chi\cos\psi &= \sin\theta\cos\phi \end{aligned}\right\} \qquad (5.5)$$

Substituting equations (5.5) into (5.1) and (5.2), we obtain

$$Q = (\tau_o - 3\tau_o\gamma_o)\sin^2 i - \tau_o\gamma_2\sin 2i + \tau_o\gamma_3(1 + \cos^2 i) \qquad (5.6)$$

$$U = 2(\tau_o\gamma_1\sin i + \tau_o\gamma_4\cos i) \qquad (5.7)$$

where

$$\tau_o = \frac{\sigma_o}{2}\int_V D(r)\, n(r,\theta,\phi)\, \frac{dV}{r^2} \qquad (5.8)$$

$$\tau_o\gamma_o = \frac{\sigma_o}{2}\int_V D(r)\, n(r,\theta,\phi)\, \cos^2\theta\, \frac{dV}{r^2} \qquad (5.9)$$

$$\tau_o\gamma_1 = \frac{\sigma_o}{2}\int_V D(r)\, n(r,\theta,\phi)\, \sin 2\theta\cos\phi\, \frac{dV}{r^2} \qquad (5.10)$$

$$\tau_o\gamma_2 = \frac{\sigma_o}{2}\int_V D(r)\, n(r,\theta,\phi)\, \sin 2\theta\sin\phi\, \frac{dV}{r^2} \qquad (5.11)$$

$$\tau_o\gamma_3 = \frac{\sigma_o}{2}\int_V D(r)\, n(r,\theta,\phi)\, \sin^2\theta\cos 2\phi\, \frac{dV}{r^2} \qquad (5.12)$$

$$\tau_o\gamma_4 = \frac{\sigma_o}{2}\int_V D(r)\, n(r,\theta,\phi)\, \sin^2\theta\sin 2\phi\, \frac{dV}{r^2} \qquad (5.13)$$

and $\frac{dV}{r^2} = \sin\theta d\theta d\phi dr$.

In the stellar frame the density distribution is simplified at the expense of complicating the integral limits. The volume integral can be expressed as three seperate volume integrals, viz

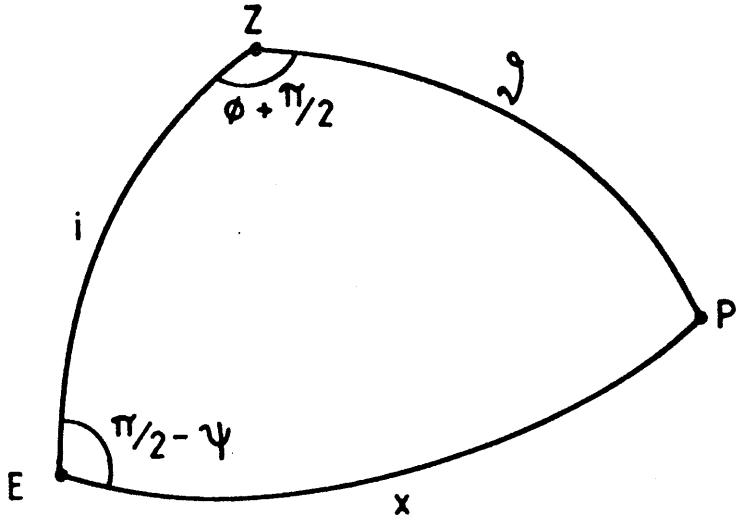

Figure 5.3

Spherical triangle from Fig. 5.1 for the tranformation from (r,χ,ψ) to (r,θ,ϕ) coordinates.

$$\int_V = \int_T - \int_{O_1} - \int_{O_2}$$

where

$$\int_T = \int_{R_*}^{\infty} \int_0^{\pi} \int_0^{2\pi} \quad (r \; \theta \; \phi)$$

$$\int_{O_1} = \int_{R_*}^{R_*/\sin i} \int_0^{2\pi} \int_{\theta(\phi,r)}^{\pi} \quad (r_1 \; \phi \; \theta)$$

$$\int_{O_2} = \int_{R_*/\sin i}^{\infty} \int_{\pi-(i+\zeta)}^{\pi-(i-\zeta)} \int_{\phi(\theta,r)}^{\pi-\phi(\theta,r)} \quad (r_2 \; \theta \; \phi)$$

with

$$\zeta = \sin^{-1}(R_*/r)$$

$$\phi(\theta,r) = \sin^{-1}\left[\frac{\cos\theta \cos i + \cos\zeta}{\sin\theta \sin i}\right]$$

$$\theta(\phi,r) = \cos^{-1}\left[\frac{\cos i \cos\zeta - \sin i \sin\phi \, (\sin^2\zeta - \sin^2 i \cos^2\phi)^{1/2}}{\sin^2 i \cos^2\phi - 1}\right] \qquad (5.14)$$

The first volume integral ($\int_T$) is the total volume of the envelope. The second volume intergal ($\int_{O_1}$) represents the volume enclosed by the occulting cylinder out to a radius $R_*\text{coseci}$ (Fig. 5.4) which is the outermost radius to which the rotation axis of the star passes through the occulting cylinder. The third integral ($\int_{O_2}$) is the volume of the occulting cylinder beyond $r = R_*\text{coseci}$.

Figure 5.4

In the stellar frame, the occulting cylinder is indicated at three different radii by the projection of the stellar disc (as viewed from E - see Fig. 5.2) on to the hemispherical surfaces.

The total volume of the occulting cylinder in the stellar frame is most conveniently considered as two separate volumes (see text). The first volume is that in which the stellar rotation axis of the star cuts through the occulting cylinder (i.e. out to a radius $R_*\text{coseci}$. The integral limits are indicated with a subscript 1). The second volume is then that in which the stellar rotation axis does not cut through the occulting cylinder. (Integral limits are indicated by a subscript 2.)

Figure 5.4

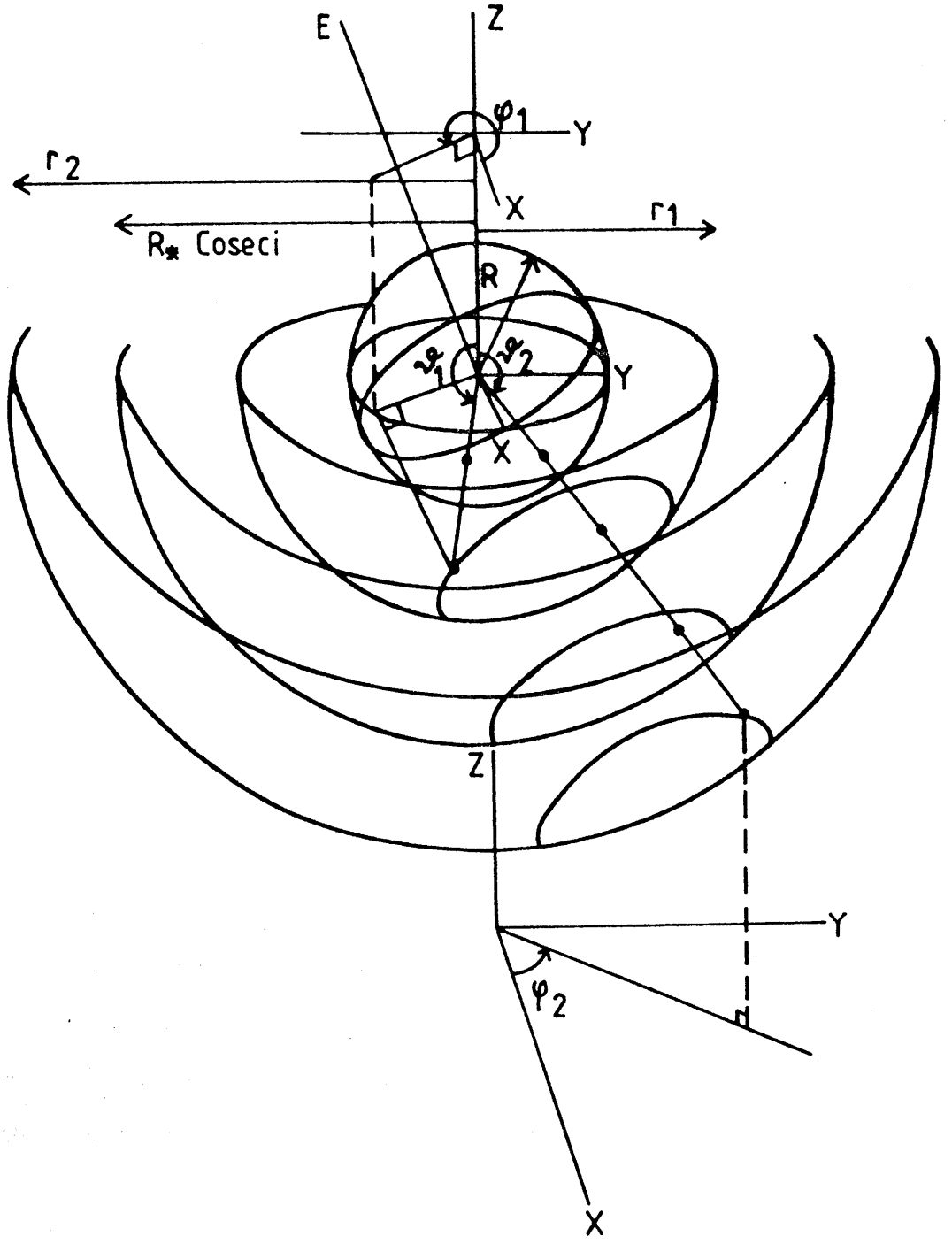

5.3 Axisymmetric Distributions.

Polarimetric observations of Be stars (Clarke and McGale 1988a, b; Clarke, 1990) have shown that the intrinsic polarisation of Be stars is variable and fluctuates about some mean value. This indicates that there exists an underlying axisymmetric envelope surrounding the star (which gives rise to the mean observed polarisation) that is subject to temporal density enhancements. These enhancements may be stochastic (Clarke and McGale, 1986, 1987) or periodic (Clarke and McGale, 1988a, b) in nature.

In Sec. 5.6 we shall investigate the variability of polarisation due to some density pertubation. Here, however, we wish to consider the time average polarisation from an axisymmetric envelope.

For an axisymmetric distribution [$n(\underline{r}) = n(r,\theta)$] the polarisation lies in a plane parallel to the axis of symmetry (i.e. the rotation axis). The net polarisation is therefore $P = Q$ ($U = 0$) and hence

$$P = Q = (\tau_o - 3\tau_o\gamma_o)\sin^2 i - \tau_o\gamma_2 \sin 2i + \tau_o\gamma_3(1 + \cos^2 i) \qquad (5.15)$$

The theoretical dependence of polarisation with certain observational parameters can be used to infer the geometry of the envelope (McLean and Brown, 1978) or to test the validity of envelope models (such as those of Doazan and Thomas, 1982; Marlborough et al., 1978) by constraining the parameter space (e.g. envelope shape and mass) to agree with polarimetric observations. Once the constraints of the model are established, it is then possible to decide whether the model is to be rejected or not. For example, if a model proposes that the scattering envelope is almost spherical, then for Be stars the model has to be rejected on the grounds that the mass of the envelope required is too large (compared to the inferred mass from

spectral observations). The polarimetric validation of envelope models is most easily achieved using the single scattering, point light source treatment of BM. It has been shown (Ch. 3 and 4) that the BM analysis overestimates the polarisation compared to when occultation and depolarisation are included and therefore the BM analysis permits a greater (and possibly different) range in the parameter space than when depolarisation and occultation are taken into account.

In order to illustrate the effects of occultation and depolarisation upon the polarisation from circumstellar envelopes (compared to the BM treatment) three geometries, similar to those of BM are considered. These are:

(i) A spherical shell with a surface density that depends on the colatitude, viz

$$\Omega = \Omega_0 \, \delta(r - R) \exp-\beta|\cos\theta|.$$

where Ω_0 is the equatorial surface density, R is the radius of the shell and β is a free parameter ($-\infty < \beta < \infty$) that describes the variation of the scattering material over the surface.

(ii) An oblate spheroidal shell with uniform density,

$$\frac{R_1}{\sqrt{1 + (A^2 - 1)\cos^2\theta}} < r < \frac{R_1 + hR_*}{\sqrt{1 + (A^2 - 1)\cos^2\theta}} \qquad n(r,\theta) = n_0$$

$$\text{otherwise} \qquad n(r,\theta) = 0$$

where $A > 1$ (for an oblate spheroid) and R_1 is the equatorial radius of the envelope. In addition (for the puposes of integration) we will assume that the shell is thin, $h << 1$.

(iii) A wedge shaped equatorial disc (cylindrical sector geometry) of infinite extent with a radial power law distribution, $n = n_0(r/R_*)^{-n}$ and a half opening angle α, where n_0 is the electron number density at

thr surface of the star [$n_o = n(r = R_*)$ and n is the power index.

5.3.1 Axisymmetric Envelopes View in the Equatorial Plane (i = 90).

Before proceeding to the general inclination case, it is instructive to compare the point light source polarisation with that when depolarisation and occultation are included for envelopes viewed in the equatorial plane.

5.3.2 Spherical shell.

(a) Point light source.

From the BM analysis the polarisation is,

$$P_o = \frac{2\pi\sigma_o\Omega_o}{\beta}\left[(1 - e^{-\beta}) - 3\left\{ \frac{2}{\beta^2} - e^{-\beta}\left[1 + \frac{2}{\beta} + \frac{2}{\beta^2}\right]\right\} \right] \qquad (5.16)$$

(b) Extended light source without occultation.

For this particular geometry depolarisation is taken into account by multiplying P_o by the depolarisation factor which is uniform over the shell, viz

$$P_1 = (1 - X^{-2})^{1/2} P_o \qquad (5.17)$$

where $X = R/R_*$ and R is the radius of the shell.

(c) Extended light source with occultation.

In Fig. 5.5 the occulted region of the shell is shown as the hatched area. This is the projection of the stellar disc (as seen from E) upon the surface of the shell (see also Fig. 5.4). The polarisation is then,

$$P_2 = (\tau_o - 3\tau_o\gamma_o) + \tau_o\gamma_3 \qquad (5.18)$$

where,

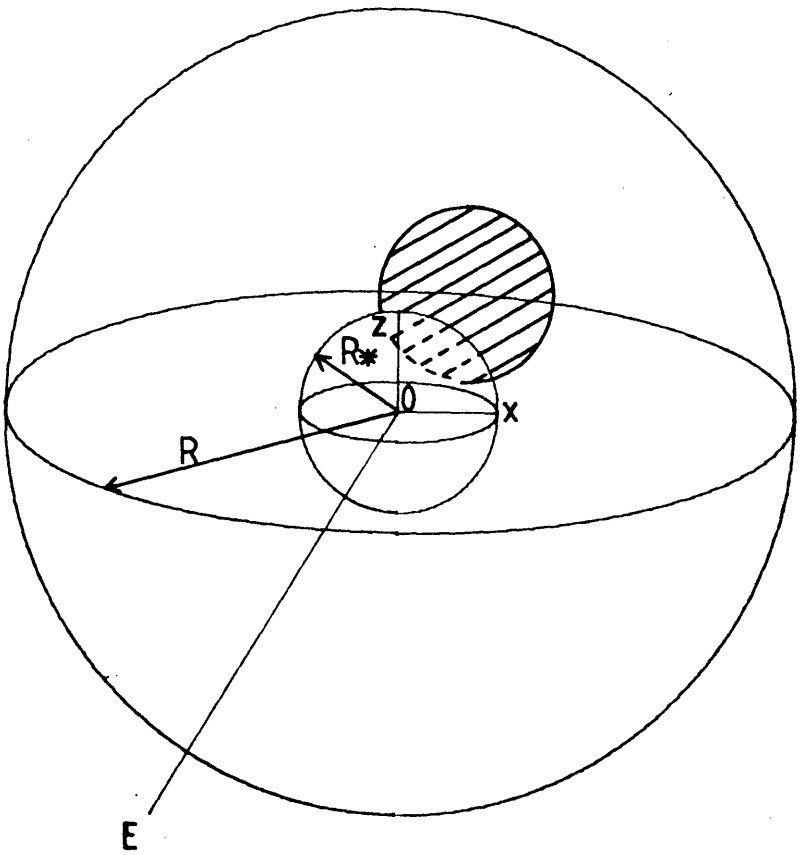

Figure 5.5

Schematic diagram of a spherical shell (radius R) surrounding a star (radius R_*) with an observer (E) in the equatorial plane. The hatched area is the occulted region of the envelope (as seen at E).

$$\tau_o = \frac{2\pi\sigma_o\Omega_o}{\beta}(1 - X^{-2})^{\frac{1}{2}}\left\{\frac{1}{2} - e^{-\beta} + \frac{e^{-\beta/X}}{2} + \frac{\beta}{\pi}\int_0^{1/X} e^{-\beta}\,\phi(\mu)\,d\mu\right.$$

$$\tau_o y_o = \frac{2\pi\sigma_o\Omega_o}{\beta}(1 - X^{-2})^{\frac{1}{2}}\left\{\frac{1}{\beta^2} - e^{-\beta}\left[1 + \frac{2}{\beta} + \frac{2}{\beta^2}\right] + \frac{e^{-\beta/X}}{2}\left[\frac{1}{X^2} + \frac{2}{\beta X} + \frac{2}{\beta^2}\right]\right.$$

$$\left. + \frac{\beta}{\pi}\int_0^{1/X} \mu^2\, e^{-\beta\mu}\,\phi(\mu)\,d\mu\right\}$$

$$\tau_o y_3 = \frac{2\pi\sigma_o\Omega_o}{\beta}(1 - X^{-2})^{\frac{1}{2}}\left\{\frac{\beta}{2\pi}\int_0^{1/X} (1 - \mu^2)\, e^{-\beta\mu}\,\sin\{2\phi(\mu)\}\,d\mu\right.$$

and $\qquad \phi(\mu) = \left[\frac{1 - X^{-2}}{1 - \mu^{-2}}\right] \qquad \mu = \cos\theta$

The variation of P_1 and P_2 (compared to P_o) are shown in Fig. 5.6 and 5.7 as functions of β and the radius of the shell ($X = R/R_*$) respectively. It can be seen that occultation is unimportant when the shell is either distant from the star ($X > 3$) or when the scattering material is concentrated towards the poles of the star ($\beta < 0$) because in both cases very little material is being occulted and thus the polarisation is adequately approximated by the inclusion of the depolarisation factor alone (i.e. $P_2 \sim P_1$). Moreover at large distances the point light source analysis is valid ($P_2 \sim P_o$). From Fig. 5.6 it appears that occultation is unimportant compared to the correction for depolarisation. However, for relatively close shells ($X < 2$) with equatorially concentrated scattering distributions ($\beta > 0$) the polarisation is overestimated by ~20% (at $X \sim 1.2$) when depolarisation is included but occultation is not.

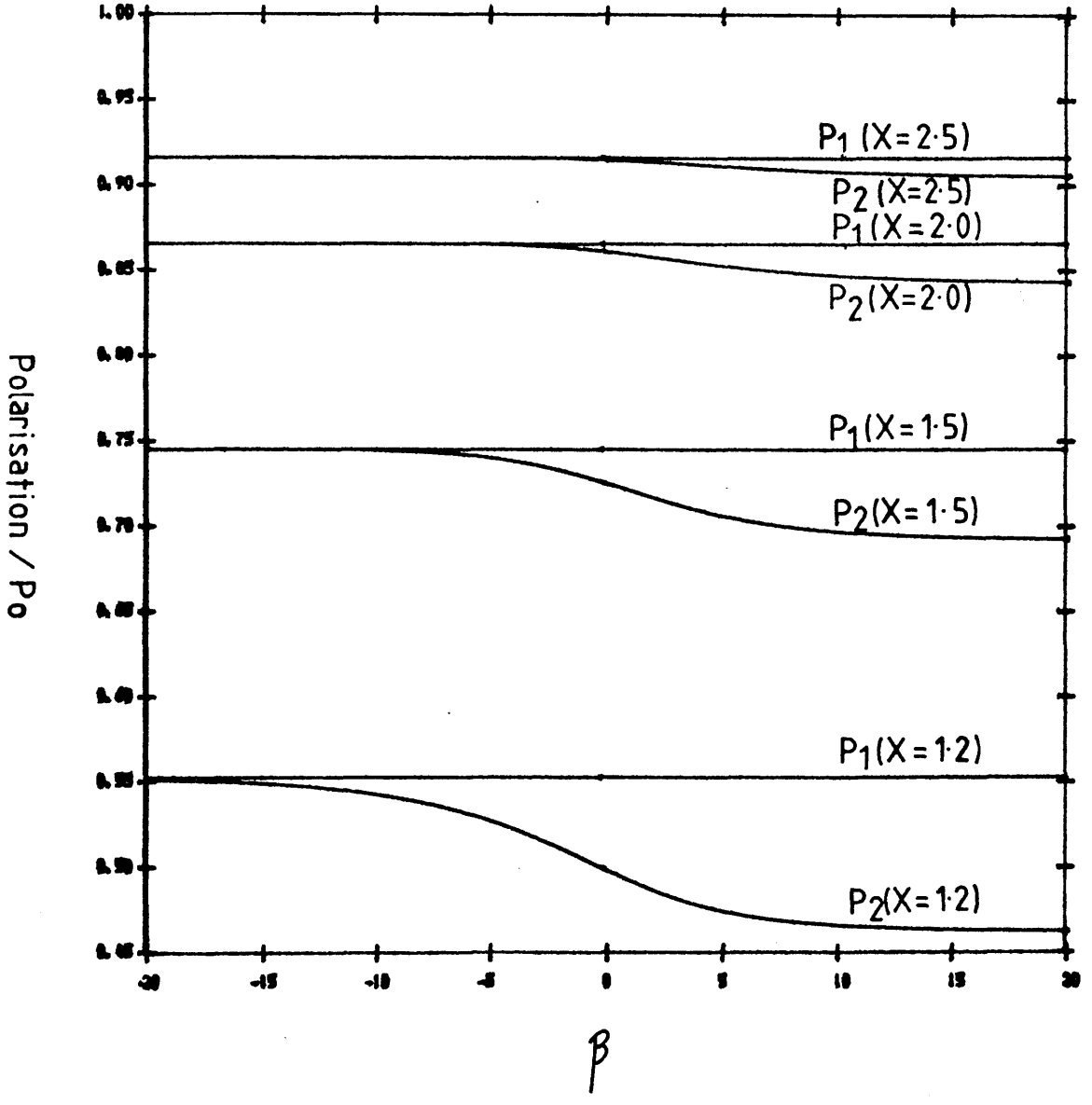

Figure 5.6

Plot of polarisation values P_1 and P_2 compared to P_o as a function of β for spherical shells of fixed radii (X).

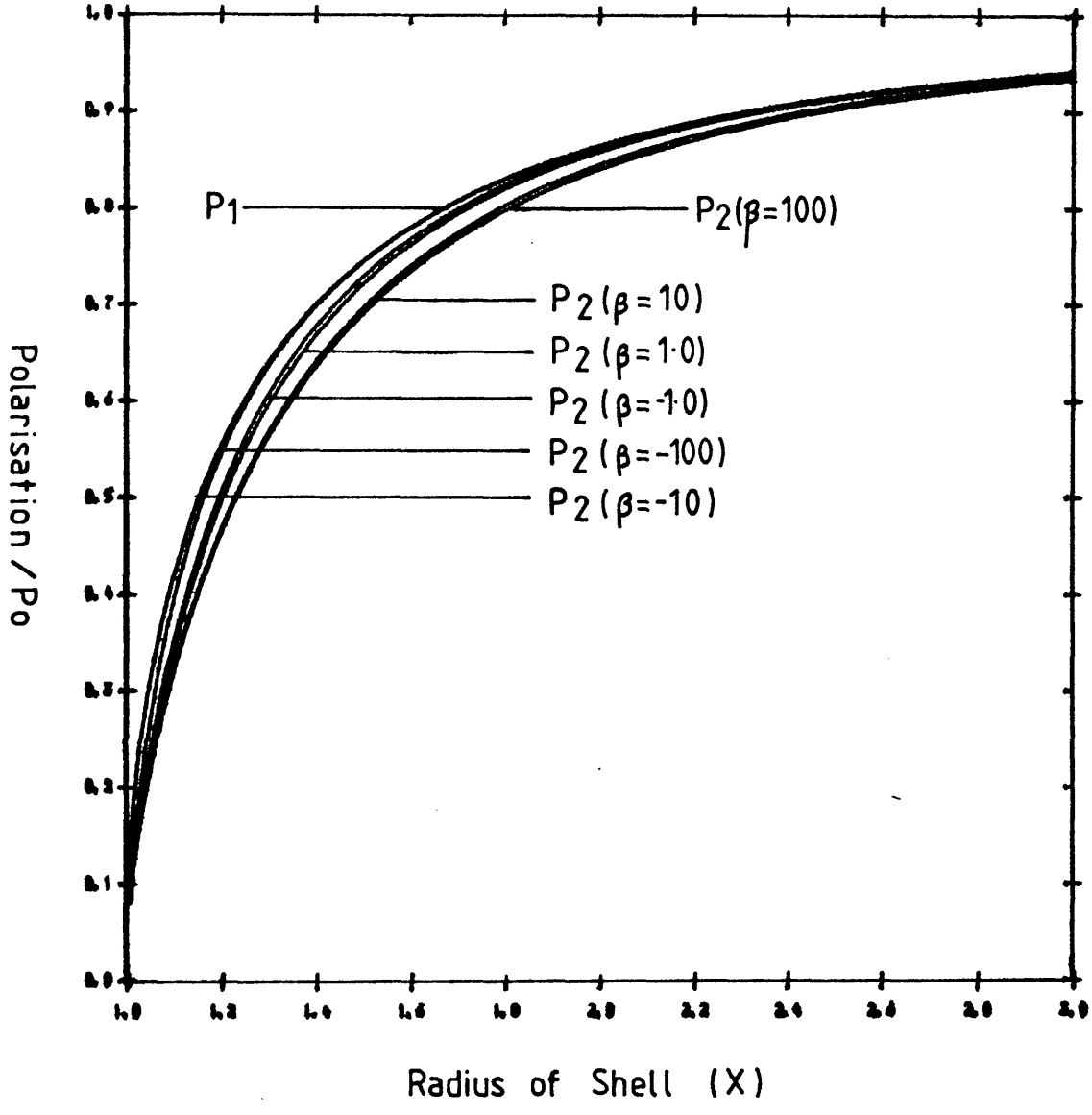

Figure 5.7

Plot of polarisation values P_1 and P_2 compared to P_o as a function of radius (X) for spherical shells with fixed β.

5.3.3 Oblate Spheroid.

(a) Point light source.

From the analysis of BM,

$$P_o = 2\pi\sigma_o n_o h R_* \left\{ \frac{1}{(A^2-1)^{1/2}} \ln\left|A + (A^2-1)^{1/2}\right| - \frac{3}{2(A^2-1)}\left[A - \frac{1}{(A^2-1)^{1/2}} \ln\left|A + (A^2-1)^{1/2}\right|\right]\right\} \tag{5.19}$$

(b) Extended Light source without occultation.

$$P_1 = 2\pi\sigma_o n_o R_* \int_0^1 \int_{x_1(\mu)}^{x_2(\mu)} (1 - x^{-2})^{1/2} (1 - 3\mu^2)\, dx d\mu \tag{5.20}$$

where $x_{1,2}(\mu)$ are given below.

(c) Extended light source with occultation.

In Fig. 5.8 the occulted region of the spheroid/ellipsoid is shown as the hatched area, which is the projection of the stellar disc upon the surface of the shell. Notice that the region is elongated towards the poles as the polar regions are closer to the star than the equatorial region. The polarisation is found to be (with the aid of Fig. 5.3)

$$P_2 = (\tau_o - 3\tau_o\gamma_o) + \tau_o\gamma_3 \tag{5.21}$$

where

$$\tau_o - 3\tau_o\gamma_o = 2\pi\sigma_o n_o R_* \left[\int_0^1 \int_{x_1(\mu)}^{x_2(\mu)} (1 - x^{-2})^{1/2} (1 - 3\mu^2)\, dx d\mu - \frac{1}{2\pi} \int_0^{\mu_o} \int_{x_1(\mu)}^{x_2(\mu)} (1 - x^{-2})^{1/2} (1 - 3\mu^2) \{\pi - 2\phi(\mu)\}\, dx d\mu \right]$$

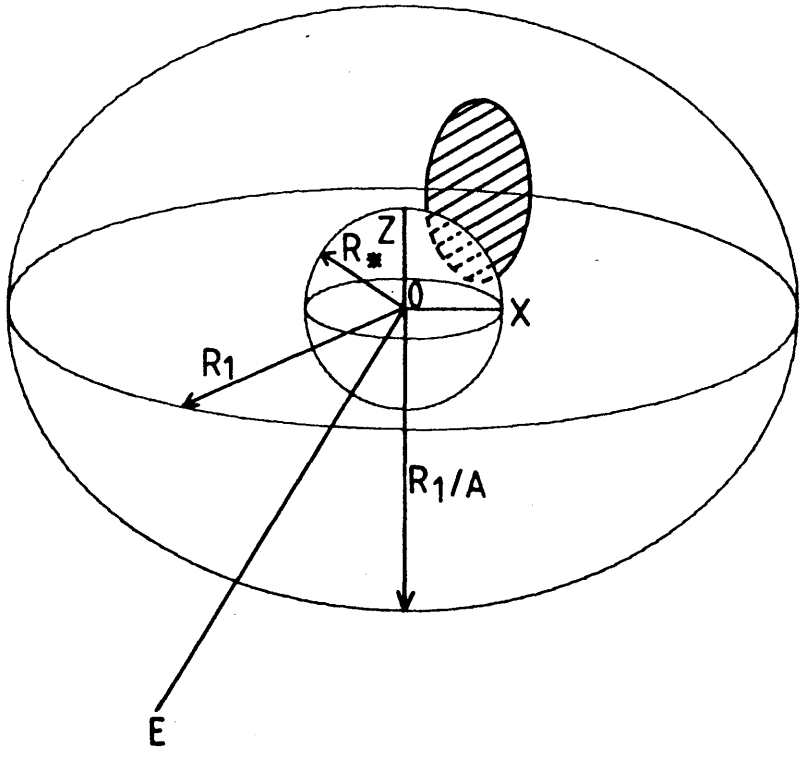

Figure 5.8

Schematic diagram of an ellipsoidal shell (equatorial radius R_1, oblateness A) surrounding a star (radius R_*) with an observer (E) in the equatorial plane. The hatched area is the occulted region of the surface (as seen from E).

$$\tau_o \gamma_3 = 2\pi\sigma_o n_o R_* \left[\frac{1}{2\pi} \int_0^{\mu_o} \int_{x_1(\mu)}^{x_2(\mu)} (1 - x^{-2})^{\frac{1}{2}} (1 - \mu^2) \sin 2\phi(\mu) \, dx d\mu \right]$$

with $x = r/R_*$ and

$$x_1(\mu) = \frac{R_1/R_*}{\sqrt{1 + (A^2 - 1)\mu^2}} , \qquad x_2(\mu) = \frac{R_1/R_* + h}{\sqrt{1 + (A^2 - 1)\mu^2}}$$

$$\phi(\mu) = \sin^{-1}\left[\frac{R_*}{R_1} \frac{[(R_1/R_*)^2 - (1 + (A^2 - 1)\mu^2]^{\frac{1}{2}}}{(1 - \mu^2)^{\frac{1}{2}}} \right] \quad (h << 1)$$

$$\mu_o = [(R_1/R_*)^2 - (A^2 - 1)]^{\frac{1}{2}} \quad (h << 1)$$

We take $h << 1$ (i.e. an ellipsoid of finite thickness but comparatively thin compared to its equatorial or polar radii) in order to simplify the complexity of the problem. The problem is further simplified as the inner intergral may then be approximated by a Taylor expansion.

The variations of P_1 and P_2 (compared to P_0) are shown in Figs 5.9 and 5.10 as functions of the oblateness (A) and the equatorial radius ($X_1 = R_1/R_*$) respectively. The most striking thing to notice is that contrary to what would be expected, the inclusion of "depolarisation" actually enhances the polarisation by almost a factor of two compared to when depolarisation is neglected. This phenomenon is due to the vector nature of polarised light. Consider the case when an ellipsoidal envelope touches the poles of the star (cf. Fig. 5.8). In the point light source case, scatterers that lie in the equatorial plane will produce polarised light that is parallel to the rotation axis, whilst scatterers at the poles will produce polarised light that is perpendicular to this plane. Since these regions produce oppositely polarised light partial cancellation occurs. Since more scatterers lie in the equatorial plane the net polarisation will lie in a plane parallel to the rotation axis and

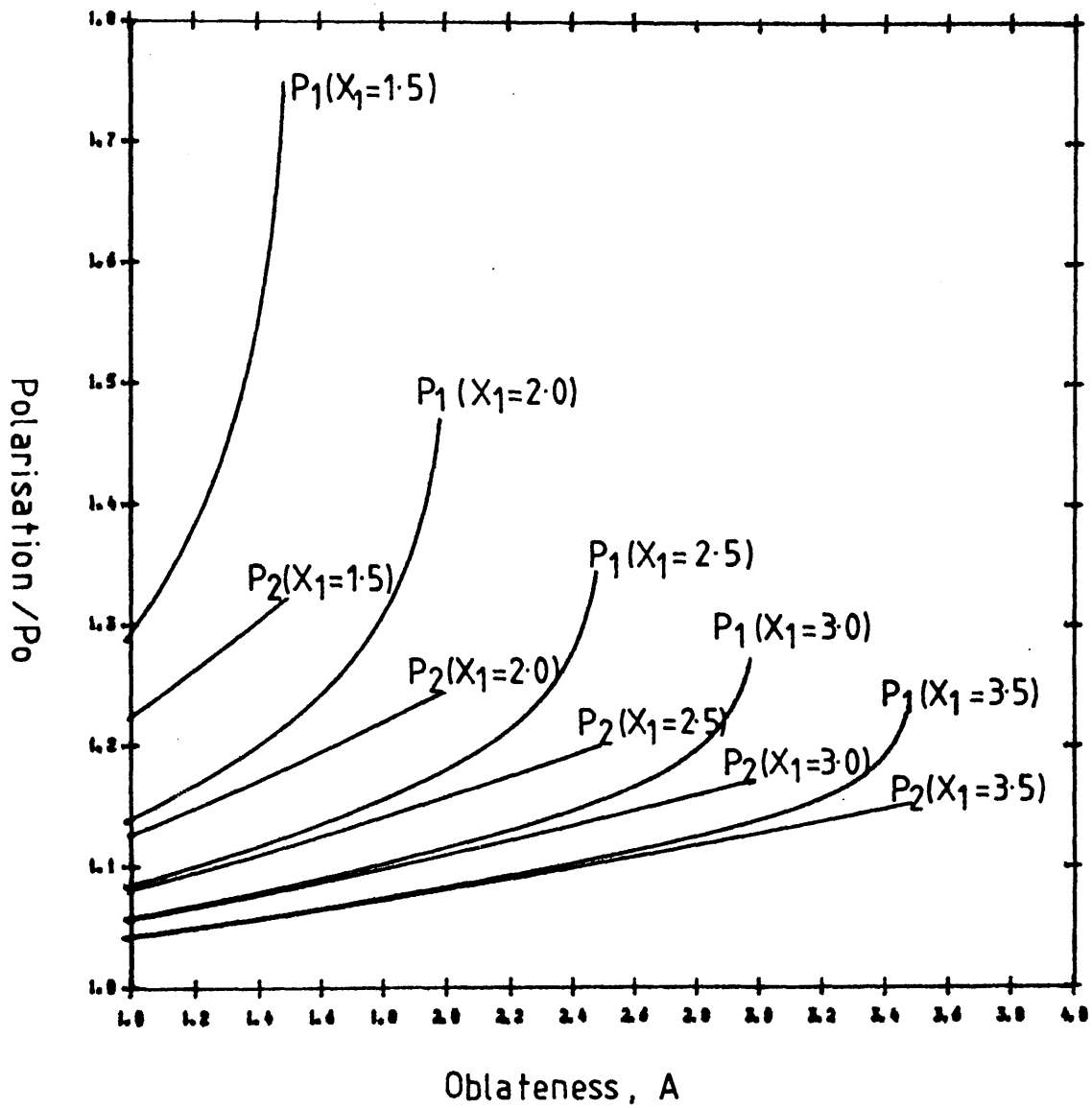

Figure 5.9

Plot of polarisation values P_1 and P_2 compared to P_o as a function of oblateness (A) for ellipsoids of fixed equatorial radii (X_1).

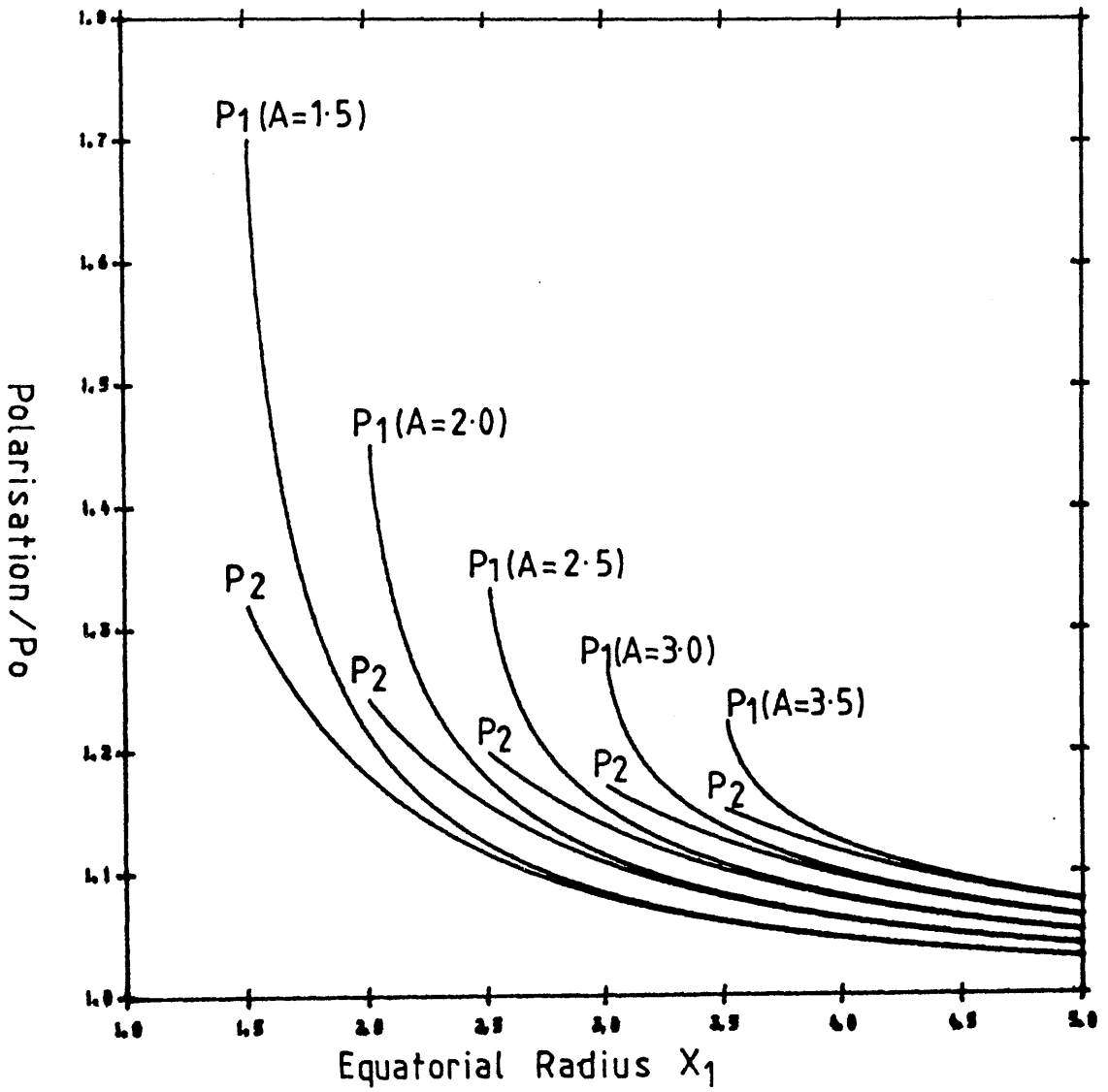

Figure 5.10

Plot of polarisation values P_1 and P_2 compared to P_o as a function of equatorial radius (X_1) for ellipsoids with fixed oblateness (A).

will be reduced compared to the polarisation from the equatorial region alone. For a finite light source material closest to the star (i.e. the poles) will be most affected by depolarisation whilst scattering material in the equatorial plane will essentially see a point light source and therefore will not be much reduced (compared to the point light source calculations). The net polarisation of the whole ellipsoid will then be approximately equal to that of the equatorial regions because there is little or no contribution from the poles (i.e little cancellation) and consequently the polarisation will be enhanced (compared to the point light source approximation) and lies in a plane parallel to the rotation axis.

The effect of occultation is to reduce the polarisation (compared with P_1) but this is a rather minor correction and only significant when the envelope is oblate and the equatorial radius is small ($X_1 < 4$) such that a significant number of scatterers are occulted.

5.3.4 Wedge Shaped Disc.

(a) Point light source.

From the analysis of BM the polarisation is

$$P_0 = 2\pi\sigma_0 n_0 R_* \frac{\sin\alpha \cos^2\alpha}{n - 1} \qquad (5.22)$$

(b) Extended light source without occultation.

$$P_1 = \frac{(n - 1)}{2} B(^{(n+1)}/_2, {}^3/_2)\, P_0 \qquad (5.23)$$

where B is the beta function.

(c) Extended light source with occultation.

In Fig. 5.11 the occulted region of the disc is shown. The polarisation arising from the volume V_2 is zero because, according to an observer

Figure 5.11

Cross-section through a wedge shaped disc (opening angle α) surrounding a star (Radius R_*) with the observer (E) in the equatorial plane. The hatched region is the total occulted volume ($V_1 + V_2$). Since V_2 is rotationally symmetric, according to the observer, the net polarisation of V_2 is zero and then the only contributing volume to the polarisation in the occulted region is V_1.

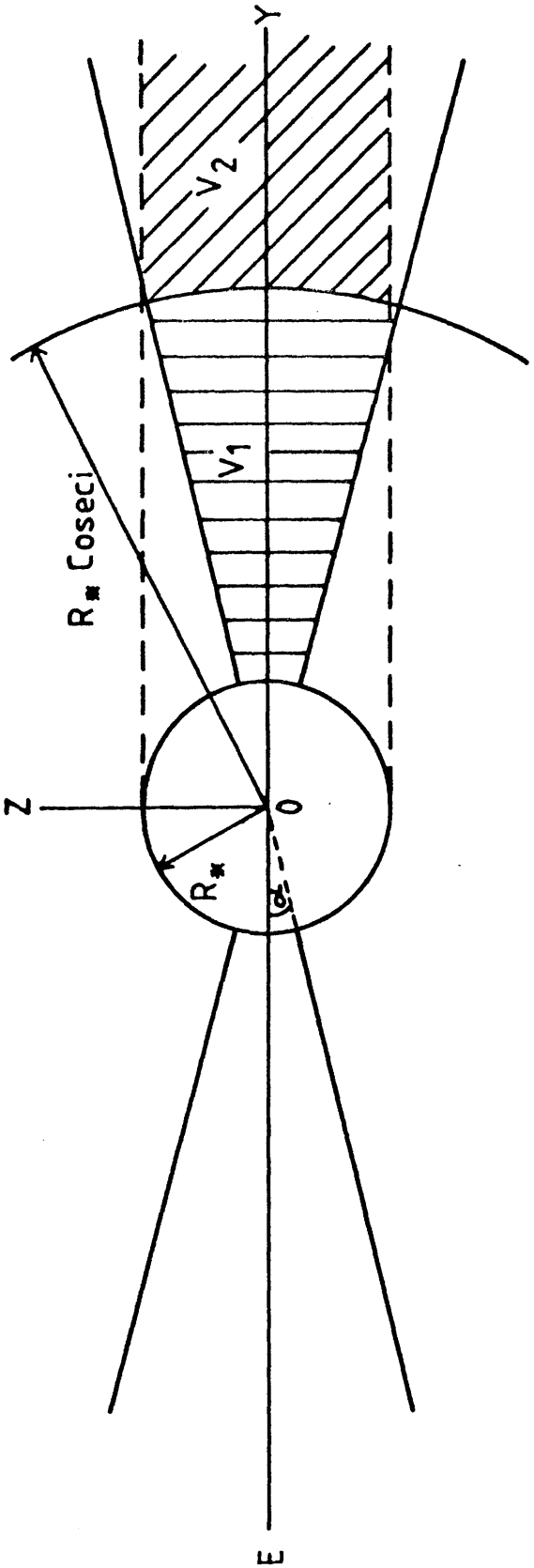
Y
V2
V1
R* Coseci
Z
O
R*
E

at E, the region is rotationally symmetric about the line of sight. The net polarisation is then,

$$P_2 = (\tau_o - 3\tau_o\gamma_o) + \tau_o\gamma_3 \qquad (5.24)$$

where

$$\tau_o - 3\tau_o\gamma_o = 2\pi\sigma_o n_o R_* \left[\frac{1}{2} B(^{(n+1)}/_2, ^3/_2) \sin^2\alpha \cos\alpha \right.$$

$$\left. - \frac{1}{2\pi} \int_{\sin\alpha}^{1} \int_{o}^{\sin\alpha} (1 - y^2)^{1/2} y^{n-2} (1 - 3\mu^2) \{\pi - 2\phi(\mu,y)\} \, d\mu dy \right]$$

$$\tau_o\gamma_3 = 2\pi\sigma_o n_o R_* \left[\frac{1}{2\pi} \int_{\sin\alpha}^{1} \int_{o}^{\sin\alpha} (1 - y^2)^{1/2} y^{n-2} \sin 2\phi(\mu,y) \, d\mu dy \right]$$

and

$$\phi(\mu,y) = \sin^{-1}\left[\left[\frac{1 - y^2}{1 - \mu^2} \right]^{1/2} \right] \quad , \; y = R_*/r$$

The variation of P_1 and P_2 (compared to P_o) are shown is Figs 5.12 and 5.13 as functions of opening angle (α) and power index (n). For a disc of infinite extent, in order that the mass of the envelope is finite the power index must be $n > 3$ (see section 5.4).

It can be seen that the effect of occultation is to reduce the observed polarisation (compared to P_1 and P_o) and is most significant for small opening angle and high values of n since then volume V_1 contains a significant number of scatterers. By increasing the opening angle the occulting volume V_1 becomes insignificant and occultation effects are then negligible (i.e $P_2 \rightarrow P_1$ as $\alpha \rightarrow 90^\circ$). Similarly as $n \rightarrow 3$, the scattering distribution is less concentrated near the star and so the volume V_1 is less significant.

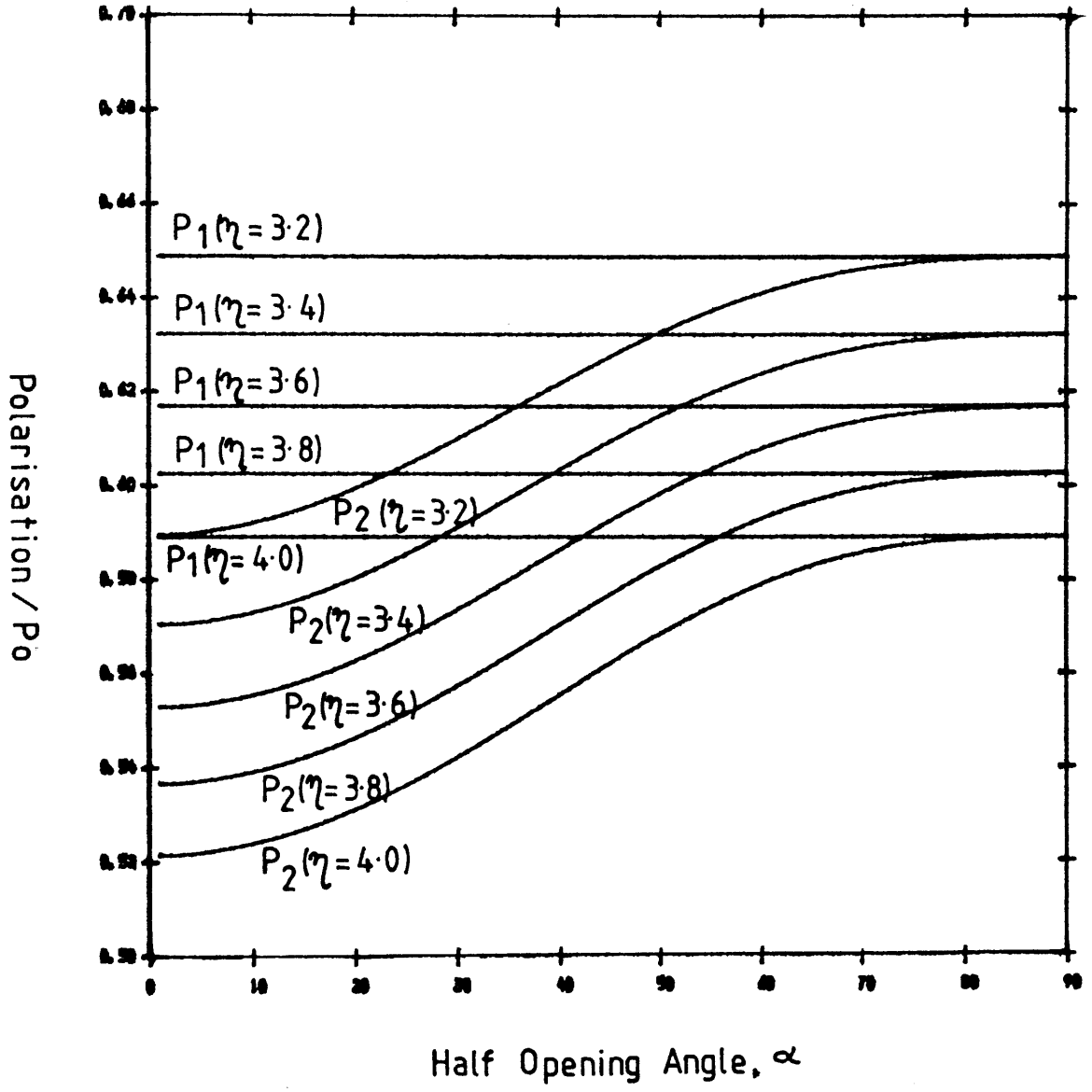

Figure 5.12

Plot of polarisation values P_1 and P_2 compared to P_o as a function of half opening angle (α) for discs with fixed power indices (n).

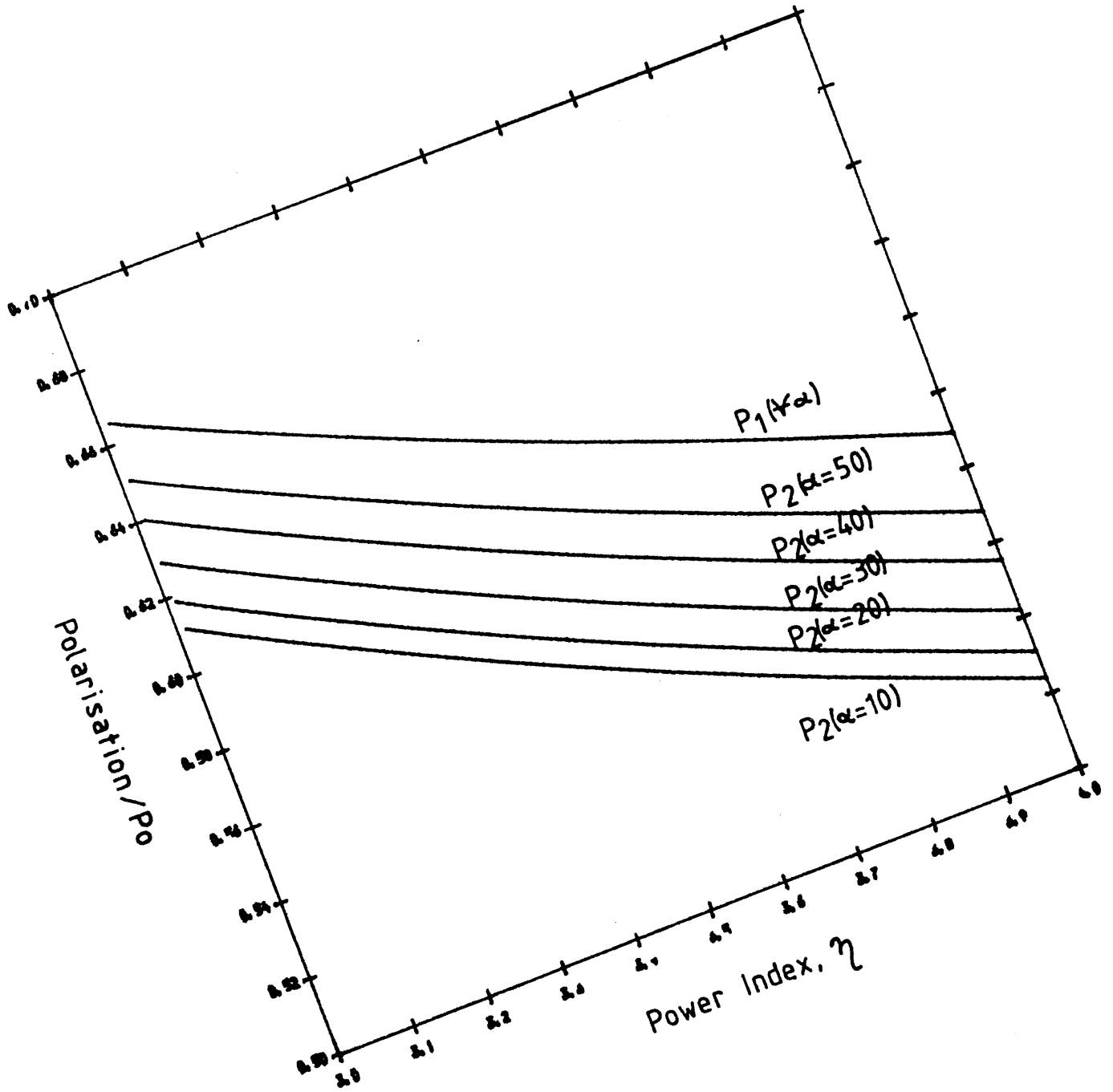

Figure 5.13

Plot of polarisation values P_1 and P_2 compared to P_o as a function of power index for discs with fixed half opening angle (α).

5.4 Absolute Polarisation.

Be stars are observed to be highly intrinsically polarised early type stars exhibiting polarisations of up to 2% (c.f. Sec. 1.5). In order to observe such a high degree of polarisation the scattering envelope surrounding the star must be highly asymmetric as viewed by an observer. To account for such a high degree of polarisation the scattering envelope has been modelled by some authors as an equatorial mass enhancement (Marlborough et al., 1978; Dachs et al., 1986; Waters, 1986) whilst others have interpreted the envelope to be ellipsoidal (Doazan and Thomas, 1982; McLean and Brown, 1978).

In our modelling of scattering envelopes we have implicitly assumed through out that the envelope is optically thin, i.e. $\tau < 1$

where $$\tau = \frac{\sigma_o N_e}{R_*^2} \qquad (5.25)$$

and N_e is the total number of scattering electrons. For $\tau \sim 1$ we may put an upper limit on the mass of the envelope to be $M_{env} \sim 10^{-8}\ M_\odot$ (assuming the envelope to be purely 100% ionised hydrogen). Spectroscopic observations of Be stars suggest a mass loss value of typically 10^{-8} - $10^{-10}\ M_\odot/yr$ from UV observations (Snow and Marlborough, 1976; Lamers and Rogerson, 1978) whilst IR observations indicate mass loss rates systematically a factor of 10 - 10^2 higher (Waters et al., 1988). The inferred mass loss rates, therefore, indicate an envelope lifetime of typically of the order of decades. This is consistent with the observed timescale of Be star phase changes (Underhill and Doazan, 1982 p. 317) and theoretical estimates (Apparao et al., 1987) which suggest a short period of enhanced mass loss from the star followed by a slower steady mass loss of the resulting

envelope which re-occurs on timescales of approximately a decade.

A useful quantity with which to compare these geometries with each other is the polarisation per unit mass (P_2/M_{env}). This can be considered as a measure of how efficiently an envelope of given mass will produce a net polarisation. If we consider a star with a polarisation of 2% (i.e the maximum polarisation of a Be star) then

$P_2 = 2\% = 0.02.$

$M_{env} = m_p N_e$ (kg) so substituing for N_e from eq. (5.25) we have

$M_{env} = m_p R_*^2 \tau/\sigma_o$ (kg)

and hence $P_2/M_{env} \sim 0.04\ (\sigma_o/2m_p R_*^2)\ kg^{-1}$ for $\tau \sim 1$.

For a shell of radius X (= R/R_*) the mass of the envelope is given by

$$M_{env} = 4\pi\Omega_o m_p R_*^2 X^2 (1 - e^{-\beta})/\beta \quad (kg) \qquad (5.26)$$

In Fig. 5.14 the variation of the function P_2/M_{env} is shown as a function of the shell radius. The curve represents the observed polarisation from a shell of constant mass (and β) expanding out from the star. As the envelope expands, the polarisation increases and reaches a maximum at X ~ 1.2 (due to a trade-off between depolarisation and the inverse square law) and thereafter decreases, falling off as X^{-2}. The distance at which P_2/M_{env} reaches a maximum can be found by differentiating P_2/M_{env} with respect to X and setting $d(P_2/M_{env})/dX = 0$, viz

$$\frac{d}{dX}\left[\frac{P_2}{M_{env}}\right] = \frac{1}{X^3}\,\frac{1}{\sqrt{1 - X^{-2}}}\left[2 - \frac{3}{X^2}\right]$$

so $\frac{d}{dX}\left[\frac{P_2}{M_{env}}\right] = 0$ when $X = \sqrt{3/2} \sim 1.2$

Polarimetric observations of ω Ori (Sonneborn et al., 1988, Brown and Henrichs, 1987) shows that the star exhibits temporal variations similiar to those of Fig. 5.14. This would suggest that the temporal

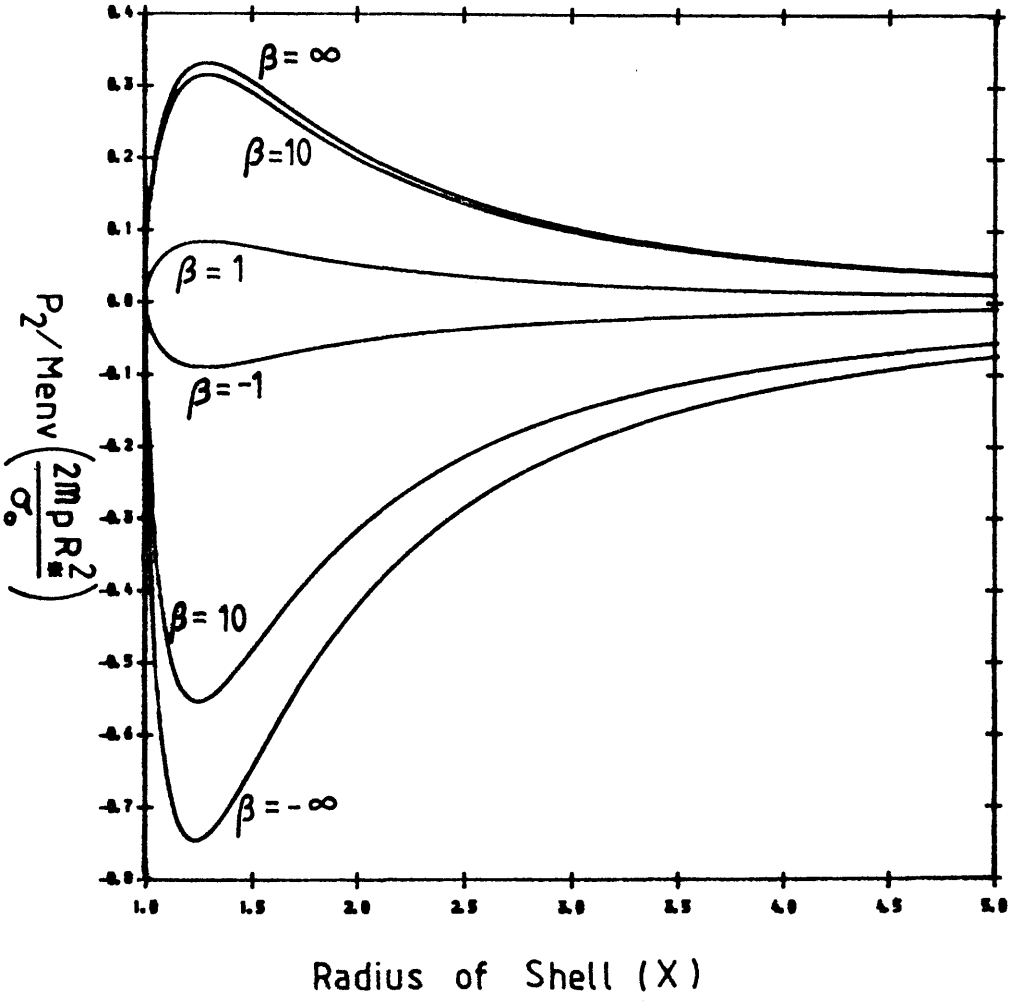

Figure 5.14

The variation of polarisation per unit mass (P_2/M_{env}) with radius (X) for a shell with fixed values of β.

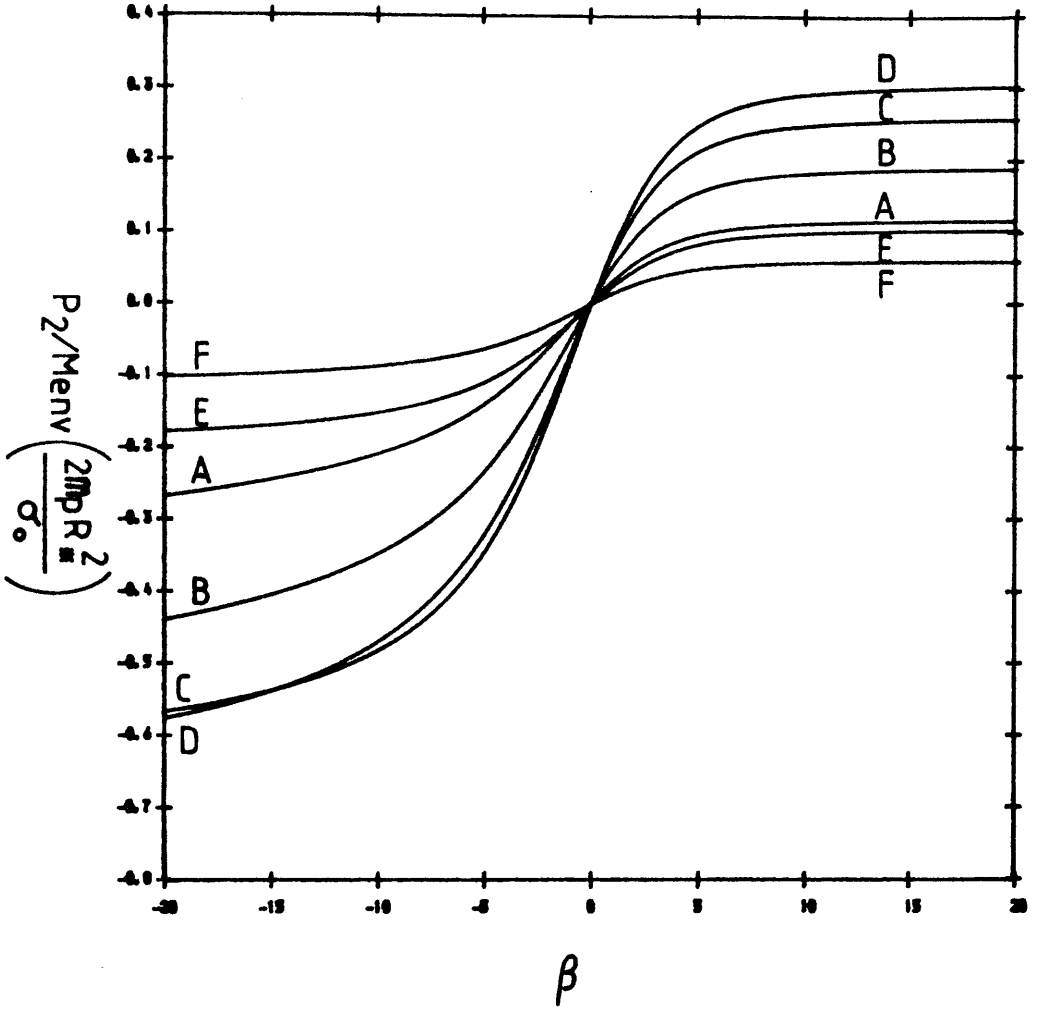

Figure 5.15

The variation of polarisation per unit mass (P_2/M_{env}) with β for a shell with fixed values of radius (X).

Legend; curve A: X = 1.02, B: X = 1.05, C: X = 1.1, D: X = 1.5

E: X = 3.0, F: X = 4.0

polarimetric variations of ω Ori may be interpreted as an expanding shell of material (for a full discussion concerning the interpretation of the polarimetric variations see Brown and Henrichs, 1987). In this interpretation, the peak in the polarimetric data occurs because the shell has expanded to a radius of ~ $1.2R_*$. It is possible, from this, to estimate the expansion velocity of such an envelope (assuming the envelope is 'lifted off' from the stellar surface and expands at a uniform rate) via

$$v \sim 1.2R_*/t_{max} \qquad (5.27)$$

where $R_* \sim 10R_\odot$ and $t_{max} \sim 1 \times 10^6$s (time taken for polarisation to change from the quiescent to maximum value, Sonneborn et al., 1988) and hence $v \sim 8.4$ kms^{-1}, which is approximately the thermal (sound) speed of the cool wind ($v \sim 10$ kms^{-1} at 10^4 K). The polarimetric variations occurring within the wind of ω Ori would therefore appear to be associated with a low velocity component of the wind, whereas the UV spectroscopic variations are associated with a high velocity component (typically $v_{uv} \sim 100$ kms^{-1}). This would suggest (but not prove - see Brown and Henrichs, 1987) that the polarisation arises from a region different from that of the UV line variations

Fig. 5.15 shows the variation of P_2/M_{env} as a function of β. Note that for $\beta = 0$ the net polarisation is zero because the envelope is spherically symmetric. When $\beta < 0$, the scattering material is concentrated towards the polar regions, the polarisation vector lies in a plane perpendicular to the rotation axis and hence the polarisation is negative in sign (by definition). From Figs 5.14 and 5.15 it can be seen that in order to produce a maximum polarisation of 2% the radius of the shell must lie between ~ 1.1 and 4.0 (R_*) and the material must be concentrated towards the polar or equatorial regions (i.e. $|\beta| > 5$).

For a geometrically thin ($h << 1$) oblate ellipsoid of equatorial radius X_1 ($= R_1/R_*$) and oblateness A, the mass of the envelope is given by

$$M_{env} = 4\pi n_o m_p R_*^3 h X_1^2/A \quad (kg) \qquad (5.27)$$

In Fig. 5.16 the variation of the P_2/M_{env} is shown as a function of the equatorial radius (X_1). The curves can be considered as envelopes (with constant oblateness) uniformly expanding away from the star and in doing so the polarisation monotonically decreases, falling approximately as X_1^{-2}. In Fig. 5.17 the variation of P_2/M_{env} as a function of oblateness is shown. Here the curves indicate the variation of polarisation for envelopes with a fixed equatorial radius expanding in the polar directions (decreasing A). As the polar radius increases the envelope becomes increasingly spherical ($A \rightarrow 1$) and hence the polarisation tends to zero. It is apparent (from Figs 5.16 and 5.17) that in order to produce a maximum polarisation of 2% the envelope must be very oblate for a given equatorial radius (i.e. envelope must be touching, or almost touching, the stellar surface at the poles) and yet the equatorial envelope cannot be too large (i.e the absolute value of the oblateness cannot be too great). In essence our results agree with the conclusions of Doazan and Thomas (1982) and McLean and Brown (1978) who suggest that extremely oblate envelopes are not necessary in order to explain the observed polarisation of Be stars. In fact extremely oblate envelopes (approximately $A > 5$) are unable to produce a polarisation of 2%. It must be remembered, however, that although the absolute value of the oblateness may not be large, in order to produce a polarisation of 2%, the envelope must be near its maximum oblateness (i.e. the envelope almost touching the stellar surface at the poles).

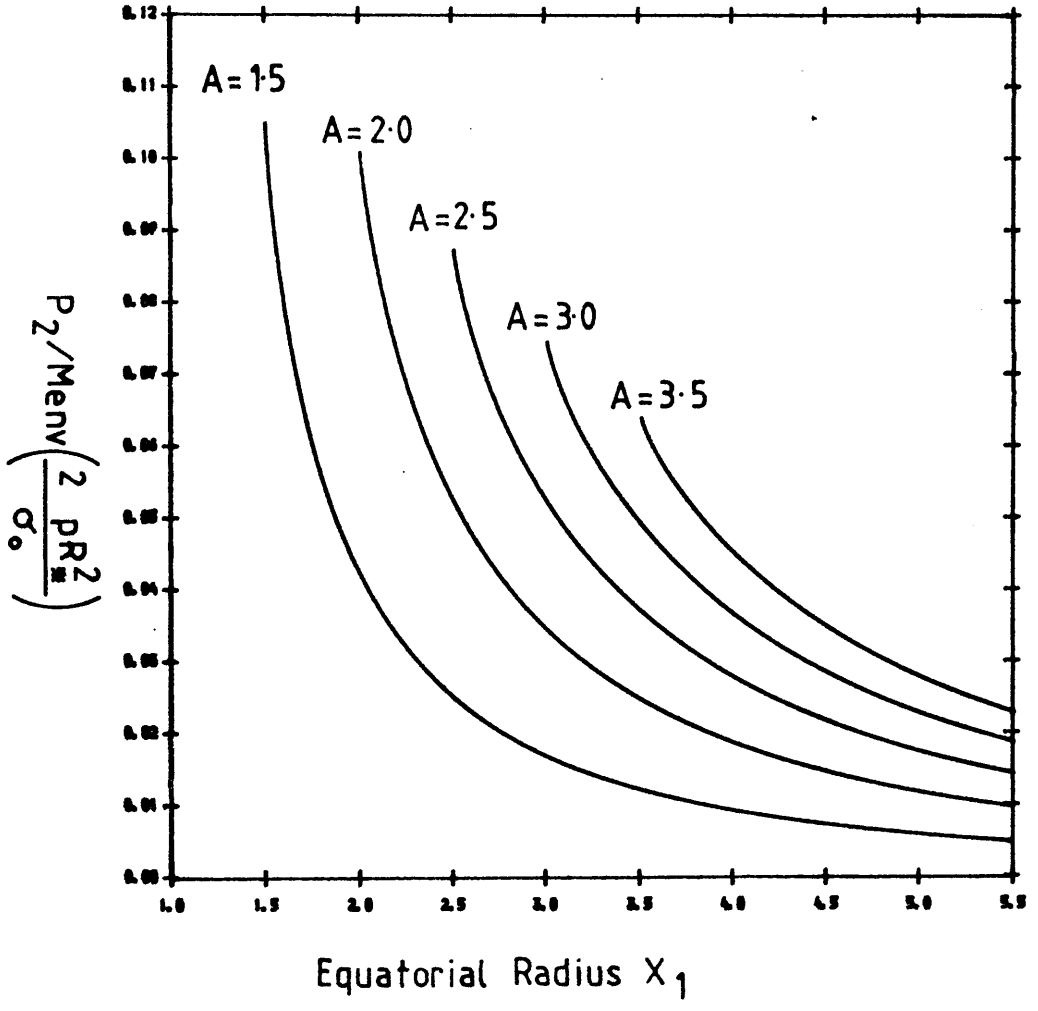

Figure 5.16

The variation of polarisation per unit mass (P_2/M_{env}) with equatorial radius (X_1) for an ellipsoid with fixed values of oblateness (A).

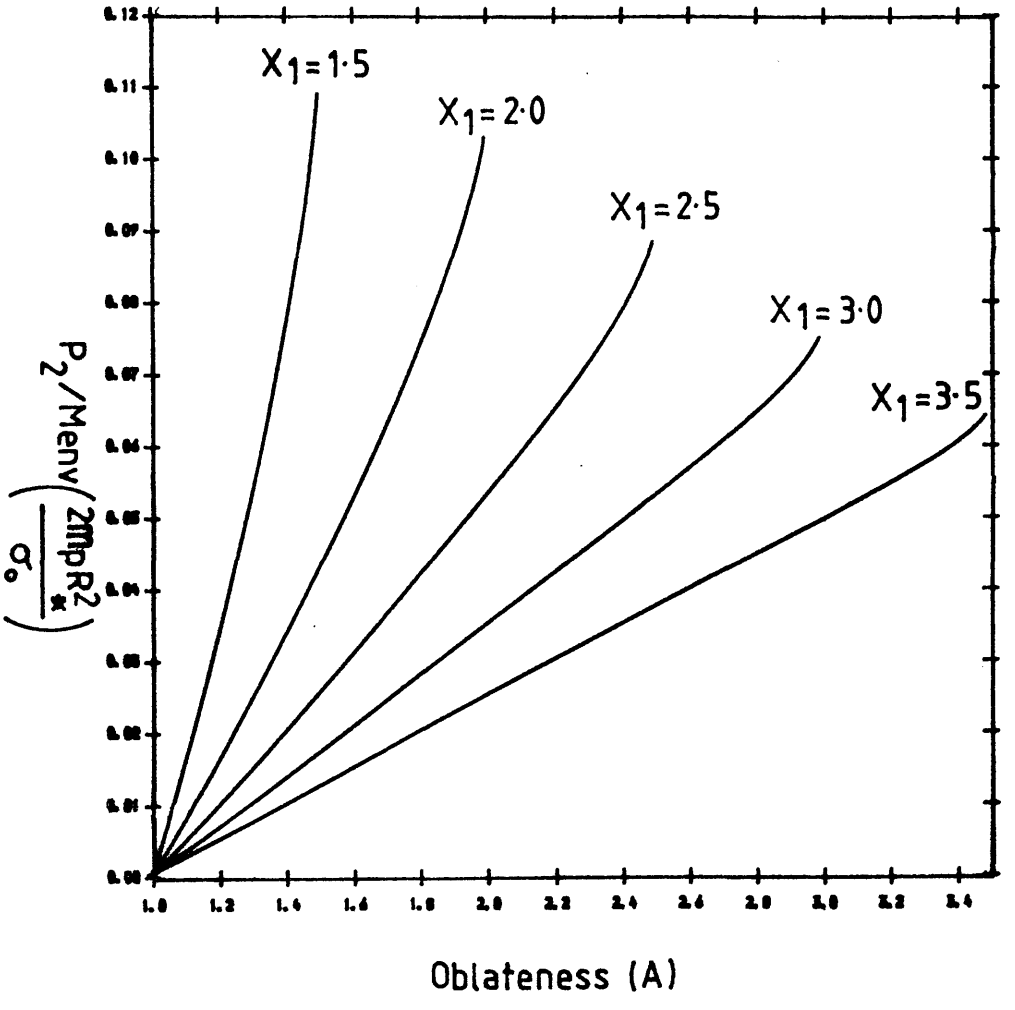

Figure 5.17

The variation of polarisation per unit mass (P_2/M_{env}) with oblateness (A) for an ellipsoid with fixed values of equatorial radius (X_1).

In Sec. 5.3.3 it was shown (for an ellipsoid) that the effect of including occultation was a negligible correction compared to including depolarisation into the BM treatment. One could envisage that this would also be the case for a geometrically thick ($h > 1$) ellipsoid. For such an ellipsoid (in the point light source treatment) the polarisation is still given by eq.(5.19) whilst the mass of the envelope is given (exactly) by

$$M_{env} = 4\pi n_o m_p R_*^3 X_1^2 \frac{h}{A}\left[1 + \frac{h}{X_1} + \frac{h^2}{3X_1^2}\right] \quad (kg) \tag{5.28}$$

Therefore, assuming that for a geometrically thick ellipsoid, occultation effects are still negligible, then the fuction P_2/M_{env} will be correspondingly smaller than shown in Figs 5.16 and 5.17 by a factor $(1 + h/X_1 + h^2/3X_1^2)$. Hence a geometrically thick ellipsoid is unlikely, for any values of X_1 and A, to be able to produce a polarisation of up to 2%.

The mass of a wedge shaped disc is given by

$$M_{env} = 4\pi n_o m_p R_*^3 \frac{\sin\alpha}{n - 3} \tag{5.29}$$

and therefore in order that the envelope has finite mass $n > 3$ ($n \leqslant 3$ is permitted only when the disc has a finite radius; see Waters, 1986).

In fig. 5.18 the variation of P_2/M_{env} is shown as a function of the half opening angle (α). As is intuitively obvious, as α increases the polarisation decreases because the envelope becomes less oblate. The polarisation is zero when $\alpha = 90°$ as the envelope is spherically symmetric. It is also apparent that for small α the polarisation (for constant mass and power index) is approximately independent of the half opening angle which would suggest that the envelope could be approximated by a planar distribution such as that considered in Ch. 3 and Ch. 4. Notice also that the function P_2/M_{env} is a monotonically

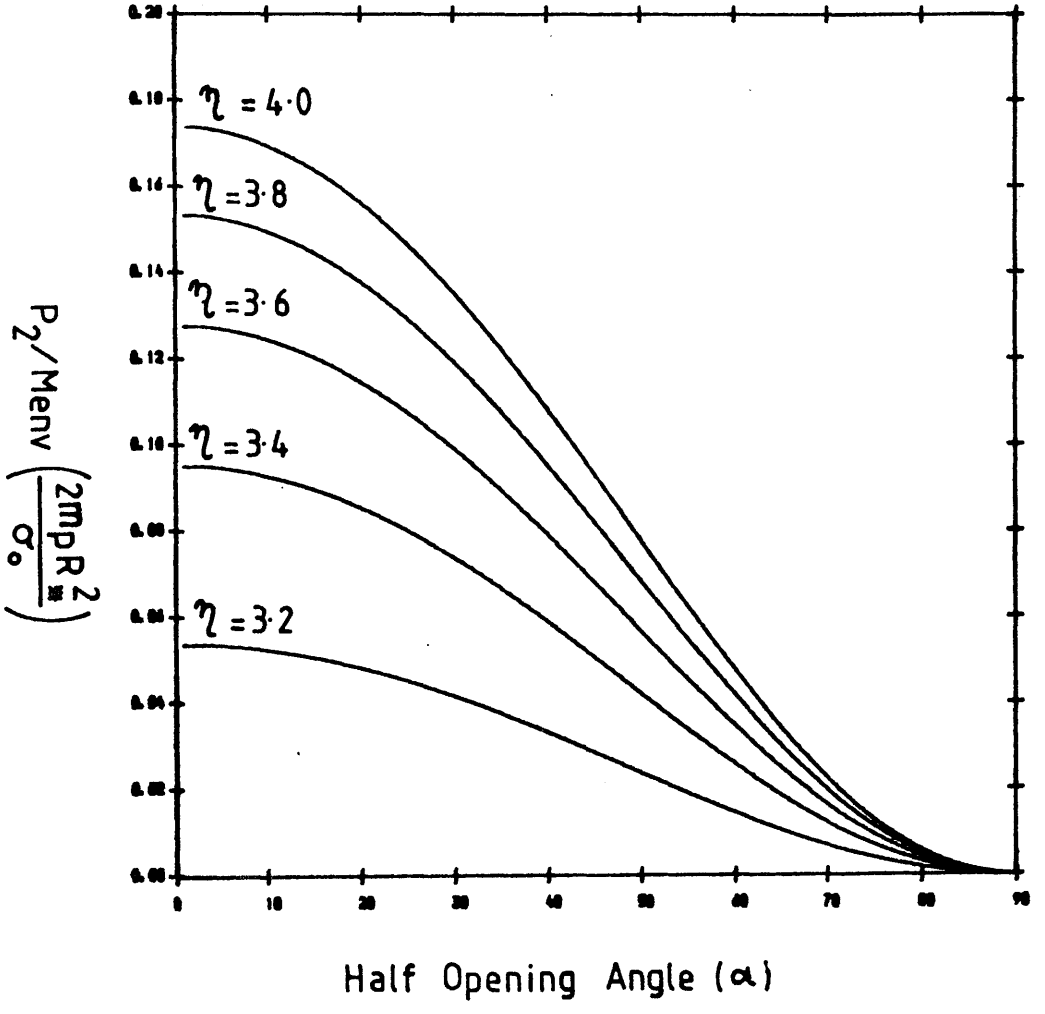

Figure 5.18

The variation of polarisation per unit mass (P_2/M_{env}) with half opening angle (α) for a disc with fixed values of power index (η).

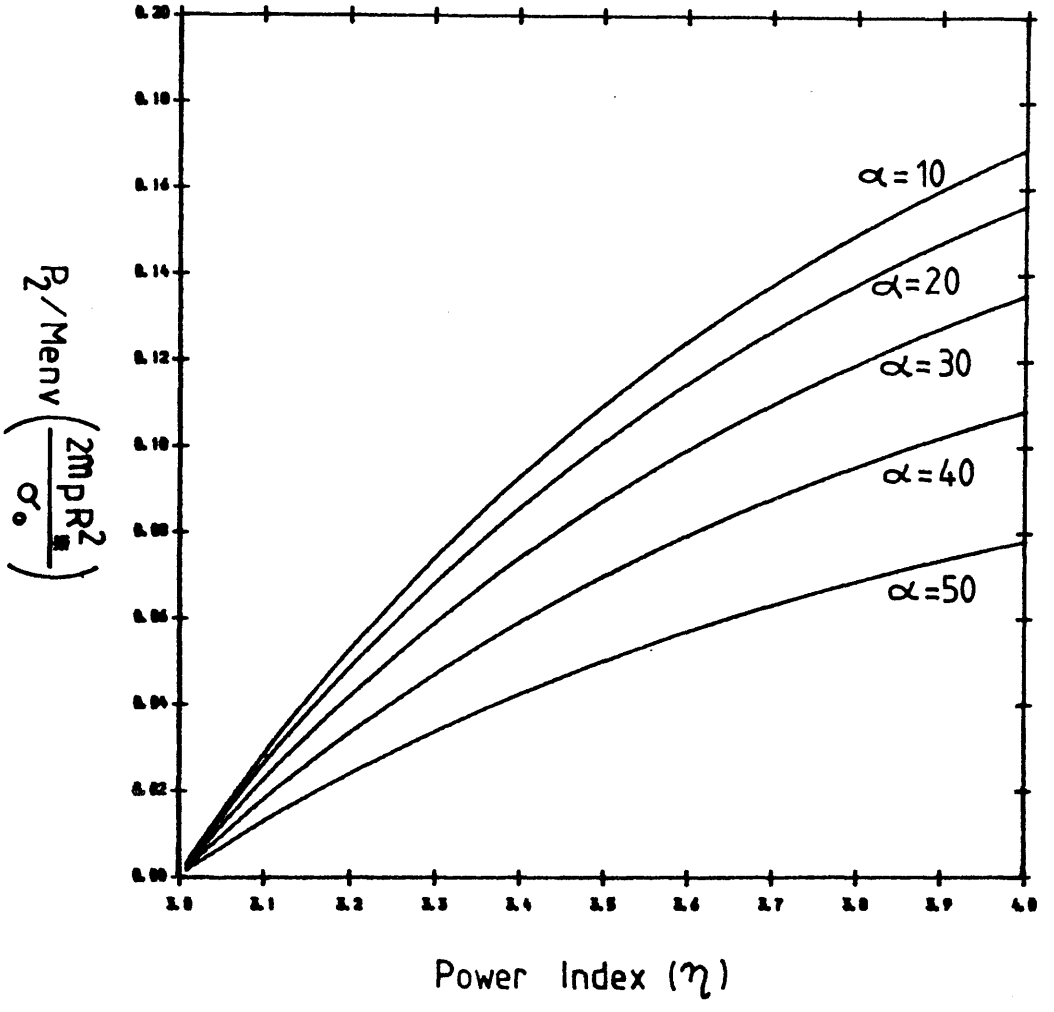

Figure 5.19

The variation of polarisation per unit mass (P_2/M_{env}) with power index (η) for a disc with fixed values of half opening angle (α).

decreasing function function of α. At first sight this would appear to be at variance with the analysis of Sec. 3.3.3 where it was claimed that the maximum polarisation of a disc is achieved for $\alpha = 35^{\circ}$. However, it must be borne in mind that in the latter case the density of the envelope was assumed to be constant whereas we are now considering the mass of the envelope to be a constant. The results shown in Fig. 5.18 (and 5.19) are, however, consistent with our previous results of Sec. 3.3.3. This can be demonstrated by finding the maximum polarisation at $\alpha = 35^{\circ}$, giving $P_{max} \sim 6.5\%$, consistent with the inequality of eq.(3.23).

In Fig. 5.19 the variation of P_2/M_{env} is shown as a function of the power index. It can be seen that the function P_2/M_{env} increases with increasing power index. This may be interpreted in two equivalent ways. One could consider an envelope of constant mass, whereby increasing the power index of the envelope results in an increased number of scatterers close to the star (e.g 28% of all scatterers are contained within a radius of $5R_*$, for $n = 3.2$, whereas for $n = 4.0$ this figure is 80%) and hence there are more scatterers that contribute strongly to the net observed polarisation. Alternatively, one could consider the mass of the envelope required to produce a given polarisation. Then, by the same argument as before, higher power indices result in a greater concentration of scatterers close to the star which are the main contributors to the polarisation. Hence by increasing the power index the evelope will need to be less massive (compared to low power indices) in order to produce the same polarisation and therefore the function P_2/M_{env} will increase with increasing power index.

In order to produce a polarisation of 2% it can be seen (Figs 5.18

and 5.19) that there is little restriction upon the choice of parameters. For example, α may be as much as 60° for high density power indices ($n > 3.6$) i.e. material highly concentrated towards the surface of the star. Even for low power indices ($n \sim 3.2$) half opening angles of up to 30° are permissible.

On the basis of these results it would appear that either a spherical shell with a polar/equatorial concentration or an equatorial disc are likely to be responsible for producing the intrinsic polarisation of Be stars rather than an ellipsoidal shell (particularly if $\tau < 1$ or the envelope is geometrically thick).

5.5 Axisymmetric Envelopes Viewed at Arbitrary Inclination.

We now consider the polarisation from an envelope viewed at arbitrary inclination. For both the point light source (P_0) and extended light source without occultation (P_1) cases the results of Sec. 5.3 are simply multiplied by $\sin^2 i$. For an extended light source with occultation the net polarisation (at arbitrary inclination) is not so easily found but may be written in the general form of

$$P_2 = (\tau_0 - 3\tau_0\gamma_0)\sin^2 i - \tau_0\gamma_2 \sin 2i + (1 + \cos^2 i)\tau_0\gamma_3 \qquad (5.30)$$

where the weighted integral moments are given in eq. (5.8 - 5.13) and are calculated in appendix B for the three geometries under consideration.

In Figs 5.20 - 5.23 the function P_2/M_{env} is shown as a function of inclination for the three geometries. Also show is the function $(P_2/M_{env})/\sin^2 i$ which is a measure of the importance of occultation. If occultation is unimportant then $(P_2/M_{env})/\sin^2 i$ will be independent of inclination such that the BM result (P = constant.$\sin^2 i$) will be valid and the polarisation of the envelope can be adequately approximated

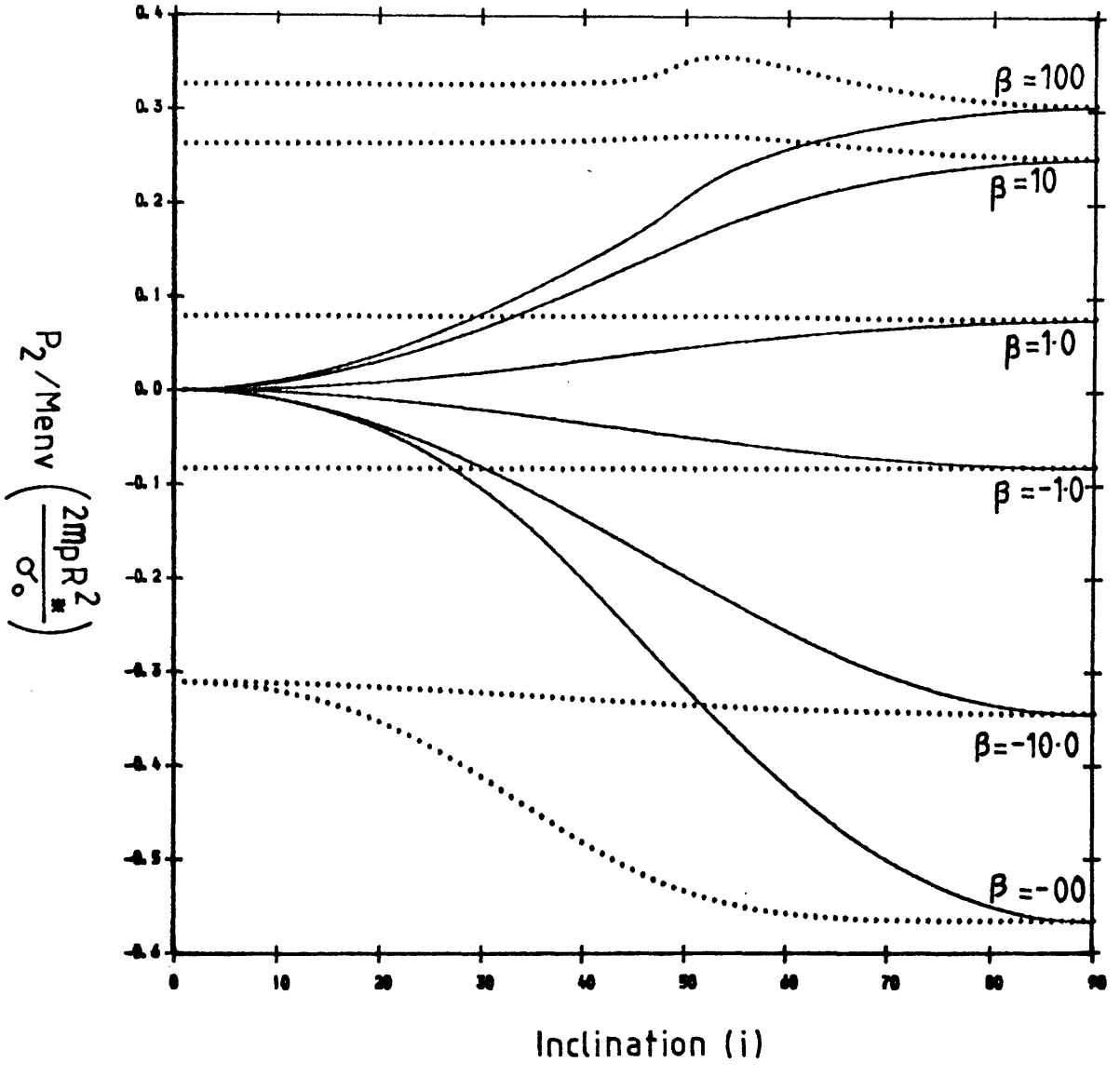

Figure 5.20

The variation of polarisation per unit mass (P_2/M_{env}) with inclination for a shell (of radius X = 1.5) with fixed values of β.

The dotted curves indicate the deviation of the variation of polarisation from the BM result (perfect agreement with the BM result would be a straight line).

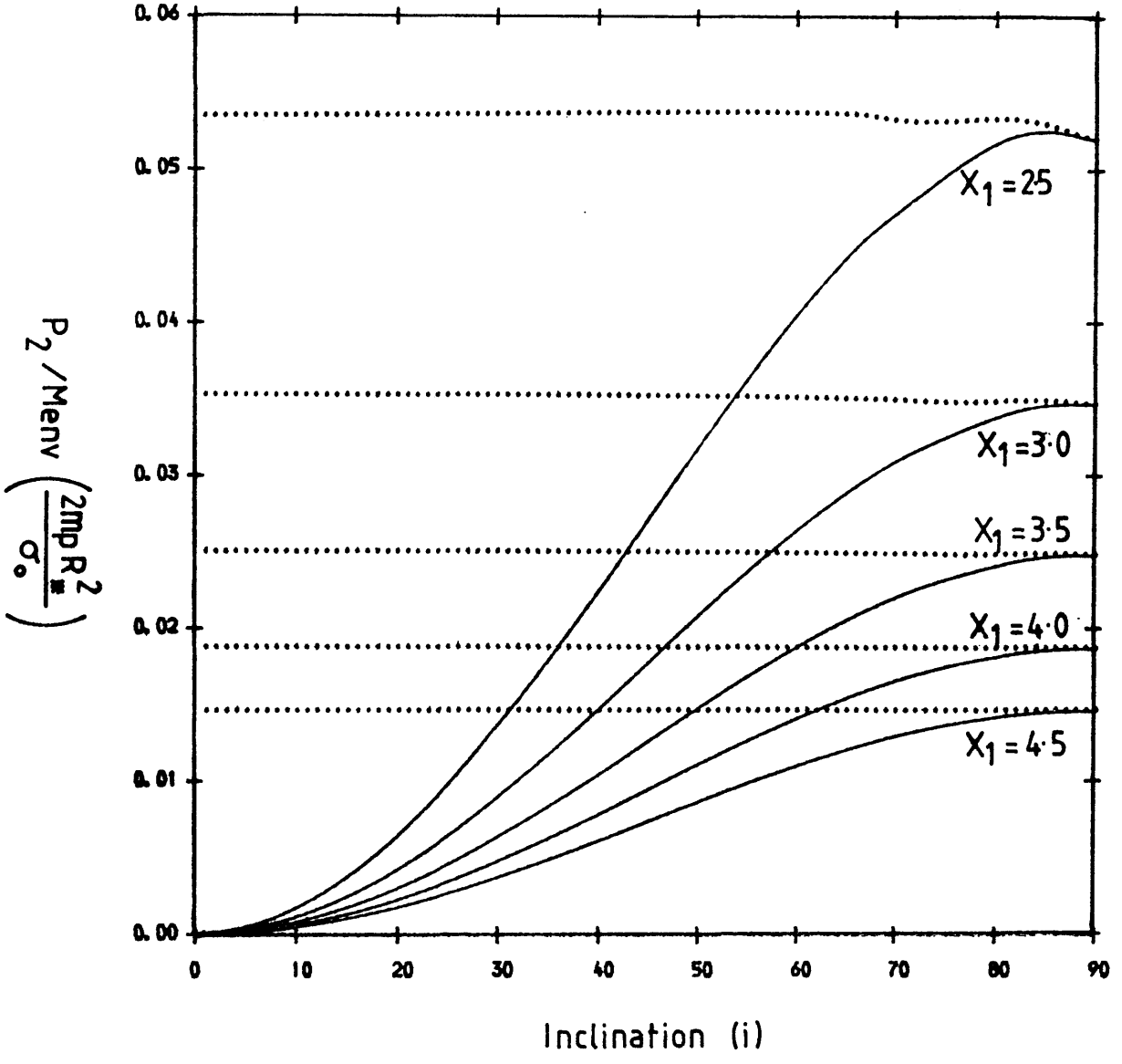

Figure 5.21

As Fig. 5.20 except for an ellipsoid (oblateness A = 2.0) with fixed values of equatorial radius (X_1).

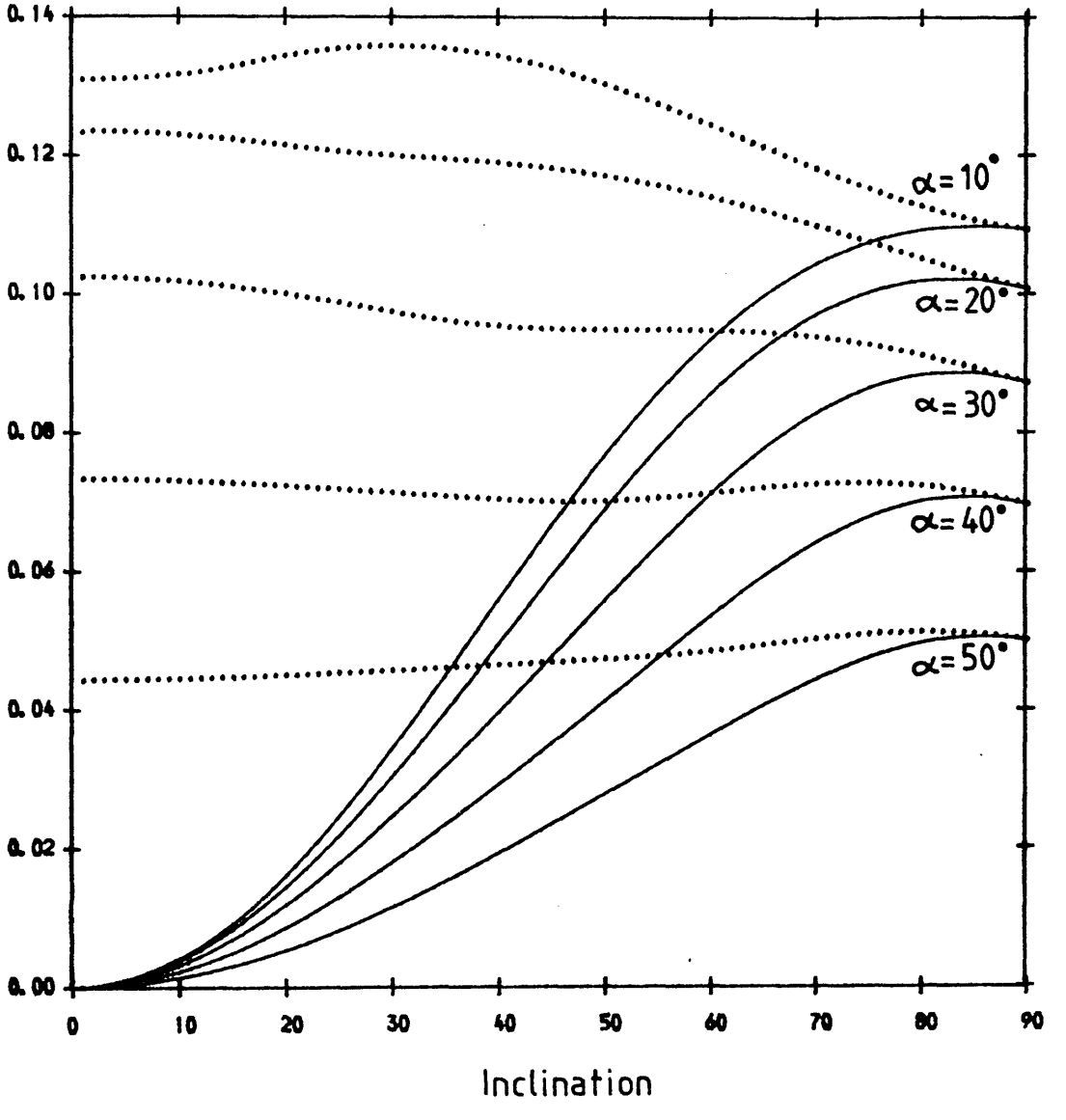

Figure 5.22

As Fig. 5.20 except for a disc (η = 3.5) with fixed values of half opening angle (α).

by incorporating depolarisation into the BM analysis.

For a spherical shell it can be seen (Fig. 5.20) that for polar concentrated distributions ($\beta < 0$) occultation is important at low inclinations where a significant number of scatterers are occulted (i.e. polar region occulted). For equatorial concentrated distributions ($\beta > 0$) occultation is important at high inclinations where a significant number of scatterers are occulted. This is particularly exemplified for the curve of $\beta = 100$, which can be considered to be an equatorial ring of material. In this case occultation does not occur until $i > \cos^{-1}(1/x)$ and hence the variation of the polarisation with inclination goes as $\sin^2 i$ (dotted curve) until $i \sim 48^\circ$ when occultation of part of the ring occurs and the BM result no longer holds. Notice that occultation is unimportant for electron distributions with $|\beta| < 10$ and so the polarisation of such distributions may adequately be approximated by the BM analysis when depolarisation is included.

For a geometrically thin ellipsoid ($h < 1$) it can be seen (Fig. 5.21) that the effects of occultation can in general be neglected. It is only when the envelope is touching (or almost touching) the stellar surface and the equatorial radius of the envelope is small that at high inclinations occultation effects are noticeable. Even in this case the effect is small and negligible (as found in Sec. 5.3.3). Therefore, the polarisation of an ellipsoid can be accurately approximated by incorporating depolarisation into the BM analysis.

It can be seen (Fig. 5.22) that for a wedge shaped disc occultation is important at all inclinations. As the half opening angle increases occultation effects become less significant but cannot be neglected and therefore the BM analysis cannot be used to describe the variation of polarisation with inclination for a disc. It may also be seen that the

maximum polarisation occurs at i ~ 85° and not at 90° as would be expected. The fact that this 'anomaly' occurs only when occultation is included suggests that the enhancement arises due to the suppresion of polarisation that is oppositely polarised to that of the whole disc. That is, the occulted region is oppositely polarised to that of the whole disc and by suppressing this polarimetric contribution leads to a suppression of cancellation that in the absence of occultation would not occur.

5.6 The Structure of General Three dimensional Envelopes.

Whilst for single stars it is reasonable to assume that the stellar envelope is axisymmetric, it may often in reality not be true. Such would be the case for instance if the envelope is gravitationally perturbed by an unseen companion (eg. a neutron star) or corotating wind structures (eg. corotating interacting regions - Mullan, 1984). In such cases the stellar envelope may be modelled as an axisymmetric envelope with a perturbation term that depends upon the rotation rate. this may be modelled by representing the number density function of the envelope by a Fourier series, viz

$$n(r,\theta,\phi) = n(r,\theta)\left[\sum_{j=o}^{\infty} x_j \cos j\phi_o + y_j \sin j\phi_o\right] \qquad (5.31)$$

where

$$\phi_o = \phi - \omega t$$

ω is the rate of rotation, t is the time from t_o when $\phi_o = \phi$. By substiuting eq. (5.31) into eq.(5.5) we may Fourier analyse the polarimetric data via

$$\begin{Bmatrix} Q \\ U \end{Bmatrix} = \sum_{j=0}^{\infty} \begin{Bmatrix} p_j \\ u_j \end{Bmatrix} \cos j\omega t + \begin{Bmatrix} q_j \\ v_j \end{Bmatrix} \sin j\omega t \qquad (5.32)$$

In order to simplify the problem we consider only sufficiently high inclination systems such that the volume integral (eq. 5.14) $\int_{O1}$ may be neglected compared to the other volumes. At high inclinations this is justified because the volume O_1 (cf. eq. 5.14) is geometrically small compared to the other regions and also it is highly depolarised (as it contains material that lies close to the star). At low inclinations, on the other hand, the absolute value of the polarisation will be small ($P \propto \sin^2 i$). Moreover at low inclinations the volume integral O_1 will appear to be almost rotationally symmetric and thus again only the regions O_2 and T will contribute significantly to the polarisation (depending somewhat upon the envelope distribution) By substituting (5.31) into (5.6), integrating with respect to Φ and equating to (5.32) we find the Fourier coefficients to be

$$p_o = a_o[(\pi A - B)\sin^2 i + G_1 \sin 2i + X_2(1 + \cos^2 i)] \quad j = 0 \qquad (5.33)$$

$$\begin{Bmatrix} p_1 \\ q_1 \end{Bmatrix} = -\begin{Bmatrix} b_1 \\ a_1 \end{Bmatrix}[C_1 \sin^2 i + \tfrac{1}{2}(\pi E - F)\sin 2i + \tfrac{1}{2}Y_1(1 + \cos^2 i)] \qquad (5.34)$$

$$\begin{Bmatrix} p_2 \\ q_2 \end{Bmatrix} = \begin{Bmatrix} a_2 \\ -b_2 \end{Bmatrix}[D_2 \sin^2 i - \tfrac{1}{2}\bar{K}_2 \sin 2i + \tfrac{1}{2}(\pi M - \bar{N})(1 + \cos^2 i)] \qquad (5.35)$$

$$\begin{Bmatrix} p_j \\ q_j \end{Bmatrix} = -\begin{Bmatrix} b_j \\ a_j \end{Bmatrix}[C_j \sin^2 i + \tfrac{1}{2}\bar{L}_j \sin 2i + \tfrac{1}{2}Y_j(1 + \cos^2 i)] \quad \begin{matrix} \text{odd } j \\ (j > 1) \end{matrix} \qquad (5.36)$$

$$\begin{Bmatrix} p_j \\ q_j \end{Bmatrix} = \begin{Bmatrix} a_j \\ -b_j \end{Bmatrix}[D_j \sin^2 i - \tfrac{1}{2}\bar{K}_j \sin 2i + \tfrac{1}{2}Z_j(1 + \cos^2 i)] \quad \begin{matrix} \text{even } j \\ (j > 2) \end{matrix} \qquad (5.37)$$

$$u_o = 0 \qquad (5.38)$$

$$\begin{Bmatrix} u_1 \\ v_1 \end{Bmatrix} = \begin{Bmatrix} a_1 \\ -b_1 \end{Bmatrix}[(\pi E - \bar{F})\sin i + \bar{Y}_1 \cos i] \qquad (5.39)$$

$$\begin{Bmatrix} u_2 \\ v_2 \end{Bmatrix} = -\begin{Bmatrix} b_2 \\ a_2 \end{Bmatrix}[K_2 \sin i - (\pi M - N)\cos i] \tag{5.40}$$

$$\begin{Bmatrix} u_j \\ v_j \end{Bmatrix} = \begin{Bmatrix} a_j \\ -b_j \end{Bmatrix}[L_j \sin i + \bar{Y}_j \cos i] \qquad \text{odd } j \ (j > 1) \tag{5.41}$$

$$\begin{Bmatrix} u_j \\ v_j \end{Bmatrix} = -\begin{Bmatrix} b_j \\ a_j \end{Bmatrix}[K_j \sin i - \bar{Z}_j \cos i] \qquad \text{even } j \ (j > 2) \tag{5.42}$$

where

$$a_j = \sigma_o n_o x_j \ , \ b_j = \sigma_o n_o y_j \tag{5.43}$$

$$A = \int_T n_{eff}(r,\theta)(1 - 3\cos^2\theta) \sin\theta \, d\theta dr \tag{5.44}$$

$$B = \int_{O_2} n_{eff}(r,\theta)(1 - 3\cos^2\theta)\left[\frac{\pi}{2} - \phi(r,\theta)\right] \sin\theta \, d\theta dr \tag{5.45}$$

$$C_j = \int_{O_2} n_{eff}(r,\theta)(1 - 3\cos^2\theta) \frac{T_j}{j} \sin\theta \, d\theta dr \tag{5.46}$$

$$D_j = \int_{O_2} n_{eff}(r,\theta)(1 - 3\cos^2\theta) \frac{S_j}{j} \sin\theta \, d\theta dr \tag{5.47}$$

$$E = \int_T n_{eff}(r,\theta)\sin 2\theta \sin\theta \, d\theta dr \tag{5.48}$$

$$F = \int_{O_2} n_{eff}(r,\theta)\sin 2\theta \left[\frac{\pi}{2} - \phi(r,\theta) + \frac{S_2}{2}\right] \sin\theta \, d\theta dr \tag{5.49}$$

$$\bar{F} = \int_{O_2} n_{eff}(r,\theta)\sin 2\theta \left[\frac{\pi}{2} - \phi(r,\theta) - \frac{S_2}{2}\right] \sin\theta \, d\theta dr \tag{5.50}$$

$$G_j = \int_{O_2} n_{eff}(r,\theta)\sin 2\theta \ \frac{T_j}{j} \sin\theta \, d\theta dr \tag{5.51}$$

$$H_j = \int_{O_2} n_{eff}(r,\theta)\sin 2\theta \ \frac{S_j}{j} \sin\theta \, d\theta dr \tag{5.52}$$

$$\left.\begin{aligned} K_j &= G_{j-1} + G_{j+1} \\ \bar{K}_j &= G_{j-1} - G_{j+1} \end{aligned}\right\} \tag{5.53}$$

$$\left.\begin{aligned} L_j &= H_{j-1} + H_{j+1} \\ \bar{L}_j &= H_{j-1} - H_{j+1} \end{aligned}\right\} \tag{5.54}$$

$$M = \int_T n_{eff}(r,\theta)\sin^2\theta \sin\theta \, d\theta dr \tag{5.55}$$

$$N = \int_{O_2} n_{eff}(r,\theta)\sin^2\theta \left[\frac{\pi}{2} - \phi(r,\theta) + \frac{S_4}{4}\right] \sin\theta \, d\theta dr \tag{5.56}$$

$$\bar{N} = \int_{O_2} n_{eff}(r,\theta)\sin^2\theta \left[\frac{\pi}{2} - \phi(r,\theta) - \frac{S_4}{4}\right] \sin\theta \, d\theta dr \tag{5.57}$$

$$W_j = \int_{O_2} n_{eff}(r,\theta)\sin^2\theta \, \frac{T_j}{j} \sin\theta \, d\theta dr \tag{5.58}$$

$$X_j = \int_{O_2} n_{eff}(r,\theta)\sin^2\theta \, \frac{S_j}{j} \sin\theta \, d\theta dr \tag{5.59}$$

$$\left.\begin{aligned} Y_j &= W_{j-2} + W_{j+2} \\ \bar{Y}_j &= W_{j-2} - W_{j+2} \end{aligned}\right\} \tag{5.60}$$

$$\left.\begin{aligned} Z_j &= X_{j-2} + X_{j+2} \\ \bar{Z}_j &= X_{j-2} - X_{j+2} \end{aligned}\right\} \tag{5.61}$$

$$n_{eff}(r,\theta) = n(r,\theta)(1 - R_{\frac{1}{4}}^2/r^2)^{\frac{1}{2}}/n_o \tag{5.62}$$

$$\left.\begin{aligned} S_j &= \sin\{j\phi(r,\theta)\} \\ T_j &= \cos\{j\phi(r,\theta)\} \end{aligned}\right\} \tag{5.63}$$

and

$$\phi(r,\theta) = \sin^{-1}\left\{ \frac{\cos\theta \cos i + (1 - R_{\frac{1}{4}}^2/r^2)^{\frac{1}{2}}}{\sin\theta \sin i} \right\} \tag{5.64}$$

By taking ratios of the observed Fourier coefficients the envelope Fourier coefficients may be eliminated, viz

$$\Gamma_j = \frac{p_j}{v_j} = -\frac{q_j}{u_j} \quad \text{for all } j > 0 \tag{5.65}$$

For distributions in which occultation is unimportant the volume integral $\int_{O2}$ may be neglected and

$$\Gamma_1 = \cos i, \quad \Gamma_2 = \frac{1 + \cos^2 i}{2\cos i}$$

agreeing with the results of Brown et al.(1978) and Simmons (1983).

The Fourier coefficient ratios Γ_1 and Γ_2 are shown as functions of inclination in Figs 5.23(a-c) and 5.24(a-c) respectively. In each case the BME results are shown for comparision.

In Fig. 5.23a it can be see that for a spherical shell deviation from the BME result ($\Gamma_1 = \cos i$) is significant for all values of β at moderate-low inclination ($i < 60^\circ$). Interpreting the observed Γ_1 in terms of the BME analysis would result in a systematically higher inferred inclination than is actually the case. At higher inclinations ($i > 60^\circ$) the converse is true for equatorially concentrated distributions ($\beta > 0$) whilst for $\beta < 0$ the curves follow the BME result, which is expected from the analysis of Sec. 5.5 where it was found that occultation is unimportant at high inclinations for polar concentrated distributions. For $\beta = 100$ (effectively $\beta = \infty$) for a given observed Γ_1 a multiplicity of inclinations is possible (i.e a maximum of four equally valid inclinations are possible). For an ellipsoid (Fig. 5.23b) it can be seen that the Fourier ratio Γ_1 follows closely the predicted curve of BME agreeing with the previous sections' findings whereby occultation was found to be negligible. When the envelope is a wedge shaped disc it is found (Fig. 5.23c) that the observed values of Γ_1 are always systematically larger for a given inclination than the corresponding BME result (i.e. if the observed Γ_1 is interpreted as being equal to cosi the inferred inclination would be systematically lower than the real inclination of the system). For envelopes with small half opening

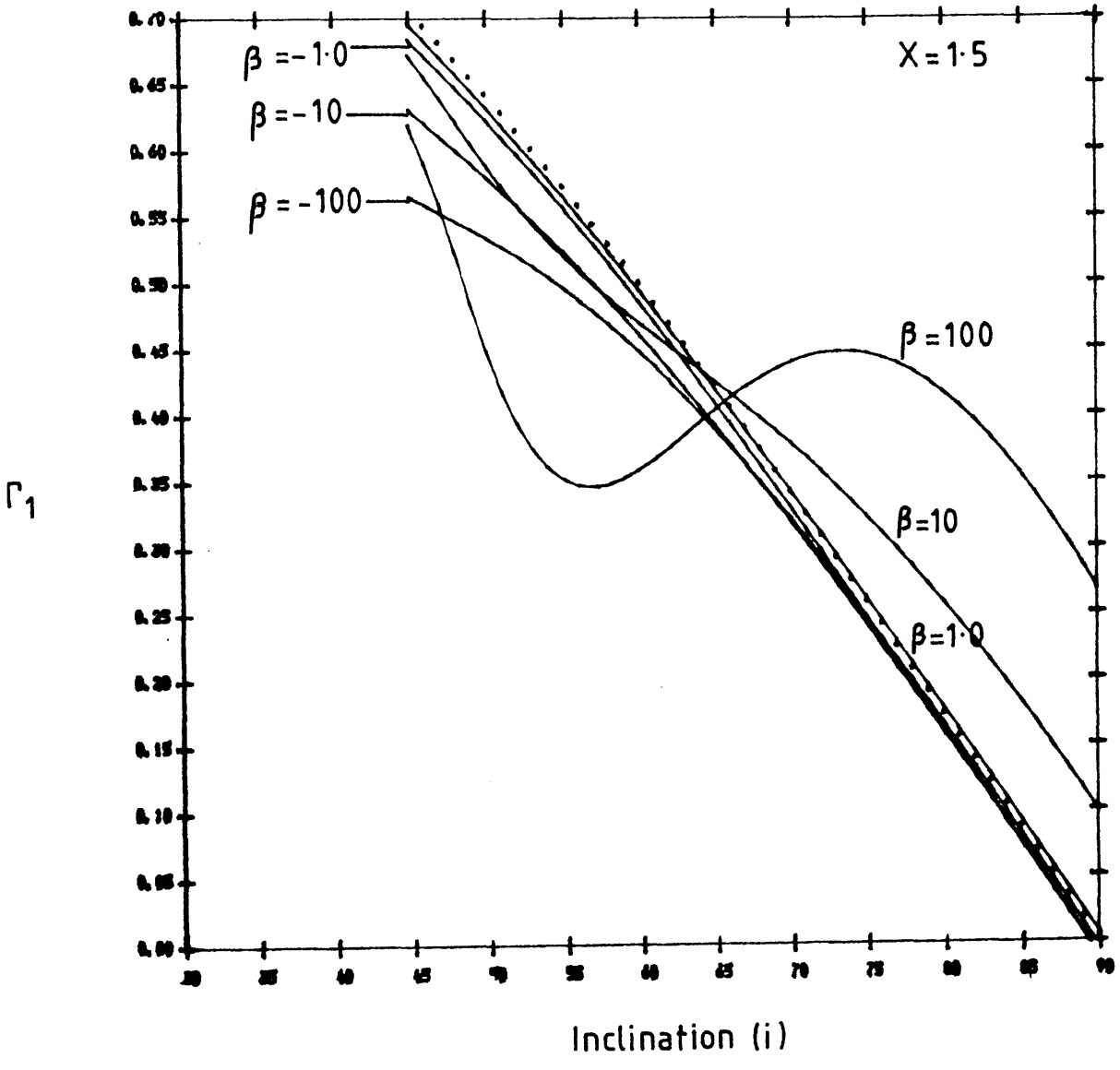

Figure 5.23a

The variation of Γ_1 with inclination for a shell (radius X = 1.5) with fixed values of β.

The dotted curve indicates the BME result, Γ_1 = cosi.

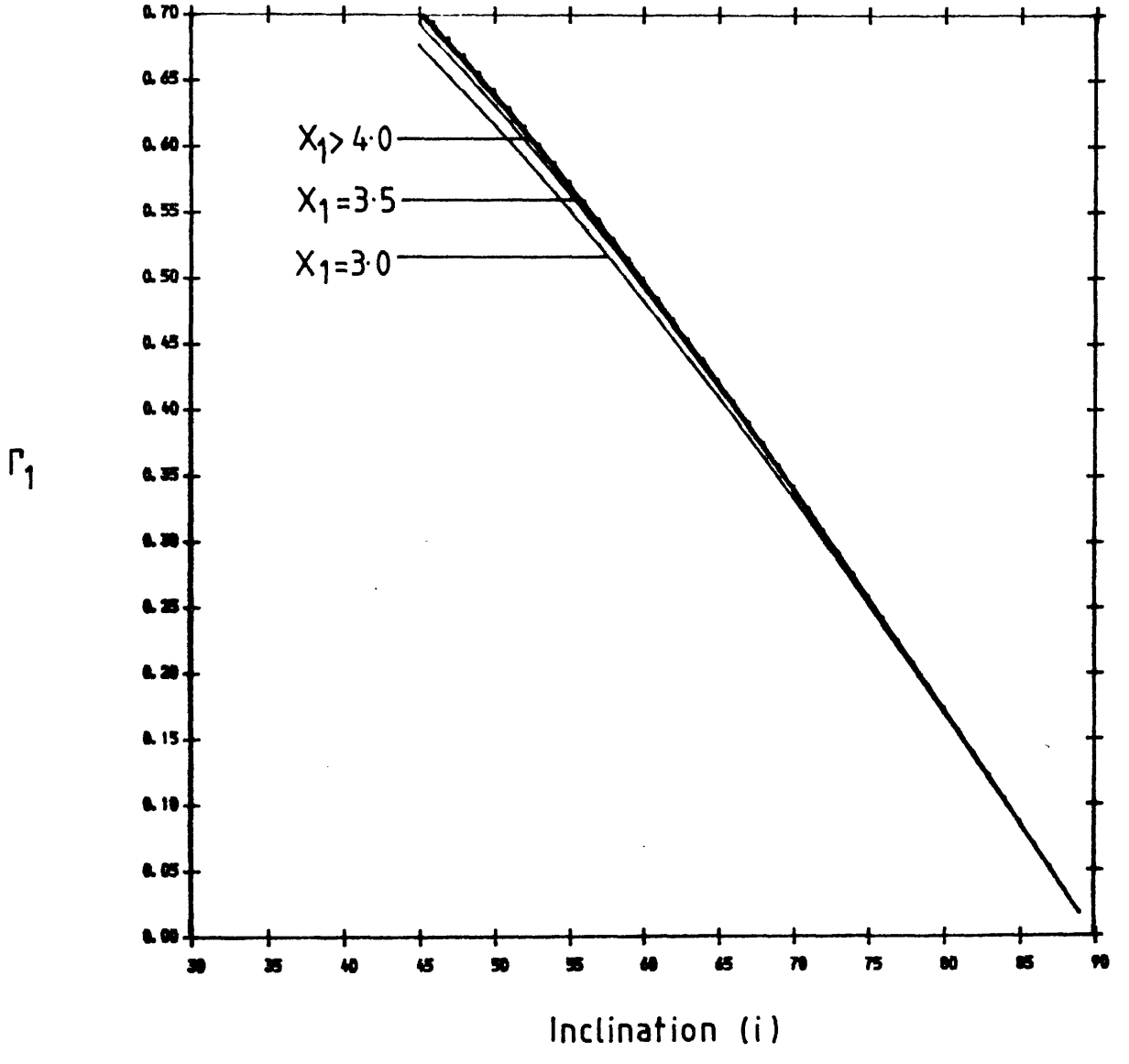

Figure 5.23b

As Fig. 5.23a except for an ellipsoid (oblateness A = 2.0) with fixed values of equatorial radius (X_1).

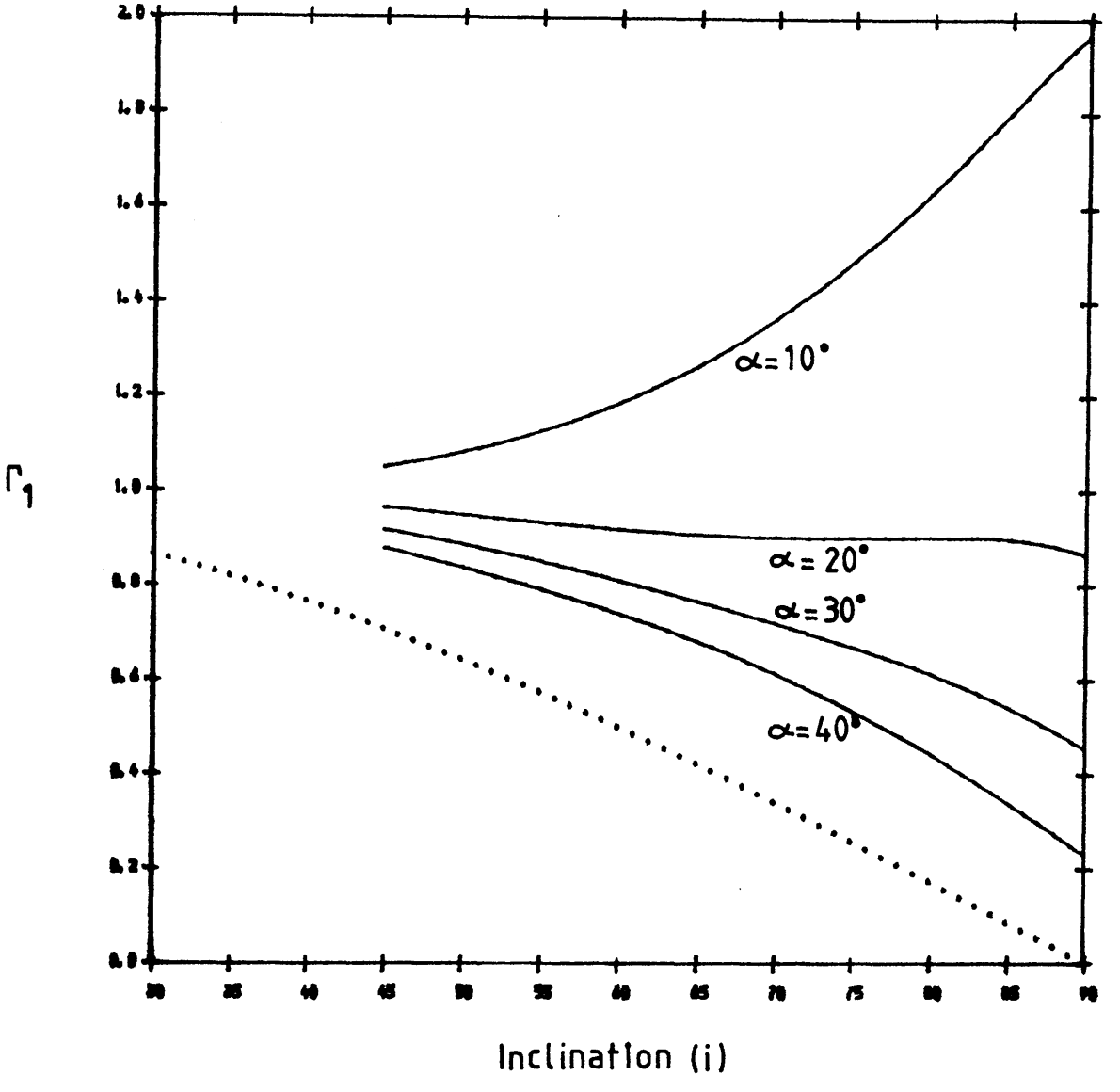

Figure 5.23c

As Fig. 5.23a except for a disc (power index n = 3.5) with fixed values of half opening angle (α).

angles it can be seen that the inclination dependence of Γ_1 is definitely not varying as cosi. For example for α =20° Γ_1 is practically independent of inclination, whilst for smaller opening angles still $\Gamma_1 >$ 1 and can only be interpreted by the canonical models in terms of an eccentric binary orbit (Brown et al.,1982).

The variation of Γ_2, unlike the variation of Γ_1, for each of the geometries (Figs 5.24a-c) shows a remarkable agreement with that of the BME result (except for a shell viewed at low inclinations are there any problems in interpreting the the value of Γ_2). This would indicate therefore that Γ_2 is a reliable indicator for the inclination of the system independent of geometry unlike Γ_1 which depends significantly upon the density distribution.

In Sec. 4.5 it was shown that it is possible by use of higher Fourier coefficient ratios (Γ_j) to obtain the inclination, the envelope Fourier harmonic coefficients and the radial envelope density distribution of the system. This was made possible only because the envelope was of a presumed known structure. In the absence of such knowledge the best that one may achieve is the inclination of the system. In order to infer the envelope density structure, short of constructing high order Fourier coefficient (Γ_j) curves for various envelope geometries (cf. Sec. 4.5) one could generalise the density distribution as an expansion of Legendre polynomials (Simmons, 1982, 1983). The general method would be to plot the curves of Γ_j up to the sixth order, say for the lowest order Legendre polynomials and then by finding the various Fourier coefficent ratios (Γ_j) to obtain a best fit, i.e to obtain consistent inclination values and thereby, at least to some extent, inferring the distribution of material with in the envelope (eg. polar or equatorial enhancements) which cannot be inferred by

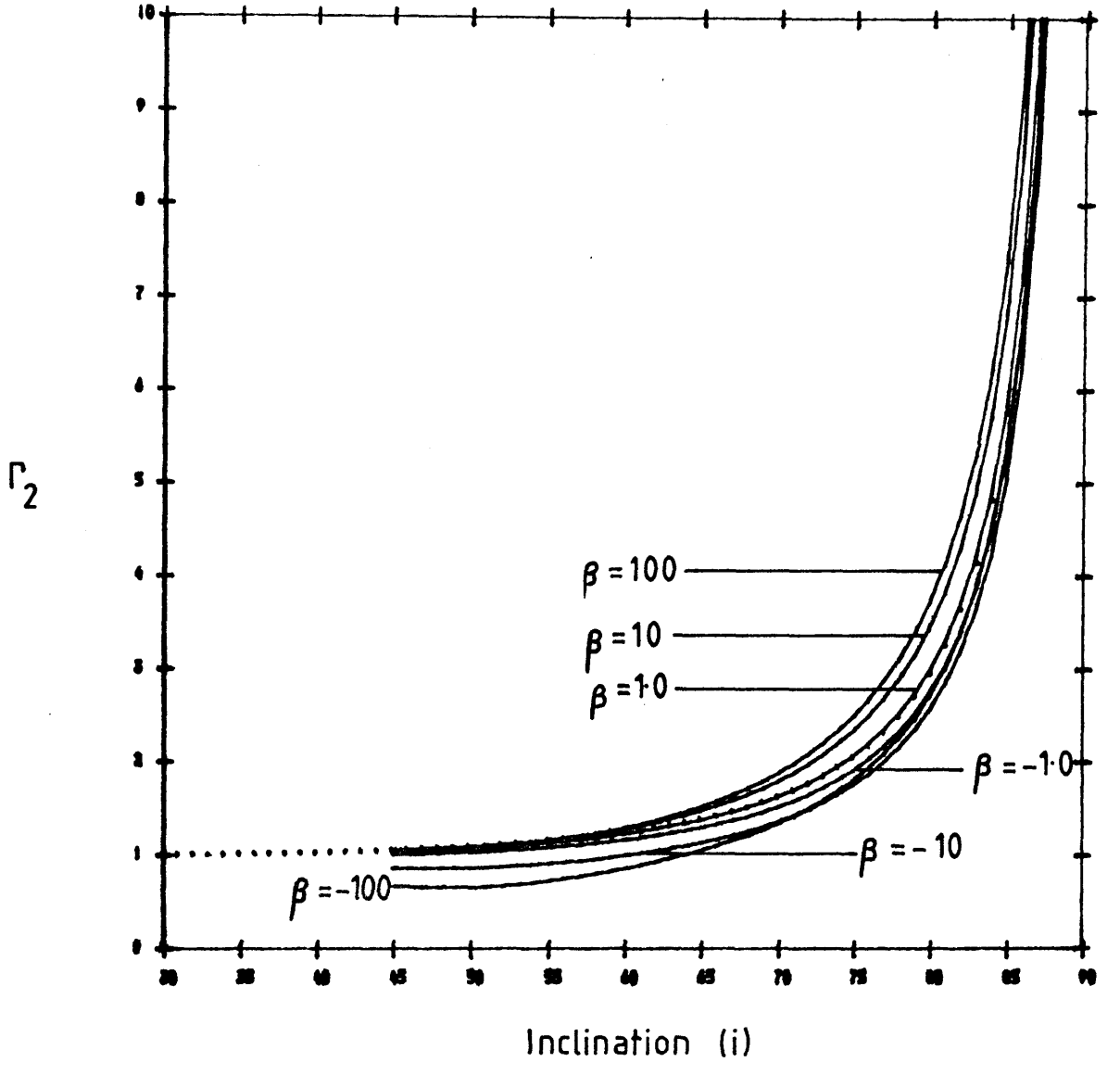

Figure 5.24a

The variation of Γ_2 with inclination for a shell (radius X = 1.5) with fixed values of β.

The dotted curve indicates the BME result, $\Gamma_2 = (1 + \cos^2 i)/2\cos i$.

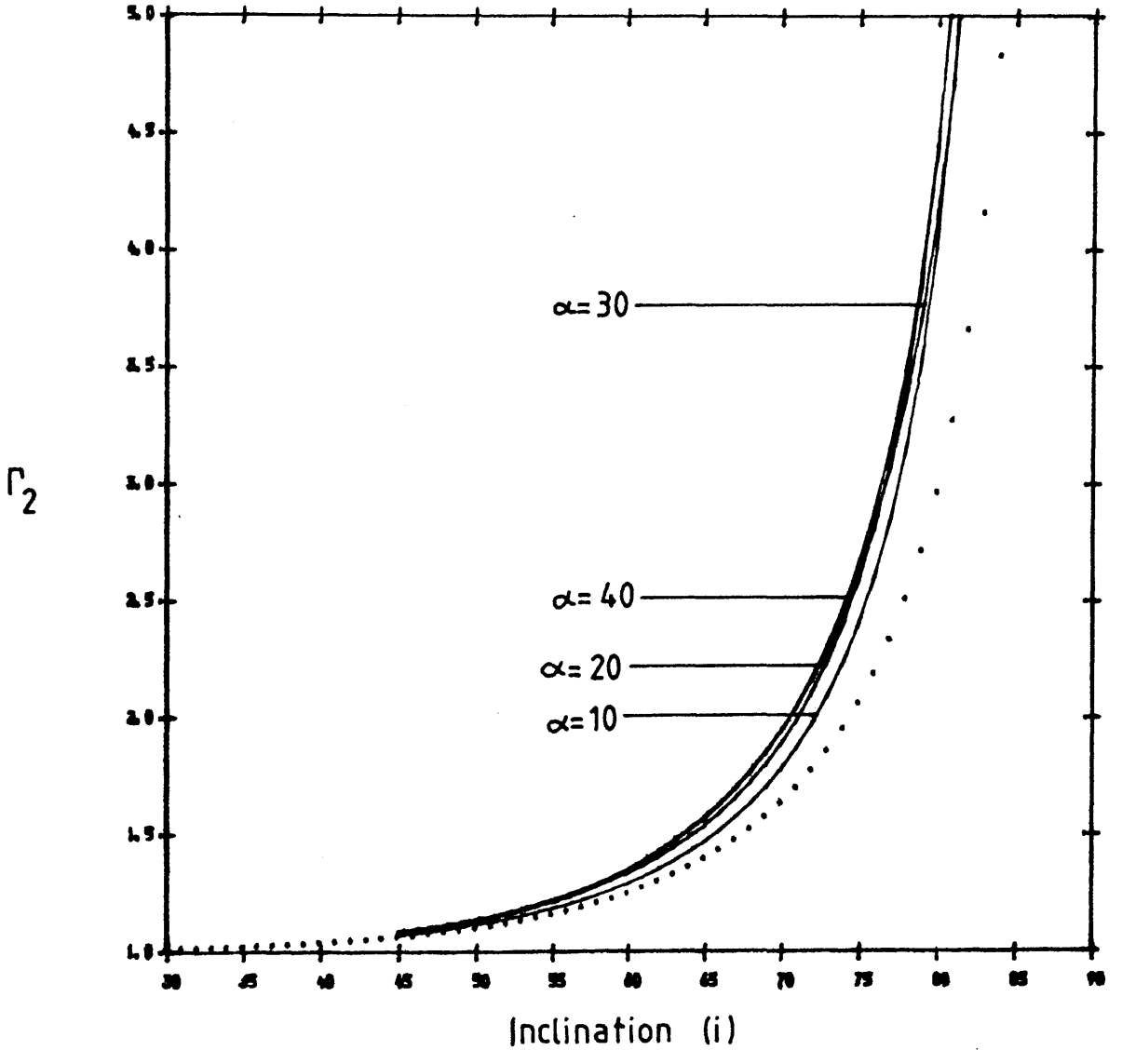

Figure 5.24b

As Fig. 5.24a except for an ellipsoid (oblateness A = 2.0) with fixed values of equatorial radius (X_1).

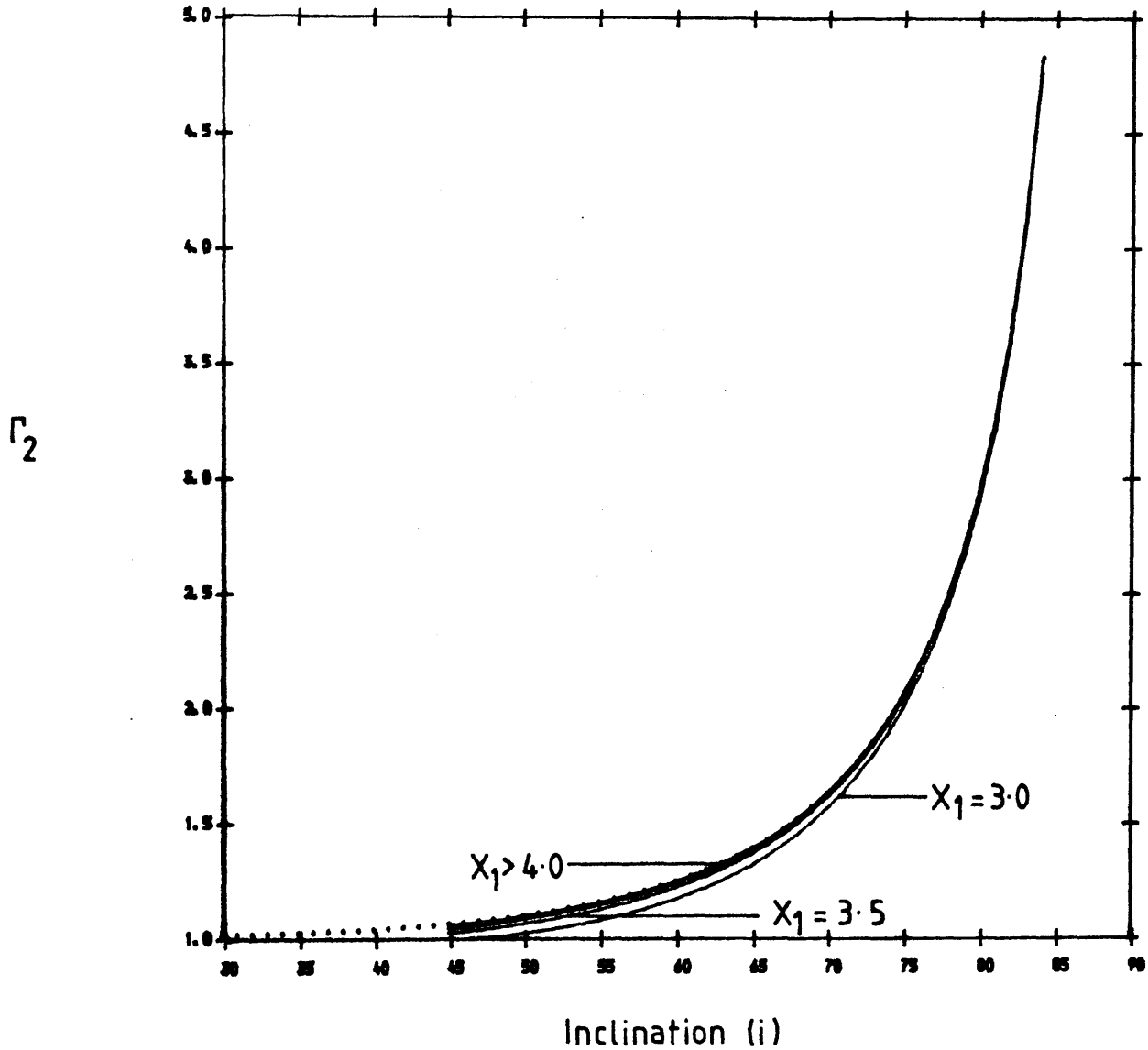

Figure 5.24c

As Fig. 5.24a except for a disc (power index $n = 3.5$) with fixed values of half opening angle (α).

the canonical analysis.

5.7 Discussion and Conclusions.

The general combined effect of incorporating both occultation and depolarisation into the single scattering polarimetric theory of Brown and McLean (1977) has been found to reduce the net polarisation by up to a factor of two (compared to point light source calculations), except for ellipsoidal envelope geometries where the net polarisation is found to be increased by a similar factor.

One important feature of incorporating occultation into the polarisation theory of BM is that the variation of polarisation with inclination is no longer $P \propto \sin^2 i$ (this is still correct if depolarisation alone is included), but instead is more complicated [cf. eq. (5.15)] where apart from the explicit complexity of the inclination dependence there is also an implicit dependence arising from the weighted integrals as they too are inclination dependent. The exact variation of polarisation with inclination therefore becomes model dependent (much in the same way as full radiative transfer treatments are model dependent).

By using geometrical models to represent the envelopes of Be stars, it was found that an equatorial enhanced density distribution (i.e. an equatorial disc or a shell with $\beta > 5$) or a polar enhanced distribution (shell with $\beta < -5$) are able to produce polarisations in excess of the observed maximum polarisation of Be stars (2%). Ellipsoidal envelopes, on the other hand, were unable to produce such a high degree of polarisation. It would appear, therefore, that the geometrical model of Marlborough et al. (1978) is,polarimetrically, an acceptable model for Be star envelopes, whereas the Doazan and Thomas (1982) model is not.

One somewhat overlooked geometrical model capable of producing

polarisations in excess of 2% is a polar enhaced density distribution. In Be stars such a scenerio is possible by the fact that these stars are rapidly rotating. The rapid rotation of the star leads to a lower local surface gravity at the equator than at the poles (cf. Sec. 1.3.1) and hence one anticipates equatorial enhanced mass loss. However, it must be borne in mind that the equatorial regions will consequently have a lower local temperature compared to the polar regions. It is conceivable that the higher temperature at the poles could lead to a reduction in the local gravity such that mass loss from the polar regions becomes more probable.

By considering corotating density perturbations within a circumstellar envelope it has been found that by Fourier (time) analysing the polarimetric variability , with occultation effects included, the inclination of the system can be reliably estimated by using the ratio of the second harmonic coefficients. In single stars this has the imporant consequence of establishing the equatorial velocity of the star from knowing the apparent rotational velocity (Vsini) which cannot be otherwise established.

CHAPTER 6

Obliquely Rotating Envelopes of Single Stars.

6.1 Introduction.

Regular polarimetric (and photometric) variations of stars are generally interpreted as arising due to binary motion despite the fact that in some cases the binary nature does not reveal itself in spectroscopic analysis. A recent alternative explanation for the regular variations has been given by Harmanec (1984) who suggested that the variations arise from an obliquely rotating envelope (ORE) about the star. The mechanism giving rise to an ORE is presumed to be be due to the magnetic field of the star whose rotation axis is not aligned with the magnetic field axis. Indeed Clarke and McGale (1988a, b: henceforth CM) have successfully interpreted polarimetric data in this way for σ Ori E and X Per by considering two localised spots of scattering material placed at the poles of an obliquely rotating magnetic dipole field.

In a binary system the external torque required to drive and maintain an ORE is provided by tidal forces when the orbital plane of the secondary does not lie in a plane perpendicular to the rotation axis of the primary with the extended envelope. Such a scenerio has been suggested by Apparao (1985) for the X-ray transient AO538-66 in which the primary star has an extended disc-like envelope and the companion -a neutron star- orbits the primary out of the plane of the disc. This model, however, has been found unnecessary in the interpetation of the polarimetric data for AO538-66 (but not excluded) in Chapter 2.

Karitskaya (1981) has considered, for Cyg. X-1, an oblique and precessing accretion disc around a neutron star orbiting the luminous primary and finds that the predicted polarimetric variations are inconsistent with the data of Kemp et al. (1978) and Kemp et al. (1979). However, it is possible in Karitskaya's model for there to be complicated occultation effects because as the disc precesses a variable amount of the disc will be occulted by the primary (with respect to the observer) which was neglected in the analysis. Brown et al. (1978: henceforth BME) have also analysed the polarimetric variations of Cyg. X-1 and they too find that the polarimetric variations are inconsistent with their model. Milgrom (1978) suggested that such occultation of scatterers would lead to inconsistences when the polarimetric data is interpretated in terms of the canonical models (which has been verified - cf. Sec. 5.6).

In this chapter we wish to analyse how significant the effects of occultation are upon the interpretation of polarimetric data when the point light source analysis of BME is used (cf. McGale, 1988) but occultation is present within the data.

First, we extend the single scattering, point light source approximation for ORE to include envelopes that exhibit some symmetry such that the envelope appears stationary in the obliquely corotating stellar frame and is a previously unpublished result. Following this, envelopes with axisymmetry in the obliquely rotating frame are considered.

We then consider the effects of including occultation and finite light sources upon the the observed polarimetric variability. Because the variablity depends upon the envelope geometry (cf. Ch. 5) we consider only two specific geometries and assess how reliable previous

point light source treatments (eg. CM) have inferred the inclination and obliquity angles of ORE when occultation is neglected but its effect are present in the polarimetric data.

Finally, we consider to what extent spectroscopic variability could be used to differentiate between envelope geometries.

6.2 General Envelopes.

Consider a point light source at O (Fig. 6.1). Let the star have some fixed cartesian coordinate system (X,Y,Z) such that the Z axis defines the rotation axis of the star. An observer at E with coordinate system (A,B,E) is defined such that th X-axis lies in the plane AE and the angle between OZ and OA is i, the inclination of the star. The scattering envelope is stationary in a frame (x,y,z) where the z axis is some symmetry axis (e.g the magnetic axis) and shall be referred to as the principal obliquity axis and the angle (zOZ) between the principal obliquity axis and the stellar rotation axis is the angle of obliquity (ξ). We shall assume that the envelope rotates uniformly about the rotation axis of the star, at a rate $\omega = {}^{2\pi}/_{T}$, where T is the orbital period and $\lambda = \omega t$ with t being the time after which the y-axis lay in the XZ-plane.

In the observer's frame the position of a general scattering point, P, in spherical polars is given by (r,χ,ψ), whilst in the star frame it will have position (r,θ,ϕ) and (r,α,β) in the corotating (oblique) frame. For an ensemble of such scatterers, with number density $n(\underline{r})$, the Stokes Flux parameters in the observer's frame are given by

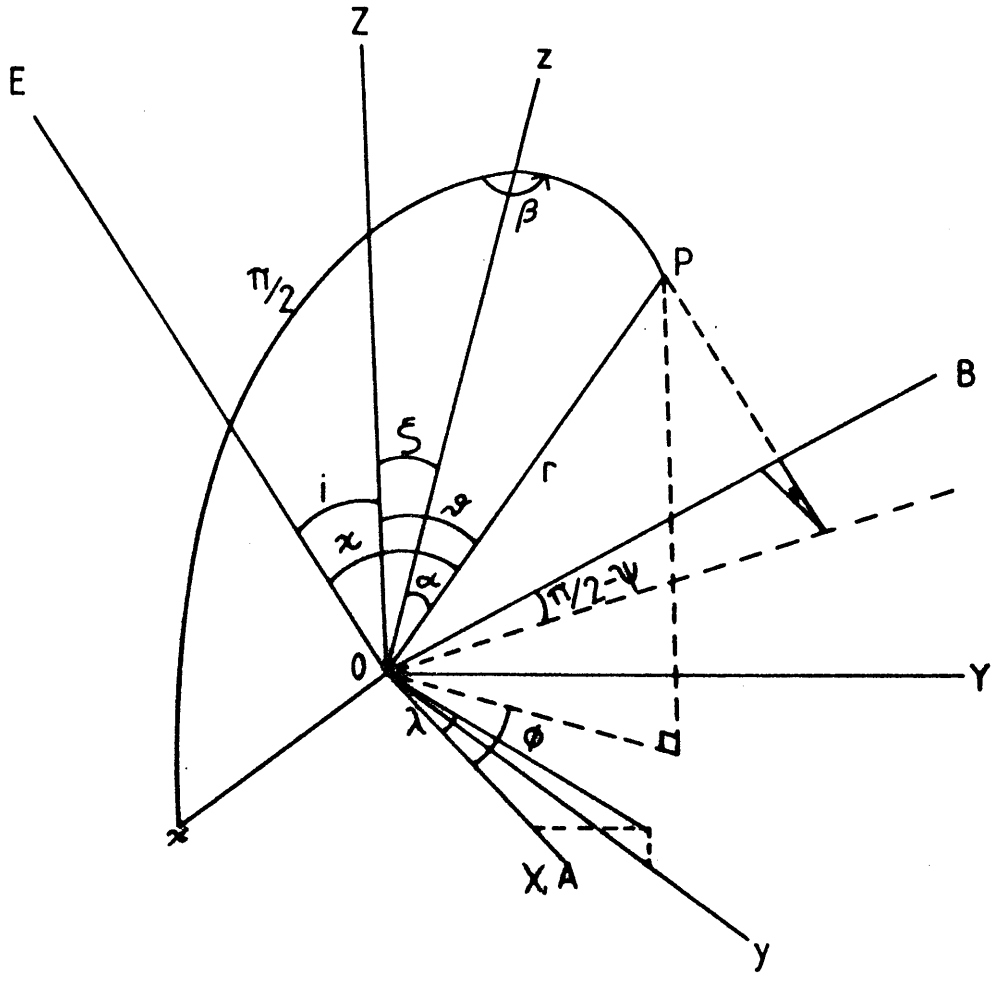

Figure 6.1

The scattering geometry for a general point, P, at a distance r from O. In the obliquely rotating frame (x,y,z) the scattering point (in spherical polars) has position (r,α,β). In the fixed stellar (X,Y,Z) frame, P is given (r,θ,ϕ). The Z-axis defines the rotation axis of the star, the z-axis is the principal obliquity axis and the angle zOZ (ξ) is the angle of obliquity.

$$\left.\begin{aligned} F_I &= \frac{L_* \sigma_o}{4\pi d^2} \int_V n(\underline{r}) \ (1 + \cos^2\chi) \ \frac{dV}{r^2} \\ F_Q &= \frac{L_* \sigma_o}{4\pi d^2} \int_V n(\underline{r}) \ \sin^2\chi \cos 2\psi \ \frac{dV}{r^2} \\ F_U &= \frac{L_* \sigma_o}{4\pi d^2} \int_V n(\underline{r}) \ \sin^2\chi \sin 2\psi \ \frac{dV}{r^2} \end{aligned}\right\} \qquad (6.1)$$

where $\sigma_o = 3\sigma_T/16\pi$, σ_T is the Thomson electron scattering cross-section, L_* is the luminosity of the star, d is the distance between the observer and the star and $dV = r^2 \sin\chi \, d\chi d\psi dr$.

It is, however, more convenient to transform from the observer to the corotating envelope frame (x,y,z) by changing the dependent coordinates (in spherical polars) from (χ,ψ) to (α,β) via (θ,ϕ) by use of Fig. 6.2.

The relevant tranforms from (χ,ψ) to (θ,ϕ) are

$$\begin{aligned} \cos\chi &= \cos\theta \cos i - \sin\theta \sin i \sin\phi \\ \sin\chi \cos\psi &= \sin\theta \cos\phi \\ \sin\chi \sin\psi &= \cos\theta \sin i + \sin\theta \cos i \sin\phi. \end{aligned} \qquad (6.2)$$

The transformations required for (θ,ϕ) to (α,β) are found from Fig. 6.1 and Fig. 6.2 in the form of a rotation matrix, viz

$$\begin{bmatrix} \sin\theta \cos\phi \\ \sin\theta \sin\phi \\ \cos\theta \end{bmatrix} = \begin{bmatrix} \sin\lambda & \cos\xi \cos\lambda & \sin\xi \cos\lambda \\ -\cos\lambda & \cos\xi \sin\lambda & \sin\xi \sin\lambda \\ 0 & -\sin\xi & \cos\xi \end{bmatrix} \begin{bmatrix} \sin\alpha \cos\beta \\ \sin\alpha \sin\beta \\ \cos\alpha \end{bmatrix} \qquad (6.3)$$

Substituting the relevant transformations into equation (6.1) we obtain after some manipulation,

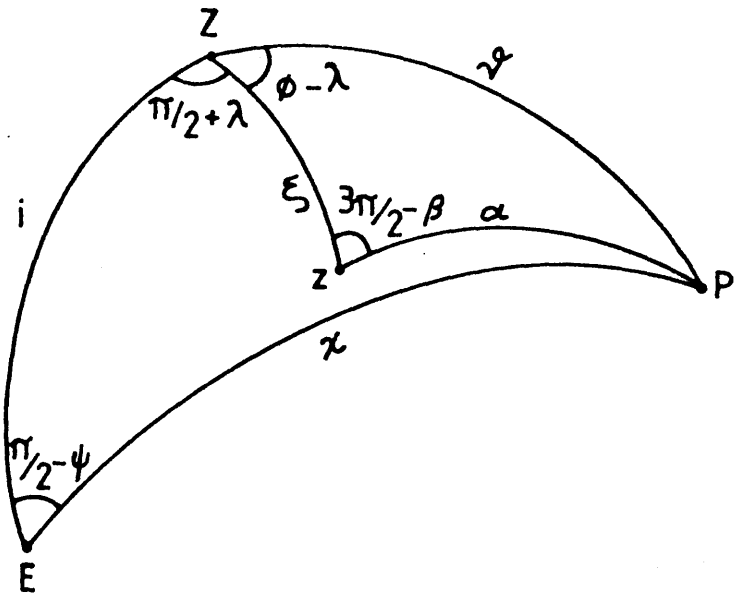

Figure 6.2

The spherical triangle from Fig. 6.1 for the transformation of (r,α,β), (r,θ,ϕ) to (r,χ,ψ) coordinates.

$$F_i = \frac{F_*}{2}\Big\{ 2(\tau_o + \tau_o y_o)(3\cos^2\xi - 1)$$

$$+(\tau_o - 3\tau_o y_o)\Big[\sin^2 i\ (3\cos^2\xi + 1) + \sin 2i \sin 2\xi \sin\lambda$$

$$+ \sin^2 i \sin^2\xi \cos 2\lambda\Big]$$

$$+ 2\tau_o y_1\Big[\sin 2i \cos\xi \cos\lambda - \sin^2 i \sin\xi \sin 2\lambda\Big]$$

$$+ \tau_o y_2\Big[(3\sin^2 i - 2) \sin 2\xi - 2\sin 2i \cos 2\xi \sin\lambda$$

$$- \sin^2 i \sin 2\xi \cos 2\lambda\Big] \qquad (6.4)$$

$$+ \tau_o y_3\Big[(3\sin^2 i - 2) \sin^2\xi - \sin 2i \sin 2\xi \sin\lambda$$

$$+ \sin^2 i\ (1 + \cos^2\xi) \cos 2\lambda\Big]$$

$$- 2\tau_o y_4\Big[\sin 2i \sin\xi \cos\lambda + \sin^2 i \cos\xi \sin 2\lambda\Big]\Big\}$$

$$F_q = \frac{F_*}{2}\Big\{(\tau_o - 3\tau_o y_o)\Big[\sin^2 i\ (3\cos^2\xi - 1) + \sin 2i \sin 2\xi \sin\lambda$$

$$- (1 + \cos^2 i) \sin^2\xi \cos 2\lambda\Big]$$

$$+ 2\tau_o y_1\Big[\sin 2i \cos\xi \cos\lambda + (1 + \cos^2 i) \sin\xi \sin 2\lambda\Big]$$

$$+ \tau_o y_2\Big[3\sin^2 i \sin 2\xi - 2\sin 2i \cos 2\xi \sin\lambda \qquad (6.5)$$

$$+ (1 + \cos^2 i) \sin 2\xi \cos 2\lambda\Big]$$

$$+ \tau_o y_3\Big[3\sin^2 i \sin^2\xi - \sin 2i \sin 2\xi \sin\lambda$$

$$- (1 + \cos^2 i)\ (1 + \cos^2\xi) \cos 2\lambda\Big]$$

$$- 2\tau_o y_4\Big[\sin 2i \sin\xi \cos\lambda - (1 + \cos^2 i) \cos\xi \sin 2\lambda\Big]\Big\}$$

$$F_u = F_*\Big\{ -(\tau_o - 3\tau_o\gamma_o)\Big[\sin i \sin 2\xi \cos\lambda + \cos i \sin^2\xi \sin 2\lambda\Big]$$
$$+ 2\tau_o\gamma_1\Big[\sin i \cos\xi \sin\lambda - \cos i \sin\xi \cos 2\lambda\Big]$$
$$+ \tau_o\gamma_2\Big[2\sin i \cos 2\xi \cos\lambda + \cos i \sin 2\xi \sin 2\lambda\Big] \qquad (6.6)$$
$$+ \tau_o\gamma_3\Big[\sin i \sin 2\xi \cos\lambda - \cos i\ (1 + \cos^2\xi)\ \sin 2\lambda\Big]$$
$$+ 2\tau_o\gamma_4\Big[\sin i \sin\xi \sin\lambda + \cos i \cos\xi \cos 2\lambda\Big] \Big\}$$

where the weighted integral moments τ_o, $\tau_o\gamma_o$, $\tau_o\gamma_1$, $\tau_o\gamma_2$, $\tau_o\gamma_3$ and $\tau_o\gamma_4$ are given in Chapter 5 [D(r) = 1], $F_* = L_*/4\pi d^2$ with d being the distance between the source and the earth.

It is evident that in the point light source approximation the polarimetric variations for a general envelope are represented by a Fourier series up to 2λ as in the case of BME. This means that polarimetrically it is not possible to distinguish between orbital and rotational motion. In order to make such a distinction will require the aid of spectral analysis.

6.3 Axisymmetric Distributions.

Here we shall concern ourselves with the polarimetric variations of an ORE with density distributions that are axisymmetric about an axis oblique to the rotation axis. For any such axisymmetric distribution, $n(\underline{r}) = n(r,\alpha)$. In the (BME) point light source approximation the only non-vanishing integral moments are τ_o and $\tau_o\gamma_o$ and the normalised Stokes parameters ($Q = F_Q/F_*$, $U = F_u/F_*$) simplify to

$$Q = \tfrac{1}{2}(\tau_o - 3\tau_o\gamma_o)\Big[\sin^2 i\ (3\cos^2\xi - 1) + \sin 2i \sin 2\xi \sin\lambda$$
$$- (1 + \cos^2 i)\ \sin^2\xi \cos 2\lambda\Big] \qquad (6.7)$$

$$U = -(\tau_o - 3\tau_o\gamma_o)\left[\sin i \sin 2\xi \cos\lambda + \cos i \sin^2\xi \sin\lambda\right] \qquad (6.8)$$

In Fig 6.3 (Q,U) loci are shown for various values of i and ξ. It can be seen that that the loci vary in shape from a double looped ellipse, for high values of ξ, to a renal shape and finally to a point lying on the Q-axis for $\xi \sim 0^\circ$ (i.e the polarisation is independent of time). The geometrical factors are contained within the expression $(\tau_o - \tau_o\gamma_o)$ and acts as a scaling factor (cf. Brown and McLean, 1977) that does not alter the shape of the (Q,U) loci for a given i and ξ.

By Fourier analysing the polarimetric data it is possible from equation (6.7) to find the values of i, ξ and $(\tau_o - 3\tau_o\gamma_o)$, viz

$$\begin{Bmatrix} Q \\ U \end{Bmatrix} = \begin{Bmatrix} p_o \\ u_o \end{Bmatrix} + \sum_{j=1}^{2} \begin{Bmatrix} p_j \\ u_j \end{Bmatrix} \cos j\lambda + \begin{Bmatrix} q_j \\ v_j \end{Bmatrix} \sin j\lambda \qquad (6.9)$$

where the only non-zero coefficients are,

$$\left.\begin{aligned} p_o &= \tfrac{1}{2}(\tau_o - 3\tau_o\gamma_o)\sin^2 i\,(3\cos^2\xi - 1) \\ q_1 &= \tfrac{1}{2}(\tau_o - 3\tau_o\gamma_o)\sin 2i \sin 2\xi \\ p_2 &= -\tfrac{1}{2}(\tau_o - 3\tau_o\gamma_o)(1 + \cos^2 i)\sin^2\xi \\ u_1 &= -(\tau_o - 3\tau_o\gamma_o)\sin i \sin 2\xi \\ v_2 &= -(\tau_o - 3\tau_o\gamma_o)\cos i \sin^2\xi \end{aligned}\right\} \qquad (6.10)$$

If $i = 0^\circ$ then only second-order harmonics exist and ξ and $(\tau_o - 3\tau_o\gamma_o)$ cannot be determined. If $p_o \neq 0$ but $q_1 = u_1 = 0$ then $\xi = 0^\circ$ or 90°. In general, however, it will be possible to determine i, ξ and $(\tau_o - 3\tau_o\gamma_o)$ by taking ratios of the Fourier coefficients, viz

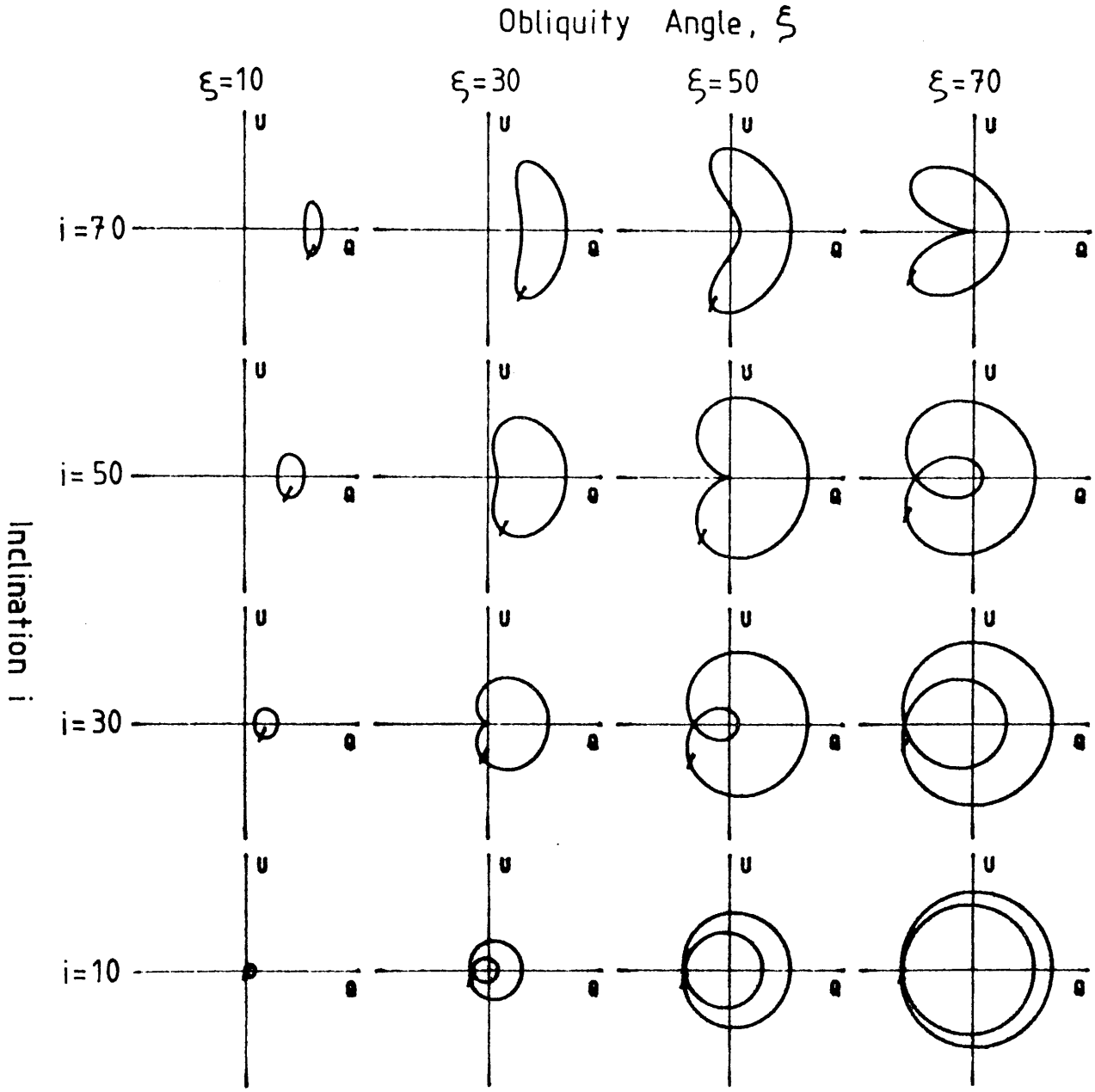

Figure 6.3

(Q,U) loci for any axisymmetric envelope for the values of inclination (i) and obliquity angle (ξ) indicated.

The loci vary in shape according to the value of ξ. As ξ varies from high values (~90°) to low values (~10°) the loci change gradually from an ellipse to a double loop ellipse through to renal shapes and finally, for $\xi \sim 0°$, a point (i.e. the polarisation is a constant and lies along the Q-axis)

$$\frac{q_1}{u_1} = -\cos i \tag{6.11}$$

$$\frac{p_0}{v_2} = \left[\frac{1 - 3\cos^2\xi}{\sin^2\xi}\right]\left[\frac{\sin^2 i}{\cos i}\right] \tag{6.12}$$

And finally $(\tau_0 - 3\tau_0\gamma_0) = -\frac{2p_2}{(1 + \cos^2 i)\sin^2\xi}$ (6.13)

It is instructive to establish how reliable this Fourier analysis is in returning the values of the inclination and obliquity angles and in order to do so polarimetric data were constructed for various values of inclination and obliquity angles (which shall be referred to as the real values) using 64 equally spaced (in time) data point. The polarimetric data were then Fourier analysed to obtain the inclination and the obliquity angles (which shall be referred to as the inferred values). It was found that, in the absence of noise, the inferred values of inclination and obliquity are consistent with the real (input) values (i.e. ξ, $i_{real} = \xi$, $i_{inferred}$).

Stars exhibiting polarimetric variations consistent with ORE have also been interpreted in terms of binary systems, e.g. σ Ori E (BME). It is possible now to see why, polarimetrically at least, that the variations of an ORE are consistent with binary variations by comparing the results of BME with those of equations (6.7) and (6.8).

In BME we set

$\lambda_1 = -\pi/2$, $\lambda_2 = 0$ or π

$G = \sin 2\xi$, $H = \sin^2\xi$, $A = \frac{1}{2}\tan\xi$

and substitute our $\frac{1}{2}(\tau_0 - \tau_0\gamma_0)$ and $3\cos^2\xi - 1$ for their τ_0 and $(\tau_0 - \tau_0\gamma_0)$ respectively. The very fact that binary motion and ORE are polarimetrically equivalent means that rotation produces the same effect whether it is due to rotation about a body axis or an orbital

axis.

For the particular case of σ Ori E both CM and BME used the data of Harman (1977). CM, using their 'method of moments' for the polarimetric analysis, find that $i \approx 80^\circ$ and $\xi \approx 85^\circ$ gives the best fit. BME, using Fourier analysis, find a best fit for $i \approx 76^\circ$ and $A > 2$, implying $\xi > 76^\circ$. Both models are thus consistent with each other within the accuracy of the available data.

CM, using their value for the inclination, infer from magnetographic data an obliquity angle of the magnetic axis to the rotation axis of $\sim 50^\circ$. Now previously they had obtained from the polarimetric data an angle of $\xi \sim 85^\circ$. This angle refers to an axis that exhibits rotational symmetry with respect to the scattering envelope and therefore it appears that the scattering envelope is not connected with the magnetic axis of the star. Indeed, if one interprets the scattering envelope to be two diametrically opposite spots (as in CM) then the polarimetric data are consistent with two spots rotating about the equator of the star (i.e. $\xi = 90^\circ$). It must be stressed however that in the point light source approximation such an interpretation regarding the envelope geometry is unjustified from the polarimetric data alone.

6.4 Extended Sources and Occultation.

It has been shown that in the point light source approximation it is not possible to say anything about the geometry of the scattering material (i.e. one cannot distinguish between different geometries as $\tau_0 - 3\tau_0 y_0$ is a number thus allowing a multiplicity of interpretations). However, by allowing the light source to be of finite extent then some of the scattering material at any given time may be occulted by the star thus allowing some probing of the envelope geometry as it

rotates. The occultation of optically thin, Thomson scattering, envelopes has been investigated in Chapters 3 - 5. In the case of an ORE the occulted scattering material will change with time and in general the problem is a complex one so only two specific geometries are considered to illustrate the effects of occultation namely localised polar spots and a near planar, equatorial disc.

6.4.1 Polar Spots.

Stellar spots are a common phenomena to stars of all spectral classes. For stars of spectral classes G - M it is believed that stellar spots are connected with convection cells that have their origin deep within the convection zone of the star. The spots appear to be of various sizes, which in later type stars (eg. RS CVn types) may cover a large portion of the stellar disc. Attempts have been made at modelling such phenomena (Strassmeier, 1988) however the recovery of such surface features from the photometric variability is a difficult one.

For early type stars (which we shall consider) the mechanism producing spot features is unknown. It is thought unlikely to be caused by a convection zone as this has been found to be negligible in size compared to late type stars (Hofmeister et al., 1964). Instead dipole magnetic fields are often invoked (Underhill and Fehey, 1984) but this appears to be unnecessary (cf. above and CM). Whatever the mechanism, observations have shown that regular photometric variability can be interpreted in terms of localised stellar spots (Balona and Englebrecht, 1986).

For one particularly well observed star, σ Ori E, spectroscopic (Bolton et al., 1987), radial velocity (Groote and Hunger, 1982) and

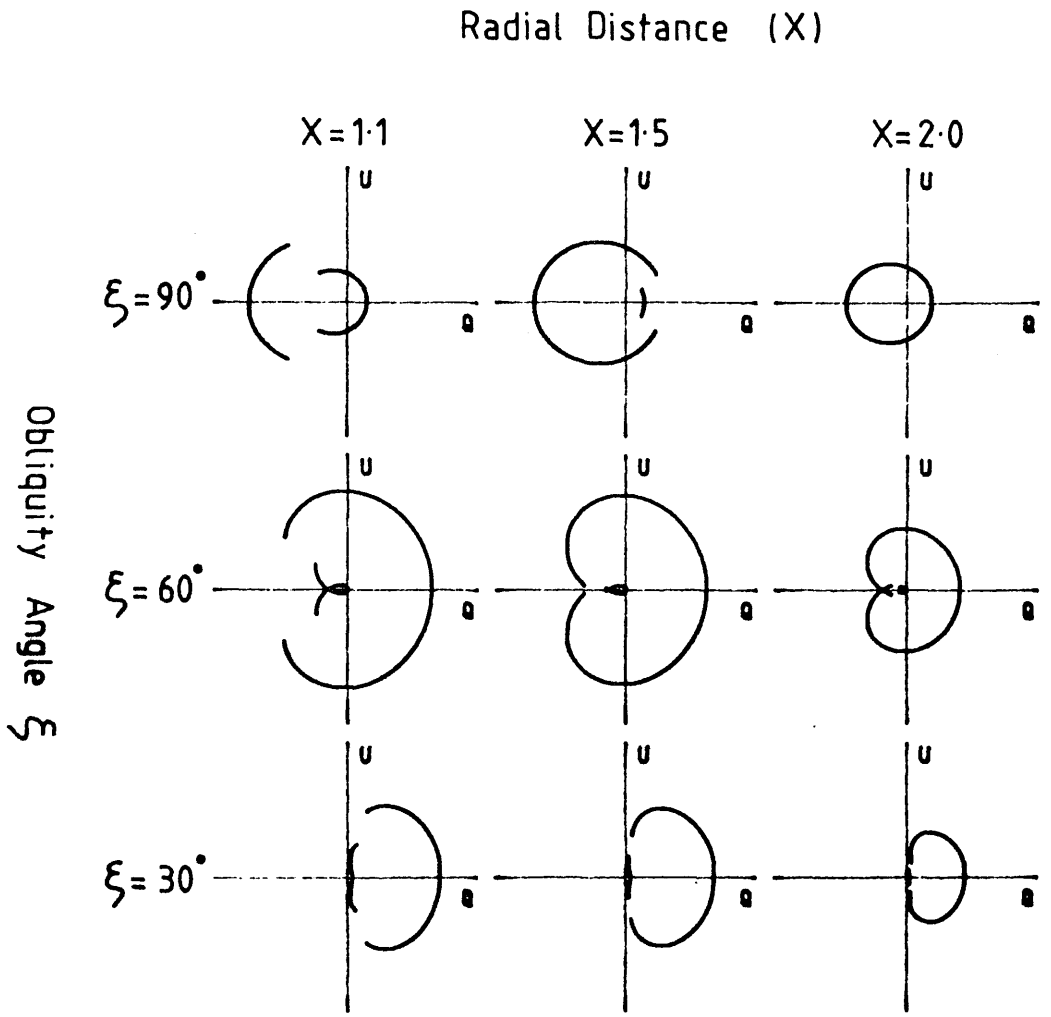

Figure 6.4

(Q,U) loci for a finite spherical light source with two localised polar spots at a distance x from the centre of the star, with the values of x, i and ζ indicated. As x increases, the period through which occultation occurs decreases.

photometric variations (Landstreet and Borra, 1978) indicate that two localised, diametrically opposite, spots are corotating with the star. In the light of such observations we consider two localised scattering regions (in the obliquely rotating frame) placed at $\alpha = 0$ and $\alpha = \pi$. We will assume that they have the same number of scatterers (n_o) and are at the same distance $r = xR_*$ (R_* being the radius of the star).

For a point source the polarimetric variations will be as in equations (6.7) and (6.8) with $(\tau_o - 3\tau_o\gamma_o) = -N\sigma_o/(xR_*)^2$ and $N = 2n_o$.

For an extended source we have

$(\tau_o - 3\tau_o\gamma_o) = -N\sigma_o(1 - x^{-2})/(xR_*)^2$ and $N = 2n_o$ except when one of the spots is occulted, viz

$$\cos i \cos\xi - \sin i \sin\xi \sin\lambda \leqslant -(1 - x^{-2})^{1/2} \qquad 0 \leqslant \lambda \leqslant \pi \tag{6.14}$$

or $\cos i \cos\xi - \sin i \sin\xi \sin\lambda \geqslant (1 - x^{-2})^{1/2} \qquad \pi \leqslant \lambda \leqslant 2\pi$

then $N = n_o$.

The resulting Q,U variations are shown in Fig. 6.4 for various i, ξ and distance x ($= r/R_*$) It can be seen that the period through which a spot is occulted decreases with increasing distance. For spots very close to the stellar surface it is possible that each of the spots may undergo occultation through some part of the period. In reality the spots will be spatially extended and so occultation will be a gradual process rather than being discontinuous as shown in Fig. 6.4.

It is obvious that by Fourier analysing polarimetric data in which occultation is evident, but no account is made of it, will result in incorrectly inferred diagnostics. In order to illustrate this, polarimetric data were constructed using equally spaced data (every $^1/_{64}{}^{th}$ phase) with occultation present for spots located at a radial

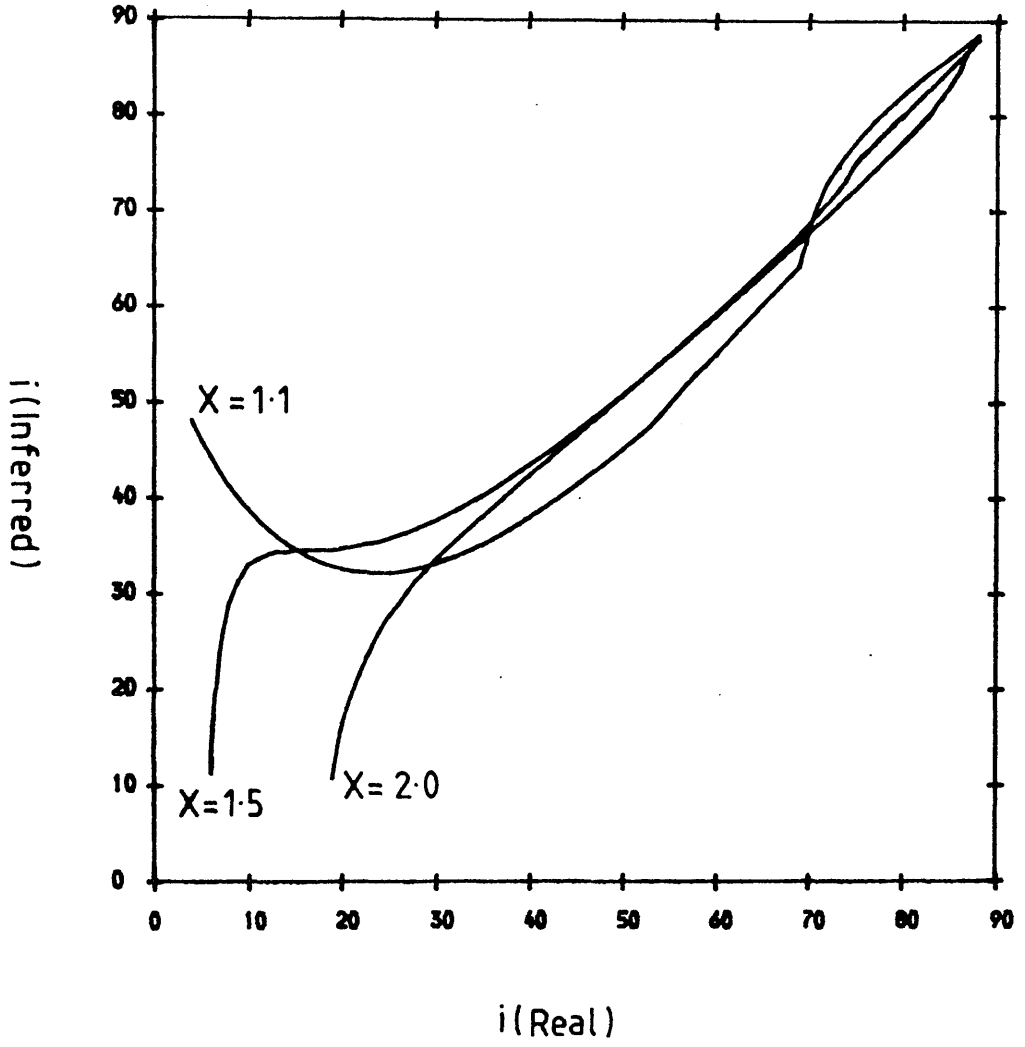

Figure 6.5a

The Fourier inferred inclination plotted against the real inclination for spots at a radial distance x = 1.1, 1.5 and 2.0 and ξ = 45°

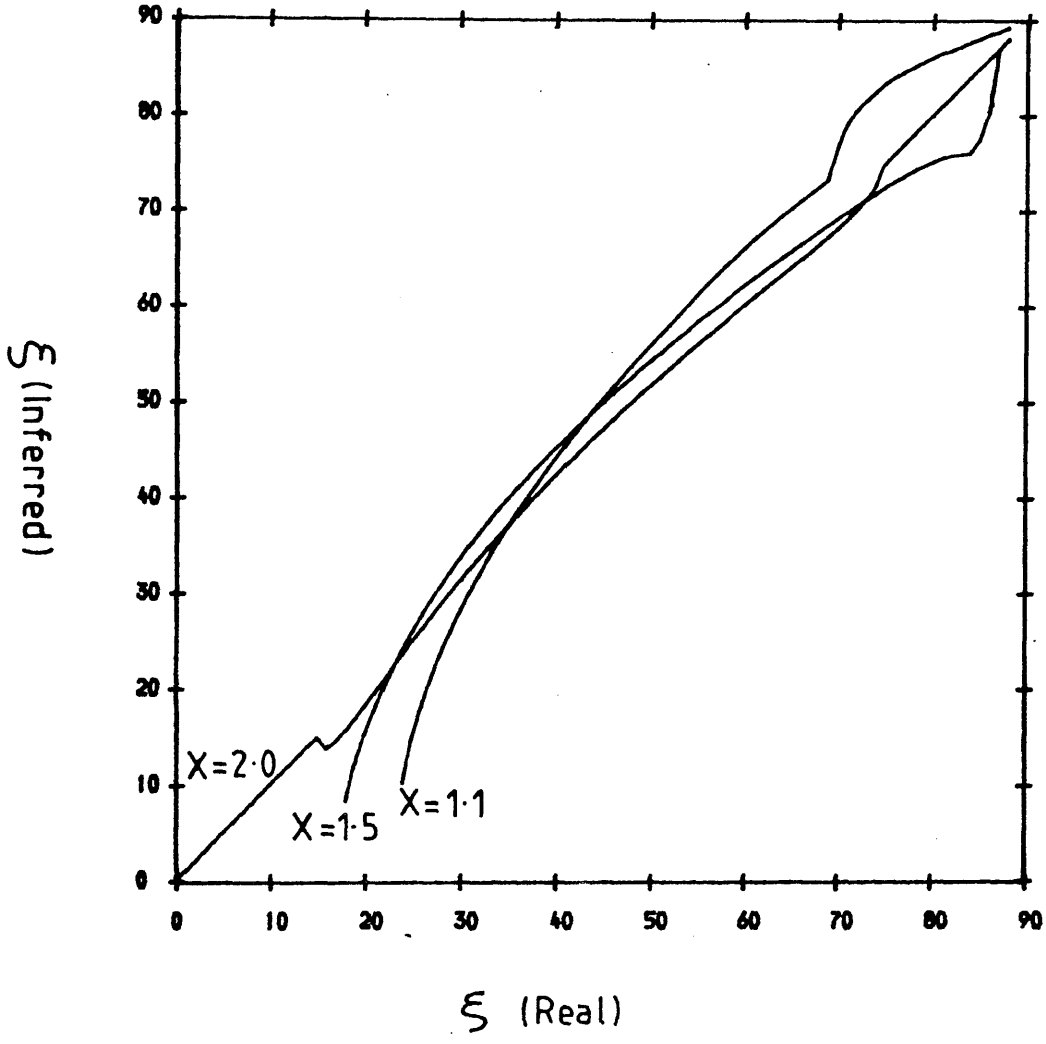

Figure 6.5b

The Fourier inferred obliquity plotted against the real obliquity for spots at a radial distance x = 1.1, 1.5 and 2.0 and i = 45°

distance of x = 1.1, 1.5 and 2.0 for fixed obliquity ($\xi = 45°$) and variable inclination. The resulting data were then Fourier analysed (using the method of Sec. 6.3). The resulting inferred inclination is shown in Fig. 6.5a against the actual (input) value. A similar plot is shown in Fig. 6.5b for variable obliquity angle with fixed inclination (i = 45°).

It can be seen that for spots distant from the star (x > 2) the inferred values of inclination and obliquity are consistent with the real (input) values, implying that occultation is negligible as shown previously (Fig. 6.4). For small radial distances the inclination or obliquity angle cannot be determined for stars with small inclinations or spots with small obliquity angles [i.e. inferred Fourier ratios are inconsistent with eqs (6.11)-(6.13)]. For large values of the inferred inclination (obliquity) angle the inferred value is consistent with the real (input) value to within an error of ±5°. In the presence of noise, however, this uncertainty will be increased. It should be noted that the curves of Figs 6.5a and b vary smoothly except at certain well defined points which are a reflection of the inclination and obliquity angles required in satisfying the conditions of eq.(6.14) i.e. the values of i and ξ at which there is a change-over in the number of spots being occulted during one rotational period.

6.4.2 Precessing Disc.

In binary systems where the primary is surrounded by an enhanced (circumstellar) density region caused (for example) by the tidal pull of the secondary (cf. Chapter 2), the enhanced density region may be modelled as a disc-like structure. Alternatively, a disc-like structure may arise from mass acretion on to a star. In

systems such that the rotation axis of the star (with the disc envelope) is not aligned with the orbital rotation axis, the envelope (confined to the orbital plane) will appear to rotate (or precess) about an axis oblique to the stellar rotation axis. Clearly such a scenario will be applicable to young systems such that the orbital and rotational axes have not yet had time to align.

In single stars obliquely rotating disk-like structures may occur by the confinement of material to the equatorial region of a magnetic field rotating obliquely to the stellar rotation axis.

We shall consider such an envelope and assume that the envelope is a near planar distribution of material in the ORE frame with surface density of the form $\Lambda(\underline{r}) = \Lambda_0 \delta(\alpha - \pi/2)/x^j$ -cf. Sec.4.3- extending to infinity, where $x = r/R_*$, j is the power index and Λ_0 is the surface density at the stellar surface. Further, we shall assume that in a binary situation the only important light source is the one surrounded by the disc. The normalised Stokes parameters are given by eqs (6.7) and (6.8). For a point light source $\tau_0 = \sigma_0 \Lambda_0 \pi / j$ and all other weighted integrals are zero. For an extended light source occultation will give rise to more complicated expressions for Q and U with additional integral moments arising because of the variable occultation (hence the general eqs 6.5 and 6.6 are employed). The weighted integrals are given by

$$\tau_0 = \frac{\sigma_0 \Lambda_0}{2}\left[\int_1^{\infty} \int_0^{2\pi} \frac{(1 - x^{-2})^{1/2}}{x^j} \frac{d\beta dx}{x} - \int_1^{x_d} \int_{\beta_1(x)}^{\beta_2(x)} \frac{(1 - x^{-2})^{1/2}}{x^j} \frac{d\beta dx}{x} \right] \quad (6.15)$$

$$\tau_0 \gamma_3 = - \frac{\sigma_0 \Lambda_0}{2} \int_1^{x_d} \int_{\beta_1(x)}^{\beta_2(x)} \frac{(1 - x^{-2})^{1/2}}{x^j} \cos 2\beta \frac{d\beta dx}{x} \quad (6.16)$$

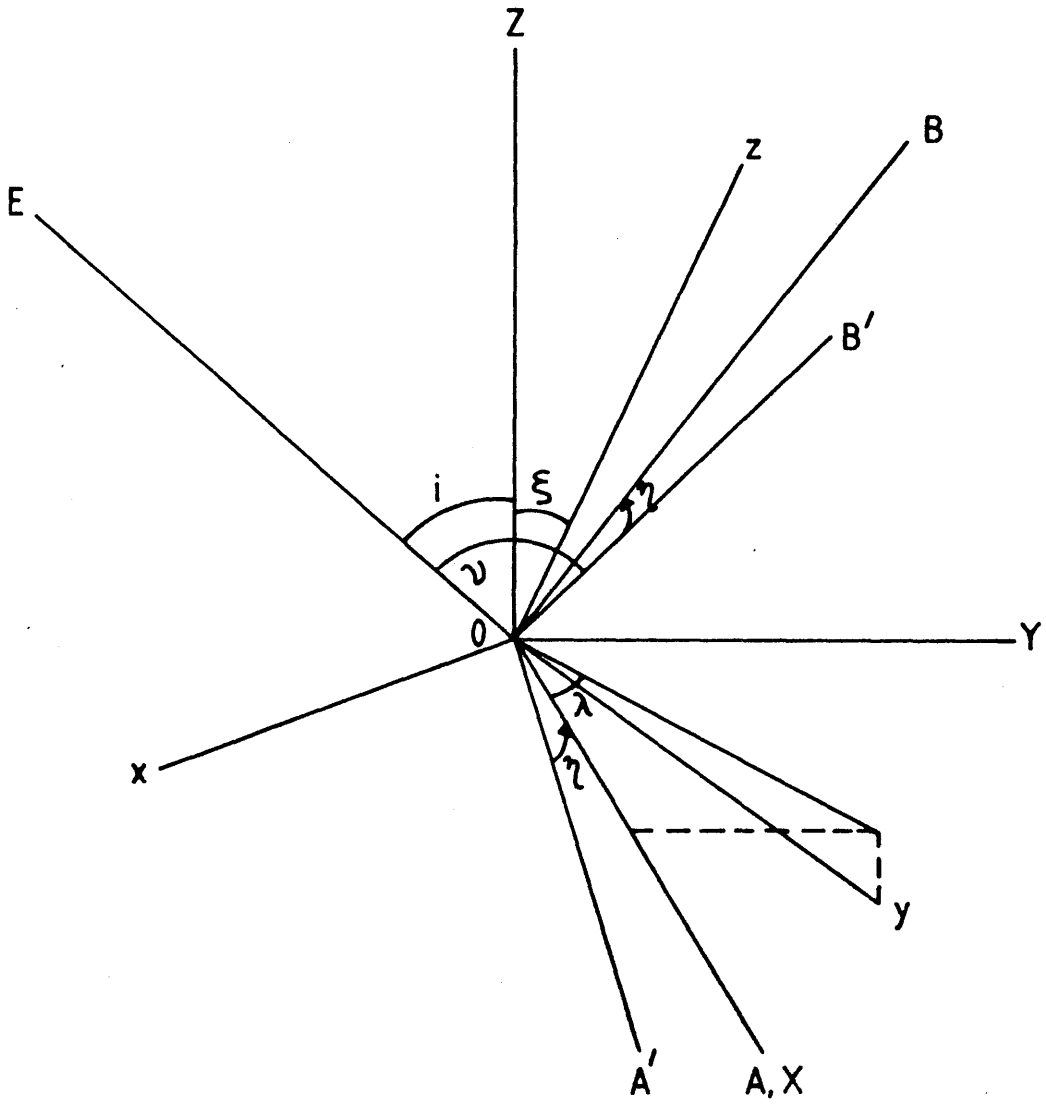

Figure 6.6

The rotated observer frame (A',B',E) shown in relation to the observer (A,B,E) and oblique frame (x,y,z). The B'-axis is parallel to the projection of the principal obliquity axis on the sky.

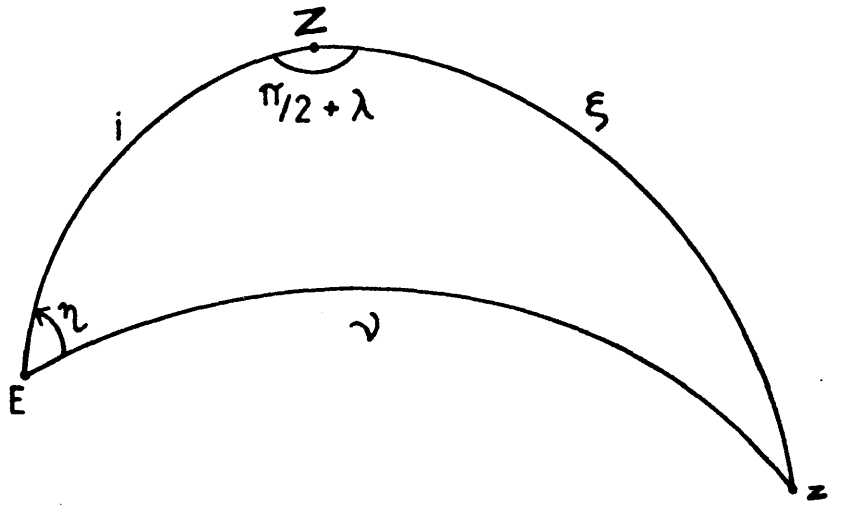

Figure 6.7

The spherical triangle for the transformation of the Stokes parameters from the privileged observer frame to the sky-observer frame.

$$\tau_o\gamma_4 = -\frac{\sigma_o\Lambda_o}{2}\int_1^{x_d}\int_{\beta_1(x)}^{\beta_2(x)}\frac{(1-x^{-2})^{1/2}}{x^J}\sin 2\beta\,\frac{d\beta dx}{x} \tag{6.17}$$

$$\tau_o\gamma_o = \tau_o\gamma_1 = \tau_o\gamma_2 = 0, \tag{6.18}$$

$$\text{where}\quad x_d = \frac{1}{|\cos i\cos\xi - \sin i\sin\xi\sin\lambda|} \tag{6.19}$$

The functions $\beta_1(x)$, $\beta_2(x)$ are found from

$$(1-x^{-2})^{1/2} = \sin\beta(\sin\xi\cos i + \sin i\cos\xi\sin\lambda) - \cos\beta\sin i\cos\lambda$$

hence

$$\cos\beta(x) = \frac{-A(1-x^{-2})^{1/2} \pm |B|(A^2+B^2+x^{-2}-1)^{1/2}}{(A^2+B^2)} \tag{6.20}$$

where $A = \sin i\cos\lambda$

and $B = \sin i\cos\xi\sin\lambda + \sin\xi\cos i$

In practice $\beta_1(x)$ and $\beta_2(x)$ are not easily determined from eq. (6.20). Since, however, we are only interested here in determining the variations of the Stokes parameters it is easier to determine the observed polarisation of the envelope in a privileged observer rotated (A',B',E) frame (Fig. 6.6) such that the plane of polarisation lies in the plane containing EB' and then to transform the observed Stokes parameters back to the observer (A,B,E) frame, via

$$\begin{bmatrix}Q(t)\\U(t)\end{bmatrix}_{(A,B,E)} = \begin{bmatrix}\cos 2\eta & \sin 2\eta\\ -\sin 2\eta & \cos 2\eta\end{bmatrix}\begin{bmatrix}Q(t)\\U=0\end{bmatrix}_{(A',B',E)} \tag{6.21}$$

where η is the (time dependent) angle BOB', measured anticlockwise from B'E to BE (Fig. 6.6) given by (Fig. 6.7)

$$\sin\eta = \cos\lambda\sin\xi/\sin\nu \tag{6.21}$$

$$\cos\eta = (\cos\xi - \cos\nu\cos i)/(\sin\nu\sin i) \tag{6.22}$$

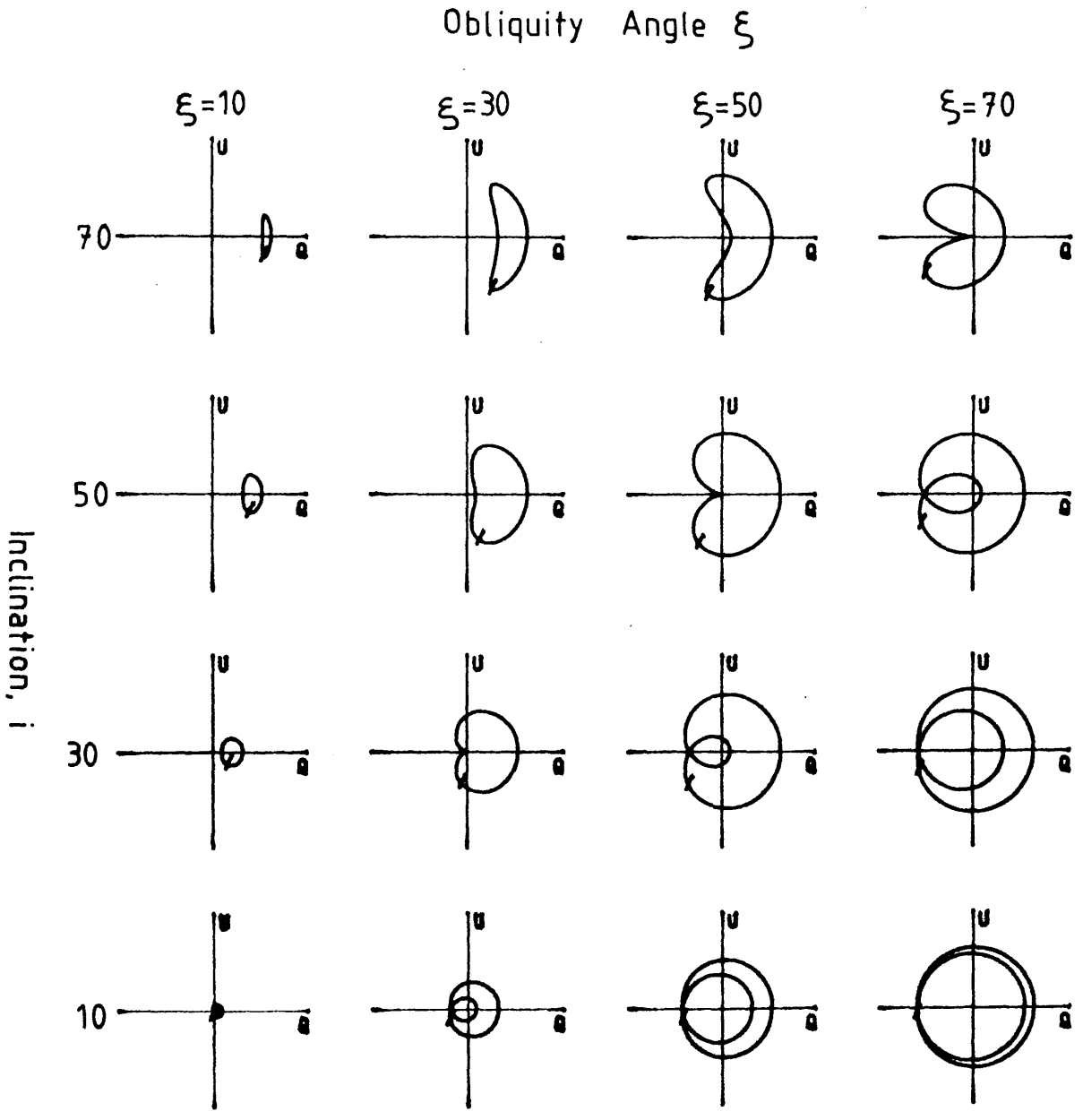

Figure 6.8

(Q,U) loci for a finite spherical light source with an obliquely rotating disc for the values of i and ξ indicated. Note that the loci resemble those of Fig.6.3.

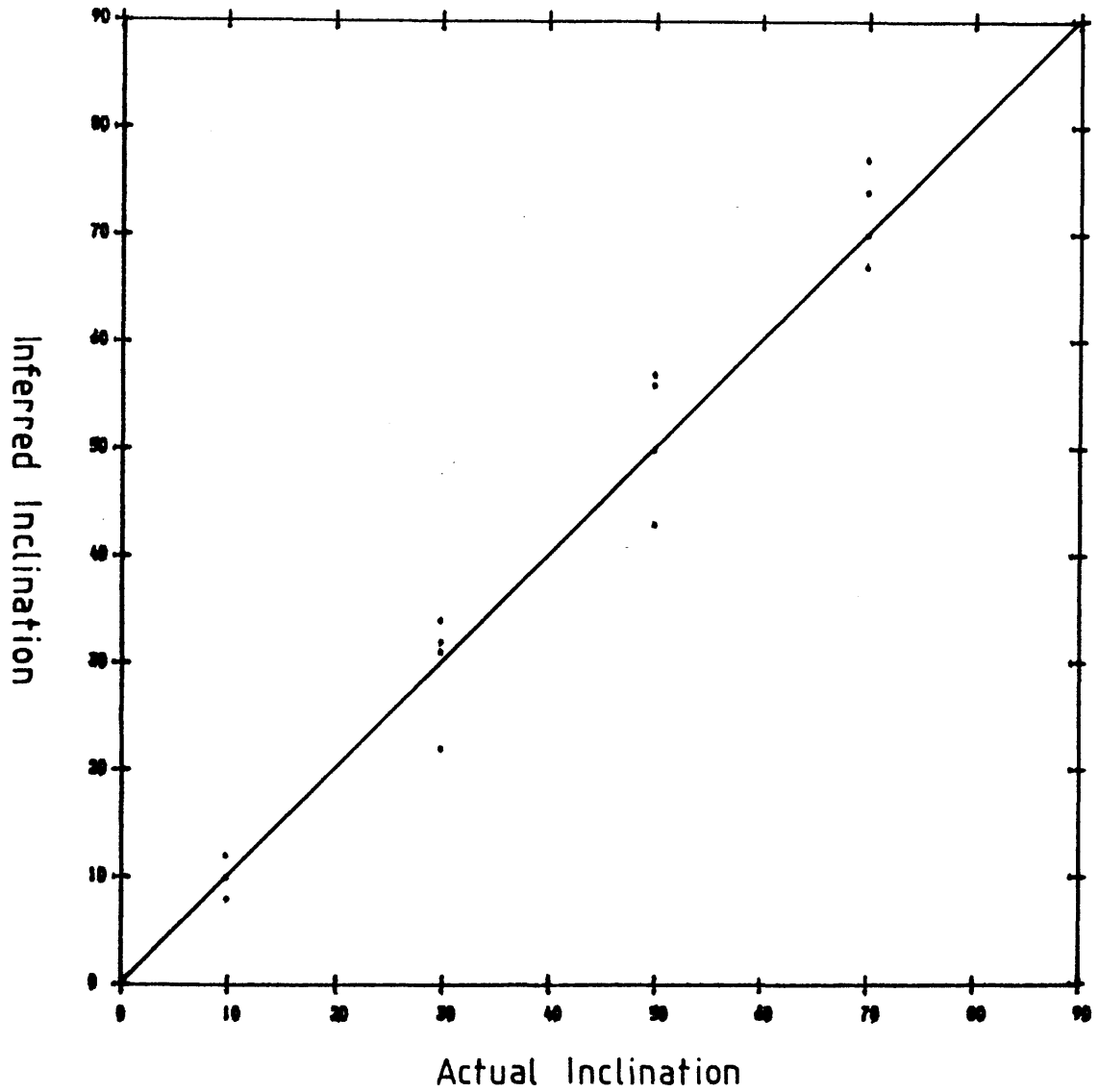

Figure 6.9a

The Fourier inferred inclination versus the 'real' inclination using the data of Fig. 6.8. The diagonal line indicates perfect agreement.

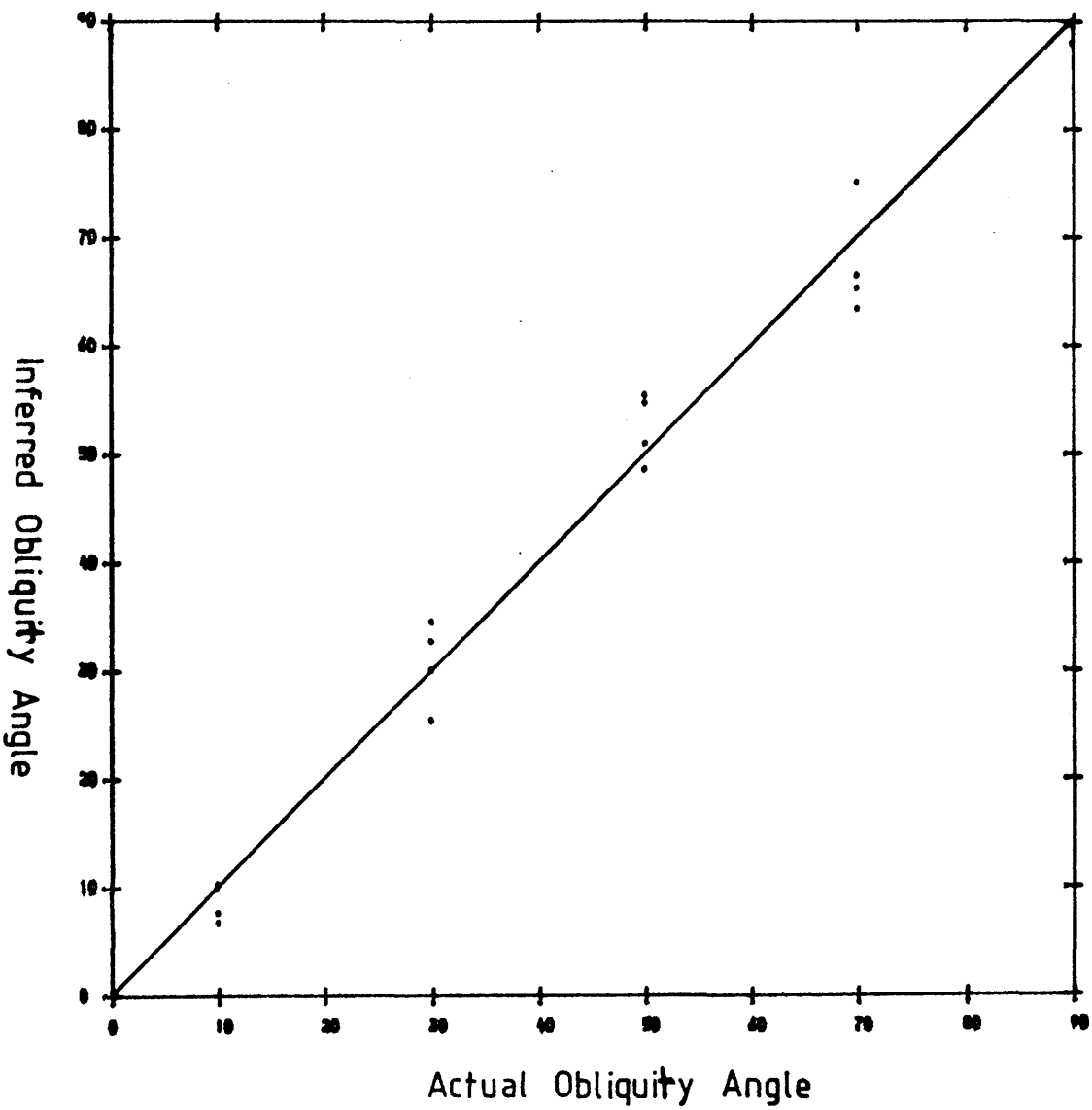

Figure 6.9b

As fig. 6.9(a) but for the obliquity angle.

The polarisation in the frame (A',B',E) is calculated using the analysis of Chapter 4 with a time dependent inclination, ν, given by (Fig. 6.7)

$$\cos\nu = \cos i \cos\xi - \sin i \sin\xi \sin\lambda \qquad (6.23)$$

The resulting (Q,U) loci for varius i, ξ (with the power index j = 2.5) are shown in Fig. 6.8.

Comparing Fig. 6.8 to Fig. 6.3 it is not visually obvious that there are any perceptable changes in the loci due to occultation, unlike the diametrically opposite spots, in which discontinuities were evident.

In order to assess the error involved in inferring the inclination and obliquity angle from polarimetric variations due to an obliquely rotating disc, equally (time) spaced polarimetric data were constructed from the data of Fig. 6.8 for every $^1/_{64}{}^{th}$ phase and then Fourier analysed using the analysis of Sec. 6.3 (the restricted number of permutations for i and ξ were considered in the analysis to save on computer time). The inferred values of the inclination and obliquity angles are plotted against the real (input) values in Fig. 6.9a and b respectively. It can be seen that in general the inferred values (for both i and ξ) are consistent with the real values to within $\pm 5^\circ$ (similar to the error found in Sec. 6.4.1). If a higher power index (j) had been chosen one could expect that the Figs 6.8, 6.9a and b would be qualitatively similar except for large values of i and ξ, where an increase in the discrepancy between the inferred and real values could be expected due to the fact that by increasing j more material will be occulted (as more material lies closer to the stellar surface).

6.5 Spectroscopic Variations.

Apart from the polarimetric variations arising from an ORE there will also be the possibility of observing such an envelope

spectroscopically.

Spectral lines arising from polar spots will have a very complicated but characteristic signature. In general there will be a blue-shifted emission line (arising from a spot approaching the observer) and a red-shifted emission line (due to a spot receding from the observer). The relative shifts of these two lines from the rest wavelength will vary (periodically) with time. If one of the spots passes across the disc of the star the line will initially appear as a blue-shifted absorption line which will become increasingly red-shifted as the spot crosses the disc of the star. Whilst one spot appears as an absorption feature the other spot will be occulted (assuming that the spots are equidistant from the centre of the star) and so only one (absorption) line will be observed. Once this absorption phase passes, the absorption line will appear as a red-shifted emission line and the occulted spot will appear as a blue-shifted emission line (neglecting light travel time effects).

The spectral variability of such spot features will only be made possible if they are sufficiently massive and have a small range in velocities (i.e. no turbulence). Observations of Be stars have indeed shown such discrete moving absorption lines (see Sec. 7.2) but features changing from absorption to emission has only been observed in one star, μ Cen (Baade, 1984b). The overall lack of observability of spots as emission features is probably due to technical/observational difficulties rather than due to a genuine lack of such features.

In the case of an obliquely rotating disc the angle between the normal of the disc and the observer will vary with time and therefore according to the analysis of Struve (1930), the Doppler broadened emission width of the disc will vary with phase. In Struve's analysis

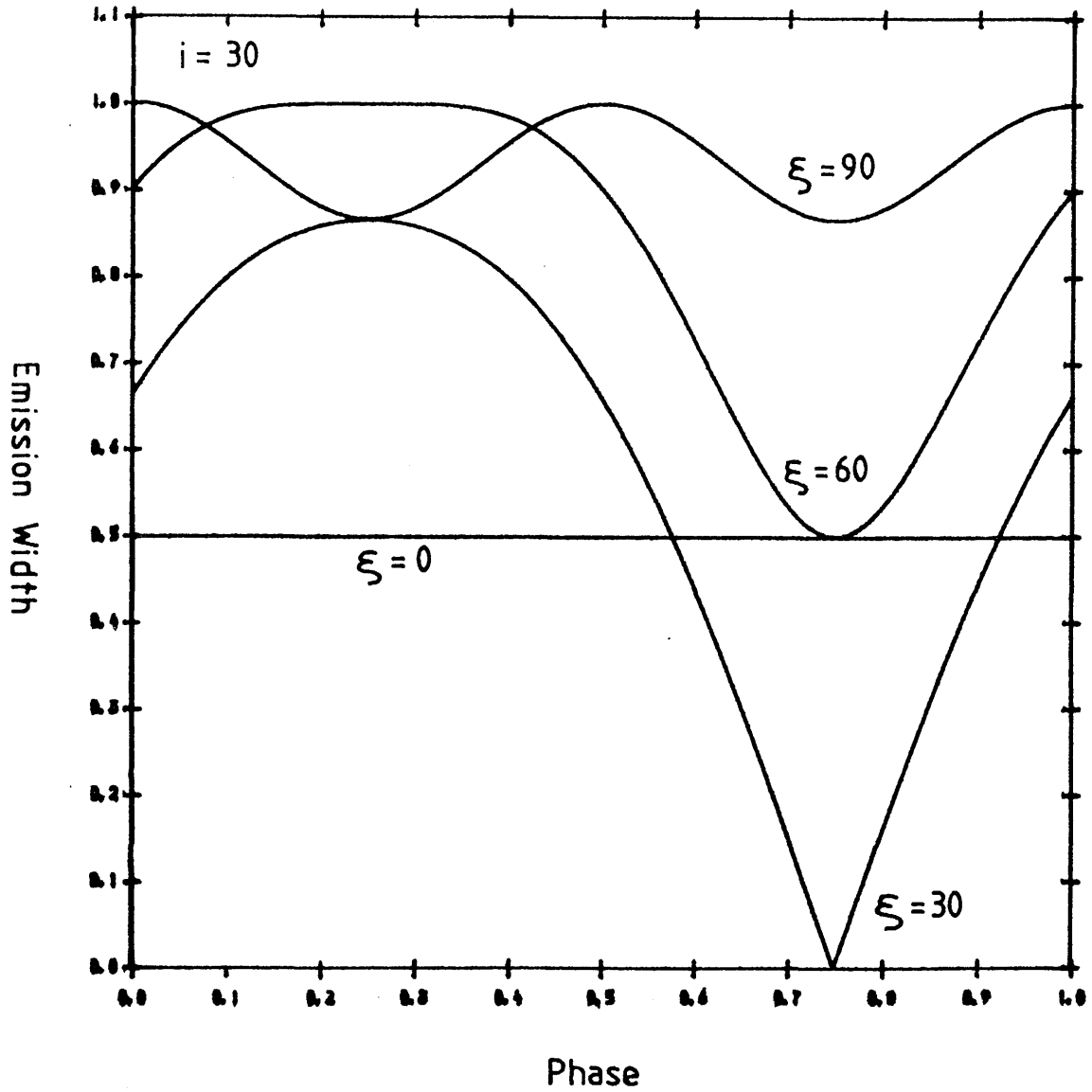

Figure 6.10a

The emission width (normalised such that it is equal to 1 when the disc is viewed in the equatorial plane, i = 90° and ξ = 0°) versus phase for i = 30° and ξ = 0°, 30°, 60° and 90°.

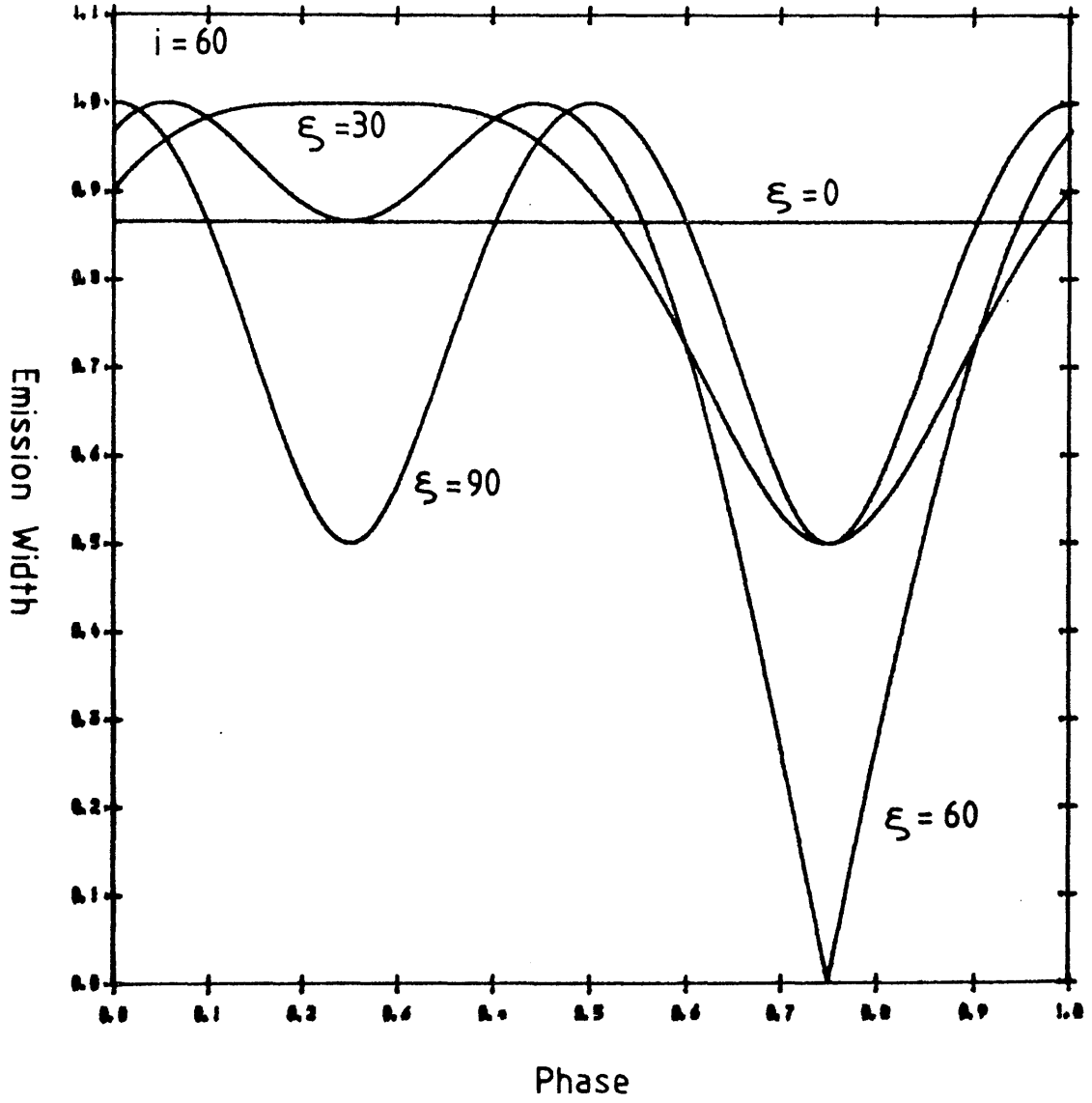

Figure 6.10b

As Fig. 6.10a but with i = 60°.

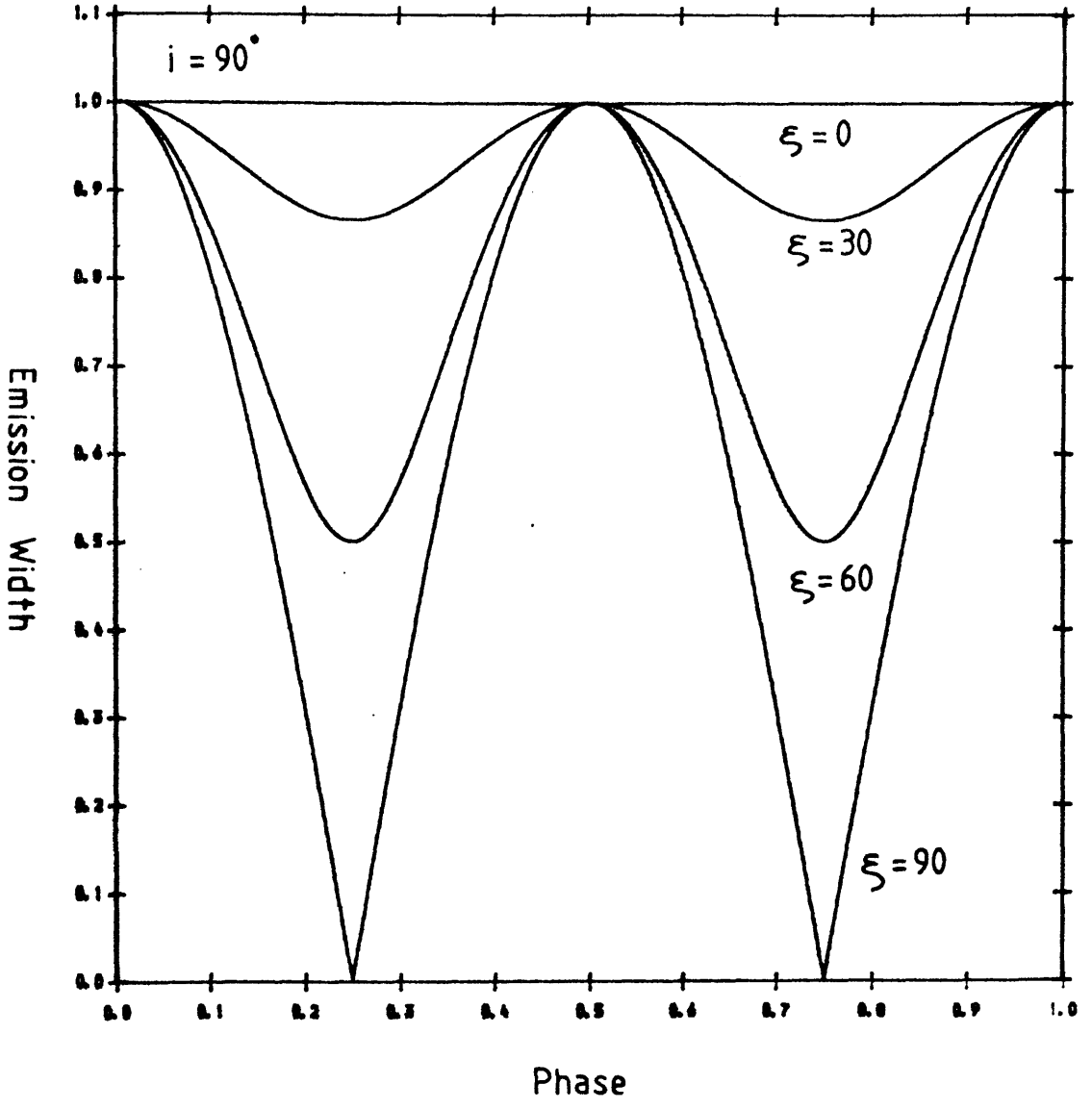

Figure 6.10c

As Fig. 6.10a but with i = 90°

his definition of i (the inclination) will be replaced by the time dependent inclination, ν, of equation (6.24). In Fig. 6.10 the variation of sin ν (which is proportional to the emission width) with phase is shown for various values of i and ξ. It can be seen that large variations in the emission width can occur, especially for large values of i and ξ. As ξ tends to zero (no obliquity) the emission tends to a constant value (i.e. as $\xi \rightarrow 0$, $\nu \rightarrow$ i). Provided that the amplitude of the variation is measurable and that the rotation period is much greater than the observation time, then such variability, if present, will be detectable. Indeed, such variability has been reported for α Eri (Balona et al., 1986) where in their Fig. 5c it can be seen that the equivalent width of the Mg II (448.1 nm) line varies in a periodic manner. The data are somewhat noisy, particularly at around phase 0.25 where it appears that there are two "peaks" in the data simultaneously (one peak occuring at ~ 0.004nm, the other at 0.007 nm) suggesting possibly that large structural changes within the envelope have occurred during the interval between observational sessions. However, pencilling in a rough curve to the data a sinusoid can be fitted that resembles the curves of Fig. 6.10c. This suggests that i ~ 90°, agreeing with their conclusions. The data are too noisy to attempt further analysis but it does suggest that the equivalent width, with careful analysis, could be a useful diagnostic tool.

6.6 Discussion and Conclusions.

It has been shown that the point light source treatment of an ORE cannot distinguish between different envelope geometries (Brown and McLean, 1977) and that an ORE is polarimetrically equivalent to a binary system with a special choice of parameters. By incorporating an

extended light source and occultation into the analysis, it is then possible to show that observable differences can exist for different geometries in the (Q,U) plane compared to the point light source predictions. In the case of polar spots the differences are readily apparent due to the discontinuous nature of the problem. For an obliquely rotating disc, however, the differences are not so apparent because the occulted region varies smoothly with time. In fact we can anticipate that for any ORE with a continuous spatial distribution the (Q,U) loci will vary smoothly such that only when the data is Fourier analysed will deviations from the point light source analysis be evident (i.e harmonics greater than second order will exist cf. Sec. 4.5).

In addition to an ORE producing polarimetric variations, spectroscopic variations may also be observable and hence if joint spectroscopic and polarimetric observations are made, it may be possible to infer something about the geometry of the system in addition to the determination of the inclination and obliquity angle.

Chapter 7

Future Work.

7.1 Introduction.

The inclusion of occultation and depolarisation into the single scattering theory of Brown and McLean (1977) enables a greater understanding of the temporal changes within stellar envelopes, by the virtue that a greater number of constraints are imposed upon the interpretation of the data. In section 7.2 we wish to outline the possible application of the previous chapters to the interpretation of polarimetric data from stellar winds that exhibit UV discrete absorption lines, subject to models that prepose to explain the spectroscopic observations. Following this the main conclusions of the previous chapters are recounted and further suggestions for future work are outlined.

7.2 Discrete Absorption Lines.

Theoretical modelling of stellar winds usually assume that the wind structure is time independent (see Section 1.3). Much data has been collected, however, which shows that this is not the case. In particular the Copernicus and IUE satellites have shown that the structure of stellar winds vary on time scales of ½ hr (approximately the flow time ~ R_*/v_∞) to months (Henrichs, 1988).

It has been found that for hot stars certain lines, such as O VI (103.2 nm, 103.8 nm), N V (123.9nm, 124.3nm) resonance lines and C III (117.6 nm) non-resonance lines, often exhibit blue shifted narrow absorption lines superposed upon the broad underlying P Cygni profile. Such lines are referred to as narrow discrete absorption lines

and typically have blue shifted velocities of up to 1000 kms^{-1} in O stars (Morton, 1976; Smith, 1972; Underhill, 1975) and also in Be stars, such as γ Cas (Hammerschlag-Hensberge, 1979) and 59 Cyg. (Doazan et al., 1980b; Doazan et al., 1985). In the case of Be stars these narrow absorption features are superposed upon the asymmetric absorption wings of the superionised line. The strength and velocity of these discrete absorption features changes over periods of time. This has been particularly observed by Henrichs et al. (1980), Henrichs (1982) in which there appears to be a correlation between the velocity and the strength of the absorption in the lines namely, the weaker the absorption the higher the velocity. Henrichs (1988) also found that even following a period of no narrow absorption features, when they did return the correlation was the same (Henrichs calls this the "memory" of the star and may last up to 5 yrs.).

Statistical studies (Henrichs, 1988) show that the narrow absorption lines are more likely to be observed in the most luminous of stars ($M_{bol} < -7$). There is, however, a lack of correlation with any other physical aspect of the star, such as Vsini, x-ray emission, binary motion etc. The lack of correlation with Vsini in particular would indicate that these UV absorption components occur throughout the wind rather than in some preferred plane. The only stars to exhibit absorption components with $M_{bol} > -7$ are Be stars and therefore the discrete absorption components would appear to be another feature and indicator of the Be phenomenon (see Barker and Marlborough, 1985).

The narrow absorption lines of superionised species indicate one of several possiblities;

(a) The existence of a velocity plateau in which the escape

probability (Sobolev, 1960) of a photon is constant over a large distance. This results in an increased path length of absorbing ions (as seen by the photon) and hence a deep narrow absorption line forms.

(b) Superionised species may exist at a preferred velocity due to ionisation effects which favour the observed ionisation fraction at that velocity, i.e. a density enhancement of superionised species at a preferred velocity.

(c) A non-monotonic velocity law caused by shocks occuring within the wind and thereby enabling velocity plateau to exist (Barker, 1987).

Models so far suggested in explaining the UV absorption components have included corotating interacting regions (Mullan, 1984; Bates and Halliwell, 1986; Prinja and Howarth; 1988), ejected parcels of material (Underhill and Fahey, 1984) and envelope ejection (Brown and Henrichs, 1987). Thus far the modelling of the UV absorption components has been primarily based upon the UV spectra alone. However, much more could be said of the envelope geometry (and structure) by including the polarimetric variations predicted by the models (Brown and Henrichs, 1987). The main reason for the neglect of polarimetric considerations has been the lack of simultaneous UV and polarimetric observations. However, with the forthcoming Astro Mission this situation will change (WUPPE Guest Observer Manual, 1985). I wish here, therefore, to make an exploratory investigation of the polarimetric variations predicted by the models of Underhill and Fahey (1984) and Mullan (1984) in order to determine what may be expected from the polarimetric variations of these models.

7.21 Corotating Interacting Regions.

Mullan (1984) suggested that a velocity plateau, used to explain the UV absorption lines, can exist when two gas streams, with different initial speeds, are ejected from the surface of a star and interact to form a shock region that results in a single velocity flow by the redistribution of momentum. Such phenonena has been observed in the solar wind from the Mariner 2 probe (Neugebauer and Snyder, 1967) and are believed to be controlled by the solar magnetic field. Numerical studies (Hundhausen, 1973, Suess et al., 1975; Pizzo, 1978, 1980, 1982) and analytical investigations (Carovillano and Siscoe, 1969; Suess, 1972; Siscoe and Finley, 1970) have attempted to quantify and explain the corotating interacting regions (CIR) in the solar wind. The analytical treatments consider the hydrodynamic equations for a non-rotating star and then include rotation as a perturbation. By considering only those perturbations that corotate with the sun, the velocity field and the density distribution for the CIR are obtained.

Mullan (1984) considers only CIR that are formed in the equatorial plane of the star. The CIR forms at some distance from the star (called the radius of interaction, r_j) and spiral outwards into the interstellar medium. As the CIR passes between an observer's line of sight and the disc of the star a deep absorption line forms which shifts in wavelength in accordance with the motion of the CIR (Prinja and Howarth, 1988).

In order to probe the geometry of the wind via the polarimetric occultation analysis of the foregoing chapters, the CIR must be occulted by the disc of the star according to an external observer. Since the CIR exist at some finite distance from the stars, only observers at sufficiently high inclinations will observe any occultation

effects.

According to Mullan, an approximation to the upper limit for the beginning of the interaction is given by

$$\frac{r_i}{R_*} = 1 + \left[\frac{V_w}{V_{rot}}\right]\pi \qquad (7.1)$$

where V_w is the average speed of the wind near the suface of the star, V_{rot} is the equatorial velocity of the star and R_* is the stellar radius.

The inclination at which occultation effects will be observable is given by

$$\sec i > r_i/R_* \qquad (7.2).$$

Typically for Be stars $V_{rot} \sim 400$ kms^{-1}, $V_w \sim 40$ kms^{-1} and thus $i > 40^{\circ}$ for the occultation of CIRs to occur.

Quantitatively eq. (7.1) states that the greater the initial wind speed is compared to the rotation of the star, the greater the distance that CIR are formed (i.e radially fast moving particles will 'see' a stationary star and will therefore not deviate from the initial radial trajectory). For Be stars the outflow velocity of the wind is comparitatively large compared to stars of later spectral classes. This large outflow velocity is, however, off-set by the rapid rotation of these stars.

In order to calculate the polarimetric variations from a CIR we need to know the density distribution. In the solar wind the iso-densities for the CIRs are Archimedian spirals. We shall assume that this is the case for Be stars and that they are confined to the equatorial plane of the star. In this case we may use the functional form for the density from the analysis of Carvillano and Siscoe (1969). The exact expression obtained by them cannot be used because the physics of Be star

winds are different from that of the sun (i.e. the rotation of the star cannot be considered as a perturbation). However, by using the functional form for the density we are in fact merely representing the density pertubation by Archimedian spirals. The density of the CIR is then,

$$\begin{aligned} \Omega(r,\phi) &= \Omega_o g(r)\ \sin j\left[\frac{r_i\omega}{V_w} + \phi - \lambda\right] && r > r_i \\ \Omega(r,\phi) &= 0 && r < r_i \end{aligned} \tag{7.3}$$

where j is the number of streams, ω is the rotation rate of the star, $\Omega(r,\phi)$ is the number density of electrons at a general point (r,ϕ) in the CIR, g(r) is the (assumed known) radial density distribution and λ is the longitude of the footpoint of the stream at r_i (Fig. 7.1). The form of eq. (7.3) is analogous to the density perturbation considered in Sec. 4.5 and this therefore suggests that the polarimetric data from a suspected CIR star should be Fourier (time) analysed. If the polarimetric variations are indeed due to CIRs, then only one set of Fourier harmonics will exist, i.e. the j^{th} harmonic (note that a zero order term will also exist which results from the constant polarisation term of the wind). By following the analysis of Sec. 4.5 with the density distribution as given by eq. (7.3) the coefficients a_j, b_j will be

$$\begin{aligned} a_j &= \sigma_o\Omega_o\ \sin j\left[\frac{r_i\omega}{V_w}\right] \\ b_j &= \sigma_o\Omega_o\ \cos j\left[\frac{r_i\omega}{V_w}\right] \end{aligned} \tag{7.4}$$

By Fourier (time) analysing the observed polarimetric data (cf. Sec. 4.5) of a CIR we may obtain the j^{th} harmonic Fourier coefficients (p_j,

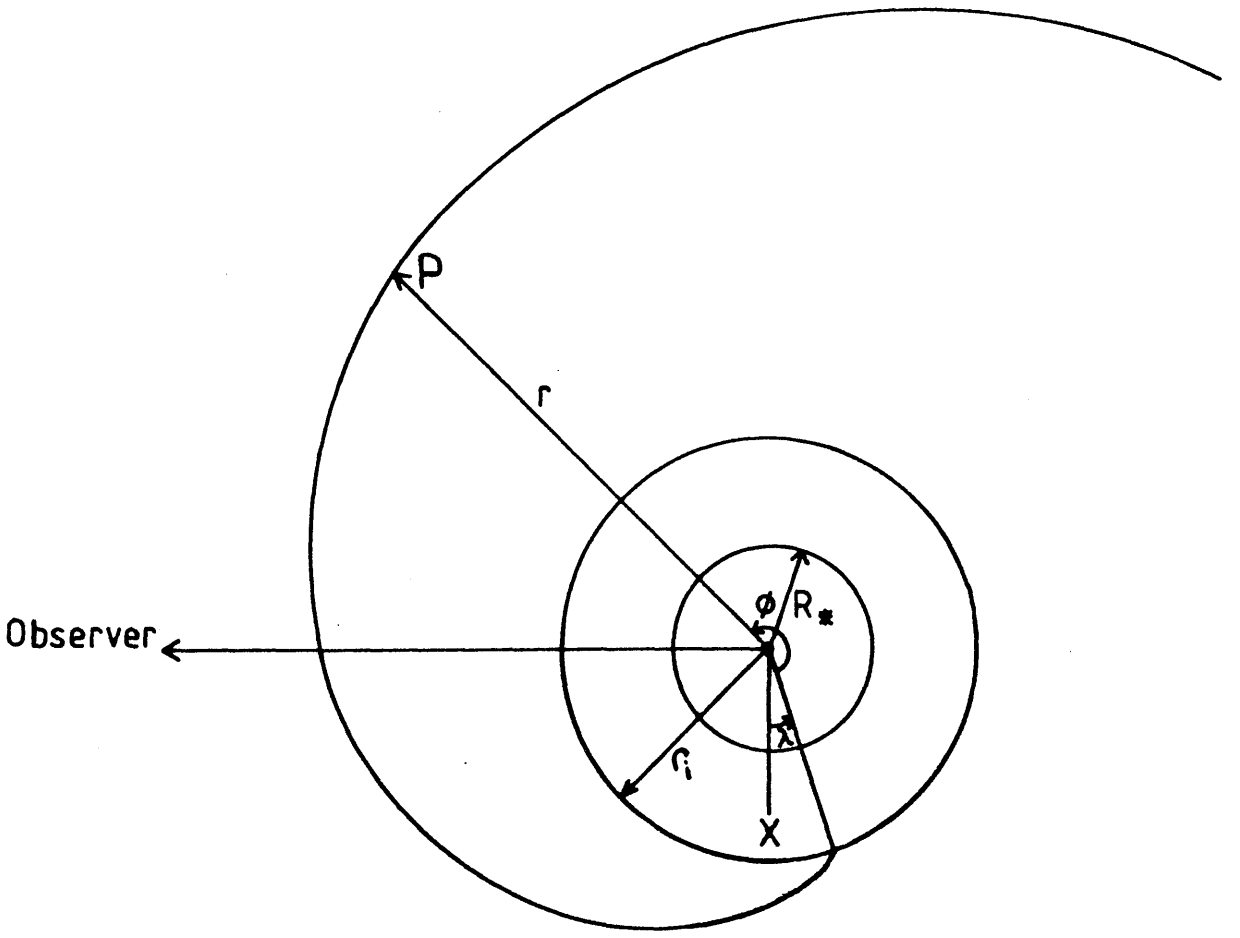

Figure 7.1

A CIR as observed in the equatorial plane of the star, viewed above the stellar rotation axis (Star rotating anticlockwise).

The CIR is an Archimedian spiral. The foot point of the CIR is at position (r_i,λ) and is the point of interaction. A general point P on the CIR has position (r,ϕ).

q_j, u_j, v_j). In order to do this however requires knowledge of the rotation period. This is gained by taking a power spectrum of the polarimetric data (see Press et al., 1986 for details). For a CIR with j streams, after a time P = T/j (T being the rotation period of the star) the CIR will look identical to that at time t = 0 (cf. Harmanec, 1989; his fig. 13) and hence duplicity occurs with a period P. The power spectrum of the polarimetric data will therefore consist of equally spaced peaks, separated by a period P. Without knowledge of T or j the only period known will be P. For a CIR we know that only the j^{th} harmonics exist and therefore in order to find the j^{th} coefficients we may (for convenience) set j = 1 and find the first order coefficients (p_1, q_1, u_1, v_1) over the time interval t = 0, P. (If we chose j arbitrarily then we would find the j^{th} harmonics but the data would be analysed over the time interval t = 0, jP and hence the coefficients would be the same.) Once the coefficients p_1, q_1, u_1 and v_1 are established it is possible, by determining the ratios p_1/q_1 ($\equiv p_j/q_j$) and v_1/u_1 ($\equiv v_j/u_j$) to estimate the ratio V_w/V_{rot} from Sec. 4.5, viz

$$\frac{1}{2}\left[\left|\frac{p_j}{q_j}\right| + \left|\frac{v_j}{u_j}\right|\right] = \tan j\left[\frac{r_j\omega}{V_w}\right] \qquad (7.5)$$

Rewriting

$$\frac{r_j\omega}{V_w} = \frac{r_j}{R_*}\,\frac{V_{rot}}{V_w}$$

then from eq. (7.3) we have the inequality

$$\frac{r_j\omega}{V_w} < \frac{V_{rot}}{V_w} + \pi \qquad (7.6)$$

Therefore

$$\frac{V_{rot}}{V_w} < \frac{1}{j}\left[\tan^{-1}\left\{\frac{1}{2}\left[\left|\frac{p_j}{q_j}\right| + \left|\frac{v_j}{u_j}\right|\right]\right\}\right] \qquad (7.7)$$

and hence the inclination of the system may be inferred from eqs

(7.1) and (7.2). Since j has not been determined then we may obtain upper limits to V_{rot}/V_w and the inclination by setting j = 1 in eq. (7.7). The rotation period of Be stars is typically of the order of 1 day (V_{rot} ~ 400 kms^{-1}, R_* ~ $10R_\odot$) and therefore the value of j maybe guessed at by j ~ Int(1/P) with P measured in days.

If, in addition to the polarimetric variations UV absorption line variations are also observed then since we have assumed that the CIR are confined to the equatorial plane, then the star is being viewed equatorially.

UV observations of Be stars show that narrow absorption lines are observed in stars with Vsini > 150 kms^{-1} and therefore some stars are clearly not being viewed equatorially. This would indicate that either CIR form throughout the wind (this is a difficult problem and has yet to be done) or some other explanation is required.

7.22 Ejected Parcels of Material.

Underhill and Fehey (1984; henceforth UF) considered the ejection of a parcel of material high above the photosphere (~ $2R_*$) of early type stars and suggested that such ejections may occur via localised magnetic dipole regions. Once the parcels are ejected, by considering the conservation of angular momentum, the trajectories can be followed (once a velocity law is prescribed). Parcels passing through the observer's line of sight and the disc of the star will appear as discrete absorption components. Parcel ejection has been criticized by Henrichs (1988) on the grounds that a parcel is required to be released at privileged times and places for the theory to correspond to observations (see Henrichs, 1988; his fig. 4.47) because for a general parcel its flightpath will be such that it will appear as a UV

discrete absorption component for only a short period of time whereas observations show them to be long lived features and as a consequence Henrichs (1988) claims the UF model to be an unlikely mechanism on the grounds that so many stars exhibit UV discrete absorption components.

According to the UF model, initially a parcel has a fixed position above the photosphere of the star (latitude θ_o, say). Polarimetrically, as the star rotates, the resulting (Q,U) loci prescribed will be the same as for an oblique rotator, with obliquity angle θ_o (Ch. 6). Once the parcel is released the polarised flux will decrease as the parcel moves away from the star ($\propto r^{-2}$ for $r >> R_*$) and consequently the (Q,U) locus will spiral into the origin. The exact way in which the (Q,U) loci will change with time will depend upon the trajectory of the parcel. Now according to the UF model, a single parcel produces the UV absorption line, consequently the parcel lies directly between the observer and the stellar disc and therefore (with a scattering angle, χ, ~ 0) the net observed polarisation of the parcel will be zero. That is there should be a lack of polarisation variability during times when UV discrete absorption components are observed and similarly a lack of UV discrete absorption when polarimetric variability is observed. To test this prediction we refer to the one and only set of polarimetric and UV correlated observations (Sonneborn et al., 1988) which has already been polarimetrically analysed by Brown and Henrichs (1987). With reference to Fig. 1 and Table 1 of Sonneborn et al. (1988) one can see that around JD 2,405,335 rapid changes in the Si IV line occured without any change in the degree of polarisation. At around JD 2,405,355 substantial polarimetric variations were observed but this time no UV changes were recorded (however, the UV data for this

period is rather sparce). The anticorrelation of these observations are exactly as predicted by the UF model. The anticorrelation of the polarimetric and UV data has also been interpreted in a different way by Brown and Henrichs (1987).

Looking more closely at the polarimetric data for ω Ori (Table 1, Sonneborn et al.) it can be seen that the polarisation is enhanced, which in order to agree with the UF model requires that the parcel is released close to the star such that initially the parcel is depolarised [$P \propto (1 - R_*^2/R^2)^{1/2}/R^2$] and as it initially moves away from the star the polarisation will increase to a maximum (at around $R = 1.2R_*$, cf. Sec. 5.4). At these close distances the speed of the parcel is $V_p \sim 0.01V_\infty$ (UF) and hence $V_p \sim 10$ kms^{-1} agreeing with the value given in Sec. 5.4 (eq. 5.27). Beyond this distance the polarisation begins to decrease ($\propto 1/R^2$ as the parcel begins to effectively see a point light source). During the period of polarimetric variation, the position angle changes by $\Delta\theta \sim 20^\circ$ consistent with the variation in position angle for parcel ejection (Bates and Halliwell, 1986) over this range in distance. Notice that prior to the polarimetric outburst the polarimetric variations do not appear to vary as one would anticipate for an obliquely rotating envelope. This is due to the fact that the data are too widely spread in time for this to be studied. To date the short term polarimetric variations (with a period of ~1 day) of ω Ori have not been studied but would clearly be of great importance for validating this interpretation of the ω Ori polarimetric data.

7.3 Conclusions.

In this thesis we have shown that the polarimetry of the X-ray transient A0538-66 indicates that when the secondary passes through

periastron the quiescent envelope around the primary is tidally disturbed. This is contrary to the Roche lobe overflow or wind accretion models that have been previously suggested (Brown and Boyle, 1984; Apparao, 1985). The spectral variability of A0538-66 during its 'on' state is similar to that of single Be stars which suggests that some mechanism akin to tidal stripping may also be working in single Be stars (Apparao et al., 1987).

It has been shown that the effects of incorporating both depolarisation and occultation into the optically thin, single (Thomson) scattering polarisation theory reduces the net theoretical polarisation by up to a factor of two compared to the point light source analysis of Brown and McLean (1977) for axisymmetric envelopes. Furthermore, the simple dependence of polarisation with inclination from the point light source treatment is found to be no longer valid when occultation is included into the scattering theory.

In order to account for the observed maximum polarisation of Be stars (~2%) it is possible, by considering geometrical models applicable to Be stars, to gain more stringent constraints upon the permitted parameter space by incorporating finite light source effects into the polarimetric theory than is possible by using the analysis of Brown and McLean (1977).

In systems in which regular polarimetric variations can be modelled in terms of a corotating density perturbation with one (predominant) light source, it has been found that by Fourier analysing the polarimetric variations the inclination of the system can be inferred from the second order harmonics and is consistent with the results of Brown et al. (1978) and Simmons (1983) even when occultation is included. This has important consequences in single stars where

knowledge of the inclination enables the equatorial rotational velocity to be estimated from the apparent rotational velocity which cannot be otherwise inferred.

We have throughout this thesis concerned ourselves with spherical light sources, which when incorporated into the single scattering theory was found to be a more important correction than occultation, though occultation itself was found not to be unimportant. For rapidly rotating stars, however, a spherical light source is only a first approximation to the shape of the stellar surface and obviously the next step would be to incorporate oblate spheriodal light sources into the analysis in order to estimate how oblate the star is required to be before the spherical light source approximation becomes inadequate. It is not at all clear what the net effect would be because the depolarisation factor will now depend on the latitude of the electron as well as its radial distance from the source. Moreover, the flux from the star itself, for an external observer, will also depend on the inclination and so the problem will become a complex one, particularly if occultation is also included.

We have illustrated to some extent the necessity for correlated spectroscopic and continuum observations in order to help distingush between different geometrical structures possible within stellar envelopes (cf. Sec. 6.5 and 7.2). Apart from joint continuum polarisation and spectral variations one could also use spectropolarimetry to study envelope geometries and geometrical changes occuring within the wind. So far, however, few such observations exist (Poeckert and Marlborough, 1978; McLean, 1979; Clarke and Brookes, 1983, 1984) and as yet no long term study has been made for any star. The lack of any such study can be attributed

to the fact that no simple theory for the theoretical wavelength dependence of polarisation across spectral lines exists. McLean (1979) attempted the problem to some extent and was able, in a qualitative way, to account for the change in polarisation (and position angle) across spectral lines. The problem could be advanced further by incorporating the Sobolev approximation (Sobolev, 1960) into McLean's analysis. The polarisation at a wavlength $\Delta\lambda$ from the line centre would then reduce to calculating the polarisation from a surface of constant apparent radial velocity. For a rotating star these surfaces are unfortunately complex (Poeckert and Marlborough, 1978; Mazzali, 1988) but it is precisely this non-spherical structure that gives rise to the observed polarisation. Such spectroscopic studies would then enable the mass flow in the stellar wind to be studied on a local scale.

One important application of spectropolarimetry could be the study of Be stars that undergo phase changes (eg. γ Cas, 88 Her, Pleione, 59 Cyg: cf Ch. 1). This would obviously need to be a long term study, but such observations could possibly pin down the changes in the density structure which appear to occur (Kogure, 1990).

References.

Abbot, D.C.: 1982, *Ap. J.*, **259**, 282

Angel, J.R.P., Landstreet, J.D.: 1970, *Ap. J.*, **160**, L47

Apparao, K.M.V.: 1985, *Ap. J.*, **292**, 257

Apparao, K.V., Antia, H.M., Chitre, S.M.:1987, *Astron. Astrophys.*, **177**, 198

Baade, D.: 1982, *Astron. Astrophys.*, **105**, 65

Baade, D.: 1984a, *Astron. Astrophys.*, **134**, 105

Baade, D.: 1984b, *Astron. Astrophys.*, **135**, 101

Baade, D.: 1987, *Physics of Be Stars*, IAU Coll. 92, p. 361 Ed. A. Slettebak and T.P. Snow (C.U.P.)

Baldwin, R.B.: 1940, *Ap. J.*, **92**, 82

Baldwin, R.B.: 1941, *Ap. J.*, **94**, 283

Balona, L.A., Englebrecht, C.A.: 1986, *Mon. Not. Roy. Astr. Soc.*, **219**, 131

Balona, L.A., Englebrecht, C.A.: 1987, *Physics of Be Stars*, IAU Coll. 92, p. 87. Ed. A. Slettebak and T.P. Snow (C.U.P.)

Balona, L.A., Englebrecht, C.A., Morang, F.: 1987, *Mon. Not. Roy. Astro. Soc.*, **227**, 123

Barker, P.K.: 1979, Ph.D Thesis (U. Colorado, Boulder). Cited within Underhill and Doazan (1982)

Barker, P.K., Brown, D.N., Bolton, C.T., Landstreet, J.D.: 1982, NASA Conf. Publ. CP-2238, p. 589

Barker, P.K., Marlborough, J.M.: 1985, *Ap. J.*, **283**, 329

Barker, P.K.: 1987, *Physics of Be Stars*, IAU Coll. 92, p. 38 Ed. A. Slettebak and T.P. Snow (C.U.P.)

Barr, J.M.: 1908, *J. Roy. Astr. Soc. Can.*, **2**, 70

Bates, B., Halliwell, H.R.: 1986, *Mon. Not. Roy. Astr. Soc.*, **223**, 673

Bocharev, N.G., Karitskaya, E.A.: 1983, *Sov. Astron. Lett.*, **9(1)**, 6

Bolton, C.T.: 1982, *Be Stars*, IAU Symp. 98, p. 181
Ed. M. Jaschek and H. -G. Groth (Reidel: Dordrecht)

Bolton, C.T., Fullerton, A.W., Bohlender, D., Landstreet, J.D.,
Geis, D.R: 1987, *Physics ofBe Stars*, IAU Coll. 92, p. 82
Ed. A. Slettebak and T.P. Snow (C.U.P.)

Bossi, M., Guerrero, G., Mantegazza, L.: 1982, *Be Stars*,
IAU Symp. 98, p. 185. Ed. M. Jaschek and H. -G. Groth.
(Reidel: Dordrecht)

Boyle, C.B.: 1984, *Ph.D Thesis*, University of Glasgow

Boyle, C.B., Walker, I.W.: 1986, *Mon. Not. Roy. Astr. Soc.*, **222**, 559

Brown, J.C., McLean, I.S.: 1977, *Astron. Astrophys.*, **57**, 141 (BM)

Brown, J.C., McLean, I.S., Emslie, A.G.: 1978, *Astron. Astrophys.*,
68, 415 (BME)

Brown, J.C., Aspin, C., Simmons, J.F.L., McLean, I.S.: 1982,
Mon. Not. Roy. Astr. Soc., **198**, 787

Brown, J.C., Boyle, C.B.: 1984, *Astron. Astrophys.*, **141**, 369

Brown, J.C., Henrichs, H.F.: 1987, *Astron. Astrophys.*, **182**, 107

Brown, J.C., Carlaw, V.A., Cassinelli, J.P.: 1989, *Ap. J.*, **344**, 341

Brown, J.C., Fox, G.K.: 1989, To appear in *Ap. J.*

Brown, J.C.: 1989, To appear in *Stellar Polarisation.*
Ed. K. Nordsieck (U. Wisconsin Press)

Carlaw, V.A.: 1988, Ph.D Thesis (Glasgow)

Carlaw, V.A., Brown, J.C.: 1988 preprint

Carovillano, R.L., Siscoe, G.L.: 1969, *Solar Physics*, **8**, 401

Cassinelli, J.P.: 1987, *Physics of Be Stars.* IAU Coll. 92., p 106
Ed. A. Slettlebak and T.P. Snow. (C.U.P.))

Cassinelli, J.P., Nordsieck, K.H., Murison, M.A.: 1987, *Ap. J.*, **315**, 290

Castor, J.I., Abbot, D.C., Klein, R.I.: 1975, *Ap. J.*, **195**, 157 (CAK)

Champeney, D.C.: 1985, *Fourier Transforms in Physics.*
(Adam Hilger)

Chandrasekhar, S.: 1950, *Radiative Transfer* (Dover)

Chandrasekhar, S., Műnch, G.: 1950, *Ap. J.*, **72**, 887

Chandrasekhar, S.: 1969, *Ellipsoidal Figures of Equilibrium* (Dover)

Charles, P.A., Booth, L., Densham, R.H., Bath, G.T.,
Thorstensen, J.R., Howarth, I.D., Willis, A.J., Skinner, G.K.
Olszewski, E.: 1983, *Mon. Not. Roy. Astr. Soc.*, **202**, 657

Clarke, D., Wyllie, T.H.A.: 1977, *Observatory*, **97**, No. 1016, p. 21

Clarke, D., Brookes, A.: 1983, *Mon. Not. Roy. Astr. Soc.*, **205**, 9p

Clarke, D., Brookes, A.: 1984, *Mon. Not. Roy. Astr. Soc.*, **211**, 737

Clarke, D., McGale, P.A.: 1986, *Astron. Astrophys.*, **169**, 251

Clarke, D., McGale, P.A.: 1987, *Astron. Astrophys.*, **178**, 294

Clarke, D., McGale, P.A.: 1988a, *Astron. Astrophys.*, **190**, 93

Clarke, D., McGale, P.A.: 1988b, *Astron. Astrophys.*, **205**, 207

Clarke, D.: 1990 *To appear in Astron. Astrophys.*

Clayton, G.C., Thompson, I.B.: 1982, *Ap. J.*, **254**, L7 (CT)

Collins, G.W.: 1987, *Physics of Be Stars.* IAU Coll. 92, p 3
Ed. A. Slettebak and T.P. Snow (C.U.P.)

Collins, G.W.: 1989, To appear in *Stellar Polarisation.*
Ed. K. Nordsieck (U. Wisconsin Press)

Corbet, R.H.D., Mason, K.O., Cordova, F.A., Branduardi-Raymont, G.
Parmer, A.N.: 1984, *Mon. Not. Roy. Astr. Soc.*, **212**, 565

Coté, J., Waters, L.B.F.M.: 1987, *Astron. Astrophys.*, **176**, 93

Cowley, A.P., Marlborough, J.M.: 1968, *Publ. Astron. Soc. Pac.*, **80**, 42

Cowley, A.P., Gugula, R.: 1973, *Astron. Astrophys.*, **22**, 203

Cowley, A.P., Rogers, L., Hutchings, J.B.: 1976, *Publ. Astron. Soc. Pac.*, **88**, 911

Coyne, G.V., Gehrels, T.: 1967, *Astron. J.*, **72**, 887

Coyne, G.V.: 1976, *Be and Shell Stars*, IAU Symp. 70, p. 233 Ed. A. Slettebak (Reidel: Dordrecht)

Craig, I.J.D., Brown, J.C.: 1986, *Inverse Problems in Astronomy.* (Adam Hilger).

Dachs, J, Hanuschik, R., Kaiser, D., Rohe, D.: 1986, *Astron. Astrophys.* **159**, 276

Daniel, J.Y.: 1980, *Astron. Astrophys.*, **86**, 198

Densham, R.H., Charles, P.A., Menzies, J.W., van der Klis, M. van Paradijs, J.: 1983, *Mon. Not. Roy. Astr. Soc.*, **205**, 1117

Doazan, V.: 1965, *Ann. Astrophys.*, **28**, 1

Doazan, V., Peton, A.: 1970, *Astron. Astrophys.*, **9**, 245

Doazan, V., Kuhi, L.V., Thomas, R.N.: 1980a, *Ap. J.*, **235**, L20

Doazan, V., Kuhi, L.V., Marlborough, J.M., Snow, T.P., Thomas, R.N.: 1980b, *2nd IAU European Conference*, p. 151. ESA-SP157

Doazan, V., Thomas, R.N.: 1982, *B Stars with and without Emission Lines*, Ch. 13. Ed. A. Underhill and V. Doazan (DT)

Doazan, V., Grady, C., Snow, T.P., Peters, G.J., Marlborough, J.M., Barker, P.K., Bolton, C.T., Bourdonneau, B., Kuhi, L.V., Lyons, R.N., Polidan, P.S., Stalio, R., Thomas, R.N.: 1985 *Astron. Astrophys.*, **152**, 182

Doazan, V., Thomas, R.N., Barylak, M.: 1986, *Astron. Astrophys.*, **159**, 75

Doazan, V.: 1987, *Physics of Be Stars*, IAU Coll. 92, p. 384
Ed. A. Slettebak and T.P. Snow (C.U.P.)

Dolan, J.F.: 1984, *Astron. Astrophys.*, **138**, 1

Dolan, J.F., Tapia, S.: 1984, *Astron. Astrophys.*, **139**, 249

Dolan, J.F., Tapia, S.: 1989, *Ap. J.*, **334**, 830

Dolginov, A.Z., Silant'ev, N.A.: 1974, *Soviet. Astron.*, **18(3)**, 289

Drissen, L., Lamontagne, R., Moffat, A.F.J., Bastien, P., Seguin, M.:
1986a, *Ap. J.*, **304**, 188

Drissen, L., Moffat, A.F.J., Bastien, P., Lamontagne, R.:
1986b, *Ap. J.*, **306**, 215

Durrant, C.J.: 1988, *The Atmosphere of the Sun* (C.U.P)

Edwards, D.L.: 1956, *Vistas in Astronomy*, **2**, 1470

Elvey, C.T.: 1930, *Ap. J.* , **71**, 221

Finsen, W.S., Worley, C.E.: 1970, *Republic Obs. Johannesburg Circ.*
129(7), 203

Friend, D.B., McGregor, K.B.: 1984, *Ap. J.*, **282**, 591

Friend, D.B., Cassinelli, J.P.: 1986, *Ap. J.*, **303**, 292

Granes, P., Thom, C. Vakali, F.: 1987, *Physics of Be Stars*,
IAU Coll. 92, p. 66. Ed. A. Slettebak T.P. Snow (C.U.P.)

Green, R.M.: 1985, *Spherical Astronomy* (C.U.P.)

Groote, D., Hunger, K.: 1982, *Astron. Astrophys.*, **116**, 64

Gulliver, A.F.: 1977, *Ap. J. Suppl.*, **35**, 441

Harmanec, P.: 1984, *Bull. Astron. Inst. Czech.*, **35**, 193

Harmanec, P.: 1989, *Bull. Astron. Inst. Czech.*, **40**, 201

Haisch, B.M., Cassinelli, J.P.: 1976, *Ap. J.*, **208**, 253

Hammerschlag-Hensberge, G.: 1979, *IAU Circ.*, 3391. Cited within
Henrichs, 1988

Hayes, D.P., Guinan, E.F.: 1984, *Ap. J.*, **279**, 721

Hearn, A.G.: 1975, *Astron. Astrophys.*, **40**, 355

Hearn, A.G. : 1988, *Circumstellar Matter*, IAU Symp. 122, p. 395
Ed. I. Appenzeller and C. Jordan (Reidel: Dordrecht)

Heintz, W.D.: 1978, *Double Stars* (Reidel: Dordrecht)

Henrichs, H.F., Hammerschlag-Hensberge, G., Lamers, H.J.G.L.M.:
1980, *2nd European Conference*, p. 147. ESA-SP157

Henrichs, H.F.: 1982, *Be Stars*, p. 431. Ed. M. Jaschek
and H. -G. Groth (Reidel: Dordrecht)

Henrichs, H.F.: 1988, *O Stars and Wolf-Rayet Stars*, Sec. 4.5.
Ed. P.S. Conti and A.B. Underhill, NASA SP-497

Hofmeister, E., Kippenhahn, R., Weigert, A.: 1964, *Z. Astrophys*,
59, 242

Holtzer, T.E.: 1988, *Circumstellar Matter*, IAU Symp. 122, p. 289
Ed. I. Appenzeller and C. Jordan (Reidel: Dordrecht)

Huang, S.S.: 1972, *Ap. J.*, **171**, 549

Huang, S.S.: 1973, *Ap. J.*, **183**, 541

Huang, S.S.: 1977, *Ap. J.*, **212**, 123

Hummer, D.G., Kunasz, C.V., Kunasz, P.B.: 1973, *Computer Physics
Communications*, **6**, 38

Hundhausen, A.J.: 1973, *J. Geophys. Res.*, **78**, 1528

Huovelin, J., Piirola, V., Vilho, O., Efimov, Y.S., Shakovskoy, N.M.:
1987, *Astron. Astrophys.*, **176**, 83

Hutchings, J.B.: 1976, *Be and Shell Stars*, IAU Symp. 70, p. 13
Ed. A. Slettebak (Reidel: Dordrecht)

Hutchings, J.B., Crampton, D., Cowley, A.P., Olszewski, E.,
Thompson, I.B., Suntzeff, N.: 1985, *Pub. Astr. Soc. Pac.*,
94, 417

Icke, V.: 1976, *Structure and Evolution of Close Binary Stars*, IAU Symp. 73, p. 267. Ed. P. Eggleton, S. Mitten and J. Whelan (Reidel: Dordrecht)

Johnston, M.D., Bradt, H.V, Doxsey, R.E., Griffiths, R.E., Schwartz, D.A., Schwartz, J.: 1979, *Ap. J.*, **230**, L11

Kalkofen, W.: 1987, *Numerical Radiative Transfer* (C.U.P.)

Karitskaya, E.A.: 1981, *Sov. Astron.*, **25**, 8

Karitskaya, E.A., Bocharev, N.G.: 1983, *Sov. Astron.*, **27**, 546

Kemp, J.C., Herman, L.C.: 1977, *Ap. J.*, **218**, 770

Kemp, J.C., Barbour, M.S., Herman, L.C., Rudy, R.J.: 1978, *Ap. J.*, **220**, L123

Kemp, J.C., Barbour, M.S., Parker, T.E., Herman, L.C.: 1979, *Ap. J.*, **228**, L23

Kemp, J.C.: 1980, *Ap. J.*, **253**, 592

Kopal, Z.: 1959, *Close Binary Systems* (Chapman and Hall: London)

Kogure, T.: 1990, *Astrophys. Space Sci.*, **163**, 7

Krautter, J., Bastian, U.: 1980, *Astron. Astrophys.*, **88**, L6

Kříž, S., Harmanec, P.: 1975, *Bull. A. Inst. Czech.*, **26**, 65

Lacy, C.H.: 1976, *Ap. J.*, **212**, 132

Lamers, H., J., G., L., M., Rogerson, J.B.: 1978, *Astron. Astrophys.* **66**, 417

Landstreet, J.D., Borra, E.F.: 1978, *Ap. J.*, **224**, L5

Limber, D.N.: 1964, *Ap. J.*, **140**, 139

Limber, D.N.: 1967, *Ap. J.*, **148**, 141

Limber, D.N.: 1969, *Ap. J.*, **157**, 785

Lucy, L.B.: 1982, *Ap. J.*, **255**, 286

Maheswaren, M., Cassinelli, J.P.: 1988, *Ap. J.*, **335**, 931

Marlborough, J.M.: 1977a, *Ap. J.*, **216**, 446

Marlborough, J.M.: 1977b, *Publ. Astron. Soc. Pac.*, **89**, 122

Marlborough, J.M., Snow, T.P., Slettebak, A.: 1978, *Ap. J.*, **224**, 157

Mazzali,P.A.: 1088, *10th IUE Meeting* GSFC, Greenbelt

McGale, P.A.: 1988, *Ph.D Thesis* (Glasgow)

McGregor, K.B., Friend, D.B.: 1987, *Ap. J.*, **312**, 659

McLean, I.S., Brown, J.C.,: 1978, *Astron. Astrophys.*, **69**, 291

McLean, I.S.: 1979, *Mon. Not. Roy. Astr. Soc.*, **186**, 265

Mihalas, D.: 1972, *Non- LTE Model Atmospheres for B and O stars.* NCAR -TN/STR-76

Milgrom, M.: 1978, *Astron. Astropyhs.*, **65**, L1

Morton, D.C.: 1976, *Ap. J.*, **203**, 386

Mullan, D.J.: 1984, *Ap. J.*, **283**, 303

Neugebauer, M., Snyder, C.W.: 1967, *J. Geophys. Res.*, **72**, 1823

Pauldrach, A., Puls, J., Kudritzki, R.P.: 1986, *Astron, Astrophys.*, **164**, 86

Persi, P., Ferrari-Toniolo, M.: 1982, *Be stars*, IAU Symp. **98**, p. 247 Ed. M. Jaschek and H.-G. Groth (Reidel: Dordrecht)

Peters, G.J.: 1982, *Be Stars*, IAU Symp. 98, p. 353, Ed. M. Jaschek and H.-G. Groth (Reidel: Dordrecht)

Pfeiffer, R.J., Koch, R.H.: 1988, *Astron. J.*, **94**, 484

Pizzo, V.: 1978, *J. Geophys. Res.*, **83**, 5563

Pizzo, V.: 1980, *J. Geophys. Res.*, **85**, 727

Pizzo, V.: 1982, *J. Geophys. Res.*, **87**, 4374

Poe, C.H., Friend, D.B., Cassinelli, J.P.: 1988, preprint

Poe, C.H., Friend, D.B.: 1986, *Ap. J.*, **311**, 591

Poeckert, R., Marlborough, J.M.: 1976, *Ap. J.*, **206**, 182

Poeckert, R., Marlborough, J.M.: 1977, *Ap. J.*, **218**, 220

Poeckert, R., Marlborough, J.M.: 1978a, *Ap. J.*, **220**, 940

Poeckert, R., Marlborough, J.M.: 1978b, *Ap. J. Suppl.*, **38**, 229

Press, W.H., Flannery, B.P., Teukolsky, S.A., Vetterling, W.T.: 1986, *Numerical Recipes*, (C.U.P.)

Prinja, R.K., Howarth, I.D.: 1988, *Mon. Roy. Astr. Soc.*, **233**, 123

Rudy, R.J., Kemp, J.C.: 1976, *Ap. J.*, **207**, L125

Rudy, R.J., Kemp, J.C.: 1977, *Ap. J.*, **216**, 767

Rudy, R.J., Kemp, J.C.: 1978, *Ap. J.*, **221**, 220

St. Louis, N., Moffat, A.F.J., Drissen, L., Bastien, P., Robert, C.: 1988, *Ap. J.*, **330**, 286

Sareyan, J.P., Alvarez, M., Chauville, J., Le Contel, J.M., Michel, R. Ballereau, D.: 1987, *Physics of Be Stars*, IAU Coll. 92, p.78 Ed. A. Slettebak and T.P. Snow (C.U.P.)

Schild, R.: 1978, *Ap. J. Suppl.*, **37**, 77

Schild, R.: 1983, *Astron. Astrophys.* **120**, 22

Secchi, A.: 1867, *Astron. Nachr.*, **68**, 63

Serkowski, K.: 1973, *Methods of Experimental Physics, Vol. 12: Astrophysics, Part A.* Eds M.L. Meeks and N.P Carleton (Academic Press, New York)

Serkowski, K., Mathewson, D.S., Ford, V.L.: 1975, *Astron. Astrophys.* **134**, 368

Shajn, G., Struve, O.: 1929, *Mon. Not. Roy. Astro. Soc.*, **89**, 222

Shakhovskoi, N.M.: 1963, *Soviet Astron.*, AJ **7**, 806

Shakhovskoi, N.M.: 1965, *Soviet Astron.*, AJ **8**, 833

Simmons, J.F.L., Aspin, C., Brown, J.C.: 1980, *Astron. Astrophys.*, **91**, 97

Simmons, J.F.L.: 1982, *Mon. Not. Roy. Astr. Soc.*, **200**, 91

Simmons, J.F.L.: 1983, *Mon. Not. Roy. Astr. Soc.*, **205**, 153

Simmons, J.F.L., Boyle, C.B.: 1984, *Astron. Astrophys.*, **134**, 368 (SB)

Simmons, J.F.L., Stewart, B.G.: 1985, *Astron. Astrophys.*, **142**, 100

Siscoe, G.L., Finley, L.T.: 1970, *J. Geophys. Res.*, **75**, 1817

Skinner, G.K.: 1980, *Nature*, **288**, 141

Skinner, G.K.: 1981, *Space Sci. Rev.*, **30**, 441

Skinner, G.K., Bedford, D.K., Elsner, R.F., Leahy, D.,
Weisskopf, M.C., Grindlay, J.: 1982, *Nature*, **297**, 568

Smale, A.P., Charles, P.A., Densham, R.H., Bath., G.T.,
van Paradijis, J., Menzies, J.W., Skinner, G.K.,1984,
Mon. Not. Roy. Astr. Soc., **210**, 855

Slettebak, A.: 1976, *Be and Shell Stars*, IAU Symp. 70, p 123
Ed. A. Slettebak (Reidel: Dordrecht)

Slettebak, A., Snow, T.P.: 1978, *Ap. J. (Letters)*, **224**, L 127

Slettebak, A.: 1982, *Be Stars*, IAU Symp. 98, p. 109
Ed. M. Jaschek and H. -G. Groth (Reidel: Dordrecht)

Slettebak, A.: 1985, *Ap. J. Suppl.*, **59**, 769

Slettebak, A., 1988, *Pub. Astron. Pac. Soc.*, **100**, 770

Smale, A.P., Charles, P.A., Densham, R.H., Bath., G.T.,
van Paradijis, J., Menzies, J.W., Skinner, G.K.,1984,
Mon. Not. Roy. Astr. Soc., **210**, 855

Smith, A.M.: 1972, *Ap. J.*, **176**, 405

Sneddon, I.N.: 1972, *The Use of Integral Transforms*. (McGraw-Hill)

Snow, T.P., Marlborough, J.M.: 1976, *Ap. J.*, **203**, L87

Snow, T.P., Marlborough, J.M.: 1980, *Ap. J.*, **235**, 269

Snow, T.P.: 1982, *Be Stars*, IAU Symp. 98, p. 109
Ed. M. Jaschek and H. -G. Groth (Reidel: Dordrecht)

Sobolev, V.V.: 1960, *Moving Envelopes of Stars*;
Translated by S. Goposchkin (Cambridge, Mass. U. Press)

Sonneborn, G., Grady, C.A., Wu, Ch.-Ch., Hayes, D.P., Guinan, E.F.,

Barker, P.K., Henrichs, H.F.: 1988, *Ap. J.*, **325**, 784

Stagg, C.R., 1987, *Physics of Be Stars*, IAU Coll. 92, p. 91
Ed. A. Slettebak and T.P Snow (C.U.P.)

Strassmeier, K.G.: 1988, *Astrophys. Space Sci.*, **140**, 223

Struve, O.: 1930, *Ap. J.*, **72**, 1

Struve, O.: 1931, *Ap. J.*, **73**, 94

Struve, O.: 1942, *Ap. J.*, **95**, 134

Suess, S.T.: 1972, *J. Geophys. Res.*, **77**, 567

Suess, S.T., Hundhausen, A.J., Pizzo, V.: 1975, *J Geophys. Res.*, **80**, 2023

Swings, J.P.: 1981, *Ap. J.*, **98**, 112

Thompson, I.B., Landstreet, J.D.: 1985, *Ap. J. (Letters)*, **289**, L9

Underhill, A.B.: 1975, *Ap. J.*, **199**, 691

Underhill, A.B., Doazan, V. (Eds.): 1982, *B Stars with and without Emission Lines*, NASA SP-456

Underhill, A.B., Fehey, R.P.: 1984, *Ap. J.*, **280**, 712 (UF)

Vaiana, G.S., Sciortino, S.: 1987, *Circumstellar Matter*,
IAU Symp. 122, p. 333. Ed. I. Appenzeller and C. Jordan
(Reidel: Dordrecht)

Van Paradijs, J., van Amerongen, S., de Kool, M., Deul, E.R.,
Lub, J., Greve, A.: 1984, *Mon. Not. Roy. Astr. Soc.*, **210**, 863

Voigt, H.H.: 1974, *Outline in Astronomy, Vol. 2* (Noordhoff: Leyden)

Wakerling, L.R.: 1970, *Mem. Roy. Astron. Soc.*, **73**, 153 (cited within
Underhill and Doazan, 1982)

Waldron, W.L.: 1984, *Ap. J.*, **282**, 256

Warren, W.H.: 1976, *Mon. Not. Roy. Astr. Soc.*, **174**, 111

Waters, L.B.F.M.: 1986, *Astron. Astrophys.*, **162**, 121

Waters, L.B.F.M.: 1987, *Ph.D Thesis* (Utrecht) Ch 7

Waters, L.B.F.M., Coté, J., Aumann, H.H.: 1987, *Astron. Astrophys.*, **172**, 225

White, N.E., Carpenter, G.F.: 1978, *Mon. Not. Roy. Astr. Soc.*, **183**, 11

Appendix A.

A.1 Structure of Two Dimensional Envelopes.

By use of equation (3.4) we permit $\Omega = \Omega_0 f(x,\theta)$ to be distributed in θ as well as x, but we still adopt the corotation condition $f(x,\theta,t) = f_0(x,\theta-\omega t)$, where $f_0(x,\theta_0)$ is $\Omega(x,\theta_0)/\Omega_0$ with θ_0 measured in a frame rotating with the envelope from a reference axis which coincides with that of θ when $t = 0$. We consider the extent to which properties of f_0 can be obtained from observations of P(t), but we shall defer model calculations to a subsequent paper.

A.1(a) $f_0(x,\theta)$ Separable with Known x-Dependence.

In this restricted case we suppose

$$f_0(x,\theta_0) = h_0(\theta_0)g_0(x) \qquad \text{(A1)}$$

where $g_0(x)$ is known but $h_0(\theta_0)$ is not. This would be the case for example for a corotating equatorial wind of known velocity profile, the same in all directions but the wind density ($\sim h_0$) varying with direction.

We proceed in this case by Fourier analysis of $h_0(\theta_0)$ via

$$h_0(\theta_0) = a_0 + \sum_{j=1}^{\infty} \{ a_j \cos j\theta_0 + b_j \sin j\theta_0 \} \qquad \text{(A2)}$$

and writing $\cos j\theta_0 = \cos j\theta \cos j\omega t + \sin j\theta \sin j\omega t$ etc.

Then inserting (A1) with (A2) into (3.5) and using the orthogonality conditions,

$$\int_0^{2\pi} \cos j\theta \cos k\theta \, d\theta = 0 \quad \text{unless } j=k$$

$$\int_0^{2\pi} \cos j\theta \sin k\theta \, d\theta = 0 \quad \text{for all } j \text{ and } k \qquad \text{(A3)}$$

we obtain after some reduction, a Fourier series for P as a function of $\theta = wt$, viz

$$\frac{2\,P(\theta)}{\Omega_o \sigma_o} = p_o + \sum_{j=1}^{\infty} \{ p_j \cos j\theta + q_j \sin j\theta \} \tag{A4}$$

with

$$p_o = a_o(2\pi I - J_o) \tag{A5}$$

$$\left.\begin{aligned} p_2 &= a_2(\pi I - J_2) \\ q_2 &= -b_2(\pi I - J_2) \end{aligned}\right\} \tag{A6}$$

$$\left.\begin{aligned} p_j &= -a_j J_j \\ q_j &= b_j J_j \end{aligned}\right\} \quad \text{for even } j \ (j \neq 2) \tag{A7}$$

$$\left.\begin{aligned} p_j &= -b_j K_j \\ q_j &= -a_j K_j \end{aligned}\right\} \quad \text{for odd } j \tag{A8}$$

where

$$I = \int_1^{\infty} g_o(x) \frac{(x^2 - 1)^{1/2}}{x^2}\, dx \tag{A9}$$

$$J_j = \int_1^{\infty} \int_{\sec^{-1}x}^{\pi - \sec^{-1}x} g_o(x) \frac{(x^2 - 1)^{1/2}}{x^2} (1 + \cos 2\theta) \cos j\theta \, d\theta \, dx \tag{A10}$$

$$K_j = \int_1^{\infty} \int_{\sec^{-1}x}^{\pi - \sec^{-1}x} g_o(x) \frac{(x^2 - 1)^{1/2}}{x^2} (1 + \cos 2\theta) \sin j\theta \, d\theta \, dx \tag{A11}$$

J_j and K_j can be simplified by integrating with respect to θ, viz

$$J_o = \pi I - \int_1^{\infty} g_o(x) \frac{(x^2 - 1)^{1/2}}{x^2} \left\{ 2\cos^{-1}(1/x) + S_2(1/x) \right\} dx \tag{A12}$$

$$J_2 = -\int_1^\infty g_o(x)\,\frac{(x^2-1)^{\frac{1}{2}}}{x^2}\left\{\cos^{-1}(1/x) - \frac{\pi}{2} + S_2(1/x) + \frac{S_4(1/x)}{4}\right\} dx \qquad (A13)$$

$$J_j = -\int_1^\infty g_o(x)\,\frac{(x^2-1)^{\frac{1}{2}}}{x^2}\left\{\frac{2S_j(1/x)}{j} + \frac{S_{j-2}(1/x)}{j-2} + \frac{S_{j+2}(1/x)}{j+2}\right\} dx \qquad (A14)$$

for even j $(j\neq 2)$

$$J_j = 0 \qquad \text{for odd } j \qquad (A15)$$

$$K_j = \int_1^\infty g_o(x)\,\frac{(x^2-1)^{\frac{1}{2}}}{x^2}\left\{\frac{2T_j(1/x)}{j} + \frac{T_{j-2}(1/x)}{j-2} + \frac{T_{j+2}(1/x)}{j+2}\right\} dx \qquad (A16)$$

for odd j

$$K_j = 0 \qquad \text{for even } j \qquad (A17)$$

where $T_j(1/x) = \cos(j\cos^{-1}(1/x))$ are the Chebychev polynomials and $S_j(1/x) = \sin(j\cos^{-1}(1/x))$.

Equations (A5)-(A8) can be inverted explicitly to obtain the Fourier coefficients of the envelope θ_o distribution in terms of the Fourier coefficients of the observed polarisation $P(\theta)$ viz

$$a_o = p_o/(2\pi I - J_o) \qquad (A18)$$

$$\left.\begin{aligned} a_2 &= p_2/(\pi I - J_2) \\ b_2 &= -q_2/(\pi I - J_2) \end{aligned}\right\} \qquad (A19)$$

$$\left.\begin{aligned} a_j &= -p_j/J_j \\ b_j &= q_j/J_j \end{aligned}\right\} \text{ for even } j\ (j\neq 2) \qquad (A20)$$

$$\left.\begin{aligned} a_j &= -q_j/K_j \\ b_j &= -p_j/K_j \end{aligned}\right\} \text{ for odd } j \qquad (A21)$$

I, J_j and K_j are computed from (A9)-(A11) (or from (A9) and (A12)-(A17)) for the known function $g_o(x)$. As examples we show in Fig. A.1a, b these integrals as functions of n for the form $g_o(x) = x^{-n}$ used

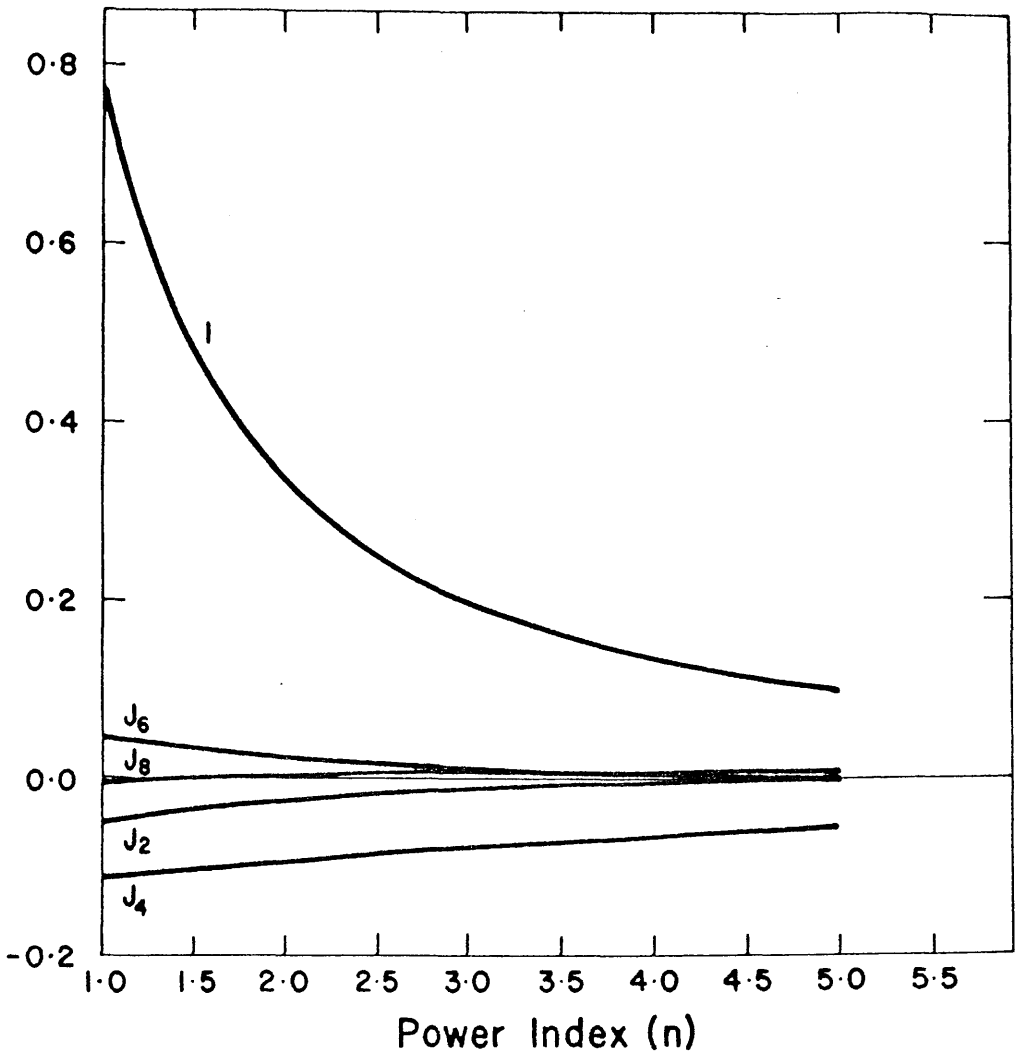

Figure A.1a

Integral moments I and J_j (for the first eight harmonics) shown as functions of the power index (n).

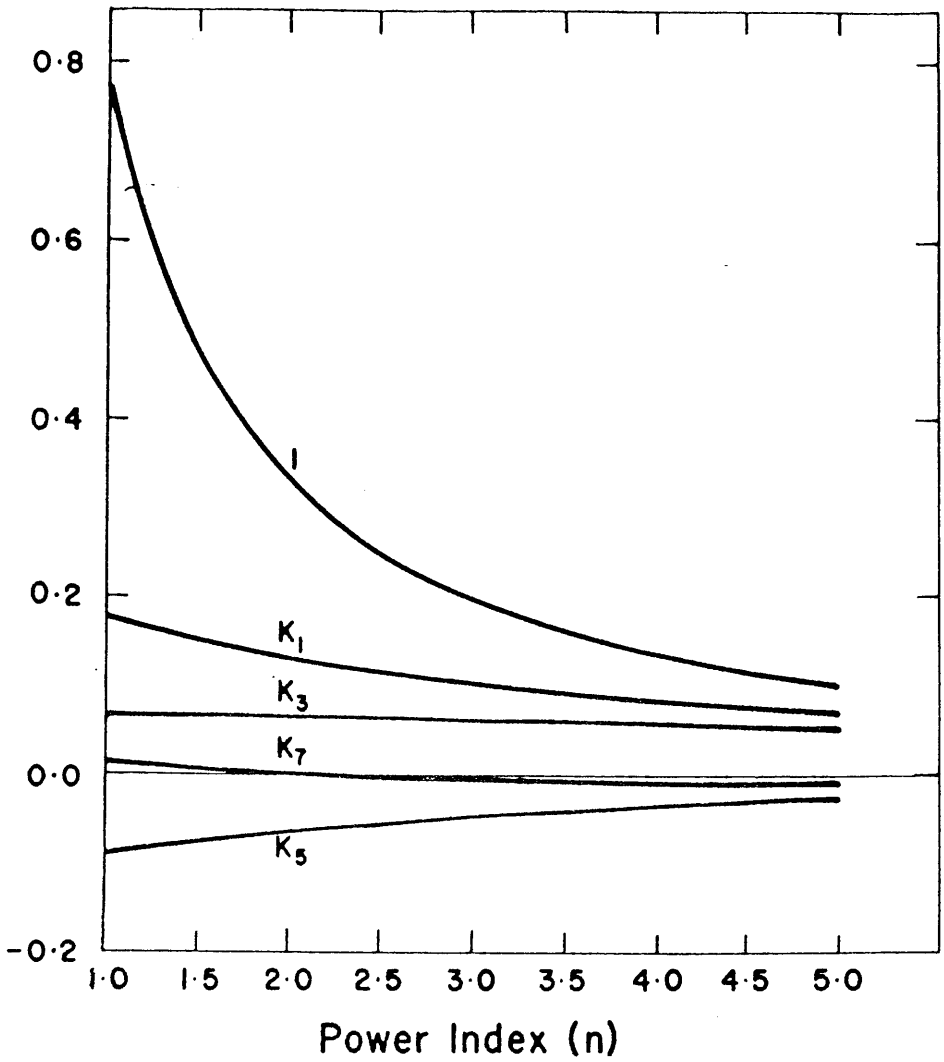

Figure A.1b

Integral moments I and K_j (for the first eight harmonics) shown as functions of the power index (n).

earlier for the first eight harmonics, which is above the maximum likely to be achievable in a meaningful fit to any polarimetric data. (In fact for integer n these integrals can be expressed in analytic form but are cumbersome and direct numerical computation is as convenient).

A.1(b) <u>General $f_o(x,\theta_o)$</u>.

In this case we again Fourier analyse $f_o(x,\theta_o)$ over θ_o but at each x, i.e

$$f_o(x,\theta_o) = a_o + \sum_{j=1}^{\infty} \{ a_j(x)\cos j\theta_o + b_j(x)\sin j\theta_o \} \qquad (A22)$$

where a_j, b_j now depend on x. Following the same proceedure as in case 4.3(a) we derive relations between a_j, b_j and the Fourier coefficients p_j, q_j of $P(\theta)$. This time however, these relations only enable us to derive a set of weighted integral moments of the $a_j(x)$, $b_j(x)$ functions from their relations to p_j,q_j namely

$$p_o = 2\pi I_{a_o} - A_o \qquad (A23)$$

$$\left.\begin{aligned} p_2 &= \pi I_{a_2} - A_2 \\ q_2 &= -\pi I_{b_2} + B_2 \end{aligned}\right\} \qquad (A24)$$

$$\left.\begin{aligned} p_j &= -A_j \\ q_j &= B_j \end{aligned}\right\} \quad \text{for even } j \ (j\neq 2) \qquad (A25)$$

$$\left.\begin{aligned} p_j &= -\tilde{B}_j \\ q_j &= -\tilde{A}_j \end{aligned}\right\} \quad \text{for odd } j \qquad (A26)$$

Again we have integrated the moment integrals with respect to θ to obtain,

$$I_{a_j} = \int_1^\infty a_j(x) \frac{(x^2 - 1)^{1/2}}{x^2} dx \tag{A27}$$

$$I_{b_j} = \int_1^\infty b_j(x) \frac{(x^2 - 1)^{1/2}}{x^2} dx \tag{A28}$$

$$A_o = \pi I_{a_o} - \int_1^\infty a_o(x) \frac{(x^2 - 1)^{1/2}}{x^2} \left\{2\cos^{-1}(1/x) + S_2(1/x)\right\} dx \tag{A29}$$

$$B_o = \pi I_{b_o} - \int_1^\infty b_o(x) \frac{(x^2 - 1)^{1/2}}{x^2} \left\{2\cos^{-1}(1/x) + S_2(1/x)\right\} dx \tag{A30}$$

$$A_2 = -\int_1^\infty a_2(x) \frac{(x^2 - 1)^{1/2}}{x^2} \left\{\cos^{-1}(1/x) - \frac{\pi}{2} + S_2(1/x) + \frac{S_4(1/x)}{4}\right\} dx \tag{A31}$$

$$B_2 = -\int_1^\infty b_2(x) \frac{(x^2 - 1)^{1/2}}{x^2} \left\{\cos^{-1}(1/x) - \frac{\pi}{2} + S_2(1/x) + \frac{S_4(1/x)}{4}\right\} dx \tag{A32}$$

$$\left.\begin{aligned} A_j &= -\int_1^\infty a_j(x) \frac{(x^2 - 1)^{1/2}}{x^2} \left\{\frac{2S_j(1/x)}{j} + \frac{S_{j-2}(1/x)}{j-2} + \frac{S_{j+2}(1/x)}{j+2}\right\} dx \\ B_j &= -\int_1^\infty b_j(x) \frac{(x^2 - 1)^{1/2}}{x^2} \left\{\frac{2S_j(1/x)}{j} + \frac{S_{j-2}(1/x)}{j-2} + \frac{S_{j+2}(1/x)}{j+2}\right\} dx \end{aligned}\right\} \tag{A33}$$

for even j ($j \neq 2$)

$$\left.\begin{aligned} A_j &= 0 \\ B_j &= 0 \end{aligned}\right\} \text{ for odd } j \tag{A34}$$

$$\left.\begin{aligned} \tilde{A}_j &= \int_1^\infty a_j(x) \frac{(x^2 - 1)^{1/2}}{x^2} \left\{\frac{2T_j(1/x)}{j} + \frac{T_{j-2}(1/x)}{j-2} + \frac{T_{j+2}(1/x)}{j+2}\right\} dx \\ \tilde{B}_j &= \int_1^\infty b_j(x) \frac{(x^2 - 1)^{1/2}}{x^2} \left\{\frac{2T_j(1/x)}{j} + \frac{T_{j-2}(1/x)}{j-2} + \frac{T_{j+2}(1/x)}{j+2}\right\} dx \end{aligned}\right\} \tag{A35}$$

for odd j

$$\left.\begin{aligned} \tilde{A}_j &= 0 \\ \tilde{B}_j &= 0 \end{aligned}\right\} \text{ for even } j \tag{A36}$$

Thus A_j, B_j, $\tilde{A}_j$ and $\tilde{B}_j$ can again be found directly from p_j and q_j .

Appendix B.

B.1.1 Spherical Shell of Arbitrary Density.

In order to calculate the net polarisation for a shell it is easier to calculate the weighted integral moments in two different regimes

(a) $X \leqslant \text{coseci}$ (polar region of the shell is occulted) then the integral moments are

$$\tau_o = 2\pi\sigma_o\Omega_o\frac{1}{\beta}\,(1 - X^{-2})^{\frac{1}{2}}\left[1 - \frac{e^{-\beta}}{2} - \frac{1}{4\pi}\int_o^{2\pi}\exp\{-\beta\mu_o(\phi)\}\,d\phi\right] \qquad \text{(B1)}$$

$$\tau_o\gamma_o = 2\pi\sigma_o\Omega_o\frac{1}{\beta}\,(1 - X^{-2})^{\frac{1}{2}}\left[\frac{2}{\beta^2} - \frac{e^{-\beta}}{2}\left[1 + \frac{2}{\beta} + \frac{2}{\beta^2}\right]\right. \qquad \text{(B2)}$$

$$\left. - \frac{1}{4\pi}\int_o^{2\pi}\exp\{-\beta\mu_o(\phi)\}\left[\mu_o^2 + \frac{2\mu_o}{\beta} + \frac{2}{\beta^2}\right]d\phi\right]$$

$$\tau_o\gamma_2 = 2\pi\sigma_o\Omega_o\frac{1}{\beta}\,(1 - X^{-2})^{\frac{1}{2}}\left[\frac{\beta}{2\pi}\int_o^{2\pi}\int_{\mu_o}^{1}\mu\,(1 - \mu^{-2})^{\frac{1}{2}}\exp\{-\beta|\mu|\}\,\sin\phi\,d\mu d\phi\right] \qquad \text{(B3)}$$

$$\tau_o\gamma_3 = 2\pi\sigma_o\Omega_o\frac{1}{\beta}\,(1 - X^{-2})^{\frac{1}{2}}\left[\frac{1}{4\pi}\int_o^{2\pi}\exp\{-\beta\mu_o(\phi)\}\left[\mu_o^2 + \frac{2\mu_o}{\beta} + \frac{2}{\beta^2} - 1\right]\cos 2\phi\,d\phi\right] \qquad \text{(B4)}$$

where

$$\mu_o = \frac{(1 - X^{-2})^{\frac{1}{2}}\cos i - \sin i\,\sin\phi(1 - X^{-2} - \sin^2 i\,\cos^2\phi)^{\frac{1}{2}}}{1 - \sin^2 i\,\cos^2\phi}$$

(b) $X \geqslant \operatorname{cosec} i$ (polar region of shell not occulted), then

$$\tau_o = 2\pi\sigma_o\Omega_o\frac{1}{\beta}(1 - X^{-2})^{\frac{1}{2}}\left[1 - e^{-\beta} - \frac{\beta}{4\pi}\int_{\mu_a}^{\mu_b} \exp\{-\beta|\mu|\}\ (\pi - 2\Phi(\mu))d\mu\right] \quad \text{(B5)}$$

$$\tau_o\gamma_o = 2\pi\sigma_o\Omega_o\frac{1}{\beta}(1 - X^{-2})^{\frac{1}{2}}\left[\frac{2}{\beta^2} - e^{-\beta}\left[1 + \frac{2}{\beta} + \frac{2}{\beta^2}\right]\right.$$

$$\left. - \frac{\beta}{4\pi}\int_{\mu_a}^{\mu_b} \mu^2 \exp\{-\beta|\mu|\}\ (\pi - 2\Phi(\mu))d\mu\right] \quad \text{(B6)}$$

$$\tau_o\gamma_2 = 2\pi\sigma_o\Omega_o\frac{1}{\beta}(1 - X^{-2})^{\frac{1}{2}}\left[\frac{\beta}{\pi}\int_{\mu_a}^{\mu_b} \mu(1 - \mu^2)^{\frac{1}{2}}\exp\{-\beta|\mu|\}\cos\Phi(\mu)d\mu\right] \quad \text{(B7)}$$

$$\tau_o\gamma_3 = 2\pi\sigma_o\Omega_o\frac{1}{\beta}(1 - X^{-2})^{\frac{1}{2}}\left[\frac{\beta}{4\pi}\int_{\mu_a}^{\mu_b} (1 - \mu^2)\exp\{-\beta|\mu|\}\sin 2\Phi(\mu)d\mu\right] \quad \text{(B8)}$$

where

$$\mu_a = -\cos(i - \sec^{-1}X)$$

$$\mu_b = -\cos(i + \sec^{-1}X)$$

and $$\Phi = \sin^{-1}\left\{\frac{\mu\cos i - (1 - X^{-2})^{\frac{1}{2}}}{\sin i\ (1 - \mu^2)^{\frac{1}{2}}}\right\}$$

B.1.2 Ellipsoidal shell.

We again consider a thin ellipsoidal shell such that the geometrical thickness of the shell is much less than the radius of the star (which allows the approximations of Sec. 5.33 to be carried over to the general inclination case). As in the previous example of the shell it is easier to calculate the weighted integral moments in two different regimes. The net polarisation at a given inclination is then given by

eq. (5.25) and the wighted integral moments are

(a) Polar radius of ellipsoid ⩽ coseci

$$\tau_o = 2\pi\sigma_o n_o h R_* \Big[\int_0^1 N(\mu)\, d\mu - \frac{1}{4\pi} \int_0^{2\pi} \int_{\xi(\phi)}^1 N(\xi)\, d\xi d\phi \Big] \tag{B9}$$

$$\tau_o \gamma_o = 2\pi\sigma_o n_o h R_* \Big[\int_0^1 N(\mu)\mu^2\, d\mu - \frac{1}{4\pi} \int_0^{2\pi} \int_{\xi(\phi)}^1 N(\xi)\xi^2\, d\xi d\phi \Big] \tag{B10}$$

$$\tau_o \gamma_2 = 2\pi\sigma_o n_o h R_* \Big[\frac{1}{2\pi} \int_0^{2\pi} \int_{\xi(\phi)}^1 N(\xi)\, \xi(1 - \xi^2)^{1/2} \sin\phi\, d\xi d\phi \Big] \tag{B11}$$

$$\tau_o \gamma_3 = 2\pi\sigma_o n_o h R_* \Big[- \frac{1}{4\pi} \int_0^{2\pi} \int_{\xi(\phi)}^1 N(\xi)\, (1 - \xi^2) \cos 2\phi d\xi d\phi \Big] \tag{B12}$$

where $N(\mu) = N(\xi) = \dfrac{1}{h} \displaystyle\int_{x_1(\mu)}^{x_2(\mu)} (1 - x^{-2})^{1/2}\, dx$ (B13)

with $x_1(\mu) = \dfrac{X_1}{(1 + (A^2 - 1)\mu^2)^{1/2}}$

$$x_2(\mu) = \frac{X_1 + h}{(1 + (A^2 - 1)\mu^2)^{1/2}}$$

X_1 is the equatorial radius, $\mu = \cos\theta$ and $\xi = -\mu$

and

$$\xi(\phi) = \left[\frac{ab + 2c^2 - 2c(c^2 + ab - a^2)^{1/2}}{b^2 + 4c^2}\right]^{1/2}$$

where

$$a = 1 - X_1^{-2} - \sin^2 i \sin^2\phi$$

$$b = (A^2 - 1)/X_1^2 + \cos^2 i - \sin^2 i \sin^2\phi$$

$$c = \cos i \sin i \sin\phi$$

(b) Polar ellipsoidal radius $\geq$ coseci

$$\tau_o = 2\pi\sigma_o n_o h R_* \left[\int_0^1 N(\mu)\, d\mu + \frac{1}{2\pi} \int_{\mu_2}^{\mu_1} N(\mu)\, d\mu - \frac{1}{4} \int_{\mu_2}^{\mu_1} N(\mu)\Phi(\mu)\, d\mu \right] \quad \text{(B14)}$$

$$\tau_o \gamma_o = 2\pi\sigma_o n_o h R_* \left[\int_0^1 N(\mu)\mu^2\, d\mu + \frac{1}{2\pi} \int_{\mu_2}^{\mu_1} N(\mu)\mu^2\, d\mu - \frac{1}{4} \int_{\mu_2}^{\mu_1} N(\mu)\mu^2\Phi(\mu)\, d\mu \right] \quad \text{(B15)}$$

$$\tau_o \gamma_2 = 2\pi\sigma_o n_o h R_* \left[-\frac{1}{\pi} \int_{\mu_2}^{\mu_1} N(\mu)\mu\, (1 - \mu^2)^{1/2} \cos\Phi(\mu)\, d\mu \right] \quad \text{(B16)}$$

$$\tau_o \gamma_3 = 2\pi\sigma_o n_o h R_* \left[\frac{1}{4\pi} \int_{\mu_2}^{\mu_1} N(\mu)\mu\, (1 - \mu^2) \sin 2\Phi(\mu)\, d\mu \right] \quad \text{(B17)}$$

where

$$\Phi(\mu) = \sin^{-1}\left\{ \frac{(1 - X^{-2} - \mu^2(A^2 - 1)/X^2)^{1/2} + \mu \cos i}{\sin i\, (1 - \mu^2)^{1/2}} \right\}$$

$$\mu_1 = -\left[\frac{ab + 2c^2 - 2c(c^2 + ab - a^2)^{1/2}}{b^2 + 4c^2} \right]^{1/2}$$

and

$$\mu_2 = -\left[\frac{ab + 2c^2 + 2c(c^2 + ab - a^2)^{1/2}}{b^2 + 4c^2} \right]^{1/2}$$

with

$$a = 1 - X_1^{-2} - \sin^2 i$$

$$b = (A^2 - 1)/X_1^2 + \cos^2 i - \sin^2 i$$

$$c = \cos i \sin i$$

B.1.3 Wedge Shaped Disc.

For a disc the net polarisation at a given inclination is again given by eq.(5.29). The weighted integrals are most conveniently calculated by considering three separate regimes, viz

(a) $i < \alpha$

$$\tau_o = 2\pi\sigma_o n_o R_* \Big[\frac{\sin\alpha}{2} B(^{(n+1)}/_2, {}^3/_2) - \frac{\sin\alpha}{4\pi} \int_0^{2\pi} \int_{y(\phi)}^1 (1 - y^2)^{1/2} y^{n-2} \, dy d\phi \Big. \tag{B18}$$
$$\Big. - \frac{1}{4\pi} \int_0^{2\pi} \int_{y(\phi)}^1 (1 - y^2)^{1/2} y^{n-2} \cos\theta(\phi,y) \, dy d\phi \Big]$$

$$\tau_o y_o = 2\pi\sigma_o n_o R_* \Big[\frac{\sin^3\alpha}{6} B(^{(n+1)}/_2, {}^3/_2) - \frac{\sin^3\alpha}{12\pi} \int_0^{2\pi} \int_{y(\phi)}^1 (1 - y^2)^{1/2} y^{n-2} \, dy d\phi \Big. \tag{B19}$$
$$\Big. - \frac{1}{12\pi} \int_0^{2\pi} \int_{y(\phi)}^1 (1 - y^2)^{1/2} y^{n-2} \mu^3(\phi,y) \, dy d\phi \Big]$$

$$\tau_o y_2 = 2\pi\sigma_o n_o R_* \Big[\frac{1}{6\pi} \int_0^{2\pi} \int_{y(\phi)}^1 (1 - y^2)^{1/2} y^{n-2} \cos\phi \, [1 - \mu^2(\phi,y)]^3 \, dy d\phi \Big. \tag{B20}$$
$$\Big. - \frac{\cos^3\alpha}{6\pi} \int_0^{2\pi} \int_{y(\phi)}^1 (1 - y^2)^{1/2} y^{n-2} \cos\phi \, dy d\phi \Big]$$

$$\tau_o y_3 = 2\pi\sigma_o n_o R_* \Big[\frac{1}{12\pi} \int_0^{2\pi} \int_{y(\phi)}^{1} (1 - y^2)^{1/2}\, y^{n-2} \sin 2\phi\, \mu^3(\phi,y)\, dy d\phi$$

$$- \frac{1}{4\pi} \int_0^{2\pi} \int_{y(\phi)}^{1} (1 - y^2)^{1/2}\, y^{n-2} \sin 2\phi\, \mu(\phi,y)\, dy d\phi \qquad \text{(B21)}$$

$$+ \frac{\sin\alpha}{4\pi}\Big[\frac{\sin^2\alpha}{3} - 1\Big] \int_0^{2\pi} \int_{y(\phi)}^{1} (1 - y^2)^{1/2}\, y^{n-2} \sin 2\phi\, dy d\phi \Big]$$

where

$$\mu(\phi,y) = \frac{-\cos i\,(1 - y^2)^{1/2} + \sin i \sin\phi\,(y^2 - \sin^2 i \cos^2\phi)^{1/2}}{(1 - \sin^2 i \cos^2\phi)}$$

and

$$y(\phi) = (1 - \{\sin\alpha \cos i + \cos\alpha \sin i \sin\phi\}^2)^{1/2}$$

(b) $\alpha < i < \pi/2 - \alpha$

$$\tau_o = 2\pi\sigma_o n_o R_* \Big[\frac{\sin\alpha}{2} B((n+1)/2, 3/2) - \frac{1}{4\pi} \int_{y_2}^{1} \int_{\xi_2(y)}^{\xi_1(y)} (1 - y^2)^{1/2}\, y^{n-2}\, d\xi dy \qquad \text{(B22)}$$

$$+ \frac{1}{2\pi} \int_{y_2}^{1} \int_{\xi_2(y)}^{\xi_1(y)} (1 - y^2)^{1/2}\, y^{n-2}\, \phi(y,\xi)\, d\xi dy \Big]$$

$$\tau_o y_o = 2\pi\sigma_o n_o R_* \Big[\frac{\sin^3\alpha}{6} B((n+1)/2, 3/2) - \frac{1}{4} \int_{y_2}^{1} \int_{\xi_2(y)}^{\xi_1(y)} (1 - y^2)^{1/2}\, y^{n-2}\, \xi^2\, d\xi dy \qquad \text{(B23)}$$

$$- \frac{1}{12\pi} \int_{y_2}^{1} \int_{\xi_2(y)}^{\xi_1(y)} (1 - y^2)^{1/2}\, y^{n-2}\, \xi^2\, \phi(y,\xi)\, d\xi dy \Big]$$

$$\tau_o y_2 = 2\pi\sigma_o n_o R_* \left[\frac{1}{\pi} \int_{y_2}^{1} \int_{\xi_2(y)}^{\xi_1(y)} (1 - y^2)^{1/2}\, y^{n-2}\, \xi (1 - \xi^2)^{1/2} \cos\phi(y,\xi)\, d\xi dy \right] \tag{B24}$$

$$\tau_o y_3 = 2\pi\sigma_o n_o R_* \left[\frac{1}{4\pi} \int_{y_2}^{1} \int_{\xi_2(y)}^{\xi_1(y)} (1 - y^2)^{1/2}\, y^{n-2}\, (1 - \xi^2) \sin 2\phi(y,\xi)\, d\xi dy \right] \tag{B25}$$

where

$$\phi(y,\xi) = \sin^{-1}\left\{ \frac{(1 - y^2) - \xi \cos i}{\sin i\, (1 - \xi^2)^{1/2}} \right\}$$

$$y_2 = \cos(i + \alpha)$$

$$\xi_1(y) = \sin\alpha \quad \text{and} \quad \xi_2 = \cos(i + \sin^{-1} y)$$

(c) $i > \pi/2 - \alpha$

$$\tau_o = 2\pi\sigma_o n_o R_* \left[\frac{\sin\alpha}{2} B\left(\frac{(n+1)}{2}, \frac{3}{2}\right) - \frac{\sin\alpha}{2} \int_{y_1}^{1} (1 - y^2)^{1/2}\, y^{n-2}\, dy \right.$$

$$- \frac{\sin\alpha}{4} \int_{y_2}^{y_1} (1 - y^2)^{1/2}\, y^{n-2}\, dy + \frac{1}{4} \int_{y_2}^{y_1} (1 - y^2)^{1/2}\, y^{n-2} \cos(i + \sin^{-1} y)\, dy \tag{B26}$$

$$+ \frac{1}{\pi} \int_{y_1}^{1} \int_{0}^{\sin\alpha} (1 - y^2)^{1/2}\, y^{n-2}\, \phi(y,\mu)\, d\mu dy$$

$$\left. + \frac{1}{2\pi} \int_{y_2}^{y_1} \int_{\mu_1(y)}^{\mu_2(y)} (1 - y^2)^{1/2}\, y^{n-2}\, \phi(y,\mu)\, d\mu dy \right]$$

$$\tau_o\gamma_o = 2\pi\sigma_o n_o R_*\Big[\frac{\sin^3\alpha}{6} B(^{(n+1)}/_2, ^3/_2) - \frac{\sin^3\alpha}{6}\int_{y_1}^{1} (1 - y^2)^{1/2}\, y^{n-2}\, dy$$

$$- \frac{\sin^3\alpha}{12}\int_{y_2}^{y_1} (1 - y^2)^{1/2}\, y^{n-2}\, dy + \frac{1}{12}\int_{y_2}^{y_1} (1 - y^2)^{1/2}\, y^{n-2}\cos^3(i + \sin^{-1}y)\, dy$$

(B27)

$$+ \frac{1}{\pi}\int_{y_1}^{1}\int_{0}^{\sin\alpha} (1 - y^2)^{1/2}\, y^{n-2}\, \phi(y,\mu)\, \mu^2\, d\mu dy$$

$$+ \frac{1}{2\pi}\int_{y_2}^{y_1}\int_{\mu_1(y)}^{\mu_2(y)} (1 - y^2)^{1/2}\, y^{n-2}\, \phi(y,\mu)\, \mu^2\, d\mu dy \Big]$$

$$\tau_o\gamma_2 = 2\pi\sigma_o n_o R_*\Big[- \frac{1}{2\pi}\int_{y_1}^{1}\int_{0}^{\sin\alpha} (1 - y^2)^{1/2}\, y^{n-2}\, \mu(1 - \mu^2)^{1/2}\cos\phi(y,\mu)\, d\mu dy$$

(B28)

$$- \frac{1}{\pi}\int_{y_2}^{y_1}\int_{\mu_1(y)}^{\mu_2(y)} (1 - y^2)^{1/2}\, y^{n-2}\, \mu(1 - \mu^2)^{1/2}\cos\phi(y,\mu)\, d\mu dy \Big]$$

$$\tau_o\gamma_3 = 2\pi\sigma_o n_o R_*\Big[\frac{1}{2\pi}\int_{y_1}^{1}\int_{0}^{\sin\alpha} (1 - y^2)^{1/2}\, y^{n-2}\, (1 - \mu^2)\sin 2\phi(y,\mu)\, d\mu dy$$

(B29)

$$+ \frac{1}{4\pi}\int_{y_2}^{y_1}\int_{\mu_1(y)}^{\mu_2(y)} (1 - y^2)^{1/2}\, y^{n-2}\, (1 - \mu^2)\sin 2\phi(y,\mu)\, d\mu dy \Big]$$

where $y_1 = \cos(\alpha - i)$, $y_2 = -\cos(\alpha + i)$

$\mu_1 = -\sin\alpha$, $\mu_2 = -\cos(i + \sin^{-1}y)$

and $\phi = \sin^{-1}\left\{\dfrac{(1 - y^2)^{1/2} + \mu\cos i}{(1 - \mu^2)^{1/2}\sin i}\right\}$.